How central and peripheral clocks and the neuroendocrine system interact to time eclosion behavior in *Drosophila melanogaster*

Wie zentrale und periphere Uhren und das neuroendokrine System zusammenwirken, um das Schlupfverhalten von *Drosophila melanogaster* zeitlich festzulegen

Doctoral thesis for a doctoral degree

at the Graduate School of Life Sciences,

Julius-Maximilians-Universität Würzburg,

Section of Integrative Biology

Submitted by

Emad Amini

From Esfahan

Würzburg, 2024

The present work was accomplished at the Chair of Neurobiology and Genetics, Biocenter at the Julius-Maximilians-Universität Würzburg.

Submitted on: 15.01.2024

Members of the Promotion Committee:

Chairperson: Prof. Dr. Rüdiger Pryss

Supervisor (first): Prof. Dr. Christian Wegener

Supervisor (second): Prof. Dr. John Ewer

Supervisor (third): Prof. Dr. Keram Pfeiffer

Table of Contents

List of abbreviations

20-E: 20-hydroxyecdysone

ARG-Luc: Activity-Regulated Gene *lola*-Luciferase reporter

ARGs: activity-regulated genes

AstA: allatostatin A

AstA-R1: AstA receptor 1

AstA-R2: AstA receptor 2

AstC: allatostatin C

AstC-R1: AstC receptor 1

AstC-R2: AstC receptor 2

BAcTrace: Botulinum-Activated Tracer

C4da: class IV dendritic arborization neurons

CA: corpora allata

Ca^{2+}: calcium ion

CaLexA: Ca^{2+}-dependent nuclear import of LexA

cAMP: cyclic adenosine monophosphate

CC: corpora cardiaca

ChAT: choline acetyltransferase

ChR2-XXL: Channel rhodopsin 2-XXL

CLK: CLOCK

CNS: central nervous system

CO_2: carbon dioxide

CRISPR: clustered regularly interspaced short palindromic repeats

CRY: CRYPTOCHROME

CT: circadian time

CWO: CLOCKWORK ORANGE

CYC: CYCLE

DBT: DOUBLETIME

DD: constant darkness

DEM: *Drosophila* Eclosion Monitor

Dh31: diuretic hormone 31

Dh31-R: Dh31 receptor

Dh44: diuretic hormone 44

ILP: insulin-like peptide

D_{ls}: dorsolateral non-canonical eclosion hormone neurons

D_{ms}: dorsomedial non-canonical eclosion hormone neurons

DN: dorsal neurons

$DN1_{as}$: anterior dorsal neurons 1

$DN1_{ps}$: posterior dorsal neurons 1

DN1s: dorsal neurons 1

DN2s: dorsal neurons 2

DN3s: dorsal neurons 3

DNA: deoxyribonucleic acid

EcR: ecdysone receptor

EH: eclosion hormone (neuropeptide)

EH-R: EH receptor

eJTK: enhanced JTK cycle

ETH: ecdysis triggering hormone (neuropeptide)

ETHR: ETH receptor (protein)

G protein: Guanine nucleotide-binding protein

GABA: γ-aminobutyric acid

GFP: Green Fluorescent Protein

GPCR: G protein-coupled receptor

GRASP: GFP Reconstitution Across Synaptic Partners

gRNA: guide RNA

Kir2.1: potassium inward rectifying channel 2.1

LD: light-dark cycles

LGR: leucine-rich repeat-containing G protein-coupled receptor

LL: constant light

lLN_vs: large ventrolateral neurons

LN: lateral neurons

LN_ds: dorsolateral neurons

LPN: lateral posterior neurons

LS: Lomb-Scargle

Luc: Luciferase

MBDL: median bundle

MDT: median dorsal abdominal tract

MESA: Maximum Entropy Spectrum Analysis

mRNA: messenger ribonucleic acid

Ms: myosuppressin

MsR1: myosuppressin receptor 1

MsR2: myosuppressin receptor 2

O_2: oxygen

Opto-DEM: Optogenetic activation and *Drosophila* Eclosion Monitoring

PBT: phosphate-buffered saline + 0.3% Triton-X100

PDF: Pigment Dispersing Factor

PDFR: PDF receptor

PDF-tri: tritocerebrum PDF neurons

PDP1ε: PAR DOMAIN PROTEIN 1ε

PER: PERIOD

PG: prothoracic gland

phm: *phantom*

PI: Pars intercerebralis

PNS: peripheral nervous system

ppk: pickpocket

PTTH: prothoracicotropic hormone

PTTHn: PTTH neurons

RA^{CS2}.CC: cold-sensitive ricin

RFP: Red Fluorescent Protein

RI: rhythmicity index

RNAi: RNA interference

ROI: regions of interest

SEZ: suboesophageal zone

SIP: superior intermediate protocerebrum neuropil

sLN_vs: small ventrolateral neurons

SLP: superior lateral protocerebrum neuropil

SMP: superior medial protocerebrum neuropil

sNPF: short neuropeptide F

sNPF-R: sNPF receptor

syb: synaptobrevin

TARGET: Temporal and Regional Gene Expression Targeting

tdTomato: tandem dimer Tomato

TIM: TIMELESS

TOR: Target of Rapamycin

v'Td: ventral' Tracheal dendrite neuron

VGAT: vesicular GABA transporter

VGlut: vesicular glutamate transporter

V_m: ventromedial neurons

VNC: ventral nerve cord

VRI: VRILLE

WC: warm-cold temperature cycles

WEclMon: Würzburg Eclosion Monitor

ZT: Zeitgeber time

Summary

To grow larger, insects must shed their old rigid exoskeleton and replace it with a new one. This process is called molting and the motor behavior that sheds the old cuticle is called ecdysis. Holometabolic insects have pupal stages in between their larval and adult forms, during which they perform metamorphosis. The pupal stage ends with eclosion, *i.e.,* the emergence of the adult from the pupal shell. Insects typically eclose at a specific time during the day, likely when abiotic conditions are at their optimum. A newly eclosed insect is fragile and needs time to harden its exoskeleton. Hence, eclosion is regulated by sophisticated developmental and circadian timing mechanisms.

In *Drosophila melanogaster,* eclosion is limited to a daily time window in the morning, regarded as the "eclosion gate". In a population of laboratory flies entrained by light/dark cycles, most of the flies eclose around lights on. This rhythmic eclosion pattern is controlled by the circadian clock and persists even under constant conditions.

Developmental timing is under the control of complex hormonal signaling, including the steroid ecdysone, insulin-like peptides, and prothoracicotropic hormone (PTTH). The interactions of the central circadian clock in the brain and a peripheral clock in the prothoracic gland (PG) that produces ecdysone are important for the circadian timing of eclosion. These two clocks are connected by a bilateral pair of peptidergic PTTH neurons (PTTHn) that project to the PG. Before each molt, the ecdysone level rises and then falls shortly before ecdysis. The falling ecdysone level must fall below a certain threshold value for the eclosion gate to open. The activity of PTTHn is inhibited by short neuropeptide F (sNPF) from the small ventrolateral neurons (sLN_vs) and inhibition is thought to lead to a decrease in ecdysone production.

The general aim of this thesis is to further the understanding of how the circadian clock and neuroendocrinal pathways are coordinated to drive eclosion rhythmicity and to identify when these endocrinal signaling pathways are active. In Chapter I, a series of conditional PTTHn silencing-based behavioral assays, combined with neuronal activity imaging techniques such as non-invasive ARG-Luc show that PTTH signaling is active and required shortly before eclosion and may serve to phase-adjust the activity of the PG at the end of pupal development. Trans-synaptic anatomical stainings identified the sLN_vs, dorsal neurons 1 (DN1), dorsal neurons 2 (DN2), and lateral posterior neurons (LPNs) clock neurons as directly upstream of the PTTHn.

Eclosion motor behavior is initiated by Ecdysis triggering hormone (ETH) which activates a pair of ventromedial (V_m) neurons to release eclosion hormone (EH) which positively feeds back to the source of ETH, the endocrine Inka cells. In Chapter II trans-synaptic tracing showed that most clock neurons provide input to the V_m and non-canonical EH neurons. Hence, clock can potentially influence the ETH/EH feedback loop. The activity profile of the Inka cells and V_m neurons before eclosion is described. V_m and Inka cells are active around seven hours before eclosion. Interestingly, all EH neurons appear to be exclusively peptidergic.

In Chapter III, using chemoconnectomics, PTTHns were found to express receptors for sNPF, allatostatin A (AstA), allatostatin C (AstC), and myosuppressin (Ms), while EH neurons expressed only Ms and AstA receptors. Eclosion assays of flies with impaired AstA, AstC, or

Ms signaling do not show arrhythmicity under constant conditions. However, optogenetic activation of the AstA neurons strongly suppresses eclosion.

Chapter IV focuses on peripheral ventral' Tracheal dendrite (v'Td) and class IV dendritic arborization (C4da) neurons. The C4da neurons mediate larval light avoidance through endocrine PTTH signaling. The v'Td neurons mainly receive O_2/CO_2 input from the trachea and are upstream of V_m neurons but are not required for eclosion rhythmicity. Conditional ablation of the C4da neurons or *torso* (receptor of PTTH) knock-out in the C4da neurons impaired eclosion rhythmicity. Six to seven hours before eclosion, PTTHn, C4da, and V_m neurons are active based on ARG-Luc imaging. Thus, C4da neurons may indirectly connect the PTTHn to the V_m neurons.

In summary, this thesis advances our knowledge of the temporal activity and role of PTTH signaling during pupal development and rhythmic eclosion. It further provides a comprehensive characterization of the synaptic and peptidergic inputs from clock neurons to PTTHn and EH neurons. AstA, AstC, and Ms are identified as potential modulators of eclosion circuits and suggest an indirect effect of PTTH signaling on EH signaling via the peripheral sensory C4da neurons.

Keywords: Prothoracicotropic hormone, Prothoracic gland, Eclosion, Eclosion hormone, C4da, v'Td, Neuropeptide

Zusammenfassung

Um zu wachsen, müssen Insekten ihr altes, starres Exoskelett abwerfen und durch ein neues ersetzen. Dieser Vorgang wird als Häutung bezeichnet, und das motorische Verhalten, bei dem die alte Kutikula abgestoßen wird, heißt Ekdysis. Holometabole Insekten haben zwischen ihrer Larven- und Erwachsenenform ein Puppenstadium, in welchem sie eine Metamorphose durchlaufen. Das Puppenstadium endet mit dem Schlüpfen des erwachsenen Tieres aus der Puppenhülle. Die Insekten schlüpfen in der Regel zu einem bestimmten Zeitpunkt am Tag, wenn die abiotischen Bedingungen optimal sind, da das frisch geschlüpfte Insekt zerbrechlich ist und Zeit braucht, um sein Exoskelett auszuhärten. Daher wird der Schlupf durch ausgeklügelte Mechanismen der Entwicklung und der inneren Uhr gesteuert.

Bei *Drosophila melanogaster* ist der Sclupf auf ein tägliches Zeitfenster am Morgen beschränkt, das als "Schlupffenster" bezeichnet wird. In einer Population von Laborfliegen, die durch Licht/Dunkel-Zyklen gesteuert wird, schlüpfen die meisten Fliegen in etwa um das Einschalten der Beleuchtung. Dieses rhythmische Schlupfmuster wird von der inneren Uhr gesteuert und bleibt auch unter konstanten Bedingungen bestehen.

Das Timing der Entwicklung wird von komplexen hormonellen Signalen gesteuert, darunter das Steroid Ecdyson, insulinähnliche Peptide und das prothorakotrope Hormon (PTTH). Die Wechselwirkungen zwischen der zentralen zirkadianen Uhr im Gehirn und einer peripheren Uhr in der Prothorakaldrüse (PG), die Ecdyson produziert, sind wichtig für die zirkadiane Zeitsteuerung des Schlupfs. Diese beiden Uhren sind durch ein bilaterales Paar peptiderger PTTH-Neuronen (PTTHn) verbunden, die in die PG projizieren. Vor jeder Häutung steigt der Ecdysonspiegel an und fällt dann kurz vor danach wieder ab. Der fallende Ecdysonspiegel muss einen bestimmten Schwellenwert unterschreiten, damit sich das Schlupffenster öffnen kann. Die Aktivität der PTTHn wird durch das kurze Neuropeptid F (sNPF) aus den kleinen ventrolateralen Neuronen (sLN_vs) gehemmt, und es wird angenommen, dass die Hemmung zu einer Abnahme der Ecdysonproduktion führt.

Das allgemeine Ziel dieser Thesis besteht darin, die Koordination zwischen der zirkadianen Uhr und den neuroendokrinen Signalwegen zur Steuerung der Eklosionsrhythmik weiter zu charakterisieren und zu ermitteln, wann diese endokrinen Signalwege aktiv sind. In Kapitel I zeigen eine Reihe von Verhaltenstests, die auf der konditionalen Ausschaltung von PTTHn basieren, in Kombination mit Techniken zur Darstellung neuronaler Aktivität, wie z. B. nicht-invasives ARG-Luc imaging, dass PTTH-Signale kurz vor dem Schlupf aktiv und erforderlich sind und zur Phasenanpassung der Aktivität der PG am Ende der Puppenentwicklung dienen könnten. Trans-synaptische anatomische Färbungen identifizierten die sLN_vs, die dorsalen Neuronen 1 (DN1), die dorsalen Neuronen 2 (DN2) und die lateralen posterioren Neuronen (LPNs) als Uhrneuronen, die dem PTTHn direkt vorgeschaltet sind.

Das motorische Schlupfverhalten wird durch das Ecdysis-auslösende Hormon (ETH) ausgelöst, das ein Paar ventromedialer (V_m) Neuronen zur Freisetzung des Eklosionshormons (EH) anregt, welches positiv an die Quelle des ETH, die endokrinen Inka-Zellen, zurückkoppelt. In Kapitel II zeigte die trans-synaptische Nachverfolgung, dass die meisten Uhrneuronen Input für die V_m- und nicht-kanonischen EH-Neuronen liefern, sodass die Uhr möglicherweise die ETH/EH-Rückkopplungsschleife beeinflussen kann. Das Aktivitätsprofil

der Inka-Zellen und V_m-Neuronen vor dem Schlupf wird beschrieben. V_m- und Inka-Zellen sind etwa sieben Stunden vor dem Schlupf aktiv. Interessanterweise scheinen alle EH-Neuronen ausschließlich peptiderg zu sein.

In Kapitel III wurde mit Hilfe von Chemoconnectomics festgestellt, dass PTTH-Neuronen Rezeptoren für sNPF, Allatostatin A (AstA), Allatostatin C (AstC) und Myosuppressin (Ms) exprimieren, während EH nur Ms- und AstA-Rezeptoren exprimieren. Eklosionsversuche mit Fliegen, deren AstA-, AstC- oder Ms-Signalübertragung beeinträchtigt ist, zeigen unter konstanten Bedingungen keine Arrhythmie. Eine optogenetische Aktivierung der AstA-Neuronen führt jedoch zu einer starken Unterdrückung des Schlupfs.

Kapitel IV konzentriert sich auf die peripheren ventralen Trachealdendritischen Neurone (v'Td) und dendritische Verzweigungsneurone der Klasse IV (C4da). Die C4da-Neuronen vermitteln die Lichtvermeidung der Larven durch endokrine PTTH-Signale. Die v'Td-Neuronen erhalten hauptsächlich O_2/CO_2-Input aus den Tracheen und sind den V_m-Neuronen vorgeschaltet, werden aber für die Schlupfrhythmik nicht benötigt. Die bedingte Ablation der C4da-Neuronen und das Knock-out von *torso* (Rezeptor für PTTH) in den C4da-Neuronen beeinträchtigten die Schlupfrhythmik. Sechs bis sieben Stunden vor dem Schlupf sind die PTTHn-, C4da- und V_m-Neuronen aktiv. Somit könnten C4da-Neuronen indirekt die PTTHn mit den V_m-Neuronen verbinden.

Zusammenfassend lässt sich sagen, dass diese Arbeit unser Wissen über das zeitliche Aktivitätsmuster und der Rolle des PTTH signalling während der Puppenentwicklung und dem rhythmisches Schlupf erweitert. Sie liefert auch eine umfassende Charakterisierung der synaptischen und peptidergen Eingänge von Uhrneuronen zu PTTHn- und EH-Neuronen. AstA, AstC und Ms wurden als potenzielle Modulatoren der neuronalen Schlupfschaltkreise identifiziert und deuten auf einen indirekten Effekt der PTTH-Signalgebung auf das EH signalling über die peripheren sensorischen C4da-Neuronen hin.

Schlüsselwörter: Prothorakotropes Hormon, Prothorakale Drüse, Eklosion, Eklosionshormon, C4da, v'Td, Neuropeptid

Introduction

1. Physiological events during ecdysis and adult emergence

Insects are members of a clade of the Animalia kingdom called Ecdysozoa. The Ecdysozoans are identified by the cuticle-covered epidermis that is periodically changed by molting to allow growth (Aguinaldo et al., 1997; Ewer, 2005a; Giribet and Edgecombe, 2017; Telford et al., 2008).

The Holometabolous insects life cycle (after hatching from the egg) is divided into larval stages and a reproducing adult stage which are separated by a pupal stage. The larval and adult stages are morphologically and physiologically different. Under normal conditions (25 °C with enough food and oxygen), *Drosophila melanogaster* passes into the third (last) larval instar (L3) in four days. During larval development, it accumulates weight and grows more than 200 times compared to when it hatched (Mirth and Riddiford, 2007; Texada et al., 2020). On day five, the third instar stops feeding, starts wandering, empties its gut, and searches for a suitable place to pupariate (Robertson, 1966). The transition from immature larva to reproductive adult requires metamorphosis that marks the pupal stages (Kristensen, 1999; Peters et al., 2014). During metamorphosis, a series of programmed deaths of larval tissues, cell division, and proliferations to make or alter adult organs and tissues happen. Especially, the development of imaginal disks creates new adult organs. Hence, the adult looks entirely different from its larval form (Locke and Huie, 1979; Weeks and Truman, 1984; Zitnan and Adams, 2012).

Molting is a series of physiological events that happen in a specific order that starts with the separation of the old cuticle from the epidermis (apolysis) and ends with ecdysis. The fully developed and ready-to-molt animal that is still bearing its old cuticle is called “pharate”. Ecdysis is a stereotyped behavior that is orchestrated by specific peptidergic neurons and in different ganglia of the central nervous system (CNS) which operate in a species-specific pattern to induce the predetermined muscular movements of ecdysis (Ewer and Reynolds, 2002; Mesce and Fahrbach, 2002).

The physiology of molting (from apolysis to ecdysis) comprises a series of specific events: Each new cuticle is directly made underneath the old one. At the beginning of molting (apolysis), the epidermal cells detach themselves from the cuticle. Inactive proteolytic enzymes, chitinases, and other proteins are secreted in space between the old cuticle and epidermis and form the molting gel (Bestman and Booker, 2003; Kimura and Truman, 1990; Riddiford, 2009). After the new cuticle is synthesized, and shortly before initiation of ecdysis, the molting gel enzymes are activated and digest the inner layer of the old cuticle, and the molting gel turns into molting fluid (Bestman and Booker, 2003; Kimura and Truman, 1990; Riddiford, 2009). The newly formed space between the old and new cuticles is called the exuvial space. Exuvial space is filled with molting fluid due to the osmotic pressure build-up by the new epidermal cells which actively pump K^+ ions out. The osmotic gradient forces water to flow from the hemolymph to the exuvial space (Jungreis, 1978). The following ecdysis is divided into pre-ecdysis, ecdysis, and post-ecdysis events. The beginning of pre-ecdysis is marked by the formation of molting fluid. The reabsorption of molting fluid into the hemolymph happens through the new cuticle and then the epidermis, or through the hindgut. A minor volume of molting fluid remains in the new tracheal system and around the airways

(Kimura and Truman, 1990). The collapse of the old trachea and consecutive air filling of the new trachea indicates the onset of ecdysis, during which the exoskeletons rupture along weak lines called seams after size expansion. A series of predetermined peristaltic movements help the animal to remove the old cuticle and with that the old lining of the trachea. Finally, the post-ecdysis processes comprise expanding and sclerotizing the exoskeleton, and cuticle pigmentation (Ewer, 2005a, 2005b; Riddiford, 2009; White and Ewer, 2014; Zitnan and Adams, 2012).

The final ecdysis or the adult ecdysis of holometabolous insects is called "eclosion", which in *Drosophila* is equal to the emergence of the adult fly from the puparium (Ewer, 2005a; Sullivan et al., 2020; Truman, 1971; Zitnan and Adams, 2012). Like ecdysis, eclosion is divided into three phases called pre-eclosion, eclosion, and post-eclosion events (Kimura and Truman, 1990). In *D. melanogaster* about six hours before eclosion, the molting fluid is reabsorbed and disappears (Kimura and Truman, 1990). The appearance of the pupal cuticle changes several times, and based on the appearance each stage was given a name. It starts with the smooth stage because of the smooth appearance due to the presence of molting fluid. The cuticle than changes from smooth, to smooth/grainy, to grainy, and finally to white (Kimura and Truman, 1990). The first transition happens due to the absorption of the molting fluid. Three hours later the fluid is completely removed, and the cuticle appears grainy (Kimura and Truman, 1990). About one hour prior to eclosion the grainy to white transition happens because of the air filling of the large trachea in the head. This gives the pharate adult a pair of white spots between the eyes (Kimura and Truman, 1990). Then air fills the space between the old pupal and new adult cuticle which marks the white stage. With the white stage, pre-eclosion starts (Kimura and Truman, 1990). The ptilinum expands and tears the pupal cuticle. Dorsoventral movements of the abdominal muscles start and the head trachea completely expands the postfrontal part of the head (Kimura and Truman, 1990). Pre-eclosion ends with a brief quiescent period. During eclosion, the ptilinum of the head expands to open the weak point of the puparium called the operculum. The motor program consisting of forward head thrusts, lateral thoracic contraction, and forward peristaltic contractions of the abdomen push the fly forward (Kimura and Truman, 1990; Park et al., 1999). After the motor program is completed post-eclosion which comprises pressurizing the exoskeleton, wing expansion and cuticle tanning happens (Dewey et al., 2004; Kim et al., 2006b, 2006a; Peabody et al., 2008).

2. Ecdysis-triggering hormone and eclosion hormone initiate eclosion

The decision for generating the predetermined motor program of the peristaltic movements is made by the brain and CNS (Diao et al., 2017; Elliott et al., 2021; Ewer, 2005a; Sullivan et al., 2020). However, the neuroendocrine decision-making for initiating eclosion is behavior-specific and hardwired. To increase the survival, the motor program of ecdysis is genetically coded and regardless of learning (Sullivan et al., 2020). The orchestration of the stereotypic all-or-none eclosion behavior depends on two key hormones that engage in a positive feedback loop interaction: ecdysis triggering hormone (ETH) and Eclosion hormone (EH; Figure 1). ETH injection into pharate adults triggers pre-eclosion behavior (Park et al., 1999).

Drosophila ETH is released from endocrine Inka cells located at the primary tracheal branches shortly before the inflation of the trachea and the onset of ecdysis behavior (Park et al., 2002).

The receptor of ETH (ETHR) is encoded by *ETHR* in two isoforms: $ETHR^A$ and $ETHR^B$ (Iversen et al., 2002; Park et al., 2003). $ETHR^B$ is shown to be 400 times more sensitive to ETH than $ETHR^A$ (Park et al., 2003). The preparation for molting is associated with hemolymph ecdysteroid levels (see Introduction 3.1; Kingan and Adams, 2000; Truman et al., 1983) which also leads to *ETHR* expression in the CNS (Kim et al., 2006a). However, ETH release does not happen until the ecdysteroid levels drop (Zitnan and Adams, 2012).

EH is produced by neurons residing in the brain. In *Drosophila*, these EH^+ neurons include the ventromedial (V_m) neurons that are located anteriorly at the anterior cell body rind of the superior medial protocerebrum (SMP) and arborize in the medial superior protocerebrum (Baker et al., 1999; Horodyski et al., 1993; Scott et al., 2020). The descending axons of these neurons run along the VNC, exit from it, and form release sites on the surface of the hindgut (Baker et al., 1999; Horodyski et al., 1993). The V_m neurons in both larval and pharate nervous systems send their parallel axonal projections dorsally down to the midline of the VNC and nearly cover the entire length of the VNC (Baker et al., 1999; Horodyski et al., 1993). In both *Drosophila* and moths, EH is released into the hemolymph to activate ETH peptide release from the Inka cells (Ewer et al., 1997; Hewes and Truman, 1991; Kim et al., 2004; Kingan et al., 1997; Zitnan et al., 2002).

Recently, a new subset of EH^+ neurons, referred to as the non-canonical EH neurons, have been discovered in *Drosophila* brain (Scott et al., 2020). The non-canonical EH neurons appear in the late third instar larval brain and persist during metamorphosis and at least some of them exist during adulthood. These neurons have diverse morphologies and complex projection patterns. Six to seven of these neurons are located in the dorsolateral part of each hemisphere of the pharate brain, hence they are called D_l neurons. Another cluster of six cells is in the dorsomedial part and midline of the brain, hence they are called D_ms (Scott et al., 2020).

Scott et al. (2020) provided evidence for an additional, non-neuronal expression of *Eh*. The anterior and posterior spiracles, mouth parts, superficial cells along the lateral and ventral body wall, epithelial cells of the trachea, and cells surrounding the Keilin organ are shown to express *Eh*-driven green fluorescent protein (GFP). In addition, the presence of *Eh* messenger ribonucleic acid (mRNA) in the trachea is confirmed by RT-PCR (Scott et al., 2020).

EH is able to start both pre-eclosion and eclosion programs in moth and fly (Kataoka et al., 1987; Kono et al., 1990; McNabb et al., 1997; Ruf et al., 2017; Truman, 1992). EH is also necessary to start the ecdysis/eclosion motor program together with ETH (Ewer and Reynolds, 2002; Truman, 2005; D. Zitnan et al., 2007; Zitnan and Adams, 2012). In flies with ablated V_m neurons, the ecdysis motor program is distorted, poorly performed, delayed, and the stillness period is missing (McNabb et al., 1997). Loss-of-function experiments targeting EH production in the V_m neurons resulted in remarkable but confusing results. Ablating the V_m neurons showed disrupted eclosion (Baker et al., 1999; McNabb et al., 1997), but on the contrary, the *Eh* null mutants showed complete eclosion failure (Krüger et al., 2015). This paradoxical finding was resolved in 2020 when Scott et al. (Scott et al., 2020) discovered the non-canonical EH neurons. While only silencing the V_m neurons is not completely lethal, silencing all EH^+ neurons is 100% lethal during larval stages (Scott et al., 2020). Conditional temperature-controlled silencing of all EH^+ neurons during pupal stages causes eclosion failure in half of the population. The majority of eclosed survivors failed to complete post-ecdysis behaviors

such as wing expansion (Scott et al., 2020). It is possible that in the case of V_m neurons ablation, the small amount of the EH released from the non-canonical EH neurons started the EH/ETH feedback and partially rescued the behavior (Scott et al., 2020).

Electrophysiological studies showed that EH^+ neurons one hour before ecdysis become excitable (Hewes and Truman, 1994). The V_m neurons of *Manduca* and *Drosophila* express ETHR and are activated in response to ETH (Kim et al., 2006a, 2006b). ETH release starts pre-ecdysis and leads to the release of EH from the V_m neurons (Ewer et al., 1997; Gammie and Truman, 1999; Kim et al., 2006a). EH acts back on the Inka cells and consecutively more ETH is released until the reservoirs of Inka cells are completely depleted (Ewer et al., 1997). It takes roughly half an hour from the beginning of pre-ecdysis to the time Inka cells receive the hemolymph EH signal (Clark et al., 2004; Kingan et al., 1997). In *Drosophila*, it is still not fully clear how the EH/ETH feedback is started in the first place, and whether EH or ETH starts the whole EH/ETH feedback. Some believe that releasing EH starts the process (Ewer et al., 1997; Gammie and Truman, 1999, 1997). On the other hand, others have suggested ETH to be the starting agent (Zitnan et al., 1996; Zitnan and Adams, 2000).

The EH receptor (EH-R) was first discovered on the surface of the Inka cells of the tephritid fly *Bactrocera dorsalis* (Chang et al., 2009). This guanylyl cyclase has two isoforms BdmGC-1 and BdmGC-1B. The BdmGC-1 has a higher affinity for EH and is sensitive to lower levels of EH. Based on immunolabeling assays, the Inka cells and possibly some of their neighboring cells in the epitracheal glands of *B. dorsalis* contain BdmGC-1. This means EH possibly influences the neighboring cells as well as ETH release from the Inka cells (Chang et al., 2009). The EH-R has not been identified in *Drosophila melanogaster* yet, but the gene CG10738 has a homolog sequence with *Bactrocera dorsalis* EH-R and is believed to be the *Drosophila* EH-R (Chang et al., 2009).

A series of additional neuropeptides control post-ecdysis (or post-eclosion) events after ecdysis (or eclosion) sequence completion (Figure 1; Kim et al., 2006a). For example, the crustacean cardioactive peptide, mioinhibitory peptide, and bursicon are required for post-eclosion events (Dewey et al., 2004; Kim et al., 2006b; Luo et al., 2005; Park et al., 2003; Peabody et al., 2008).

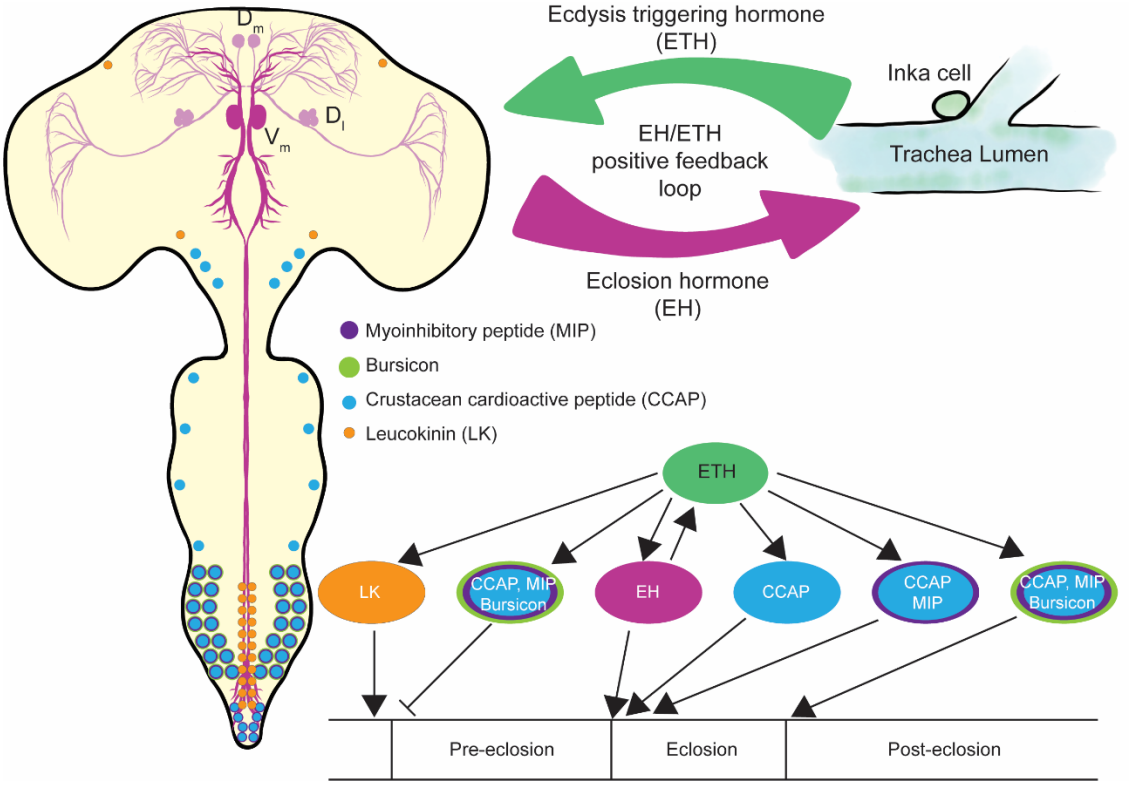

Figure 1. The interaction between EH and ETH creates a positive feedback loop that initiates eclosion. A low ecdysteroid level allows the eclosion to happen. Therefore, Inka cells located at the epitracheal glands release ETH into hemolymph. Shortly before pre-eclosion, ETH causes leucokinin release that is required for tracheal clearing after collapsing. During this time the pre-eclosion is prevented because of delay circuits that make sure everything is ready for eclosion. ETH during eclosion is picked up by EH^+ neurons, the V_ms, and in response to that V_ms release EH into the hemolymph. The circulating EH not only causes the positive EH/ETH feedback loop which encourages more EH and ETH release, but also excites crustacean cardioactive peptide (CCAP) neurons which are required for eclosion motor program initiation. Different subsets of CCAP neurons co-release myoinhibitory peptide (MIP) and bursicon which are required for pre-ecdysis delay circuits, eclosion motor program, and post-eclosion events. Based on the original model by Kim et al., 2006a, modified for P14 pharate adult nervous system.

2.1. Tracheal collapse and subsequent air filling are important physiological events

The trachea represent a cuticular structure, and hence also the tracheal cuticle has to be shed during ecdysis. During molt, the new tracheal cuticle is first built inside the old one (Keister, 1948). Then, the inner layer of the old and the newly built trachea need to separate which leads to molting fluid filling the emerging lumen of the new trachea. This process is called tracheal collapse (Kim et al., 2018). During tracheal collapse, the normal airflow is distorted and leads to a brief period of hypoxia. This temporary hypoxia might act as an extra driving force to initiate ecdysis (Greenlee and Harrison, 2005).

A class of internal sensory organ neurons that are capable of sensing oxygen (O_2) and carbon dioxide (CO_2) are the ventral' tracheal dendrite (v'Td) neurons. These peripheral nervous system (PNS) neurons project their dendrites along the internal tracheal branches (ganglionic

branch and lateral trunk) while extending their axons to the VNC (Bodmer and Jan, 1987; Merritt and Whitington, 1995; Qian et al., 2018). In abdominal segments one to six of the larva, one pair of v'Td neurons is located. Based on their positions, the neurons of each pair are categorized into v'Td1 and -2 groups. The cell bodies of both classes of neurons are located close to each other with the cell body of v'Td1 being located more ventrally. There are six v'Td1 neurons in abdominal hemisegments A1-6 and seven v'Td2 neurons in A1-7 (Qian et al., 2018). Based on their receptor profile, a role in chemical, light, and gaseous stimuli detection has been predicted for the v'Td neurons (Hückesfeld et al., 2021; Imambocus et al., 2022; Qian et al., 2018). The v'Td1 neurons are mostly regarded as O_2 sensing neurons (Morton et al., 2008; Qian et al., 2018) while v'Td2 are regarded as CO_2 sensing (Hückesfeld et al., 2021; Qian et al., 2018).

Ablation of the O_2 sensing v'Td1 neurons prevents ecdysis and most of the first instar larvae die, possibly because of suffocation inside the food. Also, conditional ablation during the pupal stage prevents eclosion (Morton et al., 2008). Time-specific conditional ablation of these neurons also caused eclosion failure (Morton et al., 2008). A recent study on the larval neuroendocrine connectome showed that the V_m neurons mostly receive somato- and entero-sensory input, and to a lesser extent CO_2 gas information from the trachea (Hückesfeld et al., 2021). However, whether this connection exists in the adult nervous system and if it plays a role in eclosion or its gating is unknown.

EH signaling is important for tracheal air filling. Two to five minutes after trachea collapse, the molting fluid is reabsorbed, and the airway is cleared and filled with air. As mentioned in molting physiology, a small portion of molting fluid remains inside the trachea (Kimura and Truman, 1990). This process is necessary to restore normal respiration (Förster and Woods, 2013; Kimura and Truman, 1990; Park et al., 2002). In *Eh* knock-out flies, tracheal air filling is mistimed and fails, resulting in dead animals that still have molting fluid present in their trachea (Baker et al., 1999; McNabb et al., 1997). As mentioned before, Scott et al. (2020) showed that *Eh* is also expressed by non-neuronal tissues such as spiracles and epithelial tracheal cells. Ubiquitous cell killing of all tissues expressing *Eh* resulted in larval death during the first ecdysis. Despite successfully completing the pre-ecdysis behavior, they fail to perform ecdysis in part due to tracheal air-filling failure (Scott et al., 2020).

3. Eclosion is developmentally and circadianly timed

The events of eclosion in *Drosophila* are not very different from those during larval ecdyses and share many similarities on the physiological and neuroendocrinal basis. Yet, an important difference is the circadian gating of eclosion, while larval ecdysis is purely developmentally timed (Pittendrigh, 1967; Pittendrigh and Skopik, 1970; Qiu and Hardin, 1996). This means eclosion does not happen automatically after developmental maturation but happens at a certain time of the day (dawn). If due to any reason flies miss their chance of eclosion when the circadian gate permits it, they must postpone eclosion to the next day (Pittendrigh, 1954; Pittendrigh and Skopik, 1970; Skopik and Pittendrigh, 1967). Since eclosion for each individual happens only once during life, rhythmic eclosion can only be observed in a population of synchronized flies. In a population of *Drosophila* flies, eclosion of most individuals is confined to the time around dawn (Bunning, 1935; Kalmus, 1935; Pittendrigh, 1954). A sophisticated neuroendocrinal circuit controls the developmental and circadian timing

of eclosion (Baker et al., 1999; Ewer, 2005a; Ewer et al., 1997; Scott et al., 2020; Truman et al., 1983; Zitnan et al., 2007; Zitnan and Adams, 2012).

3.1. The developmental timing of eclosion

In insects, the levels of steroid hormones collectively known as ecdysteroids control the timing and execution of molting and metamorphosis (Figure 2; Henrich et al., 1999; Warren et al., 2006). In *Drosophila* larvae, the ring gland is dorso-anteriorly positioned regarding to brain and is a fusion product of the corpora allata (CA, producing juvenile hormone), corpora cardiaca (CC, a production and neuroendocrine release site for peptides), and the prothoracic gland (PG, producing ecdysteroids). Nutritional cholesterols and plant sterols are used as the basis of ecdysteroid biosynthesis in the PG (Lavrynenko et al., 2015). A consortium of genes collectively known as the Halloween genes (*phantom (phm)*, *disembodied*, *noppera-bo*, *shroud*, *neverland*, *spooky*, *spookier*, *spookiest*, and *shadow*) codes for the enzymes necessary for making the ecdysteroids (Figure 2 A; Chávez et al., 2000; Kamiyama and Niwa, 2022; Pan et al., 2021). At the beginning of each molt, PG produces most ecdysteroids (Gilbert, 2004; Koelle et al., 1991; Rewitz et al., 2007; Talbot et al., 1993). This subsequently increases the hemolymph ecdysteroid levels (Huang et al., 2008). After secretion from the PG, ecdysone (the important ecdysteroid required for molting) circulates in the body and is changed to its active form, 20-hydroxyecdysone (20-E) by hydroxylation via the enzyme SHADE which is expressed by many peripheral tissues (Figure 2 A; Petryk et al., 2003; Rewitz et al., 2006). As metamorphosis proceeds, the ring gland is restructured and the PG cells progressively degenerate (Dai and Gilbert, 1991). In mature adults, the gonads produce ecdysteroids (Roy et al., 2018).

The ecdysone receptor (EcR) is a member of the nuclear hormone receptor family and thus is located intracellularly (Koelle et al., 1991). EcR together with the retinoid X receptor Ultraspiracle creates a heterodimer (Hill et al., 2013). When it is not bound to ecdysone, EcR/Ultraspiracle acts as a repressor by interacting with co-repressors such as histone deacetylases and DNA binding (Millard et al., 2013; Nakagawa and Henrich, 2009; Riddiford et al., 2000). After binding to 20-E, the co-repressors are swapped with co-activators, then EcR/Ultraspiracle binds to specific ecdysone response elements of the genomic DNA, and gene transcription is initiated or inhibited (Millard et al., 2013; Small and Arnosti, 2020). The consequent transcriptional changes cause the cellular and physiological events of development that finally end with molting (Bollenbacher et al., 1981, 1979; Jiang et al., 2000; King-Jones and Thummel, 2005; Riddiford, 1993; Sullivan and Thummel, 2003; Thummel, 2002, 1996).

The levels of ecdysteroids change during development with a peak at the beginning of each larval or pupal stage and dropping shortly before ecdysis and eclosion (Figure 2 B; Gilbert et al., 2002). To initiate eclosion, the hemolymph 20-E level needs to drop below a certain threshold which marks the end of metamorphosis (Kingan and Adams, 2000; Truman et al., 1983). The developmental pattern of ecdysteroid titers in the hemolymph was first characterized in moths because their large bodies allow extractions of large hemolymph quantities (Warren and Gilbert, 1986). However, such measurements are difficult to achieve in *D. melanogaster* because of its size. Therefore, the ecdysone titers were measured in whole-body extracts and showed that each molt is associated with rising ecdysone levels (Handler, 1982; Lavrynenko et al., 2015). From pharate *Drosophila,* about 10 pg ecdysteroids can be

isolated from each animal (Handler, 1982; Lavrynenko et al., 2015). Since dropping of ecdysteroid levels is necessary to start eclosion, injection of ecdysone into the pharate adults of *Drosophila* delays their eclosion. This delay is proportional to the amount of injected ecdysone meaning with higher injected doses pharates eclose considerably later (Mark et al., 2021). The threshold level of 20-E in hemolymph to start ecdysis in moths is measured to be 0.1 µg/ml (Davis et al., 2003).

Body weight of *Drosophila* is gained during the larval stages and body size growth ends with pupariation (Boulan et al., 2015; Juarez-Carreño et al., n.d.; Yamanaka et al., 2013). Before pupariation, *Drosophila* passes two checkpoints. Normally after 8-10 hours pass the second molt, the weight of the L3 larva reaches 0.75 mg (Stieper et al., 2008). At this weight, the larva has accumulated enough energy to complete metamorphosis. This is the first important developmental threshold that *Drosophila* should pass to allow pupariation. This developmental checking point is known as the "critical weight" (Mirth et al., 2005; Mirth and Riddiford, 2007). The second checkpoint to allow proceeding to pupariation is the complete and flawless growth of the imaginal disks (Rewitz et al., 2013). Any flaw in the growth of the imaginal disks results in defective adult organs and lowers survival chances. The coordination of growth, deciding when critical weight has reached, and checking the imaginal disk development require internal and external informational acquisition and exchange between cells and hormones involved in development (Texada et al., 2020). Two peptides control this coordination and the mentioned checkpoints via controlling ecdysone production and release (Yamanaka et al., 2015): Prothoracicotropic hormone (PTTH) and insulin-like peptides (ILPs; Figure 2 A; Pan et al., 2021).

PTTH was first isolated from the brain of *Bombyx* moth and was shown to be effective in promoting ecdysone production in PG (Kataoka et al., 1991). The transition between the developmental stages always starts with the release of PTTH which leads to the biosynthesis of ecdysteroids in PG (Fellner et al., 2005; Gilbert, 2004; Kawakami et al., 1990; McBrayer et al., 2007; Rewitz et al., 2007; Westbrook and Bollenbacher, 1990). In *Drosophila melanogaster* and *Manduca sexta*, PTTH is synthesized and released by secretory neurons in the pars lateralis which send their axons down to the PG (Agui et al., 1980, 1979; McBrayer et al., 2007; Siegmund and Korge, 2001). The receptor for PTTH is the receptor tyrosine kinase TORSO (Rewitz et al., 2009). Without PTTH signaling, ecdysone synthesis is impaired and development is delayed (Gibbens et al., 2011; Perry et al., 2020). Killing of PTTH neurons (PTTHn) on one side of the brain shrinks the corresponding PG part innervated from that side, and loss of all PTTHn causes the reduction of PG size in general (Ghosh et al., 2010; Shimell et al., 2018). PTTH signaling also contributes to critical weight gain. Removing PTTH signaling either by ablating PTTHn, removing TORSO, or in *Ptth* null mutants, delays the onset of pupariation and causes overfeeding for several more days which results in oversized larvae and pupae by more than two fold (McBrayer et al., 2007; Rewitz et al., 2009; Shimell et al., 2018). This increase in size correlates with increased cellular proliferation rather than cellular size increase (McBrayer et al., 2007).

For *Drosophila* eight different ILPs have been identified (Brogiolo et al., 2001; Colombani et al., 2012; Garelli et al., 2012; Ikeya et al., 2002; Liu et al., 2016). ILP1 to ILP5 are very similar to vertebrate insulins while ILP6 is more similar to vertebrate insulin-like growth factors (Lin and Smagghe, 2019; Nässel and Broeck, 2016; Okamoto et al., 2009). Like in vertebrates,

ILP1-6 act through an insulin receptor (InR) belonging to the membrane tyrosine kinase family (Fernandez et al., 1995). ILP7 and ILP8 are similar to vertebrate relaxin and use a different receptor. The receptor of ILP7 is believed to be a Leucine-rich repeat-containing G protein-coupled receptor (GPCR) 4 (LGR4; Imambocus et al., 2022). The receptor of ILP8 is another GPCR called LGR3 (Colombani et al., 2015; Garelli et al., 2015; Jaszczak et al., 2016; Vallejo et al., 2015). Various larval tissues produce insulin but the insulin-producing cells in the pars intercerebralis (PI) of the brain (ILP1-3, 5), the fat body (ILP6), and imaginal discs (ILP8) are active insulin-secreting sites (de Velasco et al., 2007; Gontijo and Garelli, 2018). The InR is present on the PG and activates Target of Rapamycin (TOR) and Warts signaling pathways (Texada et al., 2020). ILPs also facilitate cholesterol shuttling to the PG (Boulan et al., 2013; Caldwell et al., 2005; Colombani et al., 2005; Mirth et al., 2005; Moeller et al., 2017; Texada et al., 2019).

ILP8 is in charge of checking the status of imaginal disks and in case of flaws, it is secreted and prevents pupariation (Colombani et al., 2012; Garelli et al., 2012). Secretion of ILP8 from abnormally grown imaginal disks suppresses ecdysone production by inhibiting the PTTH neurons (Colombani et al., 2015; Garelli et al., 2015; Jaszczak et al., 2016; Vallejo et al., 2015). A population of ILP8-sensing cerebral neurons regarded as growth-coordinating $LGR3^{+}$ neurons inhibit the PTTH neurons and cause developmental delay (Colombani et al., 2015; Garelli et al., 2015; Jaszczak et al., 2016; Vallejo et al., 2015).

In the larva, both PTTH and insulin pathways are positively influenced by the neuropeptide allatostatin A (AstA). In the larval brain, both PTTHns and insulin-producing cells express the AstA receptor 1 (AstA-R1). The AstA-releasing neurons are presynaptic to the PTTHn and insulin-producing cells and increase their activity, thus increasing ecdysone production. The lack of AstA to PTTHn signaling delays the onset of pupariation (Deveci et al., 2019; Pan and O'Connor, 2019). Either silencing of the AstA neurons or knocking down the AstA-R1 in the PTTHn delays pupariation by impairing the PTTH signaling (Deveci et al., 2019).

The PG itself controls ecdysone production by autocrine signaling and indirectly affects PTTH. There are EcRs present in the PG and positively or negatively up- or downregulate the ecdysone production (Moeller et al., 2017). 20-E increases PTTH production and release from the PTTHn neurons near the time of pupariation (Christensen et al., 2020). Even though ecdysone injection is shown to postpone eclosion (McBrayer et al., 2007; Rewitz et al., 2009; Shimell et al., 2018), it does not affect the daily timing of eclosion and circadian gating. This suggests that the central clock is in charge of controlling the final stages of metamorphosis possibly by controlling the expression of the EcR in the pharates (Mark et al., 2021).

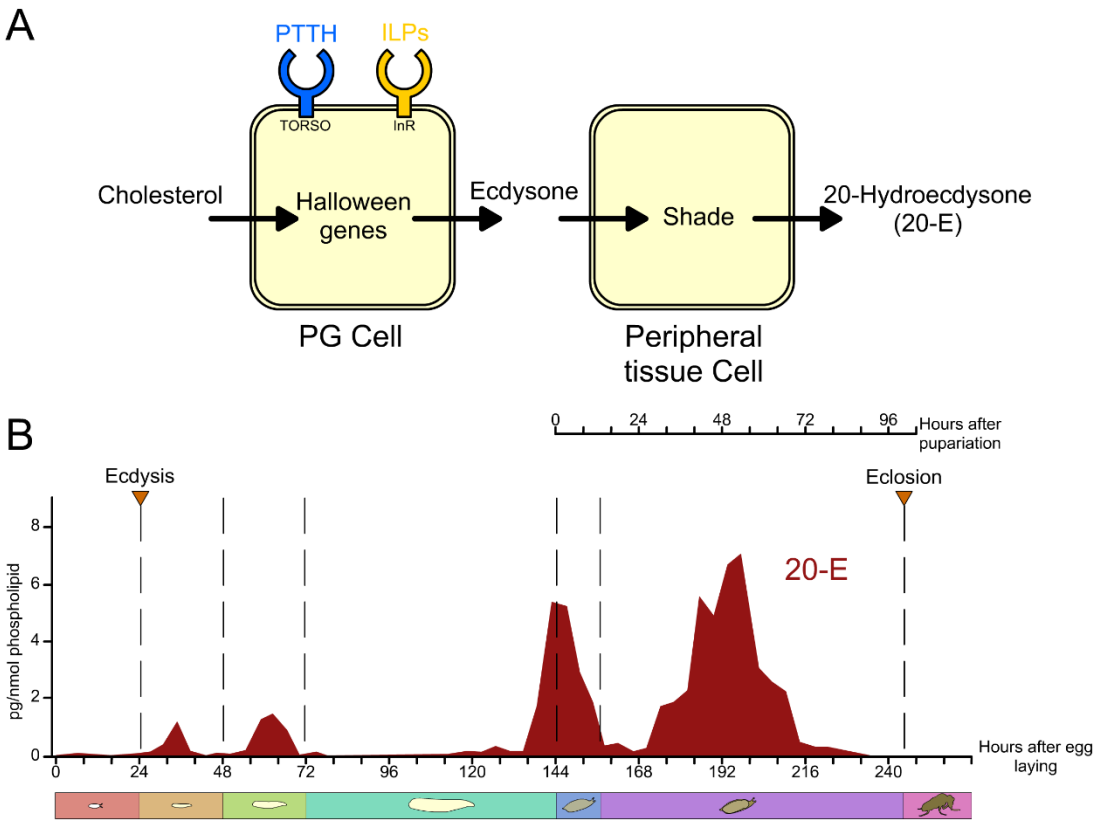

Figure 2. Molting and ecdysis depend on ecdysone titers. A Cholesterol taken up during feeding is used to produce ecdysteroids in PG cells. PG cells express TORSO receptor that binds to PTTH and InR that binds to insulin-like peptides (ILPs). These incoming signals induce ecdysteroid synthesis by Halloween genes. The most important ecdysteroid is ecdysone which is released into hemolymph. In the peripheral tissues, another enzyme called Shade turns ecdysone to its active form 20-hydroxyecdysone (20-E), which is then sensed by cells expressing EcR and initiates molting. **B** The development of *Drosophila melanogaster* heavily depends on 20-E. 20-E titers rise before and during molting and significantly drop before each ecdysis (dashed lines). Eclosion happens roughly 250 hours after egg laying and 100 hours after pupariation. 20-E titers reconstruction is based on Lavrynenko et al., 2015.

3.2. The circadian timing of eclosion

Any rhythmic circadian behavior has three distinctive characteristics: 1. It can be entrained by abiotic factors and runs with a period of 24 hours; 2. Without the presence of external cues such as light maintains its rhythmicity with a roughly 24-hour period; 3. It is temperature-compensated (Helfrich-Förster, 2005; Pittendrigh, 1954; Zimmerman et al., 1968).

Drosophila eclosion behavior when observed in the population over several days meets these clock characteristics. A functional molecular clock is necessary for eclosion rhythmicity and mutant flies with null mutations for clock genes (*e.g. period* and *timeless*; Konopka and Benzer, 1971; Sehgal et al., 1994) show arrhythmic eclosion without circadian gating (Qiu and Hardin, 1996). Secondly, eclosion can be entrained by Zeitgebers (light and temperature; Bunning, 1935; Kalmus, 1935; Pittendrigh, 1954; Wheeler et al., 1993; Zimmerman et al., 1968). Interestingly, eclosion rhythmicity can be entrained by transferring their populations from

constant light (LL) to constant darkness (DD). Light entrainment is even possible by shining a brief single light pulse under DD during early larval to late pupal stages (Brett, 1955; Bunning, 1935; Kalmus, 1935; Pittendrigh, 1954; Zimmerman, 1971). For temperature entrainment in *Drosophila*, a 2 °C change is enough to produce rhythmic eclosion (Dubowy and Sehgal, 2017; Wheeler et al., 1993; Zimmerman et al., 1968). Temperature entrainment is more important for insects that do not sense natural rhythmic photoperiod during their development. For example, for the underground pupariating onion fly (*Delia antiqua*), the Zeitgeber is the circadian temperature fluctuations in the soil instead of light (Tanaka and Watari, 2003). Lastly, eclosion is temperature compensated and does not change its period based on the environment temperature (Pittendrigh, 1954; Zimmerman et al., 1968).

To dive deeper into understanding how the circadian clock is involved in the timing of the eclosion behavior of *Drosophila*, it is important to first discuss the molecular and cellular architecture of its circadian clock.

a. The molecular clock

Circadian clocks are comprised of a series of autoregulatory expression transcription-translation feedback loops of clock genes and include consecutive phosphorylation and degradation steps with innate delays in between them that maintain a roughly 24-hour periodicity (Hardin et al., 1990; Patke et al., 2020; Takahashi, 2017). The molecular clock of *Drosophila* is very well described (reviewed in Helfrich-Förster, 2017; King and Sehgal, 2020; Patke et al., 2020). Importantly, the molecular architecture of insect clocks bears a high similarity to mammalian clocks (Helfrich-Förster, 2004; Panda et al., 2002).

The study of the molecular circadian clock was started when Konopka and Benzer found the first clock gene (*period*) after observing flies with arrhythmic eclosion patterns when screening chemically induced mutations (Konopka and Benzer, 1971). The eclosion rhythmicity of mutants was abolished in null mutants of $period^{0}$ (per^{0}), shortened to 19 hours in $period^{Short}$ (per^{S}), and lengthened to 28 hours in $period^{Long}$ (per^{L}) flies (Konopka and Benzer, 1971). Later it became clear that the three different observed phenotypes are because of these different *period* (*per*) alleles (Bargiello et al., 1984; Reddy et al., 1984; Zehring et al., 1984). After that other important clock genes such as *timeless* (*tim*; Sehgal et al., 1994), *clock* (*Clk*; Allada et al., 1998), and *cycle* (*cyc*; Rutila et al., 1998) were discovered and together produced a more complete molecular clock model of *Drosophila* (Figure 3).

The core feedback loop consists of the transcription factors CLOCK (CLK) and CYCLE (CYC) that form a heterodimer (Allada et al., 1998; Bae et al., 1998; Darlington et al., 1998; Rutila et al., 1998). This heterodimer binds to the regulatory regions of DNA known as E-boxes and drives the expression of the second heterodimerin partners, PERIOD (PER) and TIMELESS (TIM). In the middle of the day, CLK/CYC upregulates the *per* and *tim* genes (Hardin et al., 1990; Konopka and Benzer, 1971; Sehgal et al., 1994; Siwicki et al., 1988). PER and TIM also produce a heterodimer that gradually accumulates inside the cytoplasm until midnight when it shuttles into the nucleus. There, PER/TIM inhibits CLK/CYC which finally results in the downregulation of *per* and *tim* expression (Gekakis et al., 1995). Light is the most important Zeitgeber for entraining the biological clocks (Helfrich-Förster, 2020). The daily resetting of the clock requires light input and therefore needs a light-sensitive molecule that is expressed

by many clock neurons (Helfrich-Förster, 2020) and eye structures (reviewed in Senthilan et al., 2019). This blue light-sensitive (450 nm) molecule is CRYPTOCHROME (CRY; Berndt et al., 2007; Busza et al., 2004; Emery et al., 1998; Stanewsky et al., 1998). Light activates CRY which causes the degradation of TIM along with the auto-degradation of CRY (Sathyanarayanan et al., 2008). The degradation of PER requires the proteasomes that degenerate the phosphorylated molecule in the early morning. This PER and CRY degradation resets the clock daily (Lee et al., 1996; Myers et al., 1996). Clock also receives light input from rhodopsin-containing photoreceptive organs: compound eyes, ocelli, and Hofbauer-Buchner eyelets (Senthilan et al., 2019). However, since the cuticle is transparent enough for light penetration, even in the eyeless flies, light entrainment is possible directly through Hofbauer-Buchner eyelets and CRY (Rieger et al., 2003). Therefore, the only way to completely eradicate light entrainment is to remove both CRY and all eye structures (Helfrich-Förster et al., 2001).

A second transcription-translation feedback loop is also under the control of CLK/CYC. CLK indirectly affects its own transcription by transcriptionally activating the transcription activator PAR DOMAIN PROTEIN 1ε (PDP1ε) and the transcription repressor protein VRILLE (VRI; Blau and Young, 1999; Cyran et al., 2003). The competition between VRI and PDP1ε to attach to the promoter site of *Clk* (also known as VP-Box) controls the expression of *Clk*. Since PDP1ε accumulation is delayed compared to VRI, this causes rhythmic *Clk* expression.

A third feedback loop is under the control of another repressor called CLOCKWORK ORANGE (CWO; Kadener et al., 2007; Matsumoto et al., 2007; Richier et al., 2008). CWO binds to the E-box regions of *per*, *tim*, *vri*, *Pdp1ε,* and *cwo* itself and prevents their transcription.

To guarantee the 24-hour rhythmicity of the clock, the transcription-translation feedback loops must be regulated with innate delays. These regulatory delays happen at transcriptional and post-translational levels. The repression of *per* and *tim* transcription is the main regulation that happens on the transcriptional level. Other regulations include a delay between *per* and *tim* transcription and translation and a delay in PER/TIM degradation (Top and Young, 2018). For example, it has been shown that overexpressing CLK/CYC or PER shortens the period (Kadener et al., 2008; Zhao et al., 2003). On the other hand, CWO disruption and lowering *per* expression lengthen the period (Kadener et al., 2007; Lim et al., 2007; Richier et al., 2008).

The post-translational modifications (such as phosphorylation, dephosphorylation, and ubiquitination to affect clock protein synthesis, accumulation, and stability) also control the pace of the molecular clock (Top and Young, 2018). microRNAs limit TIM, CLK, and CWO production (Chen et al., 2014; Chen and Rosbash, 2016). A kinase named DOUBLETIME (DBT) phosphorylates PER (Kloss et al., 1998; Price et al., 1998) and CLK (Menet et al., 2010; Yu et al., 2009) which consequently leads to their degradation (Grima et al., 2002; Ko et al., 2002). Mutations in the *doubletime* (*dbt*) gene change the kinase activity of DBT and lead to short-period (*doubletime*^{Short} or *dbt*^{S}), long-period (*doubletime*^{Long} or *dbt*^{L}; Kloss et al., 1998) or completely arrhythmic (*doubletime*^{Arrhythmic}) phenotypes (Rothenfluh et al., 2000).

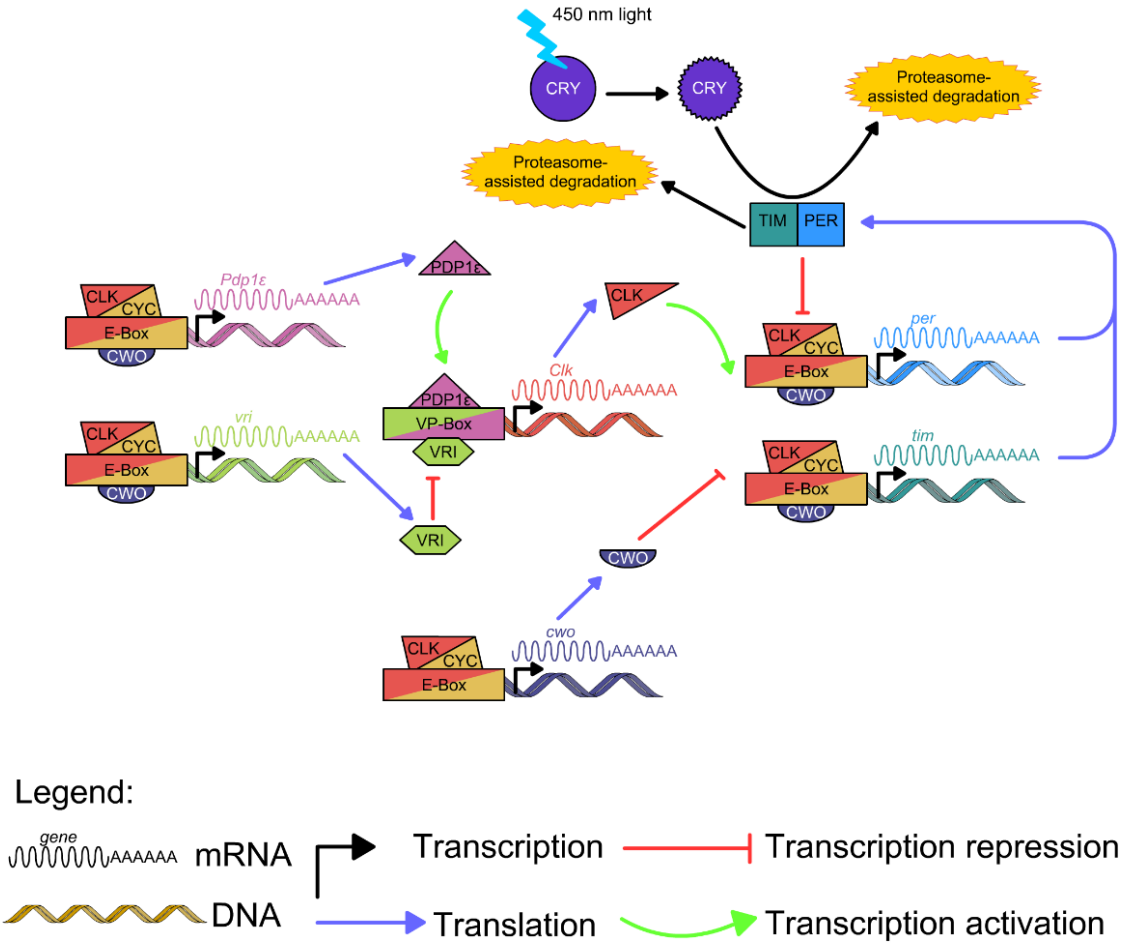

Figure 3. Combinations of transcription-translation feedback loops create a functioning molecular clock. The first loop consists of two transcription repressors, PERIOD (PER) and TIMELESS (TIM), which form a heterodimer and inhibit two transcription activators, CLOCK (CLK) and CYCLE (CYC). After degradation of PER/TIM, the loop continues, when CLK/CYC heterodimer activates *per* and *tim* mRNA transcription by binding to their E-box region in DNA. The mRNAs then translocate to the cytoplasm for translation. PER and TIM accumulate in the cytoplasm, then shuttle back to the nucleus to inhibit CLK/CYC. However, their degradation inside the nucleus is mediated by proteasome-assisted enzymatic reactions. Light restarts this cycle daily. 450 nm blue light activates CRYPTOCHROME (CRY) which starts TIM degradation in the cytoplasm and nucleus. This finally leads to PER degradation as well. The second feedback loop comprises transcription factor PAR DOMAIN PROTEIN 1ε (PDP1ε) and transcription repressor VRILLE (VRI), which control *Clk* mRNA levels by binding to VP-box. CLK/CYC controls the expression of PDP1ε and VRI. The third feedback loop requires the transcription repressor CLOCKWORK ORANGE (CWO) that binds to E-boxes and inhibits transcription of *per, tim, Pdp1ε,* and *vri* mRNAs. CWO production is also under the control of CLK/CYC heterodimer. In the schematic diagram above all transcription activators are shown binding to the top and repressors on the bottom of E-box and VP-box.

b. The neuronal arrangement of the central brain clock

The neuronal circuits of the central clock of *Drosophila* and how they drive rhythmic behaviors are well described (reviewed by Helfrich-Förster, 2017; Reinhard et al., 2022b; Top and Young, 2018).

Approximately 75 neurons in each hemisphere of the *D. melanogaster* brain form the central clock network (Figure 4 A; Ahmad et al., 2021; Beckwith and Ceriani, 2015; Helfrich-Förster, 2017; Helfrich-Förster et al., 2007; Hermann-Luibl and Helfrich-Förster, 2015; King and Sehgal, 2020; Nitabach and Taghert, 2008; Schlichting et al., 2016; Top and Young, 2018). These neurons are characterized by the expression of complete sets of clock genes including *per*, *tim*, *vri*, and *pdp1ε* (Ahmad et al., 2021; Beckwith and Ceriani, 2015; Blau and Young, 1999; Helfrich-Förster, 2017; Helfrich-Förster et al., 2007; Hermann-Luibl and Helfrich-Förster, 2015; Kaneko et al., 1997; Kaneko and Hall, 2000; King and Sehgal, 2020; Nitabach and Taghert, 2008; Rutila et al., 1998; Schlichting et al., 2016; Top and Young, 2018). Based on their location, these clock neurons can be sorted into lateral neurons (LN), dorsal neurons (DN), and lateral posterior neurons (LPN; Helfrich-Förster, 2003). These neurons are further classified into nine different clusters based on their anatomy and neurochemistry. The LNs are further categorized into four small- (sLN_vs) and four large (lLN_vs) ventrolateral neurons (Figure 4 B), six dorsolateral neurons (LN_ds), and one peculiar sLN_v known as the 5^{th} sLN_v (Figure 4 C). The sLN_vs and lLN_vs are two subsets of pigment dispersing factor expressing (PDF) neurons in each hemisphere. The four sLN_vs originate from the accessory medulla and project through the posterior lateral fascicle to the superior brain and mostly superior lateral protocerebrum (reviewed by Helfrich-Förster, 2017; Reinhard et al., 2022b; Top and Young, 2018). The lLN_vs have dendrites in the ipsilateral accessory medulla and extensively arborize in the ipsilateral medulla and project to the contralateral medulla through the posterior optic commissure (Helfrich-Förster, 2017; Reinhard et al., 2022b; Schubert et al., 2018; Top and Young, 2018). The cell bodies of the LN_ds are more dorsally located compared to the LN_vs and they project to the dorsal protocerebrum as well. Finally, the single 5^{th} sLN_v formerly due to its location was categorized with the sLN_vs is recently grouped with LN_ds based on their neurochemical similarities (Helfrich-Förster, 1997; Helfrich-Förster et al., 2007; Hermann-Luibl and Helfrich-Förster, 2015; Kaneko et al., 1997; Kaneko and Hall, 2000; Klarsfeld et al., 2004; Reinhard et al., 2023; Shafer et al., 2006).

DNs are the second major group of clock neurons (Figure 4 D). They innervate the superior protocerebrum in the dorsal brain. DNs form four different clusters, namely two anterior dorsal neurons 1 ($DN1_as$) and around 15 posterior dorsal neurons 1 ($DN1_ps$), two dorsal neurons 2 (DN2s) and roughly 40 dorsal neurons 3 (DN3s). The $DN1_a$ cell bodies are in the anterior superior cell body rind (Reinhard et al., 2022b; Shafer et al., 2006). Compared to other DNs, the morphology and neuronal projections of the $DN1_as$ are slightly different because their projections are not limited to the superior protocerebrum. They branch out in the lateral horn and superior lateral protocerebrum neuropils and protrude ventrally to the accessory medulla (Reinhard et al., 2022b). Most $DN1_ps$ (six to nine neurons) arborize in the superior protocerebrum and PI while the rest project around the lateral horn in a loop-like manner and project near the anterior optic tubercle (Lamaze et al., 2018). The cell bodies of DN2s are located near the sLN_v axonal terminals (Reinhard et al., 2022b). The projections of both DN2 neurons remain in the dorsal protocerebrum, pass to the contralateral hemisphere, and end near the cell bodies of the other DN2s (Helfrich-Förster, 2005; Reinhard et al., 2022b). DN3s are the most understudied clock cluster that comprises roughly 80 neurons (Sun et al., 2022). Perhaps one of the reasons that they were neglected for a long time is that they are considered to be less important in maintaining rhythmicity compared to the central pacemaker neurons (Rieger et al., 2006). Recently, based on their anatomy and projection they are categorized into three groups: most cells are small and project to the central brain, one pair with a large cell

body that projects to the central brain, and six neurons in each hemisphere that project to the anterior brain. Most of the cell bodies of DN3 are located in the lateral and dorsal lateral horn cell body rinds. (Sun et al., 2022).

The third major group, LPN, contains three neurons per hemisphere (Figure 4 C). Their cell bodies are located in the posterior lateral protocerebrum cell body rind and send projections dorsally to the superior protocerebrum, lateral horn, and superior clamp area (Reinhard et al., 2022a).

All clock neurons interact and form a synchronized network for timekeeping. Studying *Drosophila* circadian clock is mainly done by tracking locomotor behavior that shows two peaks at dawn and dusk with midday siesta and sleep phase during the night (characterized by low activity in between the peaks). This bimodal activity pattern helped not only to identify the gene networks behind the clock but also the function of each neuronal clock cluster involved in generating rhythmic locomotion (Axelrod et al., 2015; King and Sehgal, 2020; Patke et al., 2020). Different clock neurons are important in forming this bimodal activity pattern. One of the pioneering models to explain this behavior is the dual-oscillator model (Pittendrigh and Daan, 1976) suggesting that two different sets of oscillators cooperate to maintain the evening and morning activity. The current model includes two types of clock neurons regarded as morning and evening cells. The morning cells are comprised of sLN_vs and the CRY^+ $DN1_ps$, while the 5^{th} sLN_v, the LN_ds, and 6-8 CRY^- $DN1_ps$ form the evening cells (Emery et al., 2000; Grima et al., 2004; Murad et al., 2007; Stoleru et al., 2004; Y. Zhang et al., 2010). The activity of the sLN_vs influences the evening neurons. These two phasic feedbacks are generated by the neuropeptide PDF (Liang et al., 2017; Taghert and Nitabach, 2012). Nevertheless, newer studies consider more oscillators in play and more sophisticated models for clock neuron interactions (Jaumouillé et al., 2021; Yao and Shafer, 2014).

The clock is entrained by Zeitgebers through the LN_vs. The lLN_vs receive light and temperature input and influence the activity of sLN_vs (Dubowy and Sehgal, 2017; Schlichting et al., 2016). The temperature information perceived by the chordotonal organ is relayed to lLN_vs and entrains the clock (Chen et al., 2015). sLN_vs, lLN_vs, some LN_ds, the 5^{th} sLN_v, $DN1_as$, and DN2s project their dendrites to the accessory medulla and receive light input directly from Hofbauer-Buchner eyelets and indirectly from the compound eyes (Li et al., 2018; Schlichting et al., 2016).

The dorsal clock neurons seem to be less important for maintaining the rhythmic behaviors under constant conditions, yet important for adjusting these behaviors in the presence of Zeitgebers (Reinhard et al., 2022b). The DN1 neurons are important temperature-perceiving clock neurons and their intracellular calcium (Ca^{2+}) levels are temperature-sensitive (Guo et al., 2016). $DN1_ps$ are necessary for incorporating light and temperature in different rhythmic behaviors such as strong daily activity rhythms (L. Zhang et al., 2010; Y. Zhang et al., 2010) and sleep/waking cycles (Guo et al., 2016; Kunst et al., 2014; Lamaze et al., 2018). At lower temperatures, they promote sleep (Alpert et al., 2020; Guo et al., 2018; Reinhard et al., 2022b). It has been shown that the $DN1_ps$ projecting to the superior protocerebrum and PI are important for sleep promotion while the others promote waking (Lamaze et al., 2018). The $DN1_as$ and some DN3 receive and process light information (de Azevedo et al., 2020; Reinhard et al., 2022b; Song et al., 2021). DN2s are also entrained by temperature and are important for

temperature preference rhythms (Kaneko et al., 2012). The DNs (except for DN2) also receive and process thermal information and along with the LPNs are important temperature output neurons (Harper et al., 2016; Kaneko et al., 2012; Picot et al., 2009). The LPNs regulate sleep and metabolism. They also receive thermosensory inputs (Barber et al., 2016; Ni et al., 2019; Reinhard et al., 2022a).

Finally, it is worth mentioning that another group of neurons emerges in mid-metamorphosis and dies shortly after eclosion. These neurons are not clock neurons but produce PDF. Because of their position in the tritocerebrum and PDF expressing, they are called PDF-tri neurons. PDF-tri consists of one to two pairs of neurons sitting at the suboesophageal zone, projecting into the PI and passing around the esophagus foramen (Figure 4 B; Helfrich-Förster, 1997; Selcho et al., 2018).

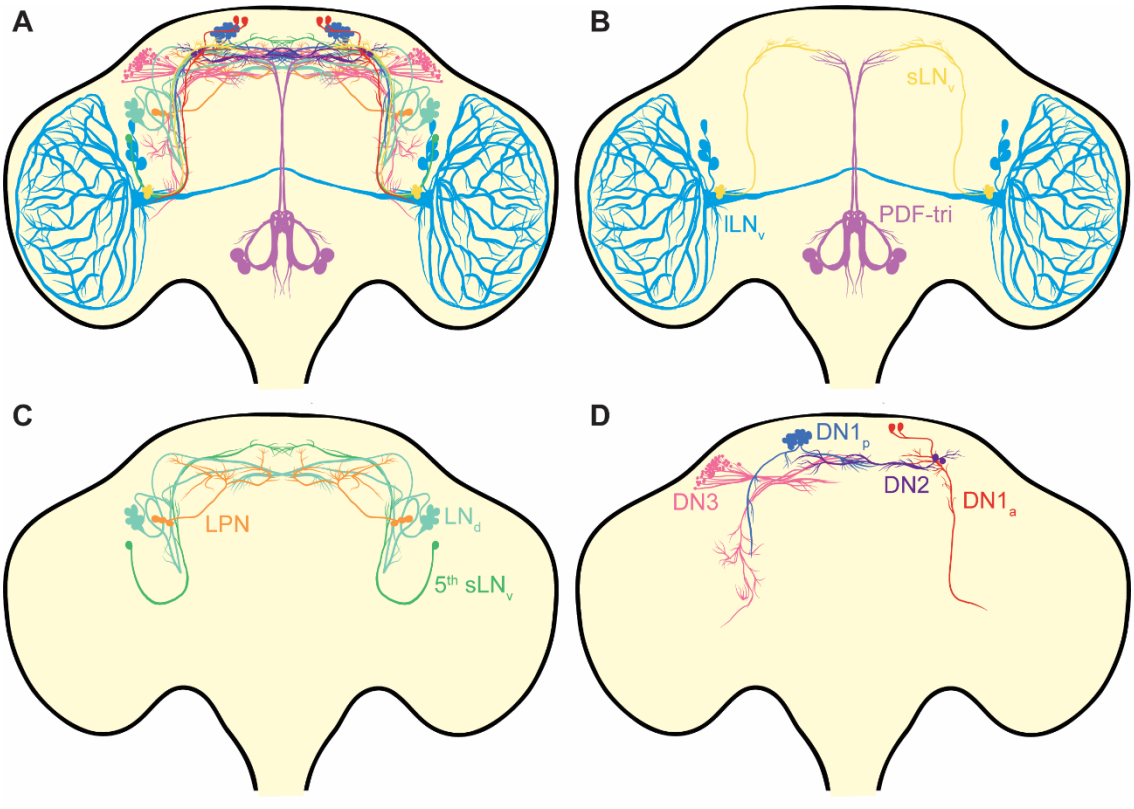

Figure 4. *Drosophila melanogaster* circadian clock consists of around 150 neurons. A All clock neurons plus non-clock tritocerebrum PDF (PDF-tri) neurons are shown together in P14 pharate brains. The processes of clock neurons heavily overlap in the superior protocerebrum. **B** The PDF^+ clock neurons are ventrolateral neurons comprised of four small- (sLN_vs) and four large ventrolateral (lLN_vs). One to two pairs of PDF-tri neurons that transiently appear in mid-metamorphosis and die shortly after eclosion are not clock neurons but are PDF^+. **C** The morphology of six dorsolateral neurons (LN_ds), one peculiar small ventrolateral neuron called 5^{th} sLN_v, and three lateral posterior neurons (LPN) are shown. **D** The dorsal clock neurons (DN) are comprised of three major groups shown by numbers DN1, DN2, and DN3. DN1 is made from two anterior ($DN1_a$) and 15 posterior ($DN1_p$) neurons. DN2s are only two neurons while DN3 are about 40 neurons. Except for PDF-tri, the morphology of other neurons is recreated after Reinhard et al., 2022a.

c. The central clock in the brain and the peripheral PG clock control eclosion rhythmicity in *Drosophila*

The idea of the involvement of two connected clocks that maintain the eclosion rhythmicity dates to more than 60 years ago. Pittendrigh believed that a "master clock" receives the environmental input and synchronizes the phase of a "slave clock" that is in charge of producing eclosion rhythmicity (Pittendrigh, 1959, 1958, 1957).

Several studies have shown the role of the central clock in maintaining eclosion rhythmicity (Blanchardon et al., 2001; Helfrich-Förster, 1998; Myers et al., 2003; Qiu and Hardin, 1996; Weiss et al., 2014). Eclosion gating is absent in flies with impaired molecular clock (Qiu and Hardin, 1996), including per^0 (Konopka and Benzer, 1971), tim^0 (Sehgal et al., 1994), and cry^b mutants (Myers et al., 2003). Expressing different alleles of *dbt* called short-period *dbt* (dbt^S) and long-period *dbt* (dbt^L) in the central clock changes the period of the clock, respectively to shorter or longer than 24 hours. Expression of these alleles also changes (shorten or lengthen) the period of eclosion rhythmicity according to the expressed allele (Price et al., 1998). Interrupting the molecular clock in the central PDF^+ clock neurons, or all tissues by overexpression of the dominant-negative form of *cyc* renders eclosion arrhythmic (Tanoue et al., 2004). Overexpression of *tim* in all clock tissues except PG or PG alone also causes arrhythmicity of eclosion (Selcho et al., 2017).

The PG expresses both TIM and PER and contains a peripheral clock necessary for proper eclosion timing (Emery et al., 1997; Myers et al., 2003; Selcho et al., 2017). Overexpression of *tim* in *Drosophila* PG stops the circadian gating and rhythmic eclosion patterns (Myers et al., 2003). Manipulations of the molecular clock solely in PG or in the entire body affect the development and timing of eclosion differently (Myers et al., 2003). Overexpression of the dominant negative allele of *cyc* in the central clock or PG showed that both clocks are required for rhythmic eclosion (Selcho et al., 2017). The oscillations of *tim* and *per* mRNA in the PG are self-sustained but can be synchronized by the central clock (Morioka et al., 2012). Studies in *Drosophila* PG (Emery et al., 1997; Morioka et al., 2012) and the bug *Rhodnius* (Saunders, 2002; Vafopoulou and Steel, 1996) suggest that the activity of the PG is dependent on the activity of the central clock. This hierarchy was first investigated using the expression of short- and long-period alleles of *dbt* in the central clock and PG. Shortening or lengthening the periodicity of eclosion is evident when both clocks or only the central clock were affected by expressing dbt^S and dbt^L alleles respectively. In contrast, a nearly normal period length was found when dbt^S and dbt^L were solely expressed in PG (Selcho et al., 2017). Collectively, these results show that both the central clock and PG are required to circadianly gate the eclosion behavior.

The central clock and PG are connected at the cellular level. Ablation of the PDF^+ LNs renders both eclosion and locomotor activity arrhythmic (Blanchardon et al., 2001; Helfrich-Förster, 1998) because PDF is necessary for maintaining the rhythmicity of eclosion (Myers et al., 2003; Renn et al., 1999). Despite the initial assumptions PTTH is the mediator of clock and PG connection (Selcho et al., 2017), not PDF. PDF is only important for intrinsic clock signaling (Yao and Shafer, 2014) since knock-down of PDF receptor in PTTH neurons does not cause arrhythmicity of eclosion (Selcho et al., 2017). In *Drosophila* pharate adults, sLN_vs are presynaptic to PTTHn and indirectly connect the central brain clock to PG (Selcho et al., 2017).

The sLN_vs-PTTH-PG connections are formed from larval stages (McBrayer et al., 2007; Siegmund and Korge, 2001) and persist through pupal development (Selcho et al., 2017). Optogenetically activated sLN_vs inhibit the PTTHn (Selcho et al., 2017). The sLN_vs express shorth neuropeptide F (sNPF; Johard et al., 2009) and sNPF is suggested to inhibit PTTHn (Figure 5; Selcho et al., 2017). Because applying sNPF on brain cultures shows rapid inhibition of PTTHn, and knock-down of sNPF receptor (sNPF-R) in the PTTHn causes arrhythmic eclosion (Selcho et al., 2017). Removing PTTH signaling by ablating or electrically silencing PTTHn or knock-down of *Ptth* in these neurons results in arrhythmic eclosion (Selcho et al., 2017). Therefore, PTTH signaling is required to synchronize the activity of both clocks. Downregulation of *torso* in both clocks, or PG alone causes arrhythmic eclosion but not when it is only knocked-down in the central clock. *torso* knock-down in PG stops the circadian oscillations of PER and impairs the molecular clock in PG. Therefore, PTTH signaling is required to keep the PG clock running (Selcho et al., 2017).

The *Drosophila* clock is one of the best-studied neuronal systems in terms of peptidergic connections (*e.g.*, Abruzzi et al., 2017; Cavanaugh et al., 2014; Liang et al., 2017; Ma et al., 2021; Nitabach and Taghert, 2008). Most of the 150 clock neurons produce and release one or several neuropeptides. A recent study using the single-cell transcriptomics of the *Drosophila* clock neurons database (Ma et al., 2021) and using in-silico, immunostaining, and trans-synaptic tracing tools reviewed the peptidergic profile of the clock neurons in detail (Reinhard et al., 2023). AstA is expressed by three of the $DN1_ps$ and all LPN neurons (Reinhard et al., 2023, 2022a). Allatostatin C (AstC) is produced by all three LPNs, both DN2s, about eight of the $DN1_ps$, and 20 of the DN3 neurons (Abruzzi et al., 2017; Reinhard et al., 2023). Studies have shown that sNPF is produced by sLN_vs, two of the LN_ds, and many $DN1_ps$ neurons (Abruzzi et al., 2017; Liang et al., 2017; Reinhard et al., 2023). Diuretic hormone 31 (Dh31) is expressed by roughly six of the $DN1_ps$ (Kunst et al., 2014; Reinhard et al., 2023). Ion transport peptide is secreted from the 5^{th} sLN_v and one LN_d (Dircksen et al., 2008; Hermann-Luibl et al., 2014; Kahsai et al., 2010; Reinhard et al., 2023). Based on the single-cell transcriptomics data, myosuppressin (Ms) is produced by some LN_ds (Abruzzi et al., 2017). However, the presence of Ms in LN_ds is not shown using immunoassays or other techniques and there is no strong evidence favoring its expression by clock neurons.

Unfortunately, not many studies have investigated the role of peptides in modulating eclosion circuits or their influence on eclosion behavior. One outstanding study looked at the effects of various peptides in eclosion through both gain- and loss-of-function experiments and showed that optogenetically activating Ms neurons promotes light-induced eclosion (Ruf et al., 2017).

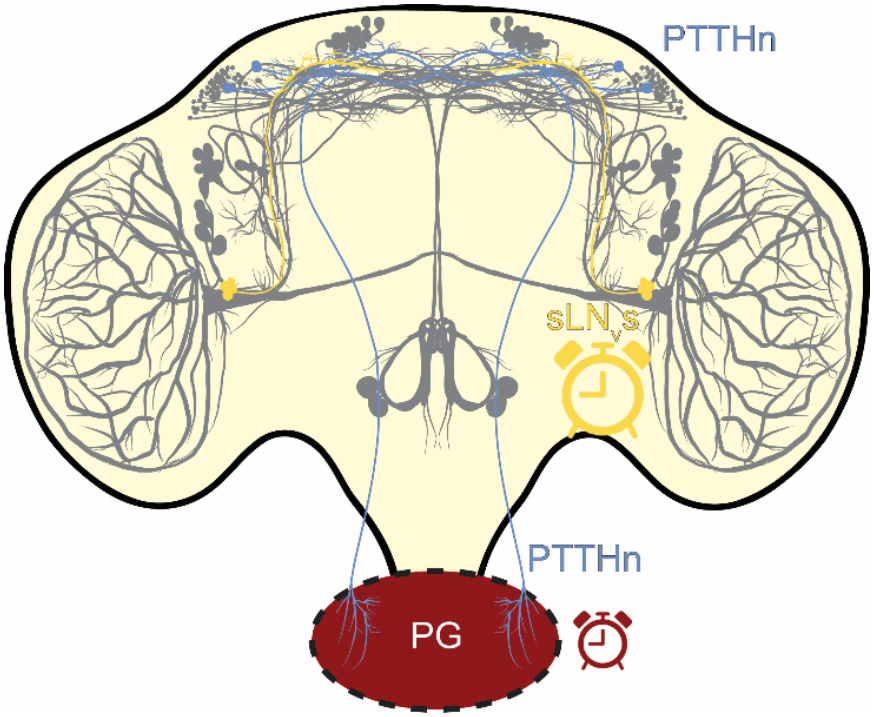

Figure 5. The current working hypothesis of how two clocks interact to gate the eclosion behavior in *Drosophila melanogaster*. The central circadian clock in the brain and prothoracic gland (PG; peripheral clock) are required for eclosion timing. These two clocks are connected by prothoracicotropic hormone neurons (PTTHn). PTTH release in PG controls ecdysteroid production. Before eclosion, the ecdysteroid levels significantly drop. The release of short neuropeptide F (sNPF) from sLN_vs inhibits PTTHn, therefore PTTH signaling to PG is over and ecdysteroids titers are lowered. Created after the model proposed by Selcho et al., 2017.

4. The Truman model of eclosion gating

A considerable amount of our knowledge of the neuroendocrine pathways that control ecdysis comes from three moth species, *Hyalophora cecropia, Manduca sexta,* and *Antheraea polyphemus*. These large insects allowed classic brain excision, transplantation, electrophysiological approach, and hemolymph extraction before genetic tools became available (Copenhaver and Truman, 1986a, 1986b; Davis et al., 2003; Gammie and Truman, 1999, 1997; Hewes and Truman, 1994; Kopec, 1917; Kopeć, 1922; Truman, 1992; Truman et al., 1983; Truman and Riddiford, 1970; Zitnan et al., 1996). The first explanation of the effects of photoperiod on the eclosion of *Manduca sexta* was presented by Jim Truman and Lynn Riddiford (Truman and Riddiford, 1974). Since eclosion in moths is confined to an eight-hour window (gate) per day, they used the term gating. PTTH release only happens within this gate, therefore ecdysis is only allowed during that daily time window and forbidden at other times, hence gated (Truman, 1972; Truman and Riddiford, 1974). The gating effect was lost when the brain was surgically excised. Surgically reimplantation of a brain (even loosely in the abdomen) would rescue the gating. Even changing the brains between the species would restore the gating based on the explanted brain gating schedule (Truman and Riddiford, 1970). These findings not only showed that a time-keeping mechanism must reside in the brain but also demonstrated that neuroendocrine mechanisms play an important role in eclosion gating.

Truman suggested the first model to explain the circadian and development-gated nature of eclosion in moths (Truman, 1984). In his model, he suggested that two mechanisms control the

activity of the V_m neurons. The first mechanism is a brain-derived gating system (G system) under the control of the circadian clock. The other mechanism is the ecdysone-controlled developmental E system. The G system excites the V_m neurons when the gate is open and when closed inhibits them. The E system does not allow V_m neurons activity until the 20-E levels drop below the threshold (Truman, 1984). The falling 20-E level forces the V_m neurons to release their EH content and commits the animal to ecdysis (Morton and Truman, 1988; Truman, 1981; Truman et al., 1983).

However, Truman model is difficult to apply to *Drosophila* eclosion gating due to two main reasons. Firstly, in *Drosophila* the timing of PTTHn activity and PTTH signaling is unknown. Secondly, how the G system excites the V_m neurons is not shown yet. A few studies have investigated the connection of clock neurons and eclosion-related neurons other than the PTTHn. Blanchardon et al. (2001) mentioned the proximity of the V_m neurons to the PDF^+ sLN_vs (Blanchardon et al., 2001). Since PDF-tri neurons are formed during metamorphosis and make synaptic contact with the V_m and crustacean cardioactive peptide neurons (Helfrich-Förster, 1997; Selcho et al., 2018), they might be involved in generating eclosion rhythmicity. However, until now no study has comprehensively investigated these connections and how they might influence the eclosion behavior and eclosion timing. Whether the newly discovered non-canonical EH^+ neurons play a role in the circadian gating of eclosion and whether any of the EH^+ neurons receive input from the clock to maintain eclosion rhythmicity is unknown. The role of the clock in starting the eclosion behavior by directly signaling to the EH^+ neurons or indirectly to Inka cells to start the EH/ETH positive feedback loop is another open question.

5. Aims of this thesis

Chapter I: PTTH signaling is important for eclosion timing during the final pupal stages

In this chapter, the important goal was to identify the temporal course of PTTHn activity. In other words, when during pupal development is PTTH signaling active and required to maintain a rhythmic eclosion pattern? Conditional silencing of the PTTHn during different developmental stages roughly marked the onset of the PTTHn activity necessary for rhythmicity. The time point of PTTHn neuronal activity was measured using the genetic Ca^{2+} sensor CaLexA (Masuyama et al., 2012) and the activity-related gene luciferase (ARG-Luc) technique (X. Chen et al., 2016). Another important question was whether other clock neurons besides the sLN_vs, provide direct input to the PTTHn. This question was addressed using immunostaining-based techniques for synaptic connection tracing. Whether PTTHn can signal via classic neurotransmitters was a further question. This question was at hand because most peptides are co-expressed and released with classic neurotransmitters (Hökfelt et al., 1987; Kim et al., 2017; Nässel, 2018). Lastly, the putative roles of *Drosophila* ILP7 and ILP8 as developmental regulators in maintaining eclosion rhythmicity have never been investigated. Therefore, the eclosion rhythmicity of null mutants of *Ilp7*, *Ilp8,* and *Lgr3* (receptor of ILP8) was measured as well.

Chapter II: The ventromedial (V_m) Eclosion hormone neurons are downstream of circadian clock neurons

The morphology of the EH neurons and their closeness to clock neuron arborization suggested a possible synaptic connection. So far, however, a comprehensive characterization of the synaptic and peptidergic connections from clock to EH neurons is missing. Thus, the overall aim of this chapter was to anatomically describe the connections of the clock to the EH neurons to identify the neuronal substrates that potentially could provide time input to the V_m neurons. For that, trans-synaptic and chemoconnectomic tracing was employed. In addition, ARG-Luc in the intact pupa was used to identify the temporal pattern of activity of the V_m neurons and Inka cells to provide deeper insight into EH/ETH feedback timing. Also, since non-canonical EH neurons were recently discovered, parts of this chapter focused on their properties such as clock connections and their lifespan in adult flies. It was shown before by electron microscopy that the EH neurons only contain dense core vesicles that carry neuropeptides but not synaptic vesicles (Selcho et al., 2018). Therefore, the presence of classic neurotransmitters in EH neurons (V_ms and D_ls) was additionally investigated.

Chapter III: Neuropeptides that localize also to clock neurons influence premature eclosion but not eclosion rhythmicity

In this chapter, chemoconnectomics was employed to identify the possibility of the peptidergic connections from the clock to PTTHn and V_m neurons. Specifically, the presence of the GPCRs corresponding to neuropeptides expressed by clock neurons (PDF, sNPF, AstA, AstC, Dh31, and Ms) in PTTHn and V_ms was tested. After the identification of these receptors on both PTTHn and V_m neurons, these peptide signaling pathways were tested for potential functions in maintaining eclosion rhythmicity or affecting premature eclosion. To do so, the rhythmicity in flies that either lack these signaling pathways (loss-of-function) or in which these peptide signaling pathways were optogenetically activated during light-induced premature eclosion (gain-of-function) was evaluated. For the promising candidates that boosted or prevented eclosion behavior, immunostaining-based synaptic tracing identified which peptidergic neurons (including clock neurons) were upstream of the PTTHn or V_m neurons. Unfortunately, the role of the investigated peptides in modulating the PTTHn and V_m activity could not be further characterized. Therefore, only predictions of their GPCRs activity were made.

Chapter IV: C4da neurons are presynaptic to V_m neurons and may be required for eclosion gating

Chapter IV focused on two types of peripheral sensory neurons. The first part investigated the potential role of O_2 and CO_2 sensing v'Td neurons in eclosion rhythmicity or the initiation of eclosion. These neurons provide input to the V_m neurons in larvae (Hückesfeld et al., 2021), but the situation in pharate adults was unknown. Therefore, the synaptic connections between v'Tds and V_ms were investigated by trans-synaptic tracing techniques. The function role of these connections in eclosion rhythmicity was investigated by time-restricted ablation and electrically silencing of v'Td neurons (loss-of-function eclosion assays). To test whether their activity can alter premature eclosion, v'Td neurons during light-induced premature eclosion were optogenetically activated (gain-of-function eclosion assays). Finally, the functionality of

v'Td-V_m connections was tested using a combination of optogenetics and functional Ca^{2+} imaging.

The second part of this chapter sought to test whether the potential peripheral targets of PTTH signaling (other than PG) were involved in eclosion timing. Since the Class IV dendritic arborization (C4da) neurons (Yamanaka et al., 2013) and fat body (based on FlyAtlas 2; Leader et al., 2018) are known to express *torso* they were chosen as the main downstream candidates for PTTH signaling.

To assess the possible role of C4da neurons in eclosion rhythmicity, they were genetically silenced, ablated, or optogenetically stimulated during light-inducing premature eclosion assays. Since these neurons pass through the midline of the VNC, it is possible that they make synaptic contact with V_m neurons. Such a connection may indirectly link the PTTHn to V_m and could act as an additional pathway that interconnects eclosion timing to initiation of eclosion. Therefore, the possibility of synaptic connections between C4da and V_m neurons was studied. Finally, using ARG-Luc it was checked whether the activity of C4da neurons correlated with the activity of PTTHn and V_m.

The FlyAtlas 2 database shows that in adult flies, the fat body shows a high expression of *torso* (Leader et al., 2018). However, the role of the fat body in the circadian or developmental timing of eclosion has not yet been investigated. Therefore, one of the aims of this chapter was to find out whether *torso* expressed by the fat body is involved in regulating eclosion timing. For that, RNA interference (RNAi) and eclosion assays were combined.

Materials and methods

1. Fly strains and rearing

Flies were kept and raised on standard cornmeal and yeast food at 25 °C, 65% humidity, and 12:12 LD cycles. A list of the fly lines that were used is collected in Table 1. The fly stock center codes are given as BL# for Bloomington *Drosophila* Stock Center (BDSC; Bloomington, IN, USA), VDRC# for Vienna *Drosophila* Resource Center (VDRC; Vienna, Austria), and Kyoto# for Kyoto *Drosophila* Stock Center (Kyoto DGGR; Kyoto, Japan). The gene nomenclature is adopted from FlyBase.

Table 1. Fly strains used in this thesis.

Full genotype	Short genotype	Source	Reference
w^{1118}	w^{1118}	BL#3605	(Hazelrigg et al., 1984)
Canton-S	*Canton S.*	BL#64349	(Lindsley, 1968)
TI{2A-GAL4}AstA$^{2A\text{-}GAL4}$	*AstA::2A-Gal4*	BL#84593	(Deng et al., 2019)
w* TI{2A-GAL4}AstA-R1$^{2A\text{-}GAL4.R}$	*AstA-R1-Gal4*	BL#84709	(Deng et al., 2019)
w*; TI{2A-GAL4}AstA-R2$^{2A\text{-}AC.GAL4}$/TM3, Sb^{1}	*AstA-R2^{AC}-Gal4*	BL#84594	(Deng et al., 2019)
TI{2A-GAL4}ChAT$^{2A\text{-}GAL4}$/TM3, Sb^{1}	*ChAT-Gal4*	BL#84618	(Deng et al., 2019)
TI{2A-GAL4}Dh31-R$^{2A\text{-}ABC.GAL4}$	*Dh31-R^{ABC}-Gal4*	BL#84625	(Deng et al., 2019)
TI{2A-lexA::GAD}Dh31-R$^{2A\text{-}C.lexA}$/CyO	*Dh31-R^{C}-Gal4*	BL#84382	(Deng et al., 2019)
w*; TI{2A-GAL4}ETH$^{2A\text{-}GAL4}$/CyO	*ETH::2A-Gal4*	BL#84631	(Deng et al., 2019)
w*; TI{2A-GAL4}Ms$^{2A\text{-}GAL4}$	*Ms::2A-Gal4*	BL#84652	(Deng et al., 2019)
w*; TI{2A-GAL4}MsR1$^{2A\text{-}B.GAL4}$/TM3, Sb^{1}	*MsR1^{B}-Gal4*	BL#84653	(Deng et al., 2019)
w*; TI{2A-GAL4}MsR2$^{2A\text{-}C.GAL4}$/TM3, Sb^{1}	*MsR2^{C}-Gal4*	Bowen Deng	(Deng et al., 2019)
TI{2A-GAL4}Pdfr$^{2A\text{-}GAL4}$ w*/FM7a	*Pdfr-Gal4*	BL#84684	(Deng et al., 2019)
w*; TI{2A-GAL4}Ptth$^{2A\text{-}GAL4}$	*Ptth::2A-Gal4*	Francisco A Martin	(Deng et al., 2019)
w*; TI{2A-GAL4}sNPF-R$^{2A\text{-}GAL4}$/TM6B, Tb^{1}	*sNPFR-Gal4*	BL#84691	(Deng et al., 2019)
TI{2A-GAL4}VGAT$^{2A\text{-}GAL4}$/CyO	*VGAT-Gal4*	BL#84696	(Deng et al., 2019)
TI{2A-GAL4}VGlut$^{2A\text{-}GAL4}$/CyO	*VGlut-Gal4*	BL#84697	(Deng et al., 2019)

Full genotype	Short genotype	Source	Reference
TI{2A-GAL4}AstC$^{2A\text{-}GAL4}$/CyO	*AstC::2A-Gal4*	BL#84595	(Deng et al., 2019)
w*; TI{2A-GAL4}AstC-R1$^{2A\text{-}GAL4}$/TM3, Sb^{1}	*AstC-R1-Gal4*	BL#84596	(Deng et al., 2019)
w*; TI{2A-GAL4}AstC-R2$^{2A\text{-}B.GAL4}$	*AstC-R2^{B}-Gal4*	Takashi Koyama	(Deng et al., 2019)
Eh^{pan}-Gal4	*Eh::2A-Gal4*	John Ewer	(Scott et al., 2020)
w^{1118}; P{y$^{+t7.7}$ w^{+mC}=GMR51H05-GAL4}attP2	*12 DN1$_{ps}$*	BL#41275	(Jenett et al., 2012)
w^{1118}; P{y$^{+t7.7}$ w^{+mC}=GMR31D10-GAL4}attP2	*R31D10-Gal4*	BL#45572	(Jenett et al., 2012)
w^{1118}; P{y$^{+t7.7}$ w^{+mC}=GMR35B01-GAL4}attP2	*R35B01-Gal4*	BL#49898	(Jenett et al., 2012)
w^{1118}; P{y$^{+t7.7}$ w^{+mC}=GMR61H08-GAL4}attP2	*R61H08-Gal4*	BL#39283	(Jenett et al., 2012)
w^{1118}; P{y$^{+t7.7}$ w^{+mC}=GMR73B01-GAL4}attP2	*R73B01-Gal4*	BL#39809	(Jenett et al., 2012)
w^{1118}; PBac{w^{+mC}=IT.GAL4}lqfR$^{0260\text{-}G4}$	*260-Gal4*	BL#62743	(Gohl et al., 2011)
P{w^{+mC}=GAL4-Eh.2.4}C21	*Eh (C21)-Gal4*	BL#6301	(McNabb et al., 1997)
y^{1} w^{1118}; P{w^{+mC}=Lsp2-GAL4.H}3	*lsp-Gal4*	BL#6357	(Yoshiyama et al., 2006)
y^{1} w* Mi{Trojan-GAL4.1}nAChRalpha7$^{MI12545\text{-}TG4.1}$	*nAChRα7-Gal4*	BL#77828	(Lee et al., 2018)
y* w*; P{GawB}NP5253	*NP5253-Gal4*	Kyoto#104922	(Hayashi et al., 2002)
y^{1} w*; P{w^{+mC}=phtm-GAL4.O}22	*phm-Gal4*	BL#80577	(Ono et al., 2006)
w*; P{w^{+mC}=ppk-GAL4.G}3	*ppk-Gal4*	BL#32079	(Grueber et al., 2007)
y^{1} w^{1118}; P{y$^{+t7.7}$ w^{+mC}=Ptth-Gal4-45,117b3}	*Ptth-Gal4*	Wegener lab	(McBrayer et al., 2007)
w*; sna^{Sco}/CyO; P{w^{+mC}=Clk-GAL4.1.5}4.1M/TM6B, Tb^{1}	*Clk4.1M-Gal4*	BL#36316	(L. Zhang et al., 2010)
w*; P{w^{+mC}=Clk-GAL4.-856}2	*Clk856-Gal4*	BL#93198	(Gummadova et al., 2009)
R43D05-p65.AD; R93B11.DBD	*DN1$_{as}$*	Taishi Yoshii	(Sekiguchi et al., 2020)
Clk9M-Gal4	*Clk9M-G4*	Fumika N. Hamada	(Kaneko et al., 2012)
R11B03-p65.AD; R65D05.DBD	*LPNs*	Taishi Yoshii	(Sekiguchi et al., 2020)
w*; P{w^{+mC}=Pdf-GAL4.G}2	*Pdf-Gal4*	Paul Taghert	(Renn et al., 1999)

Full genotype	Short genotype	Source	Reference
TI{2A-lexA::GAD}AstA$^{2A\text{-}lexA}$/TM3, Sb^{1}	*AstA::2A-LexA*	BL#84356	(Deng et al., 2019)
w^{1118}; P{Clk-lexA.4.1M}3/TM6C, Sb^{1}	*Clk4.1M-LexA*	BL#80704	(Cavanaugh et al., 2014)
w*; TI{2A-lexA::GAD}Eh$^{2A\text{-}lexA}$/TM3, Sb^{1}	*Eh::2A-LexA*	BL#84388	(Deng et al., 2019)
w*; TI{2A-lexA::GAD}Ms$^{2A\text{-}lexA}$/TM3, Sb^{1}	*Ms::2A-LexA*	BL#84403	(Deng et al., 2019)
w*; TI{2A-lexA::GAD}Ptth$^{2A.lexA}$	*Ptth-LexA*	Francisco A Martin	(Deng et al., 2019)
w^{1118}; P{y$^{+t7.7}$ w^{+mC}=GMR43D05-lexA}attP40	*R43D05-lexA*	BL#54147	(Jenett et al., 2012)
P{Pdf-lexA-VP16.S}/CyO	*Pdf-LexA*	Charlotte Förster	(Shang et al., 2008)
w*; 20xUAS-flp; lola-frt-stop-frt-luc	*ARG-Luc*	Matthias Schlichting	(X. Chen et al., 2016)
w^{1118}; P{w^{+mC}=UAS-DenMark}2, P{w^{+mC}=UAS-syt.eGFP}2; In(3L)D, mirr^{SaiD1} D^{1}/TM6C, Sb^{1}	*DenMark, syt-GFP*	BL#33064	(Nicolaï et al., 2010)
w*; P{w^{+mC}=tubP-GAL80^{ts}}20; TM2/TM6B, Tb^{1}	*tubP-Gal80^{ts}*	BL#7019	(McGuire et al., 2003)
y^{1} w^{1118}; PBac{y$^{+mDint2}$ w^{+mC}=UAS-ChR2.XXL}VK00018	*UAS-ChR2-XXL*	BL#58374	(Dawydow et al., 2014)
p{UAS-EGFP::Kir2.1}2	*UAS-Kir2.1*	Michael Pankratz	(Baines et al., 2001)
p{UAS-EGFP::Kir2.1}3	*UAS-Kir2.1*	Michael Pankratz	(Baines et al., 2001)
w*; P{y$^{+t7.7}$ w^{+mC}=10XUAS-IVS-mCD8::RFP}attP2	*UAS-mCD8::RFP*	BL#32218	(Pfeiffer et al., 2010)
w*; P{y$^{+t7.7}$ w^{+mC}=10XUAS-IVS-myr::GFP}attP2	*UAS-myr::GFP*	BL#32197	(Pfeiffer et al., 2010)
P{KK110502}VIE-260B	*UAS-Ptth^{i} (KK)*	VDRC#102043	(Green et al., 2014)
w*; P{UAS-RA}19	*UAS-RA*	BL#28999	(Allen et al., 2002)
w^{1118}; P{w^{+mC}=UAS-RA.CS2}CC	*UAS-RA^{CS2}.CC*	BL#38624	(Chen et al., 2012)
w^{1118}; P{GD2613}v4298	*UAS-torso^{i} (GD)*	VDRC#4298	(Dietzl et al., 2007)
P{KK105371}VIE-260B	*UAS-torso^{i} (KK)*	VDRC#101154	(Green et al., 2014)
P{ry$^{+t7.2}$=hsFLP}12, y^{1} w*; P{y$^{+t7.7}$ w^{+mC}=UAS-Cas9.P2}attP40	*Cas9*	BL#58985	(Port et al., 2014)
P{ry$^{+t7.2}$=hsFLP}12, y^{1} w*; P{y$^{+t7.7}$ w^{+mC}=UAS-uMCas9}attP40	*UAS-uMCas9*	VDRC#340002	(Port et al., 2020)
P{hsFLP}1, y^{1} w^{1118}; P{HD_CFD00519}attP40/CyO-GFP	*torso-gRNA*	VDRC#341451	(Port et al., 2020)

Full genotype	Short genotype	Source	Reference
w; P{y+t7.7 w+mC=13XLexAop2-IVS-NES-jRCaMP1a-p10}su(Hw)attP5*	*LexAop-jRCaMP1a*	BL#64427	(Dana et al., 2016)
w; P{y+t7.7 w+mC=13XLexAop2-IVS-myr::GFP}attP40*	*LexAop-myr::GFP*	BL#32210	(Pfeiffer et al., 2010)
w; P{y+t7.7 w+mC=13XLexAop2-IVS-myr::GFP}attP2*	*LexAop-myr::GFP*	BL#32209	(Pfeiffer et al., 2010)
w; PBac{LexAop2-Syb.GFP.P10}VK00037 PBac{LexAop2-Syb.GFP^{N146I}.TEV^{T173V}}VK00002 PBac{LexAop2-QF2.V5.hSNAP25.HIVNES.Syx1A}VK00018/CyO; P{20XUAS-B3R.PEST}attP2 PBac{UAS(B3RT.B2)BoNTA}VK00005 P{QUAS-mtdTomato-3xHA}26/TM6B, Tb1*	*BAcTrace*	BL#90826	(Cachero et al., 2020)
w; P{w+mC=LexAop-CD8-GFP-2A-CD8-GFP}2; P{w+mC=UAS-mLexA-VP16-NFAT}H2, P{w+mC=lexAop-rCD2-GFP}3/TM6B, Tb1*	*CaLexA*	BL#66542	(Masuyama et al., 2012)
y1 w; P{y+t7.7 w+mC=lexAop-rCD2::RFP-p10.UAS-mCD8::GFP-p10}su(Hw)attP5/CyO; TM3, Sb1/TM6B, Tb1*	*LexAop-rCD2::RFP, UAS-mCD8::GFP*	BL#67093	(Ren et al., 2016)
QUAS-nlsDsRed	*Qnls-RFP*	Meet Zandawala	(Snell et al., 2022)
w; P{w+mC=lexAop-nSyb-spGFP1-10}2, P{w+mC=UAS-CD4-spGFP11}2; TM3, Sb1/TM6B, Tb1*	*syb-GRASP*	BL#64315	(Macpherson et al., 2015)
y1 w1118; P{y+t7.7 w+mC=trans-TangoMkII}attP40/SM6b	*trans-Tango MkII*	BL#95317	(Sorkaç et al., 2022)
UAS-AstC.gRNA	*UAS-AstC-gRNA*	Takashi Koyama	(Kubrak et al., 2022)
w TI{RFP3xP3.cUa=TI}AstA-R1attP*	*AstA-R1attP*	BL#84452	(Deng et al., 2019)
w; TI{RFP3xP3.cUa=TI}AstA-R2attP*	*AstA-R2attP*	Bowen Deng	(Deng et al., 2019)
w; TI{RFP3xP3.cUa=TI}MsR1attP*	*MsR1attP*	BL#84524	(Deng et al., 2019)
w; TI{RFP3xP3.cUa=TI}MsR2attP*	*MsR2attP*	BL#84525	(Deng et al., 2019)
w; TI{RFP3xP3.cUa=TI}sNPF-RattP*	*sNPF-RattP*	BL#84575	(Deng et al., 2019)
Ilp7KO	*Ilp7 mutant*	Peter Soba	(Grönke et al., 2010)
Ilp8ag50	*Ilp8 mutant*	Alisson Gontijo	(Garelli et al., 2012)
Ilp8ag52	*Ilp8 BG*	Alisson Gontijo	(Garelli et al., 2012)

Full genotype	Short genotype	Source	Reference
Lgr3^{ag1}	*Lgr3 mutant*	Alisson Gontijo	(Garelli et al., 2012)
Lgr3^{ag2}	*Lgr3 BG*	Alisson Gontijo	(Garelli et al., 2012)
AstA^{SK1}	*AstA^{SK}*	Shu Kondo	(Hentze et al., 2015)
y^{1} w*; P{LN-Gal80.M4}attP40	*LN-G80*	Wegener lab	Unpublished

2. Chemoconnectomics and trans-synaptic tracing

a. Immunostaining

For immunostainings, P14 pupal stage adults were dissected, unless stated otherwise. The puparia were washed off the tubes, transferred on filter paper, and cleaned from food particles, larvae, or debris. The P14 adults were selected based on their appearance (darkened wings, completed eye pigmentation, and fully grown bristles on the abdomen; Bainbridge and Bownes, 1981). The animals were then pinned down in a silicone plate using 0.2 mm Minutiens pins (Fine Science Tools, Heidelberg, Germany). The fixed puparia were covered with HL3.1 fly ringer (Feng et al., 2004; NaCl 70 mM, KCl 5 mM, $CaCl_2.2H_2O$ 1.5 mM, $MgCl_2.6H_2O$ 4 mM, $NaHCO_3$ 10 mM, saccharose 115 mM, $Trehalose.2H_2O$ 5 mM, and HEPES 5 mM, pH 7.1). The puparium was removed by making an incision between the head and thorax in the puparium. Then gently the puparium and the thin pupal cuticle were removed. Once the animal had been exposed, the dissection was carried out. To dissect the brain, the proboscis was removed and the cuticle surrounding the brain was peeled off. To dissect the ventral nerve cord (VNC), the legs were removed. The ventral part of the thorax was cut open and after removing the trachea and muscles the VNC was exposed. Then the peripheral nerves were cut and VNC was removed. Before collecting the brains and VNCs for staining, the trachea attached to them were removed.

The dissected brains or VNCs were collected in a 0.5 ml Eppendorf tube filled with HL3.1 solution and placed on ice. After dissection, the HL3.1 solution was removed and replaced by 100 µl of 4% paraformaldehyde in phosphate-buffered saline (100 mM, pH 7.4) for fixation at 25 °C and on a shaker. After 30 minutes of fixation, the tissues were washed three times with phosphate-buffered saline plus 0.3% Triton-X100 (PBT) solution for ten minutes on the shaker at 25 °C and blocked in 5% normal goat serum in PBT for 90 minutes on the shaker at 25 °C. After blocking, the tissues were transferred into the primary antibody solution and stored at 4 °C for two days on the shaker. After that, the tissues were washed at room temperature and on the shaker six times at ten-minute intervals with PBT and stored for one day in the secondary antibody solution at 4 °C on the shaker. Finally, the tissues were washed four times at room temperature with PBT and three times with phosphate-buffered saline in ten-minute intervals and mounted on Poly-lysine-coated slides (Thermoscientific, Braunschweig, Germany) with Vectashield (Vector Laboratories, California, United States) and stored at 4 °C until imaged. For immunostainings, a variety of primary and secondary antibodies were used (Table 2).

Table 2. The primary and secondary antibodies used for immunocytochemistry.

Primary Antibody	Animal raised in	Target protein	Procedure	Company/Creator	Dilution	Batch number/Publication
Anti-mCherry	Rat	mCherry, RFP, tdTomato	Double staining, BAcTrace	Invitrogen	1:1,000	M11217
Anti-GFP	Rabbit	GFP	Double staining, BAcTrace, syb-GRASP, CaLexA	Chromotek	1:1,000	PABG1
Anti-RFP	Guinea pig	RFP	Double staining, *trans*-Tango	Susan Morton	1:10,000	-
Anti-PTTH	Rabbit	Prothoracicotropin Hormone	Double staining, *trans*-Tango	Dick Nässel & Meet Zandawala	1:10,000	Unpublished
Anti-PTTH	Rabbit	Prothoracicotropin Hormone	CaLexA	Vollborn and Korge	1:1,000	(Vollborn, 2011)
Anti-PDF C7	Mouse	Pigment Dispersing Factor	Double staining	Developmental Studies Hybridoma Bank	1:1,000	MIgG2b
Secondary Antibody	**Animal raised in**	**Fluorophore**	**Procedure**	**Company**	**Dilution**	**Batch number/Publication**
Anti-Rabbit	Goat	Alexa-488	Double staining, *trans*-Tango, BAcTrace, CaLexA, syb-GRASP	Dianova	1:500	111-545-144
Anti-Mouse	Goat	Alexa-649	Double staining	Dianova	1:500	115-605-146
Anti-Guinea pig	Goat	Alexa-555	Double staining, *trans*-Tango	Thermo Scientific	1:10,000	AB 2535856
Anti-Rat	Goat	Alexa-647	Double staining, BAcTrace	Dianova	1:500	112-605-143

b. Synaptobrevin-GFP Reconstitution Across Synaptic Partners (syb-GRASP)

Simply neurons communicating with each other build up the circuits and surly their wiring diagram generates the behavior on the higher level (Simpson, 2009). Therefore, the first step toward understanding the neuronal circuits is to identify the synaptic partners. The next logical step is to determine the direction of activity. In *Drosophila*, GFP and other fluorescent proteins were used in designing reporter systems for marking synaptic connections (Feinberg et al., 2008; Macpherson et al., 2015), and anterogradely (Sorkaç et al., 2022; Talay et al., 2017) or retrogradely (Cachero et al., 2020) trace these connections. GFP Reconstitution Across

Synaptic Partners (GRASP) uses the complementary expression of split-GFP fragments in the cellular membranes of different neurons. Based on the reconstitution of functional GFP in contacting neurons, the synaptic partners are identified. A more advanced version of GRASP which is a synaptobrevin-GRASP chimera (syb-GRASP) identifies the synaptic partners upon their activity (Macpherson et al., 2015). The syb-GRASP staining followed the immunostaining procedure outlined in 2.a., with a few extra steps (Macpherson et al., 2015). For the syb-GRASP signal to become visible, dissected P14 CNS were briefly (5-7 seconds) depolarized three times by rinsing with HL3.1 followed by HL3.1 with 70 mM KCl. Then the tissues were incubated for ten minutes in HL3.1 to reconstitute GFP at active synaptic sites. After that, the tissues were fixed for 30 minutes with 4% paraformaldehyde, and the rest of the procedure continued as described in section 2.a. The tissues were immunostained only against GFP.

c. Botulinum-Activated Tracer (BAcTrace)

One of the retrograde synaptic partnership tracing methods that is used in *Drosophila* is Botulinum-Activated Tracer (BAcTrace). This genetically encoded system is based on modified Clostridium botulinum neurotoxin A that retrogradely is transferred to the presynaptic partner. There the modified toxin initiates a series of transcriptions that end in production of red fluorescent protein tandem dimer Tomato (tdTomato) in the presynaptic neuron (Cachero et al., 2020). The BAcTrace procedure does not require any special treatment from fly rearing to staining. The BAcTrace staining is done for GFP and tdTomato. Since the antibody against mCherry was able to stain tdTomato as well, it was used for BAcTrace. The staining process is the same as described in section 2a.

d. *trans*-Tango MkII

Anterograde tracing is as important as retrograde tracing. *trans*-Tango is a system designed for anterograde synaptic partner tracing in *Drosophila*. *trans*-Tango is based on a synthetic signaling pathway that converts the activity of a membrane-tethered receptor in the presynaptic neurons into expression of a fluorescent protein in the postsynaptic neurons (Talay et al., 2017). Since it labels all postsynaptic neurons, it is possible to track neurons of interest among the labeled neurons using a second marker (for example by expressing a different fluorescent protein under the control of LexA/LexAop in neurons of interest). The second version of it or *trans*-Tango mark 2 (MkII) was designed that uses a different linker, therefore enhancing the signal accumulation in larval and pupal brain (Sorkaç et al., 2022). The *trans*-Tango signal requires a substantial amount of time to build up (Sorkaç et al., 2022; Talay et al., 2017). Therefore, the slower the flies grow, or the older they are, the better the signal accumulates. For this reason, after egg laying, flies were kept at 18 °C. P14 puparia were selected, dissected, and immunostained as explained in section 2.a. The staining for *trans*-Tango MkII was performed against GFP and red fluorescent protein (RFP).

3. Confocal Laser Scanning Microscopy

A Leica TCS SPE confocal laser scanning microscope (Leica Microsystems, Wetzlar, Germany) equipped with 488, 532, and 635 nm lasers and ACS APO 20X/0.60 IMM CORR (507904, Leica Microsystems, Wetzlar, Germany) glycerol immersion aperture and ACS APO

40X/1.15 OIL CS (507901, Leica Microsystems, Wetzlar, Germany) Type F oil immersion aperture was used for scanning at 400 Hz in the format of 1024*1024 pixels and a frame average of two and a z-step size of 1.78 µm (20x) or 0.8 µm (40x).

4. Image processing and preparation

All image processing (adjusting size, brightness, contrast, scaling, and stitching) was done using Fiji software (Schindelin et al., 2012). To produce the figures, the images were put together, cropped, and annotated using Adobe Photoshop CC 2023 (Version 24.5; Adobe Systems, San Jose, CA, USA). 2D reconstructions were drawn using Adobe Fresco (Version 4.6.1; Adobe Systems) or Adobe Animate 2023 (Version 23.0.2; Adobe Systems) and converted into vectors using Adobe Illustrator CC 2023 (Version 27.6.1; Adobe Systems).

5. Eclosion assays

a. *Drosophila* Eclosion Monitor (DEM)

For monitoring eclosion behavior, flies were raised in large plastic bottles on standard fly food. After 3-5 days of egg laying, the parental flies were removed from the bottles. The flies were always entrained at 20 °C (except for TARGET experiments and temperature entrainment) under a 12:12 light-dark (LD) light regime, and 65% relative humidity in Sanyo MIR-153 incubator (EWALD Innovationstechnik GmbH, Rodenberg, Germany). After the first wandering larvae appeared, flies were transferred to constant darkness (DD) at 20 °C. From then on, every step was done under red light. After 5-8 days (depending on the flies) in DD, most of the puparia started to darken. The puparia darkening happens at P12 stage and 75 hours after pupariation, when wings turn dark, and bristles start to grow. When approximately more than 30% of the pupariated flies were darkened (around 10-15 days after egg laying), the eclosion assays were performed.

First, the bottles were rinsed with water and after a few seconds, the puparia were removed with a brush and dried on filter paper by gently rolling using a brush. Puparia were separated from each other as much as possible without damaging them. Then, fungicide-free methyl cellulose organic glue (Tapetenkleister Nr. 389, Auro, Braunschweig, Germany; 0.9 g dissolved in 50 ml water) was used to paste the puparia onto a round acrylic plate that was mounted on top of a funnel. After several hours that the glue dried up, the funnels with the plates were mounted onto the TriKinetics *Drosophila* Eclosion Monitors (DEM; TriKinetics Inc, Waltham, MA USA), and the number of eclosed flies was recorded every minute for one week in a Sanyo MIR-553 incubator (EWALD Innovationstechnik GmbH, Rodenberg, Germany).

Using a custom-made macro in Microsoft Excel, the amount of eclosed flies per hour was calculated and plotted. The reliability of the collected data was confirmed by calculating the error (E) by counting the dead flies (n) and comparing it to the number of flies counted by the monitor (N) using the formula $\mathrm{E} = \frac{\mathrm{N}-\mathrm{n}}{\mathrm{N}} * 100$. If the error was less than 10%, the data were accepted as reliable, otherwise the data were discarded, and the assay was repeated. The rhythmicity profile of the experiments was obtained using a MATLAB (MathWorks Inc., Natick, MA, USA) toolbox (Levine et al., 2002), and rhythmicity was assessed by

autocorrelation analysis. If the Rhythmicity index (RI) was ≥ 0.3, eclosion was considered to be rhythmic. 0.3 ≥ RI ≥ 0.1 was considered weakly rhythmic and RI ≤ 0.1 was considered arrhythmic (Levine et al., 2002). The MATLAB toolbox also calculated the period of the rhythmic cycles using Maximum Entropy Spectral Analysis (MESA) method (Levine et al., 2002). Enhanced JTK cycle (eJTK) analysis was performed using BIODare2 (Zielinski et al., 2014) and Lomb-Scargle (LS) was calculated using the ActogramJ plugin for ImageJ (Ruf, 1999; Schmid et al., 2011).

b. Optogenetic activation and *Drosophila* Eclosion Monitoring (Opto-DEM)

To assess the role of the peptidergic neurons in initiating eclosion, optogenetic activation to induce premature eclosion in the Würzburg Eclosion Monitor (WEclMon) system was used (Ruf et al., 2017). The idea was to optogenetically activate certain peptidergic neurons using Channel rhodopsin 2-XXL (ChR2-XXL; Dawydow et al., 2014) within the eclosion window before the expected eclosion peak and then test for premature eclosion. In these experiments instead of 12:12 LD cycles, warm-cold temperature (25 °C-16 °C, 12:12 WC) cycles resembling day-night conditions were used for entrainment. The temperature changes happened over 1.5 hours temperature steps of 1 °C every ten minutes. After crossing the parental flies, they were placed in 12:12 WC, constant darkness at 65% relative humidity in DR-36NL incubator (Percival Scientific Inc., Perry, IA, USA). After 3-5 days of egg laying, the parental flies were removed from the bottles and the offspring remained under WC entrainment during development. When 30% darkened puparia appeared, puparia pasting and eclosion monitoring were performed as described in section 5.a. The eclosion monitors were placed in a separate incubator (Sanyo MIR-553 incubator; EWALD Innovationstechnik GmbH, Rodenberg, Germany) with the same WC entrainment, constant darkness, and 65% humidity. Given that the eclosion gate opens six hours before morning (Pittendrigh, 1954), six hours before the temperature rise at Zeitgeber time 18 (ZT18) blue light (I = 6800 $\mu W.cm^{-2}$, λ = 470 nm) was shone upon the monitors from a distance of ten cm for one hour.

The data for Opto-DEM was collected and tested for reliability as described for DEM in section 5.a. The amounts of eclosed animals were plotted as percentages of the number of flies eclosed for each day. The individual experiments were not pooled and the percentages for each ZT were plotted using OriginPro 2021b (version 9.8.5.212; OriginLab Corporation, Northampton, MA, USA). For each ZT, a Shapiro-Wilk test for normality was performed. Since the majority of the groups were not normally distributed, Mann-Whitney *U* tests followed by pairwise Wilcoxon tests were performed.

c. Conditional silencing of PTTH neurons and eclosion monitoring

The Temporal and Regional Gene Expression Targeting (TARGET) approach utilizes pan expression of a temperature-sensitive variation of Gal80 ($Gal80^{ts}$) to temporally control gene expression simply by changing the environmental temperature (McGuire et al., 2003). In this approach, $Gal80^{ts}$ protein prevents Gal4 from binding to the *UAS* site, thus preventing gene expression. By raising the temperature to 29 °C, $Gal80^{ts}$ deactivates and blocking Gal4 is over. To conditionally silence PTTHn, potassium inward rectifying channel 2.1 (Kir2.1) in combination with $Gal80^{ts}$ under the control of alphaTub84B promoter (*UAS-Kir2.1; tubP-*$Gal80^{ts}$) was used. Parental flies were crossed in large bottles. The flies were kept under LD

12:12 and 20 °C until the first wandering larvae emerged. Then the fly vials were transferred into constant darkness (DD). To electrically silence the PTTH neurons during different developmental stages the temperature was raised from 20 °C to 29 °C and back to 20 °C to revert the effect. For silencing during larval stages, the temperature was 29 °C during LD entrainment. For silencing PTTHn at the early pupal stage, the temperature was at 29 °C during DD and the first half of pupal development, for late pupal stages during the second half of the pupariation period (DD) and the eclosion monitoring time. For silencing during the entire pupal development, the temperature was at 29 °C during DD and eclosion monitoring.

d. Creating AstC knock-outs using temperature-controlled CRISPR/Cas9

The knock-out mutant of AstC was generated using clustered regularly interspaced short palindromic repeats (CRISPR) and Cas9 and knocking out the *AstC* gene in AstC neurons (Kubrak et al., 2022; Port et al., 2014). To create the knock-out mutants *AstC-Gal4; UAS-AstC-gRNA* (gRNA: guide RNA) parental flies were crossed to *UAS-Cas9; tubP-Gal80ts* in large bottles. For controls, w^{1118} flies were crossed to the mentioned parental lines. After egg laying the flies were removed from the bottles. The progeny flies were entrained in 12:12 LD and 20 °C and as soon as pupariation started and the first wandering larvae appeared, flies were given two days of 29 °C heat shock. Then the flies were moved to DD 20 °C and kept until they were ready to be pasted on acrylic plates. The eclosion assays were performed and the data were analyzed as explained in section 5.a.

e. Conditional cell ablation of neurons using cold-sensitive ricin

To conditionally restrict cellular ablation to the final pupal stages, cold-sensitive ricin (RA^{CS2}.CC) was used. RA^{CS2}.CC becomes fully activated at 29 °C and is fully inactivated at 18 °C (Chen et al., 2012). DEM eclosion assays were carried out as described in section 5.a with an added step of cell ablation by temperature change: one day before starting the eclosion assays from circadian time 1 (CT1) the temperature was raised to 30 °C for twelve hours (until CT12), followed by a decrease to 18 °C for the next twelve hours.

6. Assessment of the effect of genetic silencing by locomotor activity recording

To assess the suitability of the *UAS-Kir2.1* line for neuronal silencing, a locomotor assay was performed, using the *Drosophila* Activity Monitor 2 (TriKinetics Inc, Waltham, MA USA). This device simultaneously monitors the locomotor activity of 32 flies, but it measures circadian rhythms and sleep of every single fly individually. Flies were entrained at 20 °C and 12:12 LD. For this experiment the experiment group expressed Kir2.1 in all clock neurons (*Clk856> Kir2.1*), Gal4 and UAS controls (*Clk856>* w^{1118} and w^{1118}*> Kir2.1*) were tested. Individual flies 3-5 days after eclosion were transferred into glass tubes plugged on one end with 2% agar and 4% sucrose, sealed with a rubber plug on the other end, and placed inside the *Drosophila* Activity Monitor 2 system for at least 20 days. The monitors were placed in DD in Genheimer temperature-controlled chambers (Kälte-Klima-Technik GmbH, Hettstadt, Germany) and the data were collected every minute. Data were analyzed using ActogramJ plugin for ImageJ (Ruf, 1999; Schmid et al., 2011) and rhythmicity was calculated using the LS analysis (Ruf, 1999).

7. Imaging neuronal activity

a. Ca^{2+} imaging to assess functional connectivity

Intracellular Ca^{2+} dynamics can be used as a proxy to determine the neuronal activity (Yasuda et al., 2004). Genetically encoded Ca^{2+} indicators (GECIs) are broadly used for studying neuronal activities (Wang et al., 2003). GCaMP6 is currently the most widely used GECI in *Drosophila*. However, it has properties that make it not well-suitable for optogenetic experiments in puparia. First, the excitation spectrum of GCaMP overlaps with that of ChR2-XXL. Therefore, activation of ChR2-XXL bleaches GCaMP fluorescence, and the blue light excitation of GCaMP can lead to activation of ChR2-XXL. To circumvent these problems, red-shifted RGECO (mApple-based) and RCaMP (mRuby-based) were designed (Akerboom et al., 2013; Zhao et al., 2011). Recently, newer versions of RCaMP have been made that are comparable to GCaMP6. Among them, it has been shown that a combination of jRCaMP1a with ChR2-XXL works best (Dana et al., 2016). Therefore, the combination of ChR2-XXL and jRCaMP1a was chosen for these experiments.

The functional imaging setup (Figure 6 A) is made from an Arduino Uno board (Arduino®, Somerville, MA, USA) encased in a custom-made box (Figure 6 B) with a button that controls blue light emitting diodes ($I = 340\ \mu W.cm^{-2}$, $\lambda = 470$ nm) installed in a stand (Figure 6 C). The stand has a top and a bottom part that are attachable by magnets (Figure 6 C-D). The top part of the stand contains a replaceable holder with a chemically etched hole in the center based on pharate fly measurements (Figure 6 D). For functional imaging, the puparium and the pupal case were completely removed. Then the pharate fly was mounted on a holder as shown in Figure 6 E and F. The part of the body below the holder (Figure 6 F) and the eyes were fixed in place by instant UHU Alleskleber Super (UHU GmbH & Co. KG, Bühl/Baden, Germany) super glue. After the glue had dried, one ml of HL3.1 solution (Feng et al., 2004) pH 7.1 was added on top of the head. Using a sharp lance needle a window was cut open in between the eyes. Trachea and fat body were gently removed to expose the brain (Figure 6 G). The Ca^{2+} signal was measured using a widefield fluorescence microscope setup (Visitron Systems, Puchheim, Germany) comprising a Zeiss Axio Examiner. D1 microscope (Carl Zeiss Microscopy GmbH, Jena, Germany) with two PCO.edge sCMOS cameras (Excelitas Technologies® Corp., Kelheim, Germany), a Cairn Twin-Cam LS image splitter (89 North Inc., Williston, VT, USA), an ET filter set (Chroma, Semrock AHF, Heidelberg, Germany) and a SPECTRA-4 light engine (Lumencor, Inc., Beaverton, OR, USA). Imaging was done with a Zeiss W Plan-Apochromat 20x/1.0 water immersion lens (Carl Zeiss Microscopy GmbH, Jena, Germany) and 560 nm green light emitting diode with an intensity of 5% and an exposure of 50 ms at 2X binning. For each experiment, 30 minutes of Ca^{2+} activity were recorded at two Hz (3601 frames). During imaging to excite the neurons two 0.5s blue light pulses ($I = 340\ \mu W.cm^{-2}$, $\lambda = 470$ nm) were given at 200s and 1200s after initiation of imaging.

To analyze fluorescence changes, two regions of interest (ROI) were selected. One around the cell bodies, and one inside the brain near the first ROI as background. The ROIs fluorescence was measured using Visiview 3.2 or 6.1 (Visitron Systems, Puchheim, Germany), and movement was manually compensated for with MetaMorph software. The background fluorescence was subtracted from the cell body fluorescence. To correct for bleaching, the baseline was corrected with the peak analyzer and baseline subtraction function in OriginPro

2021b. To obtain the relative changes in the fluorescence, $\frac{\Delta F}{F0} = \frac{[(Fn-BG)-F0]}{F0}$ was calculated, in which F_0 is the average fluorescence of the cell body within the first ten seconds, Fn is the corrected fluorescence at time point n, and BG is the corrected background fluorescence. $\Delta F/F_0$ was averaged and plotted with SEM.

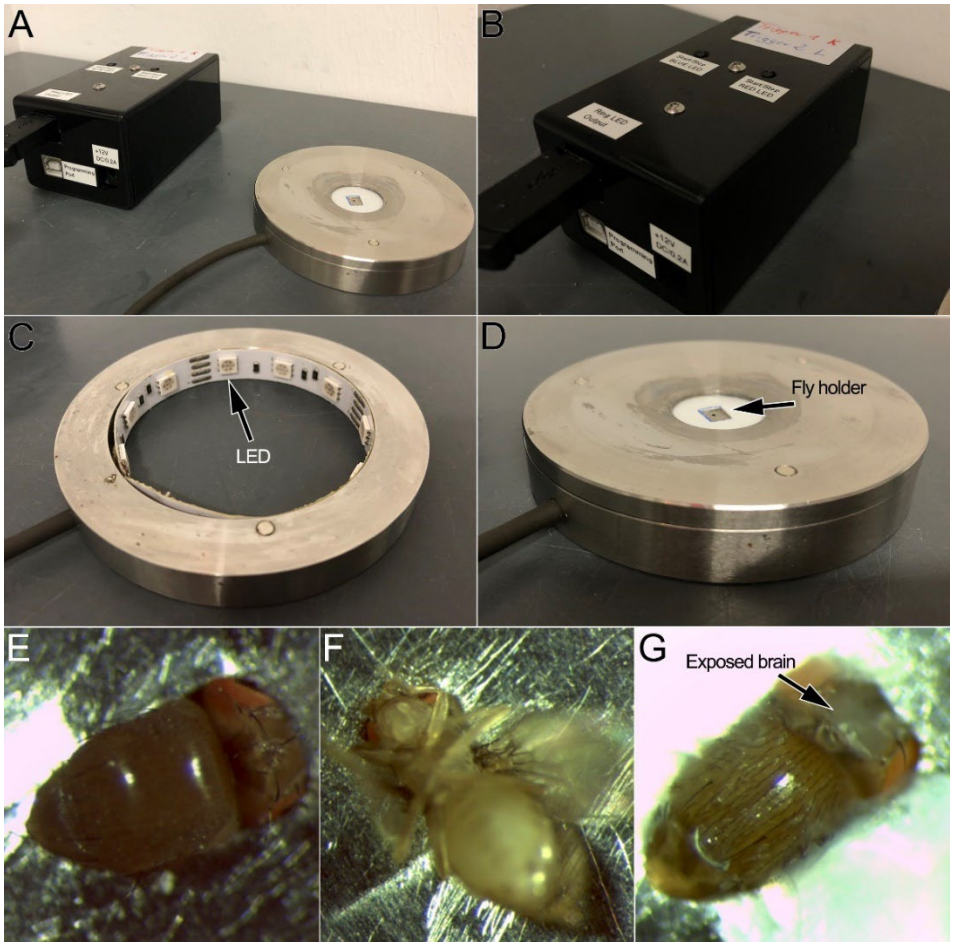

Figure 6. Make-up of the holder and functional imaging setup. A The functional imaging setup is made from a control box and a stand that is placed under the microscope. **B** The control box contains an Arduino board that controls **C** an array of light emitting diodes (LED) installed in the inner circle of the bottom part of the stand. **D** The top part of the stand has a place to contain the replaceable fly holder. **E** The fly is mounted in the holder such that its head and thorax are exposed (top view of the holder). **F** The fly is hanging (bottom view). **G** After gluing the eyes and thorax, a window between the eyes is cut to expose the brain for imaging.

b. CaLexA Ca^{2+} imaging

Ca^{2+} activity can also be measured by transcriptional reporters. CaLexA (Ca^{2+}-dependent nuclear import of LexA) uses a Ca^{2+}-responsive transcription factor linked to a mutated LexA and shuttles into the nucleus upon Ca^{2+} binding and transcribing *gfp* which is under the control of LexAop. The amount of GFP fluorescence intensity indirectly reports neuronal activity (Masuyama et al., 2012). For CaLexA (Masuyama et al., 2012), eggs were collected for five hours and kept under 12:12 LD, 25 °C, and 65% relative humidity until pupariation. P14 pupal brains were dissected in 4-hour intervals at ZT0, four, and eight under white light and 12, 16, and 20 under red light. The dissected brains were immediately fixed and stained for GFP and

PTTH as explained in section 2.a. After mounting, brains were scanned with the confocal microscope with the same setting for each preparation with 488 nm laser at 15 % laser power, ACS APO 20X/0.60 IMM CORR (507904, Leica Microsystems, Wetzlar, Germany) glycerol immersion objective, and a frame average of 2, z-step size of 1.78 µm and 1024*1024 pixels format. The PTTH cell bodies were identified by anti-PTTH staining. A z-projection with the maximum intensity for each cell body was created and that cell body was selected as ROI. Another ROI with the same size around the cell body was selected as background. Using Fiji, the GFP staining intensity was measured for each averaged ROI after background subtraction. Data were plotted and statistically analyzed using OriginPro 2021b. A Kruskal-Wallis ANOVA test and pairwise Wilcoxon test were used because the normality of the data was rejected by a prior Shapiro-Wilk test.

c. ARG-Luc imaging

The transcription of immediate early genes rapidly increases upon neuronal activation (Fowler et al., 2011). Therefore, the upregulation of these genes in mammals is widely used as a proxy to assess neuronal activity (Barth et al., 2004; Mongeau et al., 2003; Wang et al., 2006). In flies, these genes are known as activity-regulated genes (ARGs). Several tools based on ARG transcription factors linked to a *luciferase* (*luc*) reporter gene sequence were developed by the Rosbash lab (X. Chen et al., 2016). Among these tools, the *lola*-Luciferase reporter (based on a transcription factor called Lola) showed a significant and rapid signal increase and provided one of the best readouts. Therefore the Activity-Regulated Gene *lola*-Luciferase reporter (ARG-luc; X. Chen et al., 2016) was employed to measure the *in-vivo* activity of the PTTHn, EH, C4da neurons, the PG, and the Inka cells in intact puparia. Six ml of normal fly food was heated to 60 °C in a water bath and mixed with a concentration of 15 mM (4.77 g/l) luciferin (Carbosynth Ltd, Newbury, UK; dissolved in double distilled water). After mixing by stirring the food it was stored at 4 °C in darkness until use. After mated parental flies had laid eggs on the luciferin-supplemented food, they were removed. Eggs were allowed to develop until pupariation in DD at 25 °C and 65% relative humidity. One day before starting the assay, a 1h white light pulse ($I = 210\ \mu W.cm^{-2}$, λ = 200-1000 nm) was given to synchronize the flies. For the assay, puparia at different stages were collected and cleaned. They were pasted on adhesive transparent plastic sheets (TopSeal™ A Plus, PerkinElmer LAS, Rodgau, Germany) placed on top of a 96 well OptiPlate™ - 96 (PerkinElmer LAS, Rodgau, Germany) such that they were placed on every other well to avoid light contamination from neighboring wells. The plate was loaded into a TopCount Multiplate Reader (PerkinElmer LAS) and kept inside a Percival I-60LLX chamber (Percival Scientific Inc., Perry, IA, USA) that was set to DD, 25 °C, and 65% humidity. Bioluminescence data was recorded every 30 minutes for one week. Data was extracted with an MS Excel plugin. The first twelve hours were removed because of high counts caused possibly by the accumulation of Luciferase. A sCMOS camera (DMK33UX178, ImagingSource, Bremen, Germany) on top of the plate captured a picture under red light every five minutes. The time of eclosion of each fly was obtained from the captured pictures and the closest luminescence data point correlated was marked as “time of eclosion”. If eclosion occurred in the first twelve hours, or if the flies showed no activity or died before eclosion, data points were discarded and were not used in the final analysis. The luminescence data were adjusted according to the time of eclosion, the baseline was corrected, and the average and standard error of the mean (SEM) were calculated and plotted using OriginPro 2021b.

Results

Chapter I: PTTH signaling is required during the final pupal stages for circadian eclosion timing

1. Temporal profile of PTTH signaling for eclosion rhythmicity

a. Conditional silencing of the PTTHn shows that PTTH signaling is important at the final pupal stages to maintain eclosion rhythmicity

To understand when during development PTTH signaling is required for rhythmic eclosion pattern, the TARGET system (McGuire et al., 2003) was used to conditionally silence the PTTHn by ubiquitously expressing the temperature-sensitive form of the repressor Gal80 (*tubP-Gal80^{ts}*) combined with targeted expression of a Kir2.1 in the neurons of interest (*Ptth-Gal4*). By raising the temperature to 29 °C, Gal80^{ts} is inactivated, and Kir2.1 expression is disinhibited, which leads to electrically silenced PTTHn. To reverse the silencing, dropping the temperature to 20 °C is sufficient. The conditional silencing of the PTTHn was performed during either i) larval, ii) entire pupal, iii) first half, and iv) second half of pupal development (Figure 1.1). Silencing during the larval and first half of pupal stage did not impair rhythmic eclosion in the experimental (*Ptth> tubP-Gal80, Kir2.1*), and control (*Ptth> w^{1118}* and *w^{1118}> tubP-Gal80, Kir2.1*) groups, based on autocorrelation RI, LS, and eJTK analyses. In contrast, silencing the PTTHn during the entire pupal- and second half of pupal development resulted in an arrhythmic eclosion pattern as indicated by the different analysis methods. In these latter experiments, eclosion monitoring occurred at 29 °C to keep the PTTHn silenced. This resulted in faster development, and subsequently in activity diagrams that only contain 3-4 days of eclosion (Figure 1.1). Because of this, the autocorrelation analysis for the experimental and control groups resulted in negative numbers. Yet, LS and eJTK analysis confirmed arrhythmic eclosion only for the experimental groups but not the controls.

Taken together, the TARGET experiments suggest that PTTH signaling is required during the entire- or during the final pupal development stages to maintain the circadian rhythmicity of eclosion behavior.

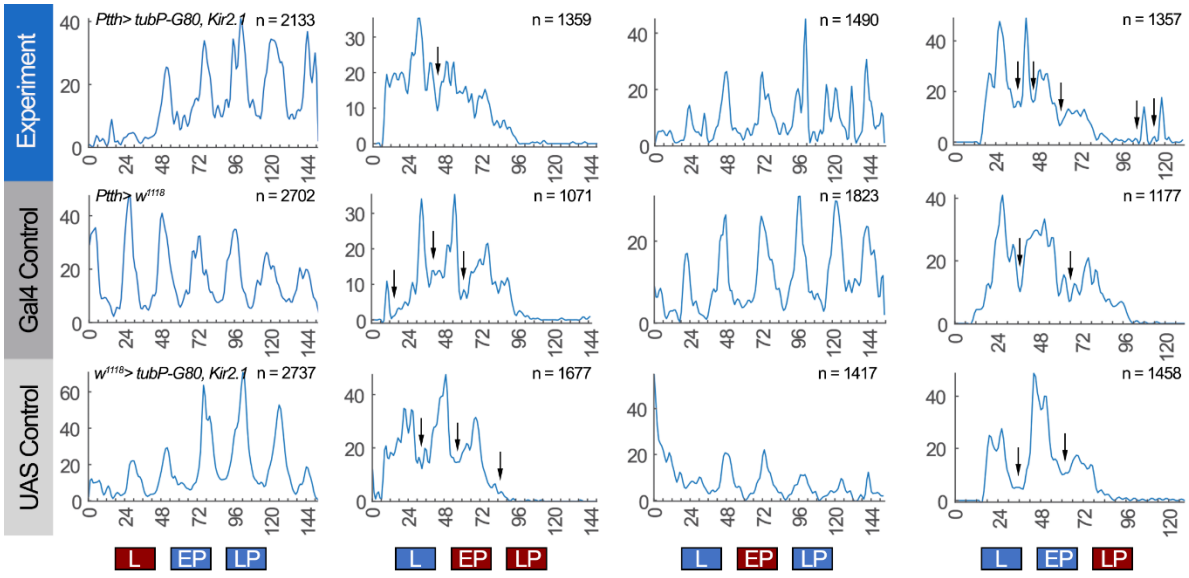

	L EP LP			L EP LP			L EP LP			L EP LP		
	Experiment	Gal4 Control	UAS Control	Experiment	Gal4 Control	UAS Control	Experiment	Gal4 Control	UAS Control	Experiment	Gal4 Control	UAS Control
RI	0.29	0.49	0.19	-0.06	-0.15	-0.19	0.16	0.45	0.25	-0.14	-0.16	-0.14
LS	13.64	35.75	20.44	0	1.80	9.64	9.98	33.80	11.65	0	7.57	2.55
eJTK	5.1×10^{-8}	2.0×10^{-23}	1.1×10^{-15}	0.06	0.001	8.4×10^{-9}	9.7×10^{-20}	3.1×10^{-16}	1.7×10^{-13}	0.03	4.7×10^{-4}	9.0×10^{-4}

Figure 1.1. Conditional silencing of the PTTH neurons during different stages of development using TARGET suggested that PTTH signaling was required at the final stages of pupal development for rhythmic eclosion. PTTHn were silenced under the control of ubiquitously expressed temperature-sensitive Gal80 (*tubP-Gal80^{ts}*) and *Ptth-Gal4*-driven potassium inward rectifying channel (*UAS-Kir2.1*) at 29 °C (red) and became activatable by decreasing the temperature to 20 °C (blue). Silencing PTTHn in larval- (L) and early pupal (EP) stages of development did not result in an arrhythmic eclosion pattern. However, silencing these neurons during entire pupal development (EP+LP) and late pupal stages (LP) rendered the eclosion pattern of the experiment group arrhythmic. Development at 29°C provided three to four days of eclosion activity. Due to more rapid development at 29 °C, autocorrelation analysis for the experiment and control groups was difficult. Therefore, the LS and eJTK were used to analyze rhythmicity. Troughs were marked by arrows. In the rhythmic control groups, these troughs were around 24 hours apart. In the experiment groups either the troughs did not exist (EP+LP) or were separated in a non-24h pattern.

b. At ZT0 the Ca^{2+} activity of the PTTHn in dissected brains is at its peak

To directly measure the Ca^{2+} activity of the PTTH neurons in pharate brains, CaLexA was first used (Masuyama et al., 2012). CaLexA uses the Ca^{2+}-dependent NFAT10 transcription factor attached to LexA which translocates to the nucleus upon Ca^{2+} increase and drives the expression of *LexAop-GFP*. Brains of pharates kept under LD 12:12 conditions were dissected every four hours and immunostained against PTTH and GFP. The GFP signal in the PTTHn showed the highest intensity around ZT0. The intensity at other measured ZTs was significantly lower or below the detection level (Figure 1.2 F). This shows that the PTTHns are active one day before eclosion prior to ZT0. As CaLexA reports the Ca^{2+} increase with a certain delay, the amount of which is unknown, the exact time of PTTHn activity remained undetermined.

c. The *in vivo* activity of PTTHn in the intact pupae shows two peaks

To assess the activity of PTTHn and the PG more precisely in intact developing pupae, the Activity-Regulated Gene-Luciferase reporter (ARG-Luc) was used (Chen et al., 2016). ARG-Luc utilizes a transgenic construct containing the transcription factor binding site of the activity-regulated gene *lola*, separated from the *luciferase* gene with a *stop* site. Expression of Flippase enzyme by *Ptth-Gal4* flips out the *stop* sequence and *lola-luciferase* becomes active. At the onset of the activity of the neuron or cell of interest, Luciferase is produced. When the substrate luciferin is added, the luciferin/Luciferase reaction emits photons that are counted and measured as a neuronal activity reporter (Figure 1.2 A).

ARG-Luc in the PTTHn was driven (*Ptth::2A> ARG-Luc*) in DD, and photons were counted. The data was then sorted according to Zeitgeber time, which revealed no clear combined temporal pattern of PTTHn activity (Figure 1.2 C). Then the data was rearranged according to the time of eclosion (Figure 1.2 B). This revealed a monophasic circadian activity (~24h) of the PTTHn with two peaks around -31h and -6h before eclosion (Figure 1.2 D). The same approach was used for the activity of PG (*phm> ARG-Luc*) and showed three peaks in the average PG activity at around -40h, -25h, and a large activity peak at the time of eclosion (Figure 1.2 E). Since the -40h peak precedes the PTTH -31h peak, it seems that PTTH signaling is not generally required for PG activity. The two other PG peaks follow the PTTH peaks with a ~6h delay which suggests that PTTH determines the phase of PG activity. It should be noted that after eclosion, a sudden increase in the photon counts is recorded from both PG and PTTHn. This increase most likely is due to the loss of the photon-absorbing puparium after eclosion. After eclosion, the PTTH peak increased about 1.6-fold and the PG peak about 2.6-fold, compared to the pre-eclosion values.

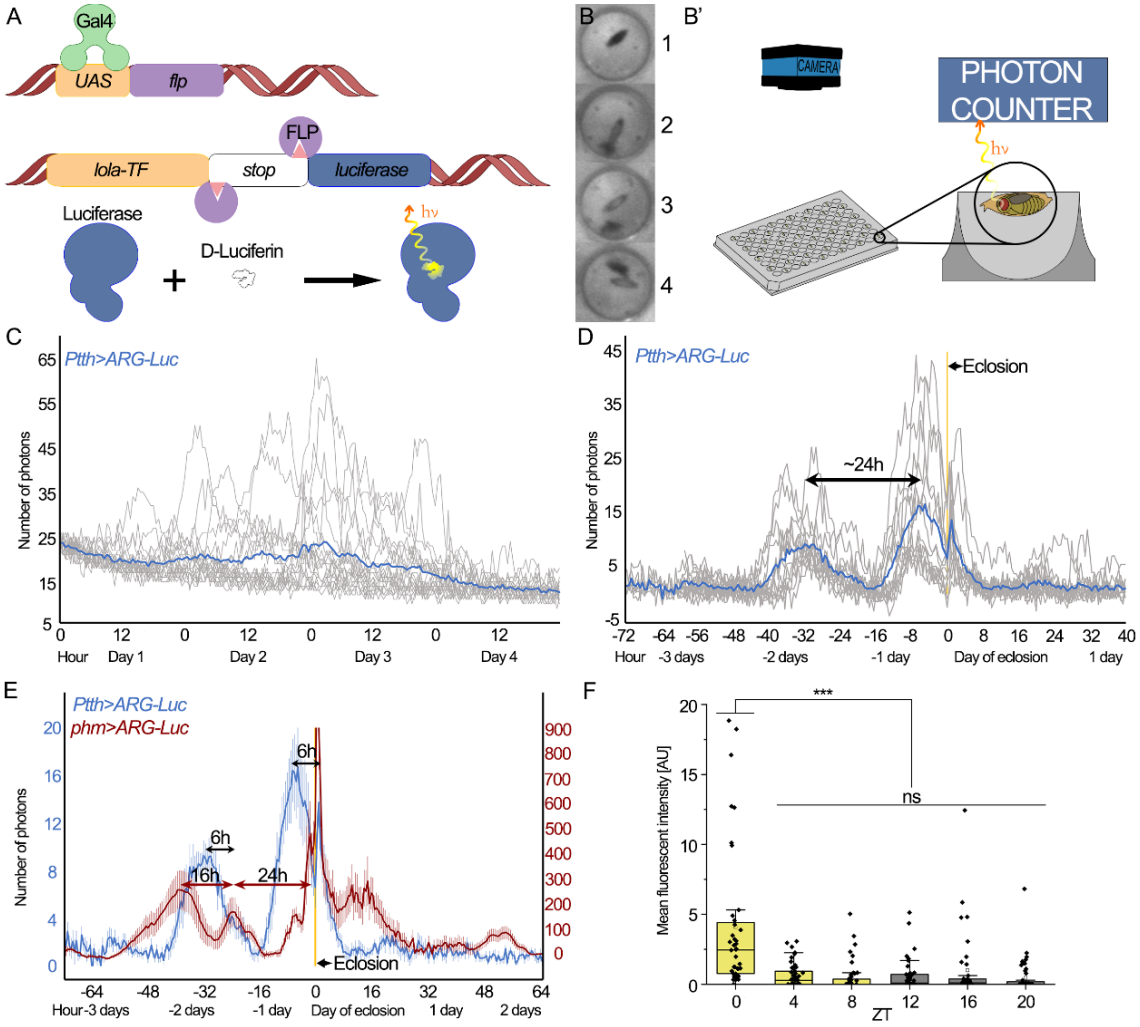

Figure 1.2. PTTHn and PG activity before eclosion as reported via ARG-Luc. A Schematic depiction of the ARG-Luc system. Gal4 drove the expression of *flp* in the cell of interest. The resulting Flippase removed the *stop* sequence between the binding site of the immediate early gene *lola* and *luciferase*. Therefore, upon activation, *lola* was expressed and drove the expression of Luciferase which bound to luciferin and emitted a photon. **B-B'** Schematic representation of the *in vivo* imaging setup. **B** A camera recorded the activity of the flies which allowed detecting the moment of eclosion for each fly. From top to bottom: **1.** Before eclosion, **2.** Eclosing fly, **3.** Fully eclosed with unexpanded wings, **4.** After wing expansion. **B'** The flies were located in 96 well plates, glued to a sheet of transparent plastic. A photon counter measured the *in vivo* activity of the tissue of interest. **C** The PTTHn activity of 21 flies was measured but the data from seven flies were removed because they showed no activity (possibly the flies were not close enough to the detector or in a bad orientation). The PTTHn activity of the remaining 14 flies (gray) was arranged based on the ZT which resulted in no notable circadian pattern of average activity (blue). **D** The activity of the flies plotted according to the eclosion time (yellow line) showed two peaks at -31h and -6h prior to eclosion in the average activity. These two peaks were about 25h apart. **E** The average activity of PTTHn (blue) and PG (dark red, n=22) plotted together with error bars indicating SEM. PG activity showed three peaks at around -40h, -25h, and a large peak at the time of eclosion. The -25h and the eclosion peaks were delayed by six hours compared to the PTTH peak. The peaks immediately after eclosion were possibly artifacts because of increased photons yielded after the fly eclosed from the puparium. **F** The mean GFP fluorescent intensity measured from *Ptth> CaLexA*. The measurements were done in 4-hour intervals and showed that at ZT0 (lights on) the mean intensity was significantly higher compared to other ZTs. ZT0 was the expected time of eclosion.

2. The sLN$_v$s are not the only clock neurons that provide synaptic inputs to the PTTH neurons

The nomenclature used for anatomical descriptions is based on Ito et al. (2014) for the brain and Court et al. (2020) for the VNC. In each brain hemisphere, a pair of PTTHn are situated such that their cell bodies are located in the pars lateralis part of the brain. Their dendrites branch through the superior neuropils and send their axons contralaterally to the esophagus orifice and then leave the brain via the nervi corporis cardiacii to innervate the PG and terminate there (Figure 1.3 A, B). The PDF$^+$ sLN$_v$s project through the posterior lateral fascicle from the accessory medulla to the superior neuropils (Figure 1.3 B"). Also, most dorsal clock neurons such as DN1$_a$s, DN1$_p$s, DN2s, LN$_d$s, and LPN project to the superior protocerebrum of the brain (Figure 1.3 A"). The axonal projections of these clock neurons come close to PTTHn dendrites in the superior protocerebrum (Figure 1.3 A', B'). To check for the presence of synaptic connections between clock neurons and PTTHn, syb-GRASP was used (Macpherson et al., 2015). This revealed a *Pdf-LexA; Ptth-Gal4> syb-GRASP* signal in this area (Figure 1.3 C). However, its low intensity suggests that the connection between the PTTHn and sLN$_v$s is not based on intense classic synaptic transmission but rather on non-synaptic peptidergic connection. This is in line with the previous description of peptidergic sNPF signaling from the sLN$_v$s to the PTTHn (Selcho et al., 2017). To test for connections between the PTTHn and DN1$_p$s, *Pdf-LexA, Clk4.1M-Gal4> syb-GRASP* was used (Figure 1.4 D). For the rest of the clock neurons (DN1$_a$s, DN2s, LN$_d$s, and LPNs), *R43D05-LexA; Ptth-Gal4> syb-GRASP* was used (Figure 1.3 E; for the specificity of R43D05 see Appendix 4 and Sekiguchi et al., 2020). In both cases (Figure 1.3 D-E) the syb-GFP signal in the superior brain was visible and spread in a large area.

To assess the directionality of connections between the clock and PTTHn, the retrograde BAcTrace and anterograde *trans*-Tango MkII tracing tools were used (Cachero et al., 2020; Sorkaç et al., 2022). For the PDF$^+$ sLN$_v$s and lLN$_v$s the *Pdf-LexA; Ptth-Gal4> BAcTrace* (Figure 1.3 F) showed that only the sLN$_v$s are upstream of PTTHn (Figure 1.3 F'-F"). For the dorsal clock neurons (DN1$_a$s, DN2s, and LN$_d$s), *R43D05-LexA; Ptth-Gal4> BAcTrace* (Figure 1.3 G, H) showed that while both DN1$_a$ neurons are presynaptic to PTTHn, only one DN2 provides input to the PTTHn (Figure 1.3 H'-H"). The *Ptth::2A-Gal4; AstA::2A-LexA> BAcTrace* showed that two out of three LPN neurons are connected to the PTTHn (Figure 1.3 I'-I"). Finally, to investigate how many DN1$_p$s are presynaptic to the PTTHn, *Ptth::2A-Gal4; Clk4.1M-LexA> BAcTrace* was used. Unfortunately, these flies never passed the L1 stage and died. We therefore used forward tracing with *trans*-Tango in combination with immunostaining against PTTH (Figure 1.3 J, K). Both sparse *Pdf> trans-Tango* and broad clock *Clk856> trans-Tango* showed that PTTH neurons are postsynaptically located to the clock neurons (Figure 1.3 J', K').

The presence of GRASP signal in the superior protocerebrum between the dorsal clock neurons and PTTHn suggested the presence of synaptic connections between the PTTHn and clock neurons (other than the sLN$_v$s). BAcTrace and *trans*-Tango together showed that both PTTHns receive input from The DN1$_a$s, one DN2, and two LPNs.

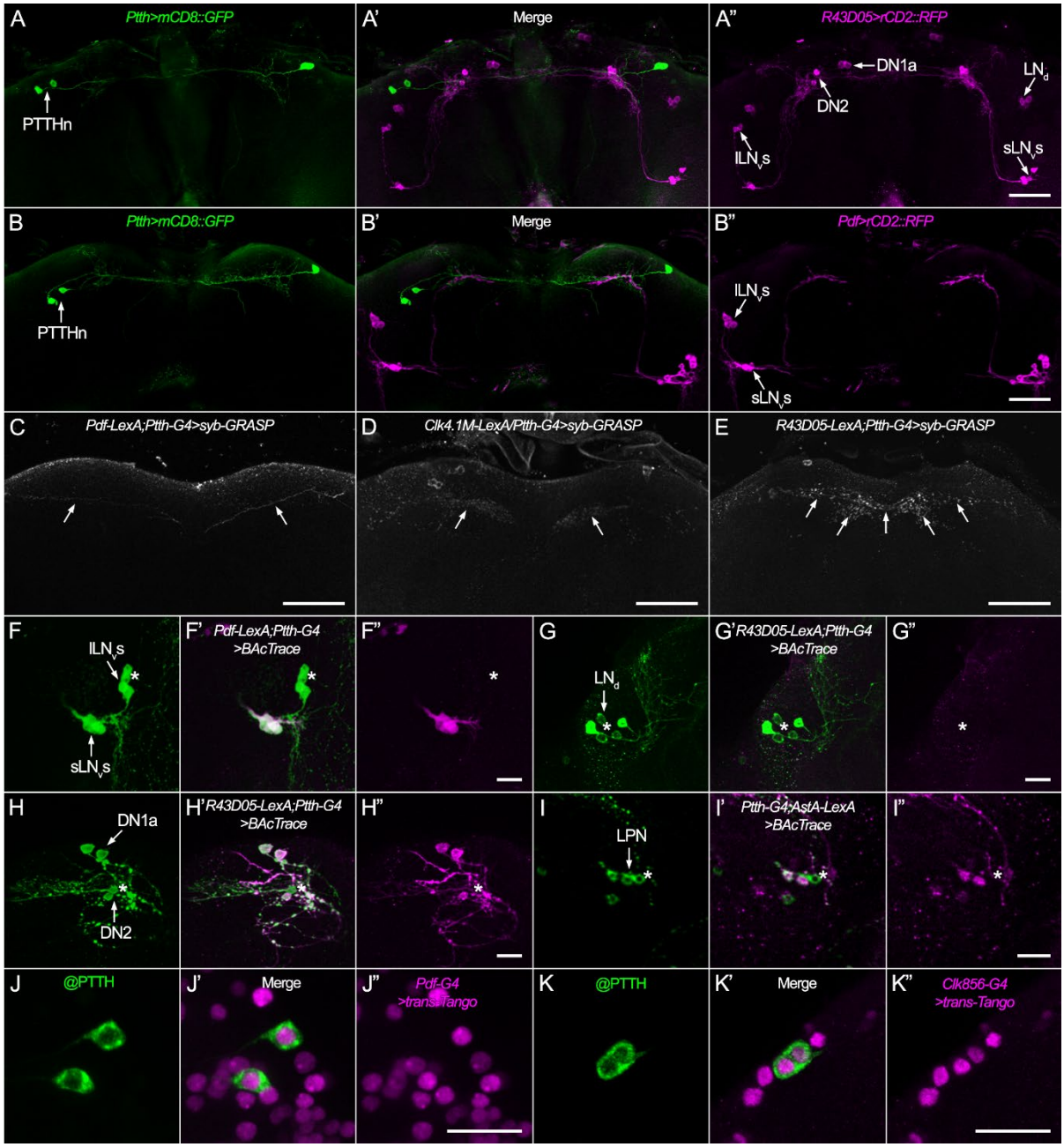

Figure 1.3. The PTTHns were postsynaptic to different clock neurons. A-A" Expression of GFP in PTTHn and RFP in clock neurons showed that PTTHn and clock neurons processes overlapped in the superior protocerebrum. **A** Expression of mCD8::GFP in PTTHn (arrows). PTTHn projections arborized in the superior brain. **A'** In the superior region of the brain the processes of PTTHn and clock neurons overlapped. A" Using *R43D05-LexA* driver rCD2::RFP was expressed in sLN_vs, LN_ds, $DN1_a$ and DN2 neurons (arrows). All these clock neurons had processes located in the superior brain region. **B-B"** The PDF^+ sLN_vs also terminated in the superior brain where they met PTTHn processes. **B** Again mCD8::GFP was expressed in PTTHn (arrows). **B'** PTTHn and sLN_vs overlapped in the superior brain regions but lLN_vs and PTTHn projections did not overlap anywhere in the brain. **B"** The expression of rCD2::RFP was driven by *Pdf-LexA* in sLN_vs and lLN_vs (arrows). These proximities suggested that the synaptic connection between different clock neurons and PTTHn was possible. To check for these synaptic connections syb-GRASP was used (**C-E**). **C** The syb-GRASP signal between the sLN_vs and PTTHn was weak (arrows), suggesting that the clock information from the sLN_vs is non-synaptically relayed to the PTTHn. **D** Using *Clk4.1M-LexA* driver to drive the presynaptic part of syb-GRASP

expression in eight $DN1_p$s, the synaptic connection between PTTHn and $DN1_p$s was tested. Presence syb-GRASP signal in the superior protocerebrum (arrows) showed this synaptic connection existed. However, it was not possible to identify how many of them participate in signaling to the PTTHn due to the lethality of the appropriate BAcTrace flies. **E** *R43D05-LexA* neurons comprised $DN1_a$, DN2s, LN_ds, and LPNs. Using *R43D05-LexA; Ptth-Gal4* in combination with syb-GRASP showed $DN1_a$, DN2s, LN_ds, and LPNs provided synaptic input to PTTHn. To check which clock neurons provided synaptic input to PTTHn BAcTrace was used (**F-I**). **F** BAcTrace using *Pdf-LexA; Ptth-Gal4* showed all PDF^+ sLN_vs and lLN_vs in GFP channel (arrows). **F'-F"** BAcTrace between the PDF^+ clock neurons and PTTHn showed that only sLN_vs were presynaptic to PTTHn not lLN_vs (asterisk). **G** BAcTrace using *R43D05-LexA; Ptth-Gal4* showed five LN_ds in GFP channel (arrows). **G'-G"** Lack of tdTomato expression in all neurons (asterisk) meant none of the LN_ds were presynaptic to the PTTHn. **H** BAcTrace using *R43D05-LexA; Ptth-Gal4* showed two $DN1_a$s and two DN2s in GFP channel (arrows). **H'-H"** While both $DN1_a$s provided input to the PTTHn, only one of the DN2s was involved in signaling to the PTTH neurons (the DN2 that did not express tdTomato is marked by an asterisk). **I** BAcTrace using *Ptth::2A-Gal4; AstA::2A-LexA* showed three LNPs in GFP channel (arrows). **I'-I"** Two out of three LPNs expressed tdTomato meaning they were presynaptic to the PTTH neurons (the LPN that did not express tdTomato was marked by an asterisk). To test if both PTTHn received input from clock neurons *trans*-Tango was used. **J** PTTHns were marked by anti-PTTH (green). **J'** The nucleus of both PTTHns was marked by the RFP expressed by *Pdf> trans-Tango.* **J"** *Pdf> trans-Tango* expressed RFP in the nucleus of all neurons postsynaptically located to PDF^+ neurons (magenta). **K** PTTHns were marked by anti-PTTH (green). **K'** The nucleus of both PTTHn was marked by the RFP expressed by *Clk856> trans-Tango.* **K"** *Clk856> trans-Tango* expressed RFP in the nucleus of all neurons postsynaptically located to all clock neurons except lLN_vs (magenta). Positive *trans*-Tango signal in both PTTH stainings (**J'** and **K'**) showed that both PTTH neurons were postsynaptic to many clock neurons including the sLN_vs. *Scale bars*: A-E 50 µm and F-K 20 µm.

3. The role of clock neurons in temperature-entrained eclosion rhythmicity

Performing eclosion assays and data acquisition of this part was done by Sina Grimm (part of her MSc thesis supervised by Emad Amini) and Emad Amini, and data analysis by Emad Amini (Grimm, 2023).

Clock neurons are capable of receiving Zeitgeber information such as light and temperature to entrain their internal molecular clock. The role and molecular mechanism of temperature entraining is well studied (Glaser and Stanewsky, 2005; Stanewsky et al., 1998; Yoshii et al., 2005, 2002). The DN2s are important clock neurons for temperature entrainment and receive temperature input (Kaneko et al., 2012). To check which clock neurons are involved in temperature entrainment of eclosion rhythmicity, the different subgroups of clock neurons were silenced using Kir2.1 under temperature entrainment as described for the Opto-DEM (see Materials and Methods 5.b) with a 12:12 warm-cold cycle WC/DD during larval stages. As soon as wandering larvae appeared, the flies were moved to constant DD and 20 °C. The eclosion monitoring was also done under constant DD and 20 °C. Different driver lines were used to drive Kir2.1 expression in different clock neurons. These drivers were *Clk856-Gal4* for all clock neurons, *Pdf-Gal4* for PDF^+ LN_vs, *R43D05-p65.AD; R93B11.DBD* split Gal4 driver for $DN1_a$s, *R51H05-Gal4* for 12 $DN1_p$s, *Clk-9M-Gal4; LN-Gal80* for DN2s and finally *R11B03-p65.AD; R65D05.DBD* for LPNs.

Silencing all clock neurons led to an arrhythmic eclosion pattern (Figure 1.4). Even though the autocorrelation RI indicated rhythmicity, multiple MESA peaks with a main period of 19.5 and

an LS power close to 0) speak for arrhythmic eclosion (Table 1.1). Silencing of the PDF^+ clock neurons strongly affected the rhythmicity and rendered it arrhythmic. While RI did not show arrhythmicity, multiple MESA peaks and an LS power of 0 again indicated arrhythmicity. Since, the *Pdf-Gal4* line is a stronger driver than *Clk856-Gal4*, a more effective silencing was expected. Silencing with other driver lines for the $DN1_a$s, twelve of $DN1_p$s, DN_2s, and LPNs (see Appendix 5 and Figure 6.5) did not impair rhythmic eclosion (Figure 1.4, Table 1.1). However, $DN1_p$s and DN2s showed irregularly broad peaks with reduced amplitudes compared to controls.

In conclusion, silencing all clock neurons or PDF^+ neurons only resulted in arrhythmic eclosion, suggesting that these neurons are important for temperature entrainment of eclosion. It also seems that $DN1_p$ and DN2s play a role. At the moment there is no effective driver line to silence the LN_ds and they may as well play a role in temperature entrainment of the eclosion, which was not investigated in this thesis.

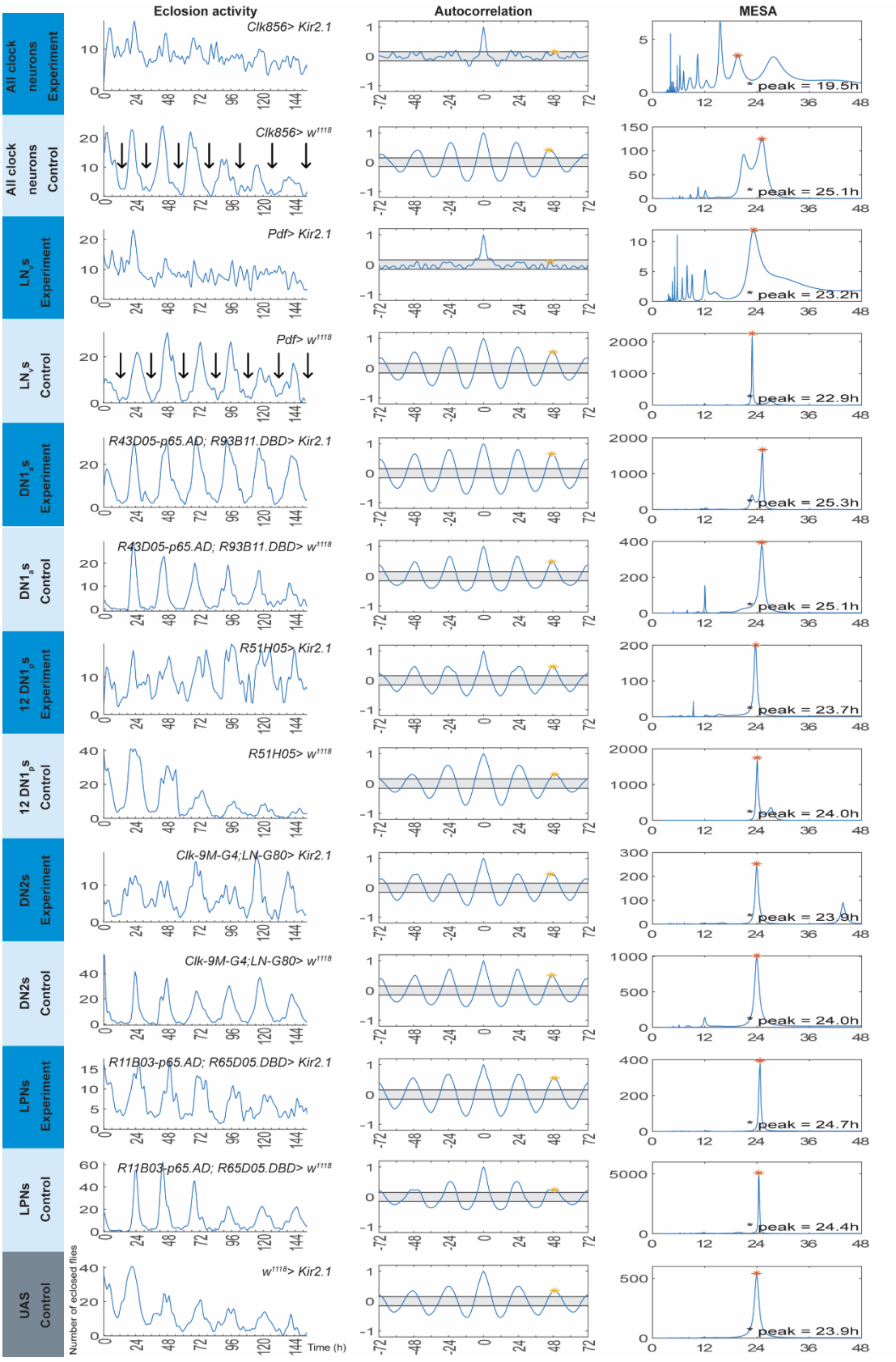

Figure 1.4. Silencing all or only the PDF^{+} clock neurons caused arrhythmic eclosion in temperature-entrained flies. Silencing all clock neurons using *Clk856-Gal4> Kir2.1* showed an arrhythmic eclosion pattern. Compared to controls (*Clk856-Gal4> w^{1118}* and *w^{1118}> Kir2.1*) peaks and valleys separated by nearly 24h intervals (arrows in Gal4 control) were not distinguishable. However,

the RI and eJTK analyses indicated rhythmicity (see Table 1.1) while LS power and MESA several peaks with a 19.5h period support arrhythmicity. The Gal4 control also showed a broad two-peaked MESA but with a period close to 24h. Silencing the PDF^{+} LN_vs (*Pdf> Kir2.1*) resulted in an arrhythmic eclosion pattern without ~24h peak intervals. Again, MESA showed several peaks and RI resulted in weak rhythmic value. LS and eJTK analyses both showed arrhythmic values. Silencing $DN1_a$s (*R43D05-p65.AD; R93B11.DBD> Kir2.1*), twelve of the $DN1_p$s (*R51H05> Kir2.1*), DN_2s (*Clk-9M-G4; LN-G80> Kir2.1*), and LPNs (*R11B03-p65.AD; R65D05.DBD> Kir2.1*) did not impair rhythmicity in temperature-entrained flies. However, eclosion patterns of $DN1_p$ and DN2 silenced experiments when compared to their controls, showed broad eclosion peaks with about two times lowered amplitude.

Table 1.1. Rhythmicity index (RI; derived from autocorrelation analysis), Lomb-Scargle (LS), and eJTK (Benjamini-Hochberg corrected) analyses for eclosion rhythmicity after silencing different clusters of clock neurons in temperature-entrained flies. Arrhythmic values are shown in red (see Figure 1.4).

Genotype	Silenced clock cluster	Total number of flies	Error	Period	Rhythmicity index	Lomb-Scargle	eJTK BH bf corrected p
Clk856> Kir2.1	All	1383	3.3%	19.5h	0.15	0.3	0.01
Clk856> w^{1118}	All control	1253	3.3%	25.1h	0.41	27.0	$3.6*10^{-17}$
Pdf> Kir2.1	LN_vs	1483	6.1%	23.2h	0.11	0.0	0.06
Pdf> w^{1118}	LN_vs control	1453	5.2%	22.9h	0.55	39.8	$9.5*10^{-27}$
R43D05-p65.AD; R93B11.DBD> Kir2.1	$DN1_a$s	1943	1.5%	25.3h	0.65	52.5	$1.1*10^{-28}$
R43D05-p65.AD; R93B11.DBD> w^{1118}	$DN1_a$s control	1015	0.1%	25.1h	0.49	32.4	$2.7*10^{-26}$
R51H05> Kir2.1	12 $DN1_p$s	1535	4.9%	23.7h	0.47	22.7	$2.8*10^{-17}$
R51H05> w^{1118}	12 $DN1_p$s control	1693	7.4%	24.0h	0.31	18.5	$1.5*10^{-16}$
Clk-9M-G4; LN-G80> Kir2.1	DN2s	1067	5.0%	23.9h	0.46	30.4	$6.0*10^{-17}$
Clk-9M-G4; LN-G80> w^{1118}	DN2s control	1827	6.1%	24.0h	0.51	40.2	$4.4*10^{-34}$
R11B03-p65.AD; R65D05.DBD> Kir2.1	LPNs	1135	0.1%	24.7h	0.55	33.5	$8.0*10^{-19}$
R11B03-p65.AD; R65D05.DBD> w^{1118}	LPNs control	1877	3.5%	24.4h	0.24	30.2	$8.1*10^{-28}$
w^{1118}> Kir2.1	UAS control	2457	3.0%	23.9h	0.35	13.3	$7.0*10^{-09}$

4. The PTTH neurons are exclusively peptidergic

Often, peptidergic neurons co-express classic neurotransmitters along with peptides (Hökfelt et al., 1987; Kim et al., 2017; Nässel, 2018). To understand whether PTTHns only release PTTH neuropeptide or also co-release neurotransmitters, intragenic T2A-Gal4 lines for vesicular glutamate transporter (*VGlut*), vesicular γ-aminobutyric acid (GABA) transporter (*VGAT*), and choline acetyltransferase (*ChAT*) were used to drive nuclear mCherry expression in glutamatergic, GABAergic, and cholinergic neurons, respectively. The PTTHn were not labeled by the glutamate (Figure 1.5 A-A"), GABA (Figure 1.5 B-B"), or acetylcholine markers (Figure 1.5 C-C"). Unfortunately, due to the lack of a suitable driver line for glycinergic neurons, the colocalization of PTTH with glycine could not be tested. Yet only very few glycinergic neurons have so far been identified in the fly brain. Therefore, the PTTH neurons most likely solely use peptidergic transmission and lack classic neurotransmitters.

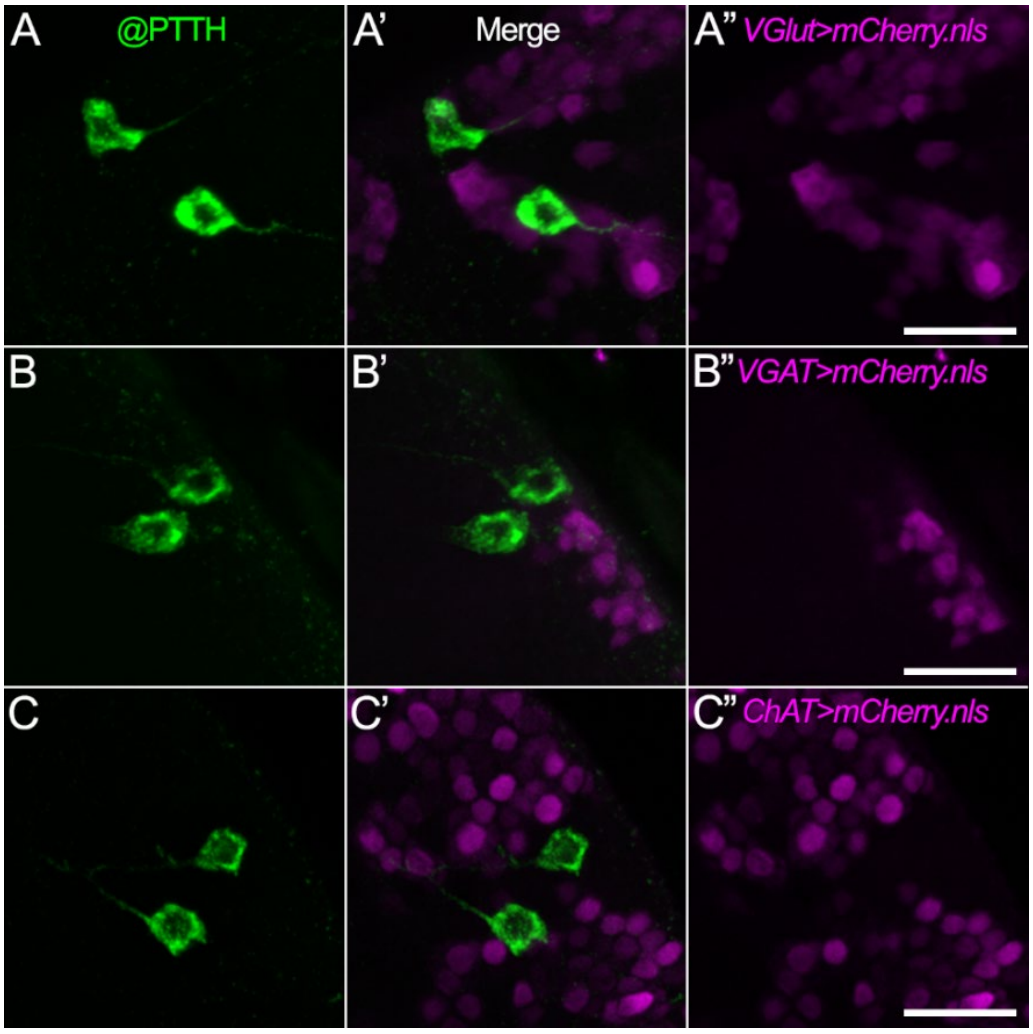

Figure 1.5. The PTTH neurons are exclusively peptidergic. The PTTHn were stained with anti-PTTH (green; **A**, **B**, and **C**). Nuclear mCherry (magenta) was driven in glutamatergic (VGlut**; A"**), GABAergic (VGAT**; B"**), and cholinergic neurons (ChAT**; C"**). Lack of colocalization between PTTH and glutamate (**A'**), GABA (**B'**), or acetylcholine (**C'**) suggested that PTTHn were exclusively peptidergic and did not produce classic neurotransmitters. *Scale bars*: 20 μm.

5. *Drosophila* insulin-like peptide 7 and -8 signaling is not necessary to maintain eclosion rhythmicity

ILPs assist cholesterol shuttling to the PG therefore important for ecdysteroids production (Boulan et al., 2013; Caldwell et al., 2005; Colombani et al., 2005; Mirth et al., 2005; Moeller et al., 2017; Texada et al., 2019). *Drosophila* produces eight different ILPs (Brogiolo et al., 2001; Colombani et al., 2012; Garelli et al., 2012; Ikeya et al., 2002; Liu et al., 2016). The insulin-producing cells located in the PI of the brain produce ILP1, -2, -3, and -5, and the fat body produces ILP6 (de Velasco et al., 2007; Okamoto et al., 2009). ILP 1-6 act through InR (Fernandez et al., 1995). PG expresses InR which activates TOR and Warts signaling pathways (Texada et al., 2020). ILP7 and -8 act through LGR4 (Imambocus et al., 2022), and LGR3 respectively (Colombani et al., 2015; Garelli et al., 2015; Vallejo et al., 2015). ILP8 is produced by the imaginal disks (Gontijo and Garelli, 2018). ILP8 secretion from abnormally grown imaginal disks suppresses ecdysone production and inhibits the PTTHn (Colombani et al., 2015; Garelli et al., 2015; Jaszczak et al., 2016; Vallejo et al., 2015). Therefore, different insulin signaling pathways are involved in developmental timing.

A recent study tested the eclosion rhythmicity of *Ilp2*, *-3*, *-5*, and *InR* null mutants and reported rhythmic eclosion for all of them (Cavieres-Lepe et al., 2023). To assess if the ILP7 and ILP8 signaling pathways affect the rhythmicity and timing of eclosion, we performed eclosion assays using *Ilp7* (Grönke et al., 2010) and *Ilp8* mutants (Garelli et al., 2012). In addition, mutants for the ILP8 receptor LGR3 were tested. For both *Ilp8* and *Lgr3*, the nonmutant background lines were available, they were used as control groups. The results of the eclosion assays are summarized in Figure 1.6 and Table 1.2. All mutants showed a rhythmic eclosion pattern in DD according to autocorrelation and eJTK analysis. Furthermore, all lines except for the *Ilp8* control (*Ilp8* BG), were found to be rhythmic by LS analysis. In case of *Ilp8* BG, the low RI and LS power were probably due to the low rhythmicity after day four during the assay. The lower eclosion rate in final days was caused by high lethality rate. Other than *Ilp7* mutants, the rest of the tested groups showed a strong reduction of the number of eclosion events over time.

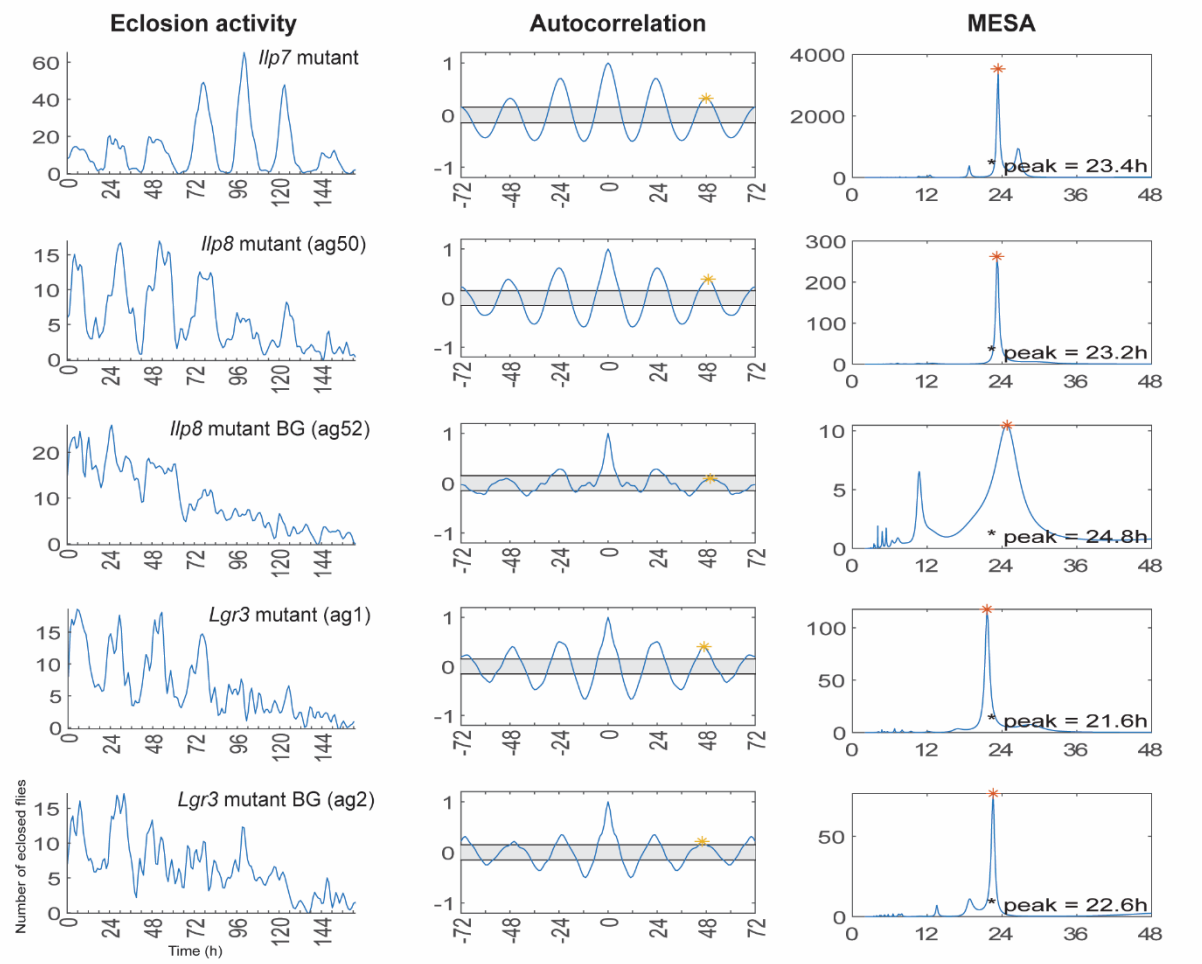

Figure 1.6. Eclosion profiles of *Ilp7* and *-8*, as well as *Lgr3* mutants. All mutant groups showed rhythmic eclosion activity according to autocorrelation and MESA analysis. However, in *Ilp8* mutant (ag50) and its control (ag52), and *Lgr3* mutant (ag1) and its control (ag2), the amplitude of the activity peaks reduced over time. This reduction was a result of high lethality rates until eclosion in these lines. *Ilp8* control also showed a very broad MESA peak. The number of flies, RIs, and results of LS and eJTK analysis of these experiments are shown in **Table 1.2**.

Table 1.2. Rhythmicity analysis of the eclosion in *Ilp7*, *-8*, and *Lgr3* mutants (see Figure 1.6). Arrhythmic values are shown in red.

Genotype	Number of flies	Error	Period	Autocorrelation	Lomb-Scargle	eJTK BH bf corrected p
Ilp7 mutant	2231	2.3%	23.4h	0.32	31.5	$2.5*10^{-31}$
Ilp8 mutant (ag50)	1014	4.3%	23.2h	0.39	20.7	$3.9*10^{-14}$
Ilp8 BG (ag52)	1730	1.0%	24.8h	0.09	0.0	0.06
Lgr3 mutant (ag1)	1143	5.6%	21.6h	0.40	11.3	$9.1*10^{-08}$
Lgr3 BG (ag2)	1154	3.5%	22.6h	0.22	2.8	$5.0*10^{-05}$

Chapter II: Connections between circadian clock neurons and the Eclosion hormone neurons

1. Anatomical characterization of synaptic inputs from clock to EH neurons

The staining experiments explaining the connections of the clock to the EH neurons and their data acquisition are performed by Sina Grimm (part of her MSc thesis; Grimm, 2023). The analysis of these data was done by Emad Amini. The rest of the experiments were entirely performed and analyzed by Emad Amini.

In the larval brain, V_m neurons processes are close to the sLN_vs (Blanchardon et al., 2001). The arborizations of PDF-tri and V_m neurons are close together in the pharate brain (Selcho et al., 2018). However, PDF-tri neurons are not clock neurons (Gatto and Broadie, 2011) and no one has ever shown that V_m neurons receive input from the clock neurons. Recently, the non-canonical EH neurons have been discovered, and it is still unclear if they are important for the initiation or timing of eclosion. To find out whether V_m and non-canonical EH neurons receive input from the clock seems very important in the context of eclosion initiation, as it is unknown what starts the EH/ETH feedback loop. Clock input to the EH^+ neurons is one putative way how eclosion could be initiated and timed. The focus of this part of this chapter therefore is to characterize the synaptic connections from the clock to the EH^+ neurons and to identify which clock neurons possibly provide these inputs.

The cell bodies of the V_m neurons were located superficially at the anterior cell body rind of the SMP. The dendrites of these neurons were arborized in the median region of SMP and around the esophagus orifice (Figure 2.1 A'-A"). In the brain, the arborization of each V_m neuron bifurcated ventral to the cell body. While the medial branch projected through the median bundle (MBDL) another loop-shaped lateral process ran in parallel but outside of the MBDL. Both projections descended and met around the esophagus orifice (Figure 2.1 A-A'). Each neurons axon projected ventral to the esophagus orifice and arborized in the ventral suboesophageal zone (SEZ). Then the axonal neurite descended through the cervical connective to the midline of VNC through the median dorsal abdominal tract (MDT) and descended to the abdominal ganglia (Figure 2.1 B-B'). In the VNC midline, the descending neurites of V_ms also had dendritic boutons (Figure 2.1 B") that formed synapses with PNS input neurons (see IV.1.b and IV.3.a). In *Drosophila*, another set of V_m fibers was found previously that passed through nervi corporis cardiacii projected to CC (Clark et al., 2004; Horodyski et al., 1993; Selcho et al., 2018).

In the median region of the SMP, the V_m neuron dendrites came in close contact with the sLN_vs, $DN1_as$, $DN1_ps$, DN2s, LN_ds, and LPNs (Figure 2.2 A'). To test whether there were synaptic connections between the PDF^+ sLN_vs and V_m neurons, *Pdf-Gal4; Eh::2A-LexA> syb-GRASP* was used. In the SMP region, a strong syb-GRASP signal was discernable that was limited to a small region of the SMP (Figure 2.2 C). To test for synaptic connectivity between the other clock and V_m neurons, *Clk856-Gal5; Eh::2A-LexA> syb-GRASP* flies were used that showed a signal in a larger less confined area of SMP, which was however weaker than the *Pdf-Gal4* associated GRASP signal (Figure 2.2 D). Since the sLN_vs are included in both driver line

expression patterns, the weaker signal is possibly due to the weaker driving properties of the *Clk856-Gal4* line in sLN$_v$s compared to *Pdf-GAL4*. Since *Clk856-Gal4* expression pattern includes nearly all clock neurons, other clock neurons may be presynaptic to V$_m$s.

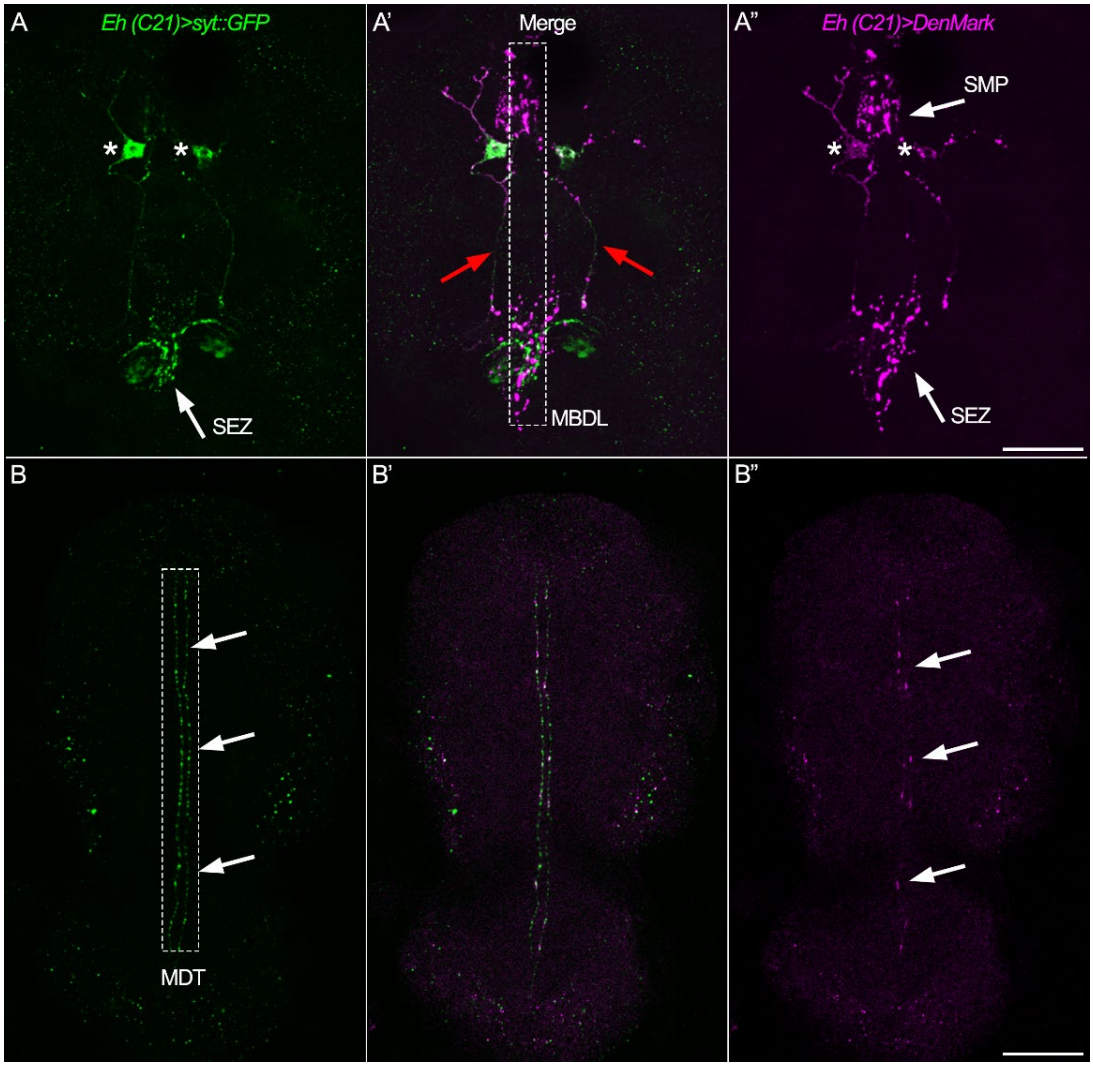

Figure 2.1. The dendritic boutons and terminals of the V$_m$ neurons. To check the input and output sites on V$_m$ neurons projections in brain and VNC, the presynaptic marker DenMark together with the postsynaptic marker syt::GFP was expressed using *Eh (C21)-Gal4*. **A** The V$_m$ neuron cell bodies (asterisks) were located superficially at the superior medial protocerebrum (SMP) cell body rind part of the brain. In the brain, the syt::GFP expression was limited to the suboesophageal zone (SEZ; arrows). **A'** The arrangement of dendritic boutons (DenMark signal) and terminals (syt::GFP signal) of the V$_m$ neurons in the brain. The processes of the V$_m$ neurons ventral to their cell bodies bifurcated and produced two branches. The medial branch descended through the median bundle (MBDL; dashed box) and the lateral branch produced a loop (red arrows) outside of the MBDL. Both branches descended to the SEZ and ran around the esophagus orifice. **A"** The dendritic boutons were mostly scattered in SMP, ventral to the esophagus orifice and around it (arrows) and along the neurons. **B-B"** The V$_m$ neurons sent their projections down to the midline of the VNC through the cervical connective to the median dorsal abdominal tract (MDT; dashed box). **B** In the VNC, the syt::GFP signal was scattered along the neuronal processes (arrows). **B'** The arrangement of presynaptic (DenMark signal) and postsynaptic (syt::GFP signal) sites of the V$_m$ neurons in the VNC midline showed possible input and output sites of the V$_m$s. **B"** The dendritic boutons (DenMark signal) were sparsely located along the neuronal processes (arrows) and possibly make synaptic contact to the PNS neurons. *Scale bars*: 20 µm.

The *Eh::2A-LexA* driver line was able to drive expression in four of the non-canonical D_l neurons (Figure 2.2 B") and very rarely in two D_m neurons. However, the expression was much weaker compared to the V_m neurons. The cell bodies of the four D_ls are located superficially in the posterior cell body rind close to the posterior slope part and they project into dorsal-posterior and lateral-posterior regions of the brain. One D_l neuron projects into the medulla of the optic lobe. The morphology of these non-canonical neurons fits the description by Scott et al. (2020). The D_l arborizations in the superior protocerebrum and especially superior lateral protocerebrum (SLP) are closely located near the axonal region of clock neurons except for the lLN_vs (Figure 2.2 B'). However, the single D_l that projects to the layer M7/8 of medulla comes close to the lLN_vs projections in the medulla. To check for the possibility of synaptic input from the clock to the D_l neurons, syb-GRASP was used again. *Pdf-Gal4; Eh::2A-LexA> syb-GRASP* flies showed a strong and scattered signal in the SLP regions (Figure 2.2 C). On the other hand, *Clk856-Gal5; Eh::2A-LexA> syb-GRASP* did not produce a clear GFP signal between the clock and the D_l neurons (Figure 2.2 D).

To investigate the directionality and to find further synaptic partners, BAcTrace (Figure 2.2 E-H) and *trans*-Tango (Figure 2.2 I-L) were used. The *Pdf-LexA; Eh::2A-Gal2> BAcTrace* expression showed a positive tdTomato signal in both sLN_vs and lLN_vs (Figure 2.2 E'). The only possible candidate to form synapses with the lLN_vs was the medulla projecting D_l neuron. To check for the rest of the clock neurons, *R43D05-lexA; Eh::2A-Gal2> BAcTrace* was used. *R43D05-lexA* drove BAcTrace expression in two LN_ds (Figure 2.2 F), both $DN1_a$s and both DN2s (Figure 2.2 G). Positive BAcTrace signal (tdTomato) was only very weakly visible in one LN_d neuron (Figure 2.2 F'-F"), all $DN1_a$s and DN2s (Figure 2.2 G'-G"). It was only possible to check the connection between the V_m and LPNs using *Eh (C21)-Gal4; AstA::2A-LexA> BAcTrace* flies. The resulting stainings showed tdTomato signal in two out of three LPNs (Figure 2.2 H'-H"). *trans*-Tango labeling showed that V_m is a postsynaptic partner to PDF^+ sLN_vs (*Pdf> trans-Tango*; Figure 2.2 I-I") and other clock neurons (*Clk856> trans-Tango*; Figure 2.2 J-J"). Moreover, *trans*-Tango showed that D_ls neurons are connected to PDF^+ clock neurons (*Pdf> trans-Tango*; Figure 2.2 K-K") but not to other clock neurons (*Clk856> trans-Tango*; Figure 2.2 L-L"), possibly again due to the weaker driving properties of the *Clk856-Gal4* line.

In summary, from syb-GRASP, BAcTrace and *trans*-Tango results it is clear that V_m neurons are strongly connected to the clock neurons and are downstream of the clock. Their strongest connections are made to the sLN_vs. The non-canonical D_ls are postsynaptic to all PDF^+ LN_vs possibly both sLN_vs and lLN_vs.

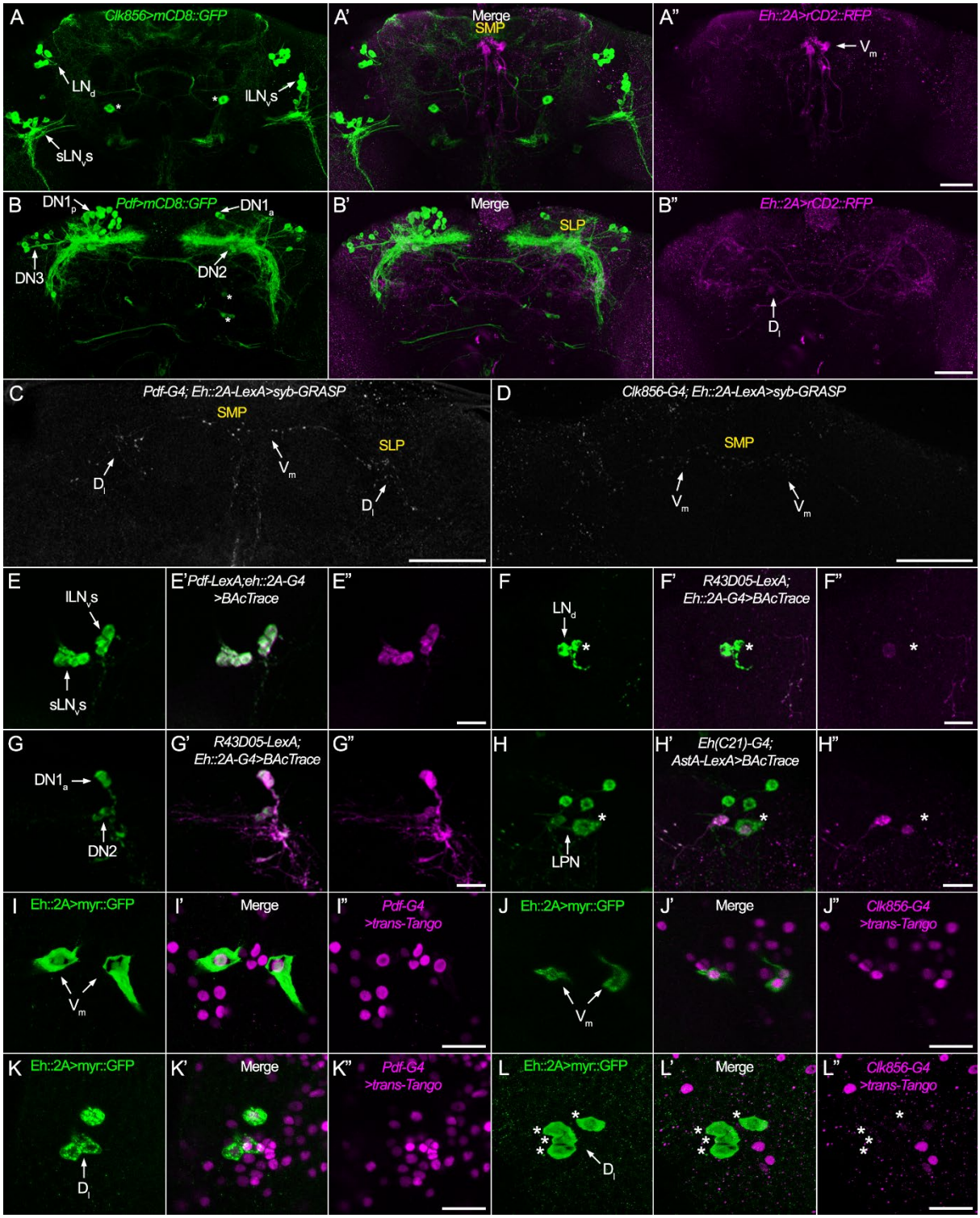

Figure 2.2. The EH neurons (V_m and non-canonical D_ls) receive synaptic input from clock neurons. A-A" The V_m neurons dendrites protruded to the medial superior medial protocerebrum (SMP), where they came into close contact with the dorsal terminal branches of sLN_vs axons and other clock neurons such as DN1s, DN2s, LN_ds, and LPNs. **A** Expression of mCD8::GFP in clock neurons using *Clk856-Gal4* (anterior plane). GFP expression in sLN_vs, lLN_vs, and LN_ds was visible (arrows), nevertheless, the driver line expressed GFP in some non-clock neurons as well (asterisks). **A'** In the medial SMP, the projections of the dorsal clock neurons and the sLN_vs (green) overlapped with V_m dendrites (magenta). **A"** Expression of rCD2::RFP in V_m neurons using *Eh::2A-LexA*. **B-B"** The non-canonical D_ls arborized in the superior lateral protocerebrum (SLP) neuropil and in the proximity of

dorsal clock neurons and sLN_vs. **B** Expression of mCD8::GFP in clock neurons using *Clk856-Gal4* (posterior plane). $DN1_a$, $DN1_p$, and DN3 neurons (arrows) as well as non-clock neurons were visible (asterisks). **B'** In the SLP, the projections of D_Is (magenta) and dorsal clock neurons (green) overlapped. **B"** Expression of rCD2::RFP marked D_Is. However, expression was not as strong as in V_ms. One D_I cell body was visible in the posterior slope cell body ring (arrow). **C** *Pdf-Gal4; Eh::2A-LexA> syb-GRASP* showed synaptic contact between the sLN_vs and both V_m neurons in the SMP and between D_Is and sLN_vs in the SLP. **D** *Clk856-Gal4; Eh::2A-LexA> syb-GRASP* showed synaptic contact between the V_m and clock neurons in the SMP but not between the clock and the D_Is. However, *Clk856-Gal4* driven GRASP signal was weaker than the GRASP signal from the *Pdf-Gal4* driver line, possibly due to the weaker driving properties of the *Clk856-Gal4* line. **E** BAcTrace using *Pdf-LexA; Eh::2A-Gal4* expressed GFP in sLN_vs and lLN_vs (arrows). **E'-E"** BAcTrace driven tdTomato in all PDF^+ neurons showed that both PDF^+ LN_vs were presynaptic to EH neurons. **F** *R43D05-LexA; Eh::2A-Gal4> BAcTrace* expressed GFP only in two of the LN_ds. **F'-F"** The positive tdTomato signal was only weakly expressed in one of the LN_ds (the cell body without tdTomato expression is marked with an asterisk). Therefore, only one of these LN_ds was synaptically connected to the EH neurons. **G** *R43D05-LexA; Eh::2A-Gal4> BAcTrace* successfully expressed GFP in both $DN1_a$ and DN2s (arrows). **G'-G"** Expression of tdTomato in $DN1_a$ and DN2 showed these neurons were providing input to the EH neurons. The expression of tdTomato in $DN1_a$ was stronger than in DN2s. **H** *Eh (C21)-Gal4; AstA-LexA* was used to check if LPNs were presynaptic to the V_m neurons. This driver marked all three LPNs with GFP expression (arrows). **H'-H"** From the three LPN neurons, two of them were involved in signaling to V_m neurons (the LPN without tdTomato expression was marked by an asterisk). **I** V_m neurons were marked by expression of myr::GFP (arrows). **I'-I"** *Pdf> trans-Tango* showed nuclear RFP expression in both V_m neurons meaning V_ms were postsynaptically connected to the sLN_vs. **J** myr::GFP expression in V_ms (arrows). **J'-J"** *Clk856-Gal4> trans-Tango* again showed that V_m neurons were the target of clock cells. **K** myr::GFP expression in D_Is (arrows). **K'-K"** *trans*-Tango with *Pdf-Gal4* confirmed that all D_Is were targets of PDF^+ clock neurons. **L** myr::GFP expression in D_Is (arrows). **L'-L"** *Clk856-Gal4> trans-Tango* was unable to express nuclear RFP in any of the D_Is (asterisks), therefore it was unclear whether D_Is received input from other clock neurons. The names of the neuropils were indicated with yellow letters. *Scale bars:* A-D 50 µm and E-L 20 µm.

2. All EH neurons are exclusively peptidergic

To test for the colocalization of classic neurotransmitters with EH, a small set of transmitter-related specific intragenic T2A-Gal4 lines was used. Similar to the PTTHn (see I.4), neither V_m nor any of the D_Is colocalized glutamatergic (Figure 2.3 A' and B'), GABAergic (Figure 2.3 C' and D'), or cholinergic (Figure 2.3 E' and F') marker expression. This suggests that the EH neurons only use peptides as intercellular messengers.

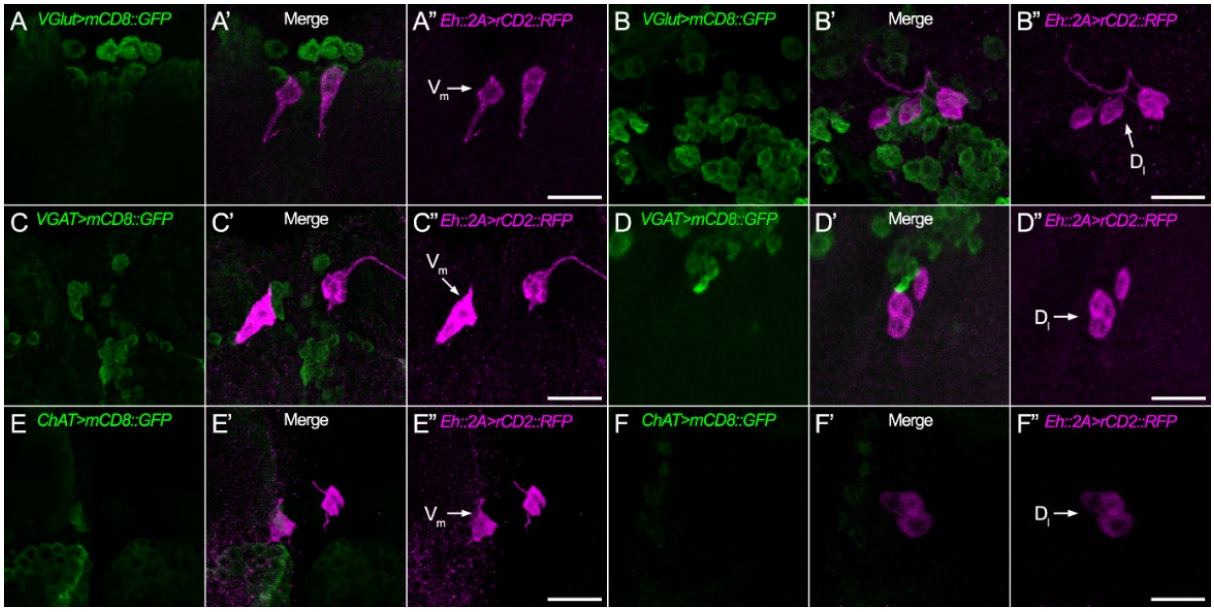

Figure 2.3. All EH neurons seem to be exclusively peptidergic. Lack of GFP staining driven with specific intragenic lines for glutamatergic (*VGlut;* **A-B**), GABAergic (*VGAT;* **C-D**), and cholinergic (*ChAT;* **E-F**) neurons, and RFP staining in V_m and D_Is, does not support the expression of classic neurotransmitters in EH neurons. The arrows marked the V_ms and D_Is. *Scale bars*: 20 μm.

3. The temporal profile of V_m and Inka cell activity

The activity of both V_m neurons and Inka cells is necessary to start the eclosion behavior. However, it is unknown which of these cells starts to become active first. Therefore, ARG-Luc imaging was used to measure the temporal activity of the V_m neurons (*Eh (C21)> ARG-Luc*) and Inka cells (*ETH::2A> ARG-Luc*) during pupal development. Similar to PTTH neurons (see I.1.c and Figure 2.4 A), the average V_m activity showed two peaks of activity around -28h and -7h before eclosion. While the -28h peak is short and broad, the -7h peak is large and narrow (Figure 2.4 A). The average ARG-Luc signal of the Inka cells showed major peaks at around -6h before eclosion, at the time of the eclosion, and a large peak two days after eclosion (Figure 2.4 B). The -6h activity coincides nearly with the -7h activity of V_m (Figure 2.4 C) and the -6h peak of PTTHn (Figure 2.4 D). At the time of eclosion, Inka cell activity shows a sharp and large peak. This large peak is probably an artifact of leaving the puparium. Compared to PTTHn and V_m neurons, the artifact peak is much larger (8.75 times) possibly because Inka cells are more peripherally located compared to the neurons.

The EH/ETH feedback loop that starts the eclosion program is initiated before but close to the time of eclosion (Kim et al., 2006a). Here ARG-Luc showed that V_m activity precedes Inka cell activity by one hour. Possibly, V_ms and Inka cells were prepared for eclosion six hours before initiation of eclosion. The gate for eclosion opens around six hours before dawn (Pittendrigh, 1954). The coincidence of PTTHn, V_ms, and Inka cells activity seven to six hours before eclosion (Figure 2.4 D) might be connected to the eclosion gate opening and readiness of the system. The peak in Inka cells activity that occurred two days after eclosion (Figure 2.4 B) had the highest amplitude variation among different individuals (hence showing large error bars). This peak was probably due to sexual maturation in adult flies (Meiselman et al., 2017, 2018) and not related to the eclosion program.

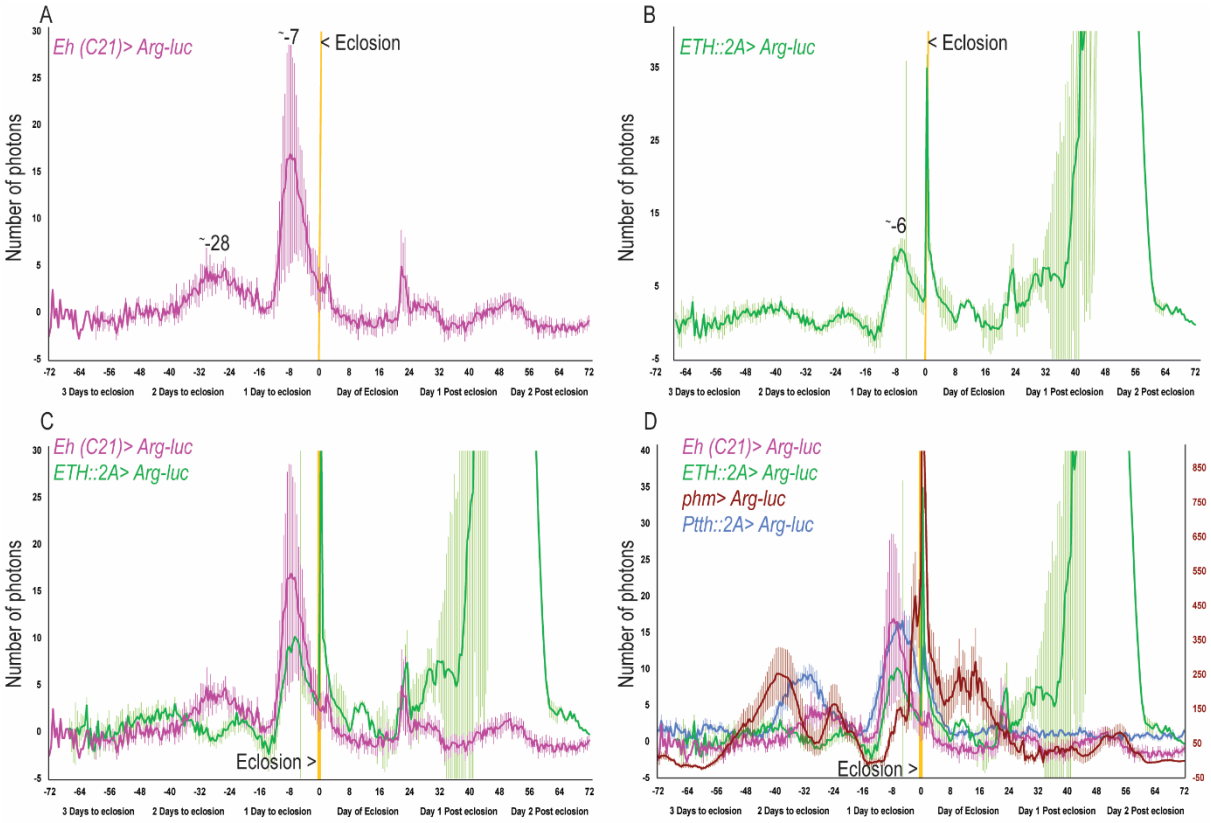

Figure 2.4. ARG-Luc imaging showed that around seven hours prior to eclosion the V_m and Inka cells become active. A Average activity of the V_m neurons (magenta; error bars = SEM) suggested they were active around -28h and -7h before eclosion. The activity of 25 animals was measured, but five were excluded because they showed no activity, and nine were excluded because the animals eclosed within the first twelve hours of starting the experiment (n=11). **B** The average Inka cell activity (green) showed that the Inka cells were active around -6h prior to and at the time of the eclosion. Around two days after eclosion, a massive activity peak was visible, probably due to the role of ETH in sexual maturation. Initially, 24 flies were recorded but the data of three flies were excluded because they eclosed within the first twelve hours (n=21). **C** The average activity of V_m (magenta) and Inka cells (green) plotted together showed that both V_ms and Inka cells became ready around seven to six hours before eclosion. At the time of eclosion, the eclosion program was started by releasing EH and ETH which led to EH/ETH feedback loop. **D** The average activity of V_m, PTTHn (blue, data from Chapter I), Inka cells, and PG (dark red, data from Chapter I) were plotted together. Around six hours before the eclosion, PTTHns, V_ms, and Inka cells activity coincided. Error bars indicate SEM.

4. The non-canonical D_l neurons do not undergo apoptosis after eclosion

Whether the non-canonical EH neurons survive or undergo apoptosis after eclosion is currently not known, and we did not investigate their survival using apoptosis markers. Instead, the post-eclosion morphology of different EH neurons was investigated by expressing CD8::RFP with the *Eh::2A-LexA* driver. Brains were dissected one, four, and seven days after eclosion. The dissected brains were stained for RFP and the morphology of the neurons was observed. For one day after eclosion, six brains were imaged (Figure 2.5 A-B). The cell bodies of the V_ms persisted (considering two V_m neurons per brain, 83.33% of cell bodies were present; Figure 2.5 A) but only in two brains V_m arborizations were completely stained. In the other four brains, V_m arborizations were completely or partially missing at least in one hemisphere. In contrast,

the cell bodies of the D_{lS}s were labeled on both sides (Figure 2.5 B). Usually, on average in each hemisphere, four D_{lS}s exist but the *Eh::2A-LexA* driver line was not consistently expressing RFP in all D_l neurons (typically expression was found in two to four cell bodies). Therefore, considering four cell bodies in each hemisphere, RFP was expressed in all D_{lS}s (eight neurons per brain) more than half of the time (54%), and D_l arborizations looked normal (Figure 2.5 B). For four days after eclosion, eight brains were analyzed (Figure 2.5 C-D). All V_m arborizations were completely or partially absent and the V_m cell bodies were mostly missing (only four out of 16 cell bodies; Figure 2.5 C). The D_{lS}s cell bodies were again present (54% of 64 cell bodies expressed CD8::RFP) and their arborization seemed normal (Figure 2.5 D). Except for two brains, only the optic lobe projecting D_l lost its neuronal processes. For seven days after eclosion, seven brains were examined (Figure 2.5 E-F). In all cases, the V_m neuron arborizations were completely absent (Figure 2.5 E) except in one case. That brain showed abnormally large V_m cell bodies (two to three times larger than usual) with inflated arborizations. However, the overall shape of the arborizations and morphology was the normal bifurcated V_m morphology. Two other brains showed only one V_m cell body, while the rest had completely lost the V_ms. The D_{lS}s cell bodies were not affected (59% present) but their projections seemed less dense, and the optic lobe-projecting D_l neuron was mostly missing (Figure 2.5 F), and most brains did not contain its arborizations and cell bodies.

In conclusion, the *Eh::2A-LexA* driver did not express RFP in V_m neurons one day post-eclosion and the V_m neurons were nearly completely missing after four days. On the other hand, RFP expression in non-canonical D_{lS}s was continued for longer. This suggests an unknown role for EH from the D_{lS}s after eclosion.

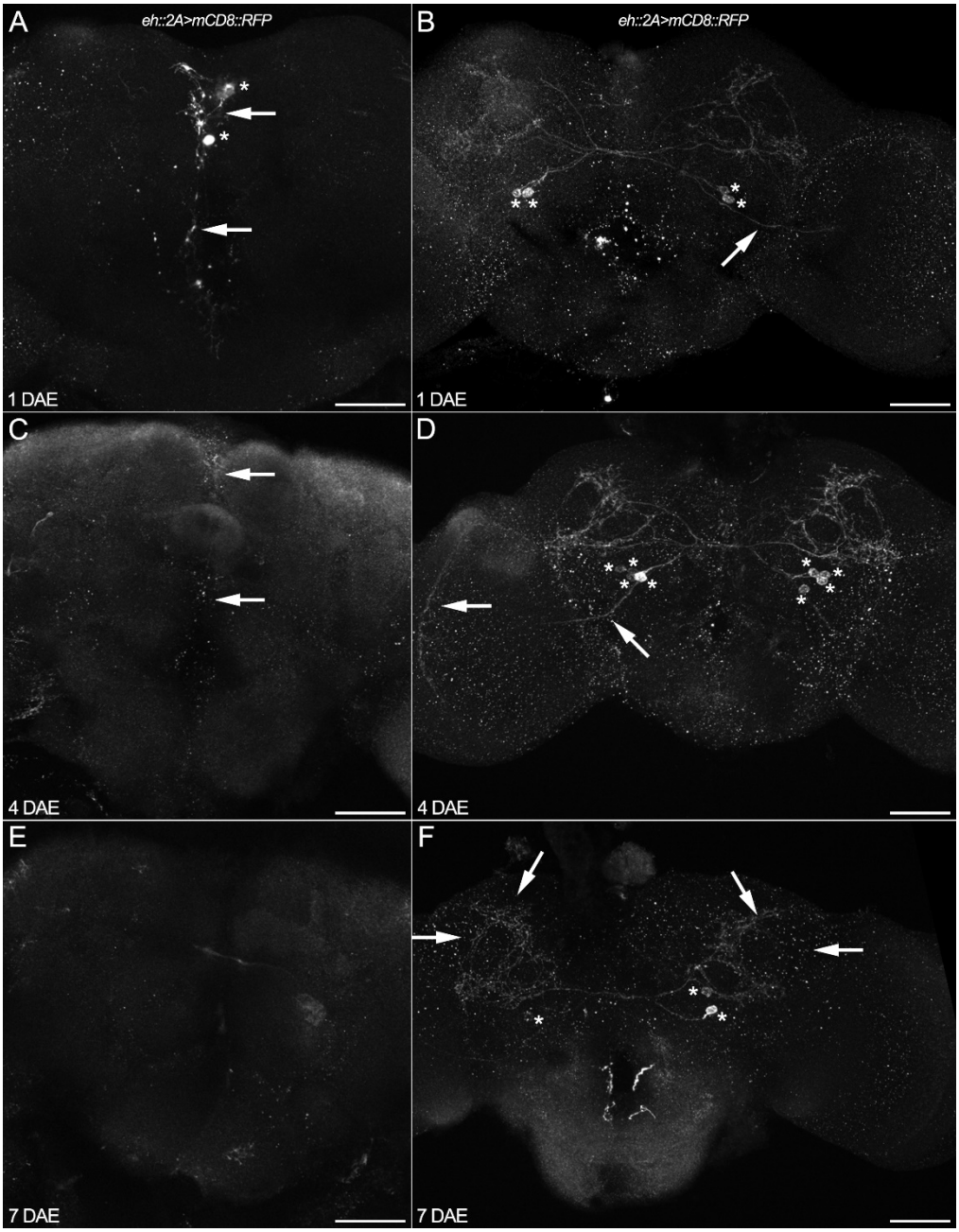

Figure 2.5. RFP expression pattern in V_ms and D_ls after eclosion. A One day after eclosion (one DAE) the cell bodies of the V_m neurons were still visible (asterisks) but RFP was partially present in their projections (arrows). **B** RFP fully marked the D_ls, and D_ls morphology was normal at one DAE. Their cell bodies (asterisks) were present (two to four cell bodies in each hemisphere), and their projections seemed normal in the superior protocerebrum. The arrow pointed to the optic lobe-projecting D_l. **C** Four days post eclosion, the V_m neurons did not show RFP expression. Arrows pointed to the remainder of RFP in V_m processes. **D** At four DAE, the D_ls still appeared normal. All projections and cell bodies (asterisks) were present and RFP staining in the superior protocerebrum was more pronounced. The arrow points to the arborization of the optic lobe-projecting D_l. **E** After seven DAE, the V_ms showed no RFP. **F** At seven DAE, RFP expression in D_ls seemed to be reduced and fewer cell bodies (asterisks) were visible. Especially in processes located at the lateral horn and superior protocerebrum RFP intensity was less pronounced (arrows). The optic lobe-projecting D_l does not show any RFP signal. *Scale bars:* 50 µm.

Chapter III: Neuropeptides influence premature eclosion but not eclosion rhythmicity

1. PTTH neurons express various GPCRs for clock-related neuropeptides and myosuppressin

Most clock neurons produce and release at least one peptide (Reinhard et al., 2023). PDF is released from sLN_vs and lLN_vs (Helfrich-Förster, 1995; Renn et al., 1999), sNPF from sLN_vs, two LN_ds and many $DN1_ps$ (Abruzzi et al., 2017; Liang et al., 2017; Reinhard et al., 2023) AstA from three of the $DN1_ps$ and all LPNs (Reinhard et al., 2023, 2022a), AstC by LPNs, DN2s, eight of the $DN1_ps$, and 20 of the DN3s (Abruzzi et al., 2017; Reinhard et al., 2023). Other peptides such as Dh31, Dh44, ion transport peptide, Proctolin and Trissin are also expressed by clock neurons but each from a smaller subset (Abruzzi et al., 2017; Dircksen et al., 2008; Hermann-Luibl et al., 2014; Kahsai et al., 2010; Kunst et al., 2014; Ma et al., 2021; Reinhard et al., 2023). DH31 is expressed by roughly six of the $DN1_ps$ (Kunst et al., 2014; Reinhard et al., 2023) and ITP is expressed by the 5^{th} sLN_v and one LN_d (Dircksen et al., 2008; Hermann-Luibl et al., 2014; Kahsai et al., 2010; Reinhard et al., 2023). Single-cell transcriptomics data predicted that Ms is expressed by some LN_ds, nonetheless, so far there is no compelling evidence to support that (Abruzzi et al., 2017). The role of clock-related peptides in influencing eclosion rhythmicity is poorly understood. Selcho et al. (2017) showed that sNPF inhibits the PTTHn, nonetheless, the expression of the sNPF-R by PTTHn has not been shown so far. However, the possible role of other clock-related peptides remains unclear.

Therefore, this chapter focuses on the clock-related peptides PDF, sNPF, AstA, AstC, and Dh31 plus Ms. First, the expression of their receptors in PTTHn is investigated to find evidence of whether those peptides might modulate the rhythmicity of eclosion. While there is only one receptor for PDF, sNPF, and Dh31 (Feng et al., 2003; Johnson et al., 2005; Mertens et al., 2002), AstA, AstC, and Ms have two receptors (Egerod et al., 2003; Kreienkamp et al., 2002).

Specific intragenic T2A lines were used to report the expression of these receptors in the PTTHn However, the genes of some of these GPCRs code for more than one splice form, and more than one driver line was created for them (Deng et al., 2019). For example, for Dh31-R, two different drivers for Dh31-R^{ABC} and Dh31-R^{C} were available. Other used driver lines in this thesis are PDF receptor (PDFR), sNPF-R, AstA-R1, AstA-$R2^{AC}$, allatostatin C receptor 1 (AstC-R1), AstC-$R2^{C}$, myosuppressin receptor 1 ($MsR1^{B}$), and $MsR2^{C}$, all created by Deng et al. (2019). Nuclear mCherry was driven in the receptor-expressing neurons (*receptor-Gal4> UAS-mCherry.nls*) and brains were double-stained against mCherry and PTTH in P14 pharate brains. The results are summarized in Figure 3.1 and Table 3.1.

PDFR was not expressed by the PTTHn (Figure 3.1 A'), while the sNPF-R was expressed in the PTTHn (Figure 3.1 B'). This finding confirms a previous study that suggested signaling from the clock to the PTTHn is through sNPF but not PDF (Selcho et al., 2017). Both AstA receptors, AstA-R1 and AstA-$R2^{AC}$, were expressed in PTTHn (Figure 3.1 C' and D'), with AstA-$R2^{AC}$ present in 68% of the analyzed PTTHn (Figure 3.1 D'). In addition, both AstC receptors (Figure 3.1 E' and F') and both Ms receptors (Figure 3.1 I' and J') were consistently expressed by the PTTHn. Finally, neither of the Dh31-R isoforms seem to be expressed by

PTTHn (Figure 3.1 G' and H'). Based on the stainings, we calculated the expression frequency of the investigated GPCRs in PTTHn (number of neurons showing expression/number of all neurons*100). The results are summarized in Table 3.1. The frequency of expression for all the GPCRs expressed by PTTHn, except AstC-R2^{AC} was > 80%.

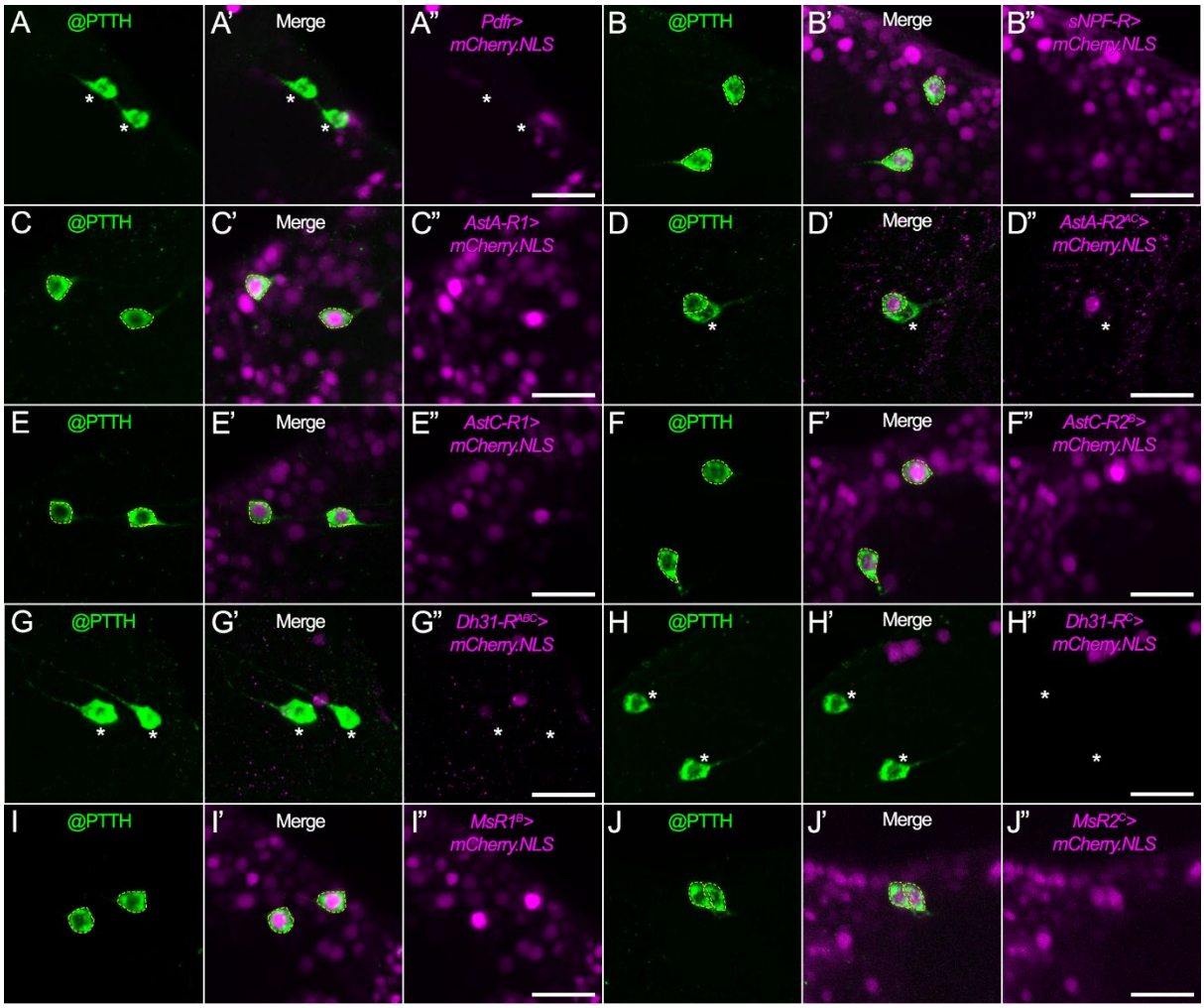

Figure 3.1. PTTHns express receptors for clock-related peptides and myosuppressin. Nuclear mCherry was expressed in the neurons expressing the receptor of interest (magenta), and preparations were co-stained with anti-PTTH (green). The contours of the PTTHns that expressed the receptor were marked with dashed lines. The cell bodies of PTTHns not expressing the receptor were marked with asterisks. **A-A"** The PTTHns did not express the PDFR. **B-B"** The PTTHns expressed the sNPF-R. **C-C"** AstC-R1 was nearly always expressed by PTTHns. **D-D"** The AC isoform of AstA-R2 (AstA-R2^{AC}) was mostly expressed by only one of the PTTHns. **E-E"** Both PTTHns expressed AstC-R1. **F-F"** Both PTTHns also always expressed AstC-R2^{B}. **G-G"** The PTTHns never expressed Dh31-R^{ABC}. **H-H"** PTTHns neither expressed Dh31-R^{C} isoform of Dh31-R. **I-I"** The MsR1^{B} was always expressed in PTTHns. **J-J"** The PTTHns also expressed MsR2^{C} but not as prominently as MsR1^{B}. *Scale bars*: 20 µm.

Table 3.1. The expression frequency of investigated peptide receptors, present on PTTH and EH neurons are shown as percentages and colored gradients. Prediction of GPCR α-subunit binding based on PRED-COUPLE 2 (Sgourakis et al., 2005b, 2005a). N=number of counted cell bodies, n=number of cell bodies expressing the receptor.

	Neuronal cluster				
Receptor	**PTTHn**	**V_m**	**D_ms**	**D_ls**	**α_s Prediction**
PDFR	0% N=26; n=0	0% N=24; n=0	NA N=0	0% N=85; n=0	$G\alpha_{i/o}$ (↓cAMP)
sNPF-R	95.35% N=43; n=41	12.12% N=33; n=4	0% N=2; n=0	15.7% N=121; n=19	$G\alpha_{i/o}$ (↓cAMP)
AstA-R1	97% N=60; n=58	54.17% N=24; n=13	0% N=4; n=0	29.11% N=79; n=23	$G\alpha_{i/o}$ (↓cAMP)
AstA-R2^{AC}	68.33% N=60; n=41	69.23% N=26; n=18	NA N=0	8.64% N=81; n=7	$G\alpha_{i/o}$ (↓cAMP)
AstC-R1	90% N=20; n=18	13.36 N=22; n=3	16.67% N=6; n=1	34% N=100; n=34	$G\alpha_{q/11}$ (↑Ca^{2+})
AstC-R2^{B}	100% N=28; n=28	0% N=12; n=0	0% N=1; n=0	27.27% N=44; n=12	$G\alpha_{q/11}$ (↑Ca^{2+})
Dh31-R^{ABC}	0% N=30; n=0	0% N=19; n=0	0% N=2; n=0	0% N=73; n=0	$G\alpha_s$ (↑cAMP) or $G\alpha_{i/o}$
Dh31-R^{C}	0% N=45; n=0	21.43% N=14; n=3	0% N=2; n=0	15.25% N=59; n=9	$G\alpha_{i/o}$ (↓cAMP) or $G\alpha_s$
MsR1^{B}	100% N=50; n=50	73.08% N=26; n=19	23.08% N=13; n=3	16.84% N=95; n=16	$G\alpha_{i/o}$ (↓cAMP)
MsR2^{C}	80.77% N=52; n=42	0% N=23; n=0	0% N=5; n=0	0% N=80; n=0	$G\alpha_{i/o}$ (↓cAMP)

2. EH neurons express receptors for allatostatin A and myosuppressin

The stainings of EH neurons receptor profile, their data acquisition, and data analysis were performed by Sina Grimm (part of her MSc thesis supervised by Emad Amini) and Emad Amini (Grimm, 2023).

The stereotypic motor pattern during ecdysis is orchestrated by a well-characterized peptidergic cascade starting with the ETH/EH feedback loop (Ewer et al., 1997; Gammie and Truman, 1999; Kim et al., 2006a). In contrast, we know very little about whether peptides (including clock-related ones) also modulate the timing of eclosion at the level of ETH/EH. Ruf et al. (2017) used optogenetics to activate a variety of peptidergic neurons during light-induced premature eclosion. They showed that optogenetic activation of Inka cells, V_m, and Ms neurons significantly increase premature eclosion (Ruf et al., 2017). However, other peptidergic neuron, including clock neurons, were not tested. Therefore, we first looked for peptide receptors on EH^+ neurons, again relying on T2A-based driver lines for the receptors of AstA, AstC, Dh31, Ms, PDF, and sNPF GFP expression was driven by the respective receptor driver line

(*receptor-Gal4> UAS-mCD8::GFP*), and RFP was driven in all EH neurons (*Eh::2A-LexA> LexAop-rCD2::RFP*). Then, we compared expression in the V_m (Figure 3.2 and Table 3.1) and D_l EH-expressing neurons (Figure 3.3 and Table 3.1). The frequency of expression of the GPCRs for EH^+ neurons is summarized in Table 3.1. From the investigated receptors, only AstA-R1 (54% expression frequency; Figure 3.2 C'), AstA-$R2^{AC}$ (69%; Figure 3.2 D'), and $MsR1^B$ (73%; Figure 3.2 I') were significantly expressed by the V_m neurons. sNPF-R, AstC-R1, and Dh31-R^C were expressed at a much lower frequency by the V_m neurons (12%, 13%, and 21% respectively). Since the expression frequency of sNPF-R, AstC-R1, and Dh31-R^C was much lower than 50%, these receptors are not considered part of the core V_m receptor profile of a pharate fly. Possibly the V_m neurons changed their receptor profile while they were approaching eclosion time. Or simply the receptor expression of the V_m neurons was not homogenous and the V_ms were not identical in receptor profile. PDFR, AstC-$R2^B$, Dh31-R^{ABC}, and $MsR2^C$ were not expressed by V_m neurons in pharate adults. These results suggest that the V_m neurons are likely modulated by AstA and Ms since both AstA-Rs and $MsR1^B$ had the highest expression frequency, and possibly AstA and Ms can start or delay eclosion. As mentioned before, a positive influence of Ms in promoting premature eclosion has indeed been found (Ruf et al., 2017).

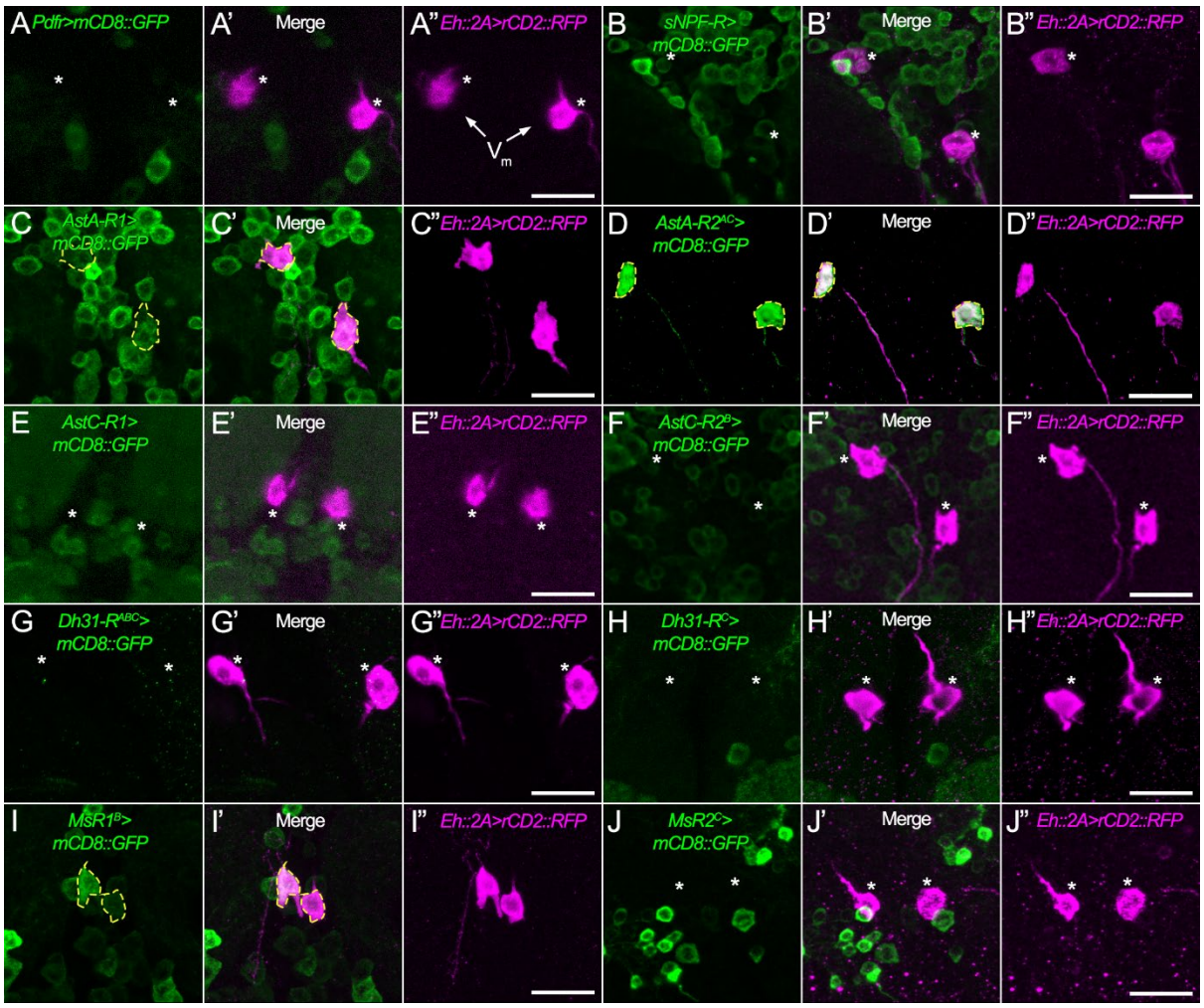

Figure 3.2. The V_m neurons expressed receptors for allatostatin A and myosuppressin. mCD8::GFP was driven using specific T2A driver lines for GPCRs (green) in P14 brains, while simultaneously expressing rCD2::RFP in V_m neurons (magenta) using *Eh::2A-LexA*. The contours of

V_m neurons with successful colocalization of RFP and GFP were marked with dashed lines. The neurons that did not express the receptor of interest were marked with asterisks. **A-A"** Lack of RFP and GFP colocalization in V_m neurons tested for PDFR expression showed PDFR was not expressed by V_m. **B-B"** Also, most V_m neurons did not express sNPF-R in P14 pharates (see Table 3.1 for expression frequencies). **C-C"** Most V_m neurons expressed AstA-R1. **D-D"** Also, AstA-$R2^{AC}$ was expressed by most V_ms. **E-E"** In most V_m neurons AstC-R1 was not expressed. **F-F"** AstC-$R2^{B}$ was never expressed by V_m neurons. **G-G"** Also V_m neurons never expressed isoform ABC of Dh31-R. **H-H"** However, in some V_m neurons isoform C of Dh31-R was expressed. **I-I"** The $MsR1^{B}$ was expressed by most V_m neurons. **J-J"** However, $MsR2^{C}$ was never expressed by any V_m. *Scale bars*: 20 μm.

The receptor profile of D_ls turned out to be more diverse than that of the V_m neurons. Unfortunately, due to the dense arborization of D_ls in the superior protocerebrum, it was not possible to anatomically tell apart individuals. Therefore, all four D_l neurons were considered as one cluster and their pharate receptor profile was measured for all of them collectively (Table 3.1). None of the expressed receptors reached an expression frequency higher than 29% (Table 1.3). AstA-R1 (29%; Figure 3.3 C'), AstC-R1 (34%; Figure 3.3 E'), and AstC-$R2^{B}$ (27%; Figure 3.3 F') showed the highest expression frequencies, with at least one of the D_ls always expressing one of these receptors. Taken together, AstA and AstC are candidate modulators of D_l neuron activity. AstA-$R2^{AC}$, sNPF-R, Dh31-R^{C}, and $MsR1^{B}$ were found in some of the D_ls but were not consistently expressed (Table 3.1).

The *Eh::2A-LexA* driver line was not consistent in driving RFP expression in the D_m neurons. Therefore, in many P14 brains, it was not possible to mark the D_ms. Only in a few brains, AstC-R1 (six cell bodies in three brains, 16%) and $MsR1^{B}$ (13 cell bodies in seven brains, 23%) were found to be expressed in D_ms (Table 3.1). However, the number of observed neurons was not sufficient to draw a firm conclusion. In none of the brains tested for PDFR and AstA-$R2^{AC}$ expression, RFP was expressed in D_m neurons (Table 3.1). Therefore, whether PDFR and AstA-$R2^{AC}$ are expressed by D_ms remains unknown.

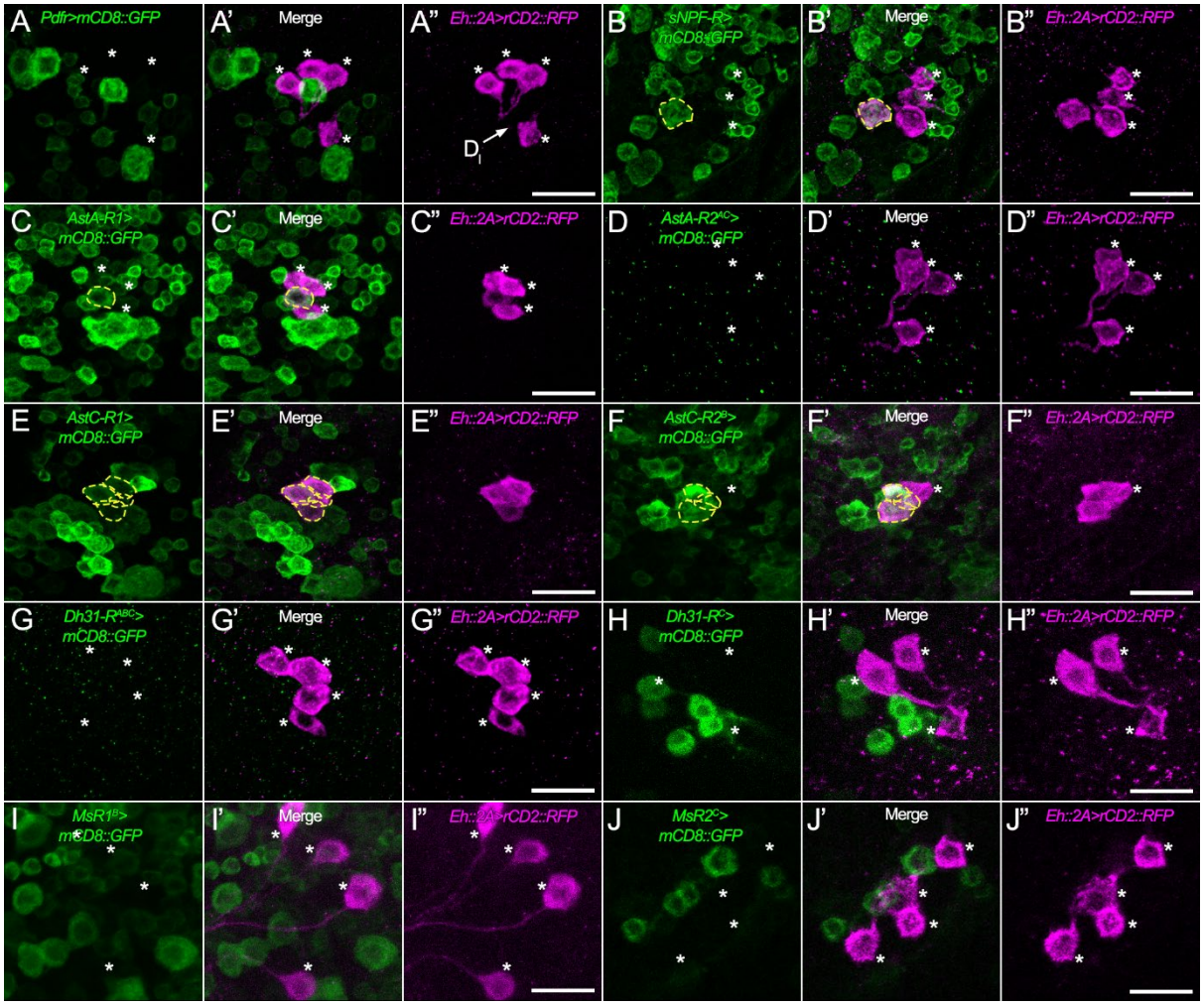

Figure 3.3. The D_l neurons expressed receptors for allatostatin C and other clock-related peptides and Ms. In P14 brains, rCD2::RFP was expressed in D_l neurons using *Eh::2A-LexA* while at the same time, mCD8::GFP was driven using specific T2A driver lines for GPCRs. The contours of D_l neurons with successful colocalization of RFP and GFP were marked with dashed lines. The neurons that did not express the receptor of interest were marked with asterisks. **A-A"** None of the D_l neurons expressed PDFR. **B-B"** D_ls rarely expressed sNPF-R in P14 pharates (see Table 3.1 for expression frequencies). **C-C"** At least one of the D_l neurons always expressed AstA-R1 (29%) **D-D"** but AstA-$R2^{AC}$ was not expressed by most D_ls. **E-E"** The highest receptor expression frequency by D_ls was for AstC-R1. **F-F"** AstC-$R2^{B}$ was almost always expressed by at least one of the D_ls. **G-G"** The D_ls never expressed Dh31-R^{ABC} **H-H"** but a few expressed the other isoform, Dh31-R^{C} in the pharate brain. **I-I"** Few D_l neurons expressed $MsR1^{B}$. **J-J"** And none of them expressed $MsR2^{C}$. *Scale bars*: 20 µm.

3. The highly Ca^{2+} permissive nAChRα7 is not expressed by the V_m neurons

The nicotinic Acetylcholine Receptors (nAChRs) are a member of the cys-loop ligand-gated ion channel superfamily. Different subtypes of nAChRs are highly Ca^{2+} permeable. However, the α7 subtype is among the highest Ca^{2+} permissive channels that rapidly increases the intracellular Ca^{2+} level of the neurons (Fucile, 2004). As for the peptidergic neurons, Ca^{2+} as the second messenger is required for peptide release. To check if this subtype is expressed by the V_m neurons double staining was performed. With the double expression of the RFP in the V_m neurons and GFP in all neurons expressing *nAChRα7* (Using a *Mi{MIC}-Gal4* line) it

became evident that the V_m neurons are not expressing this nicotinic receptor subtype (Figure 3.4 A-C). Hence, nAChRα7 is not involved in increasing the cytoplasmic Ca^{2+} and EH releasing from the V_m neurons.

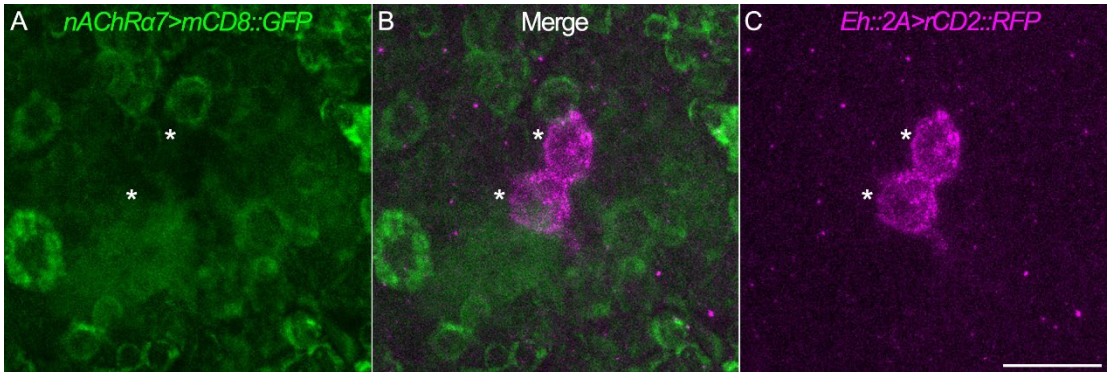

Figure 3.4. The V_m neurons did not express the common nicotinic receptor *nAChRα7* subunit. The lack of colocalization (**B**) between *nAChRα7* expressing neurons (**A**) and the V_m neurons (**C**) suggests that nAChRα7 was not involved in increasing the intracellular Ca^{2+} required for peptide release. *Scale bar*: 20 µm.

4. Eclosion of flies lacking individual clock-related peptide and Ms signaling pathways is rhythmic

In section III.1, it was shown that PTTHns express sNPF-R, AstA-R1, AstA-$R2^{AC}$, AstC-R1, AstC-$R2^{B}$, $MsR1^{B}$, and $MsR2^{C}$ GPCRs. To assess the role of sNPF, AstA, AstC, and Ms neuropeptides in rhythmic eclosion behavior, eclosion assays on flies lacking these peptides and/or their receptor(s) were performed. For AstA and its receptors (Figure 3.5 A), Ms receptors (Figure 3.5 E), and sNPF-R (Figure 3.5 C), knock-out mutant flies were available (Deng et al., 2019; Hentze et al., 2015). To create AstC knock-out mutants (Figure 3.5 B), *AstC-Gal4; UAS-AstC-gRNA* flies were crossed to *UAS-Cas9; tubP-Gal80^{ts}*. For controls, *w^{1118}* flies were crossed to the parental lines. To knock-out *AstC, the* temperature was raised to 29 °C for two days at the beginning of the pupal stages. For Ms, conditional cell killing using *UAS-RA^{CS2}.CC* (cold-sensitive ricin) was performed (Figure 3.5 D; Chen et al., 2012). In all genotypes (experiments and controls if available) the eclosion activity pattern assessed by autocorrelation RI and LS remained rhythmic (Figure 3.5, Table 3.2). The same was found after eJTK analysis, except for the controls of Ms neurons ablation (Table 3.2). This exception was possibly caused by the required temperature changes (for removing RA) that create sharper eclosion peaks.

Since eclosion in flies lacking one of the peptide signaling pathways remained rhythmic, it seems that these peptides are not required for eclosion rhythmicity. Nevertheless, it cannot be excluded that they are mutually redundant, and all together modulate the activity of the PTTHn. *i.e.*, removing them individually could be compensated by other signaling pathways.

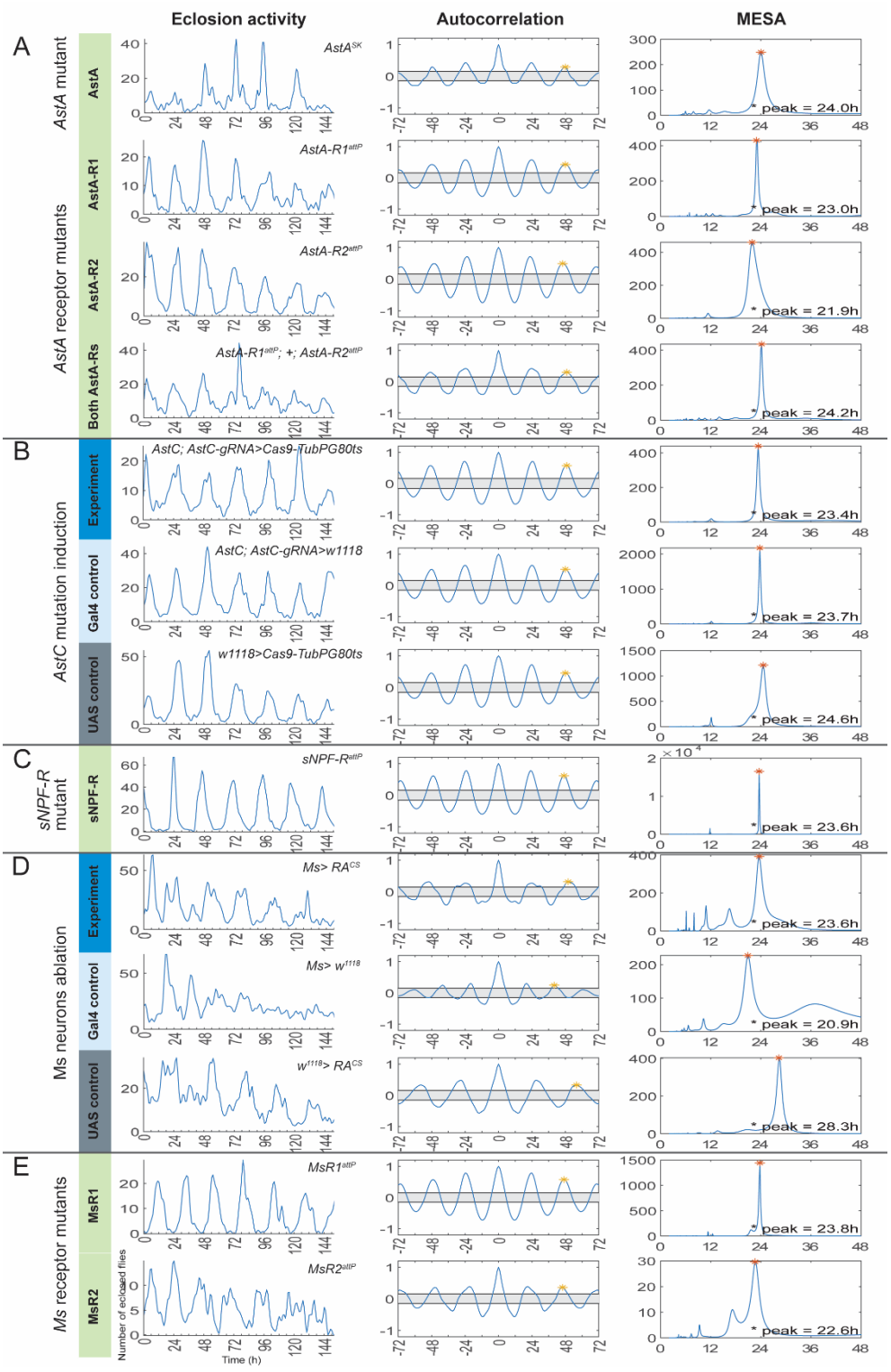

Figure 3.5. Removing AstA, AstC, sNPF, and Ms signaling individually did not impair eclosion rhythmicity. A The *AstA*^{SK} mutant, *Ast-R1*^{attp}, *AstA-R2*^{attp}, and double AstA-R mutants remained highly rhythmic in DD. **B** The AstC knock-out flies, and its controls were very rhythmic as well. **C** The *sNPF-R*^{attp} mutant was also rhythmic. **D** The Ms neurons ablated experiment and control groups were rhythmic. However, the eJTK analysis of the control groups showed arrhythmicity. This was probably due to the decreasing amplitude of the eclosion in the final days which weakened rhythmicity. **E** The *MsR1*^{attp} and *MsR2*^{attp} mutants also showed rhythmic eclosion.

Table 3.2. Rhythmicity analysis of the eclosion of flies bearing mutations in clock-related peptides and in Ms mutant or in their associated receptor mutant strains (see Figure 3.5). Arrhythmic values are shown in red.

	Genotype	Number of flies	Error	Period	Rhythmicity index	Lomb-Scargle	eJTK BH bf corrected p
AstA	*AstA^{SK}*	1248	7.9%	24.0h	0.29	16.4	$2.8*10^{-13}$
AstA-R	*AstA-R1^{attp}*	1103	0.6%	23.0h	0.43	35.6	$1.1*10^{-25}$
	AstA-R2^{attp}	1773	2.5%	21.9h	0.49	42.4	$2.0*10^{-23}$
	AstA-R1^{attp}; +; AstA-R2^{attp}	1715	1.1%	24.2h	0.30	17.6	$2.6*10^{-21}$
AstC	*AstC; AstC-gRNA> Cas9-TubPG80^{ts}*	1292	0.0%	23.4h	0.58	39.5	$1.1*10^{-27}$
	AstC; AstC-gRNA> w^{1118}	2106	2.9%	23.7h	0.52	48.1	$1.5*10^{-33}$
	w^{1118}> Cas9-TubPG80^{ts}	2063	1.8%	24.6h	0.45	40.0	$7.5*10^{-37}$
sNPF-R	*sNPF-R^{attp}*	2638	0.3%	23.6h	0.61	47.3	$1.1*10^{-28}$
Ms	*Ms> RA^{CS}*	2953	4.6%	23.6h	0.32	12.6	$4.6*10^{-9}$
	Ms> w^{1118}	3667	8.8%	20.9h	0.25	4.4	0.69
	w^{1118}> RA^{CS}	2639	7.2%	28.3h	0.33	16.6	1
MsRs	*MsR1^{attp}*	1332	8.6%	23.8h	0.58	54.4	$1.3*10^{-39}$
	MsR2^{attp}	957	9.8%	22.6h	0.36	13.7	$3.1*10^{-10}$

5. Allatostatin A and allatostatin C impede premature eclosion

The Opto-DEM assays of AstC::2A and R61H08 and their data acquisition were performed by Abdullah Sert (part of his BSc thesis supervised by Emad Amini) and their data were analyzed by Emad Amini (Sert, 2022).

Most flies eclose in the early morning. Also, in populations that are entrained by temperature instead of light, most of the flies eclose during the transition from colder to warmer temperatures. Yet, the eclosion gate is already open six hours before morning. This allows to induce premature eclosion prior to the normal eclosion peak by giving a light pulse (masking effect) when the gate is opened even before the subjective morning (Pittendrigh, 1954). This principle was used in WEclMon experiments (Ruf et al., 2017). Six hours before the temperature rise, a one-hour blue light (λ = 470 nm) pulse was given that induced premature eclosion. To test whether certain peptides affect eclosion, ChR2-XXL was expressed in peptidergic neurons releasing the peptide of interest. The blue light pulse thus excited the

ChR2-XXL-expressing neurons (Dawydow et al., 2014) and possibly induced peptide release, while at the same time inducing premature eclosion.

In section III.2, it was shown the V_m neurons express AstA receptors and MsR1 at a high frequency. V_ms also showed lower expression frequency for sNPF-R, AstC-R1, and Dh31-R^C. The V_m neurons together with Inka cells start the EH/ETH positive feedback loop and initiate the eclosion program (Ewer and Reynolds, 2002; Truman, 2005; D. Zitnan et al., 2007; Zitnan and Adams, 2012). Therefore, modulatory effects of AstA, Ms, sNPF, AstC, and Dh31 on V_m neurons may affect eclosion initiation. Ruf et al. (2017) activated a variety of peptidergic neurons during light-induced premature eclosion to test which of those peptidergic neurons influenced the number of eclosed flies. They found that optogenetic activation of Ms, ETH, and EH cells triggered a bout of premature eclosion. In contrast, activation of $sNPF^+$ and $Dh31^+$ neurons was without an effect (Ruf et al., 2017).

Here, we tested the effect of activating $AstA^+$ and $AstC^+$ neurons. For that, we combined the optogenetic properties of ChR2-XXL with the TriKinetics *Drosophila* Eclosion Monitoring (DEM) system (opto-DEM). Eclosion assays were performed under temperature cycle in DD. At ZT18, which is six hours before subjective morning (ramping up of the temperature from ZT 24-01), an intense blue light pulse was shone for one hour upon the flies mounted into Opto-DEM to activate the neurons of interest and test for premature eclosion. The percentage of eclosed flies during each ZT was calculated (number of eclosed flies during each ZT/number of eclosed flies during the day*100) and plotted. Since blue light activates ChR2-XXL, any significant difference between the experiment group and controls is due to the optogenetic activation (Figures 3.6-3.10).

To validate the Opto-DEM approach, eclosion assays with exciting the V_m neurons were performed (Figure 3.6) as a positive control. The Opto-DEM data for eclosion in experimental group flies during the blue light pulse showed a 39.0±2.5% (mean ± SEM%) increase in eclosion. In the controls, the positive light effect reached a significantly lower mean (22.7±2.3% for Gal4 and 20.1±2.6% for UAS control; Figure 3.6 A-B). Therefore, the Opto-DEM approach delivered similar results as the WEclMon system. Since the receptors for AstA, AstC, and Ms are expressed by both PTTHn and the V_m neurons, and T2A-Gal4 lines capable of expressing ChR2-XXL in these neurons were available (Deng et al., 2019), these driver lines were selected for Opto-DEM (Figures 3.7-3.10).

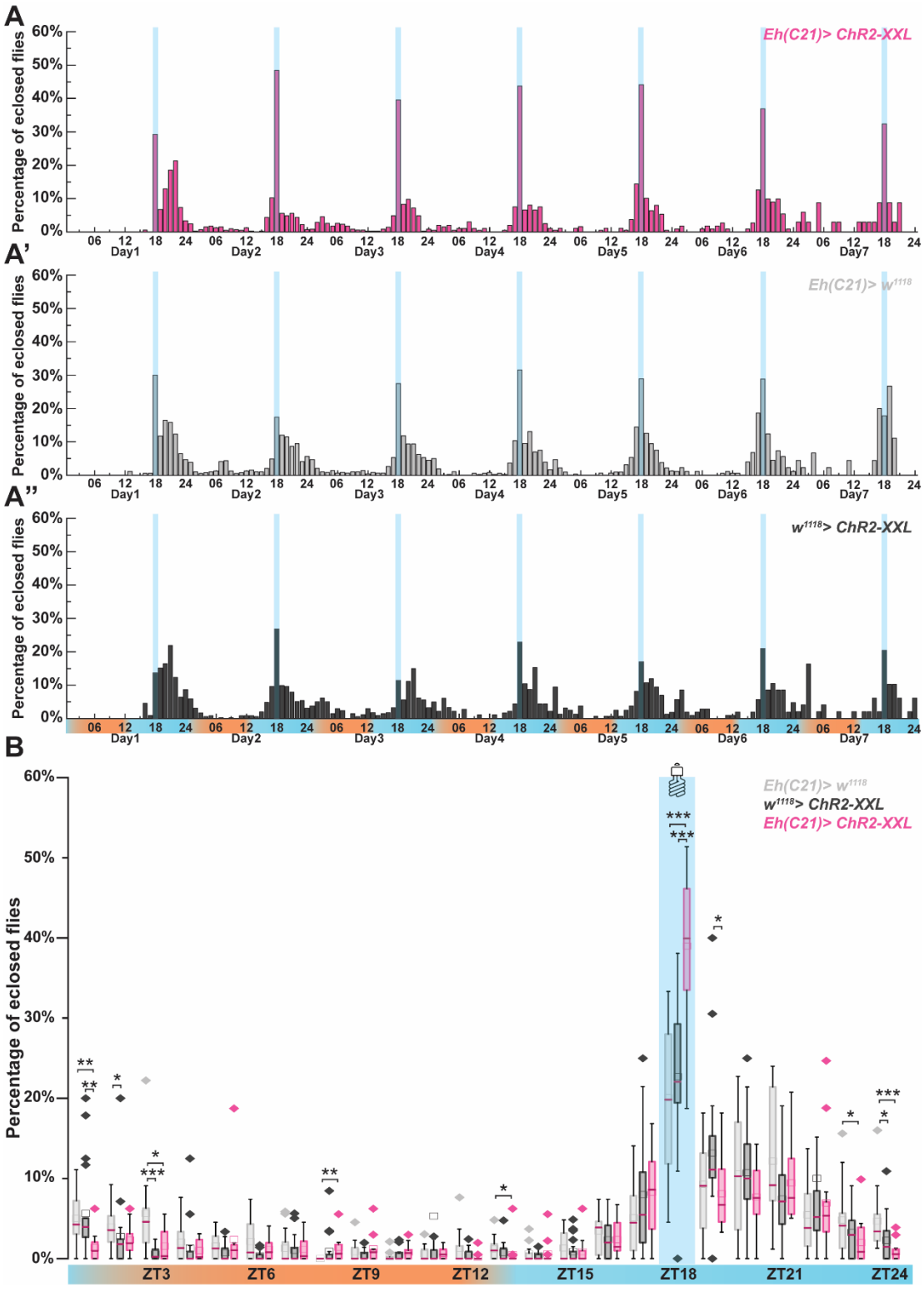

Figure 3.6. Blue light-induced premature eclosion and simultaneous optogenetic activation of the V_m neurons increased the eclosion rate. The flies were entrained to temperature changes (WC, indicated by an orange-blue gradient). Using Opto-DEM, six hours before subjective morning (ZT24-1 when the temperature changes from cold to warm) at ZT18 one one-hour pulse of intense blue light was shone on the flies (blue bars). The percentage of eclosed flies per hour compared to the entire day is plotted on the y-axis. **A-A"** Shining light on flies caused a higher eclosion rate in the *Eh (C21)> ChR2-XXL* flies (39.0±2.5%; **A**) compared to their Gal4 (22.7±2.3%; **A'**) and UAS (20.1±2.6%; **A"**)

controls. This overall eclosion percentage of the experiment group compared to the controls remained higher during the week. **B** At ZT18 (blue light pulse) the eclosion rate of the experiment group was significantly higher compared to the controls, At ZT24 and ZT1, there were additional significant differences in eclosion. The eclosion rate of the experiment group was lower because most flies had eclosed during the blue light pulse, while more control flies eclosed in the morning. Mann-Whitney *U* analysis followed by a one-sample Wilcoxon signed-rank test: * = $p \leq 0.05$, ** = $p < 0.001$, and *** = $p < 0.0001$.

With WEclMon it has been shown that the activation of the Ms neurons significantly increases premature eclosion during the light pulse (Ruf et al., 2017). However, the opto-DEM system with *Ms::2A> ChR2-XXL* flies produced different results. On the first day, optogenetic activation of *Ms::2A> ChR2-XXL* flies showed an increased premature eclosion rate (46.5%; Figure 3.7 A) but this increase drastically decreased during the next days. Moreover, the percentage of the eclosed flies during the light pulse was comparable to the Gal4 control group (Figure 3.7 A'). At all ZT (including ZT18), we found no significant difference between *Ms::2A> ChR2-XXL* and control flies (Mann-Whitney U test, Figure 3.7 B).

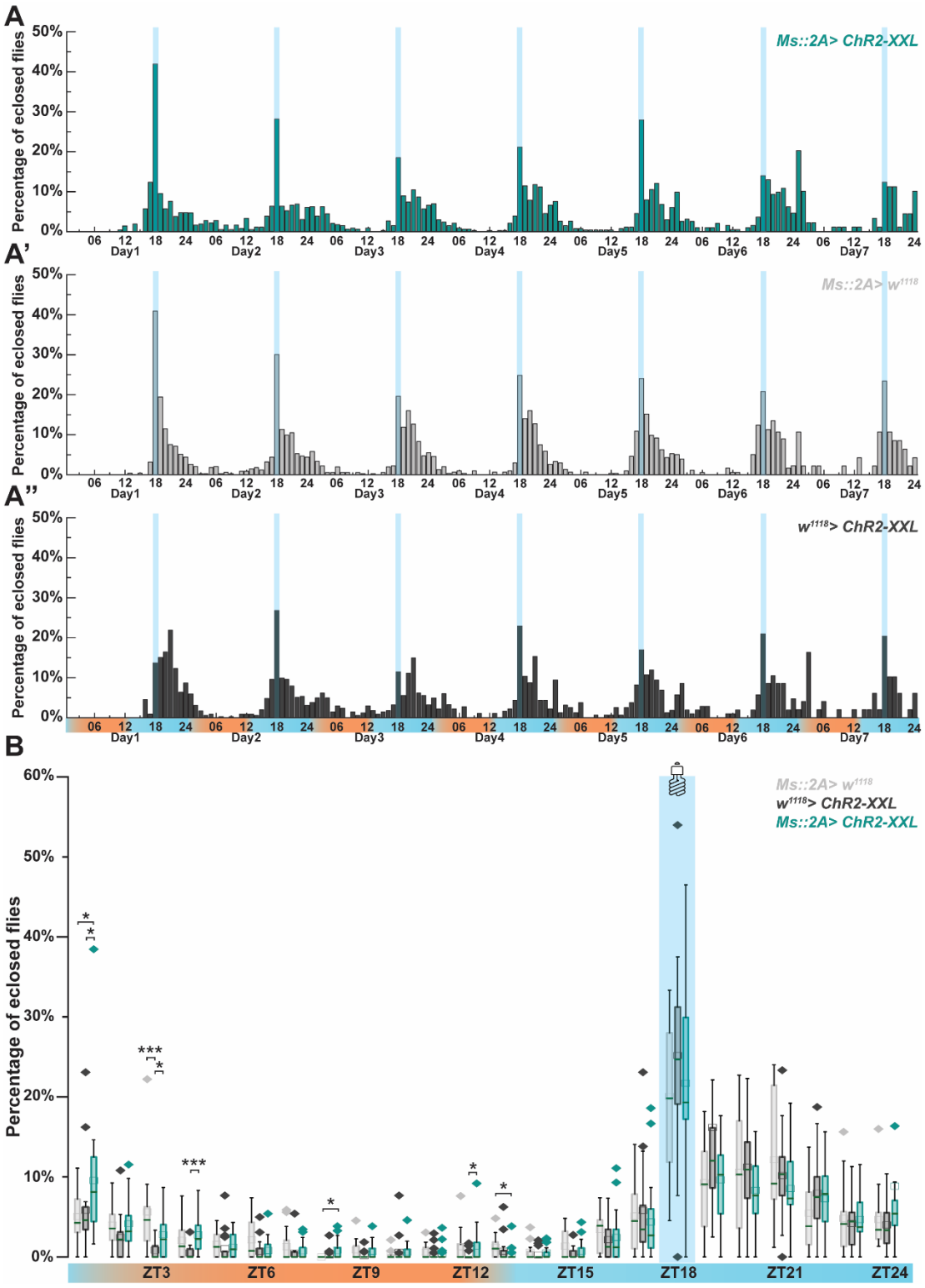

Figure 3.7. Blue light-induced premature eclosion and simultaneous optogenetic activation of the Ms neurons with *Ms::2A-Gal4* did not affect the eclosion rate. The flies were entrained to temperature changes (WC, indicated by an orange-blue gradient). Using Opto-DEM, six hours before subjective morning (ZT24-1 when the temperature changes from cold to warm) at ZT18 one one-hour pulse of intense blue light was shone on the flies (blue bars). The percentage of eclosed flies per hour compared to the entire day is plotted on the y-axis. **A-A"** A high eclosion rate on the first day) was recorded for *Ms::2A> ChR2-XXL* flies (21.7±2.4%; **A**) and their Gal4 control (25.2±2.5%; **A'**) but not the UAS control (20.1±2.6%; **A"**). The overall eclosion percentage for both the experimental group and

Gal4 control dropped (~15%) during the week. In contrast, the eclosion rate remained constant for the UAS control group. **B** At ZT18 (blue light pulse), the eclosion rate of *Ms::2A> ChR2-XXL* flies was not significantly different compared to the controls. Mann-Whitney *U* analysis followed by a one-sample Wilcoxon signed-rank test: * = $p \leq 0.05$, ** = $p < 0.001$, and *** = $p < 0.0001$.

In contrast, a very strong effect on eclosion rate was observed in *AstA::2A> ChR2-XXL* flies. Optogenetic activation of the AstA neurons during light-induced premature eclosion heavily suppressed eclosion; during the light pulse, nearly no fly eclosed ($0.0\pm6.5*10^{-4}$%; Figure 3.8 A). In comparison, both control groups showed significantly higher premature eclosion at ZT18 (28.1±2.3% for Gal4 and 20.1±2.6% for UAS control; Figure 3.8 A'-A"). At ZT19, the hour after the blue light pulse, the effect of optogenetic activation was reversed and more *AstA::2A> ChR2-XXL* flies eclosed (41.3±3.3%; Figures 3.8 A-B and 3.11 B) compared to Gal4 and UAS control groups (1.2±1.0% for Gal4 and 9.2±1.4% for UAS control; Figures 3.8 A-B and 3.11 B). Based on Mann-Whitney *U* analysis, the difference between the experiment and control groups in both ZT18 and ZT19 was highly significant ($p < 10^{-8}$, Figure 3.8 B). This shows that activation of the AstA neurons strongly prevents light-induced premature eclosion.

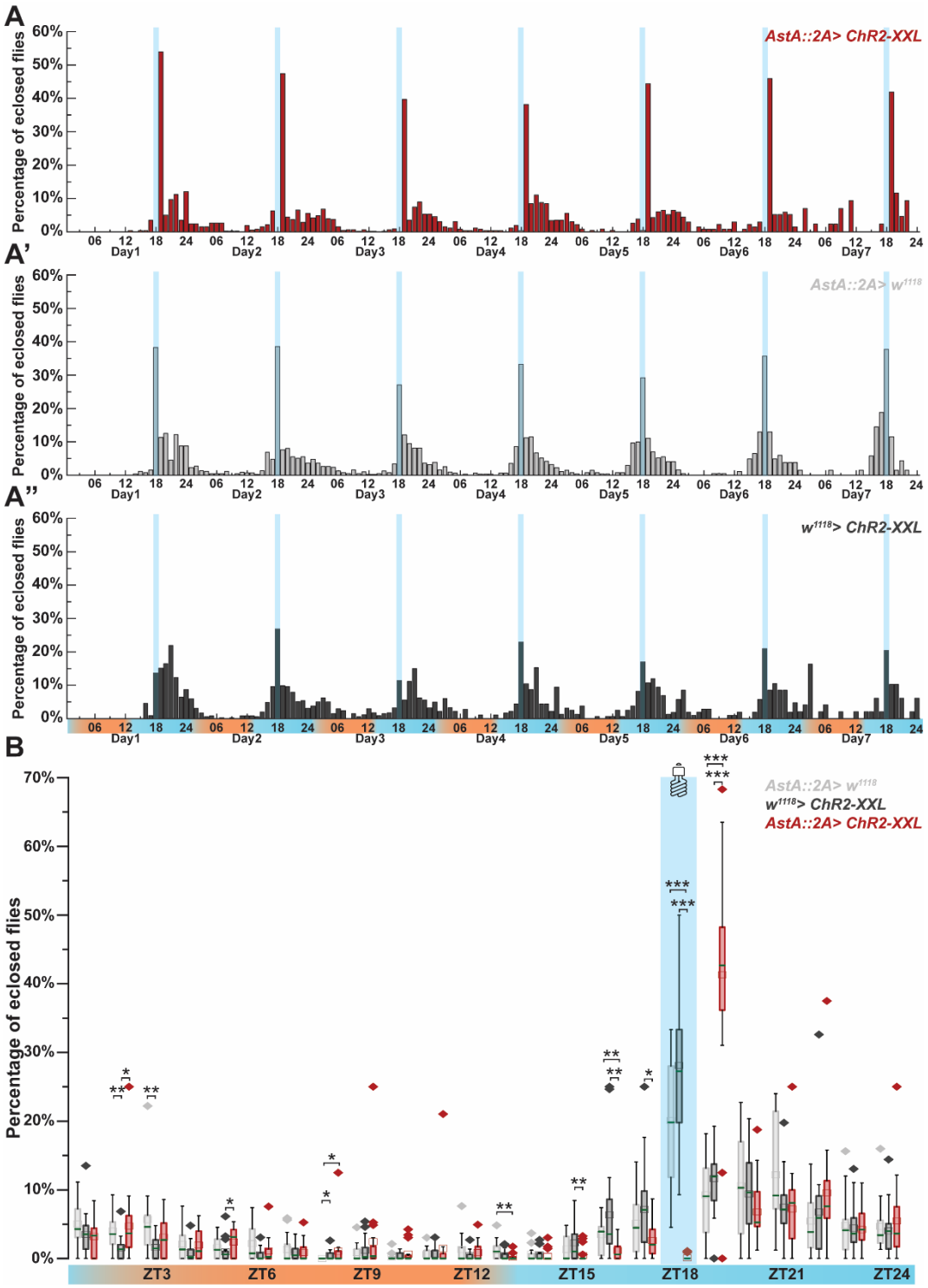

Figure 3.8. Blue light-induced premature eclosion and simultaneous optogenetic activation of the AstA neurons strongly decreased the eclosion rate. The flies were entrained to temperature changes (WC, indicated by an orange-blue gradient). Using Opto-DEM, six hours before subjective morning (ZT24-1 when the temperature changes from cold to warm) at ZT18 one one-hour pulse of intense blue light was shone on the flies (blue bars). The percentage of eclosed flies per hour compared to the entire day is plotted on the y-axis. **A-A"** Blue light triggered eclosion in *AstA::2A>ChR2-XXL* flies but flies did not eclose (0.0±6.5*10-4%; **A**) while their Gal4 control (28.1±2.3%; **A'**) and UAS control (20.1±2.6%; **A"**) eclosed. It seems after the light pulse, experiment group flies that could not eclose, perhaps due to the inhibitory effect of AstA neurons, emerged. The overall eclosion trend remained

constant during the week for the experiment and control groups. **B** At ZT18 and ZT19 the eclosion rates of *AstA::2A>ChR2-XXL* flies were significantly different compared to both control groups. At ZT18, *AstA::2A> ChR2-XXL* flies did not eclose and excitation of the AstA neurons suppressed light-induced premature eclosion. Mann-Whitney *U* analysis followed by a one-sample Wilcoxon signed-rank test: * = $p \leq 0.05$, ** = $p < 0.001$, and *** = $p < 0.0001$.

Activation of the AstC neurons using *AstC::2A> ChR2-XXL* did not show a significant difference at ZT18 (Figures 3.9 B and 3.11 A). Even though at ZT18 the experimental group showed a lower eclosion mean (16.4±2.2%) compared to its controls (18.3±1.8% for Gal4 and 20.1±2.6% for UAS control; Figures 3.9 B and 3.11 A), Mann-Whitney *U* analysis did not show any significant difference between them. According to Mann-Whitney *U* analysis, no other ZT eclosion rate of the experiment group was different from both control groups. However, the *AstC::2A-Gal4* is homozygous lethal and because the second chromosome balancer is not morphologically identifiable in puparia, an unknown subset of experimental flies (*CyO> ChR2-XXL*) did not express *ChR2-XXL* Therefore, the result of that experiment was compromised (Figure 3.9). The experiment was therefore repeated using a different AstC driver line (*R61H08-Gal4*; Figure 3.10). Activation of the AstC neurons using the *R61H08> ChR2-XXL* showed a significantly lower premature eclosion rate (11.2±2.3%) at ZT18 compared to its controls (16.0±1.1% for Gal4 and 20.1±2.6% for UAS control; Figures 3.10 B and 3.11 A). Nevertheless, the negative effect was not as strong as the AstA experiment. At ZT19 compared to the controls, more *R61H08> ChR2-XXL* flies eclosed (Figures 3.10 B and 3.11 B). However, the difference was not significantly higher. It is noteworthy that both *AstC::2A> ChR2-XXL* and *R61H08> ChR2-XXL* groups showed a higher eclosion percentage at ZT18 on the first day (Figures 3.9 A-A" and 3.10 A-A").

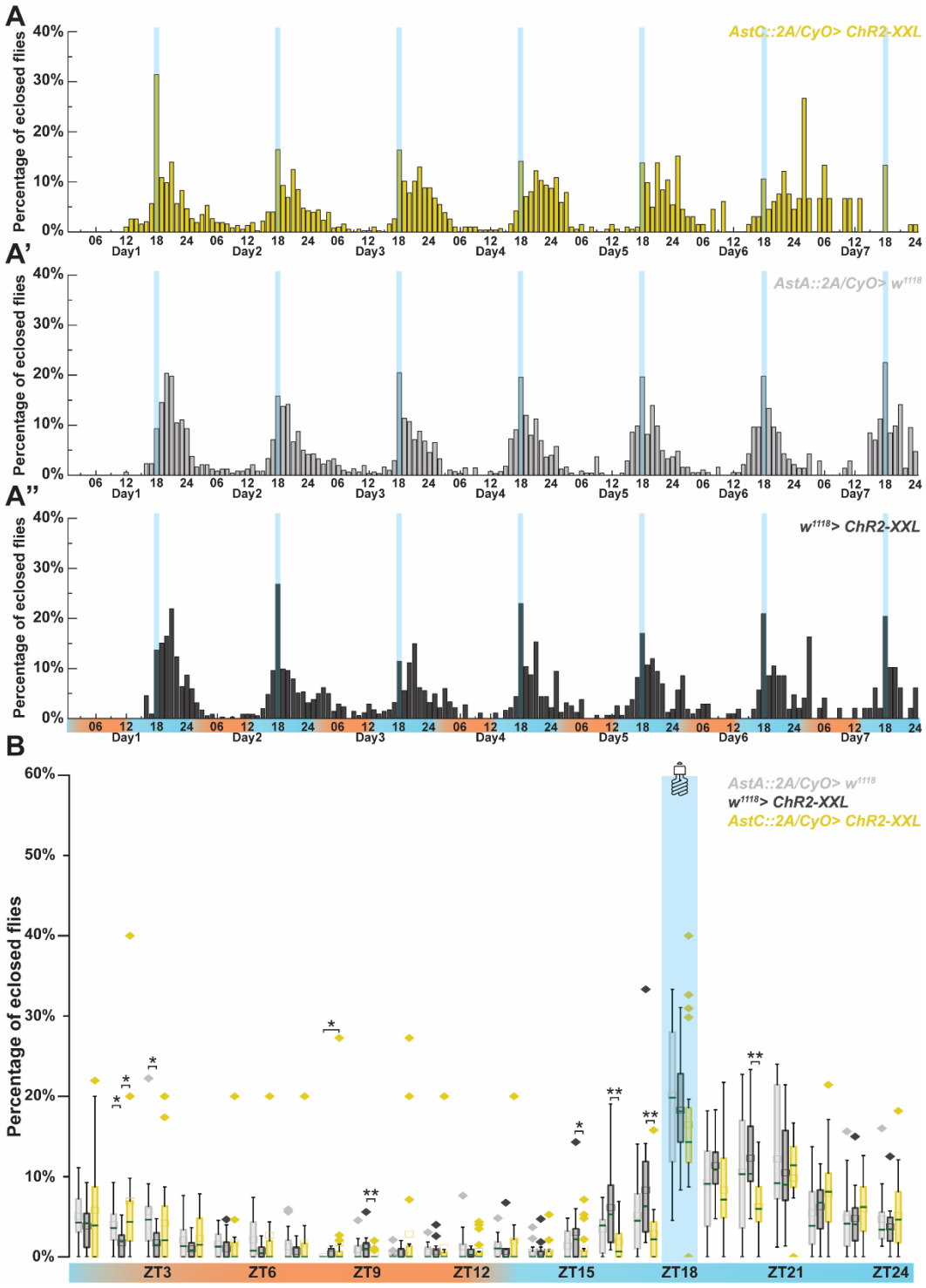

Figure 3.9. Blue light-induced premature eclosion and simultaneous optogenetic activation of the AstC neurons with *AstC::2A-Gal4* did not affect the eclosion rate. The flies were entrained to temperature changes (WC, indicated by an orange-blue gradient). Using Opto-DEM, six hours before subjective morning (ZT24-1 when the temperature changes from cold to warm) at ZT18 one one-hour pulse of intense blue light was shone on the flies (blue bars). The percentage of eclosed flies per hour compared to the entire day is plotted on the y-axis. **A-A"** Opto-DEM measured a higher eclosion rate on the first day for *AstC::2A> ChR2-XXL* flies (~30%; **A**) that drops to ~15% in the next days (on average 16.4±2.2%). The Gal4 control group started lower (~10%; **A'**) and reached up to ~20% over the week (on average 18.3±1.8%). The UAS control remained at ~20% throughout the week (on average

20.1±2.6%; **A”**). **B** Even though at ZT18 the eclosion rate of the experiment group is lower, it was not significantly different compared to the controls ($p \geq 0.05$). The experiment group showed no significant difference to both control groups at any other ZT either. Mann-Whitney *U* analysis followed by a one-sample Wilcoxon signed-rank test: * = $p \leq 0.05$, ** = $p < 0.001$, and *** = $p < 0.0001$.

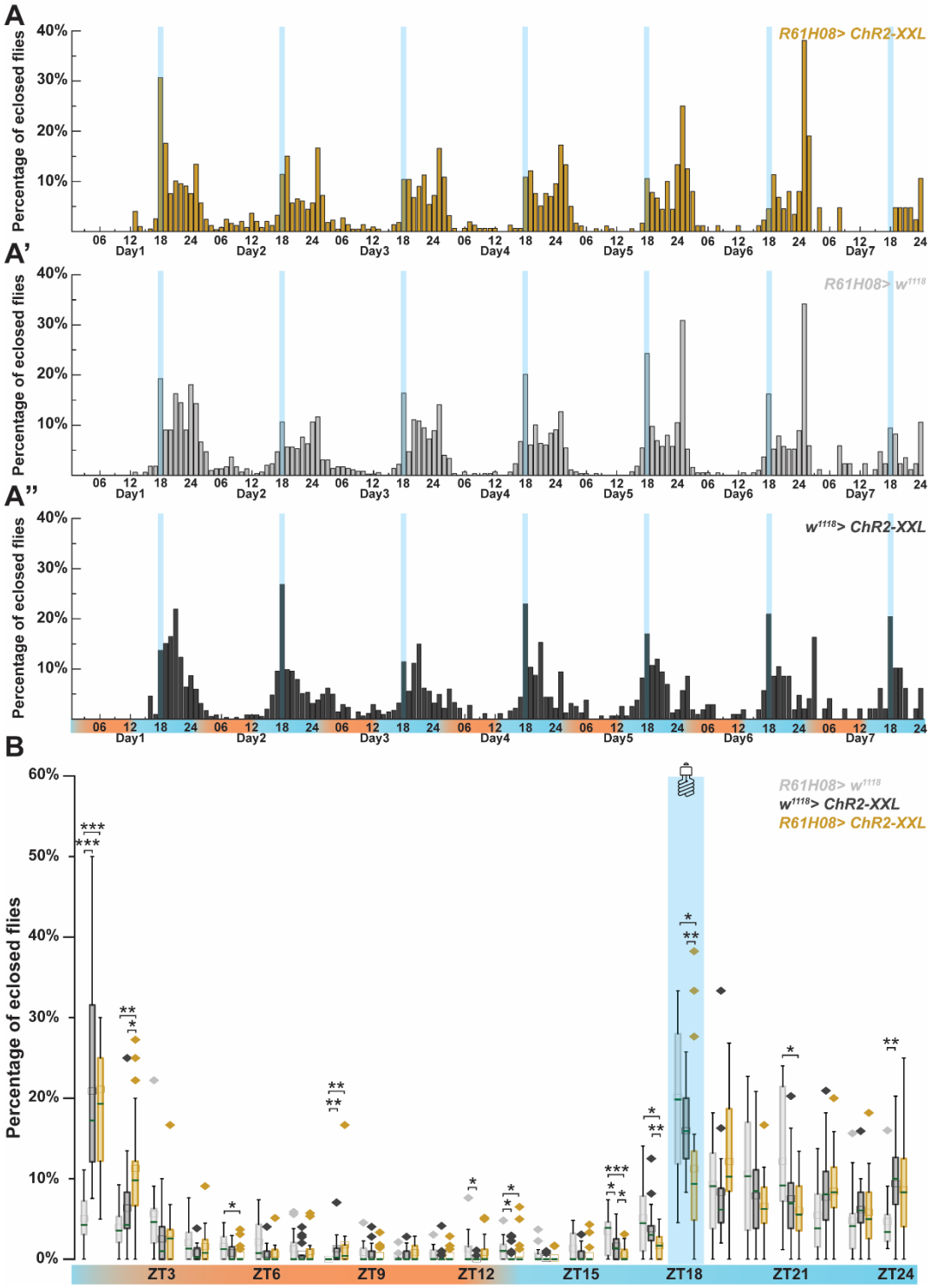

Figure 3.10. Blue light-induced premature eclosion and simultaneous optogenetic activation of the AstC neurons with *R61H08-Gal4* decreased the eclosion rate. The flies were entrained to temperature changes (WC, indicated by an orange-blue gradient). Using Opto-DEM, six hours before subjective morning (ZT24-1 when the temperature changes from cold to warm) at ZT18 one one-hour

pulse of intense blue light was shone on the flies (blue bars). The percentage of eclosed flies per hour compared to the entire day is plotted on the y-axis. **A-A"** While the eclosion rate at ZT18 on the first day for *R61H08> ChR2-XXL* flies was higher (~30%; **A**) it gradually dropped to 0% over the week (on average 11.2±2.3%). Their respective Gal4 control eclosion rate at ZT18 fluctuated between ~10% to ~25% (on average 16.0±1.1%; **A'**) and the UAS control remained constant (20.1±2.6%; **A"**). **B** At ZT18 the eclosion rate of the experiment group was significantly different compared to the Gal4 control ($p < 0.01$) and UAS control ($p < 0.05$) groups. The experiment group showed significant differences to both control groups at ZT2 (higher), ZT16, and ZT17 (lower) as well. Mann-Whitney *U* analysis followed by a one-sample Wilcoxon signed-rank test: * = $p \leq 0.05$, ** = $p < 0.001$, and *** = $p < 0.0001$.

To conclude, optogenetic activation of peptidergic neurons using Opto-DEM significantly decreased light-induced premature eclosion rate in *AstA::2A> ChR2-XXL* and *R61H08> ChR2-XXL*. AstA neurons activation strongly prevented eclosion, possibly either by inhibiting V_m neurons or the neurons that control the motor program of eclosion. Even though activation of AstC neurons prevented eclosion, the exerted effect was not as strong as AstA neurons. The increasing effect upon Ms neuron activation described by Ruf et. al (2017) with a P-element promotor-based Gal4 line was not replicated with *Ms::2A> ChR2-XXL*.

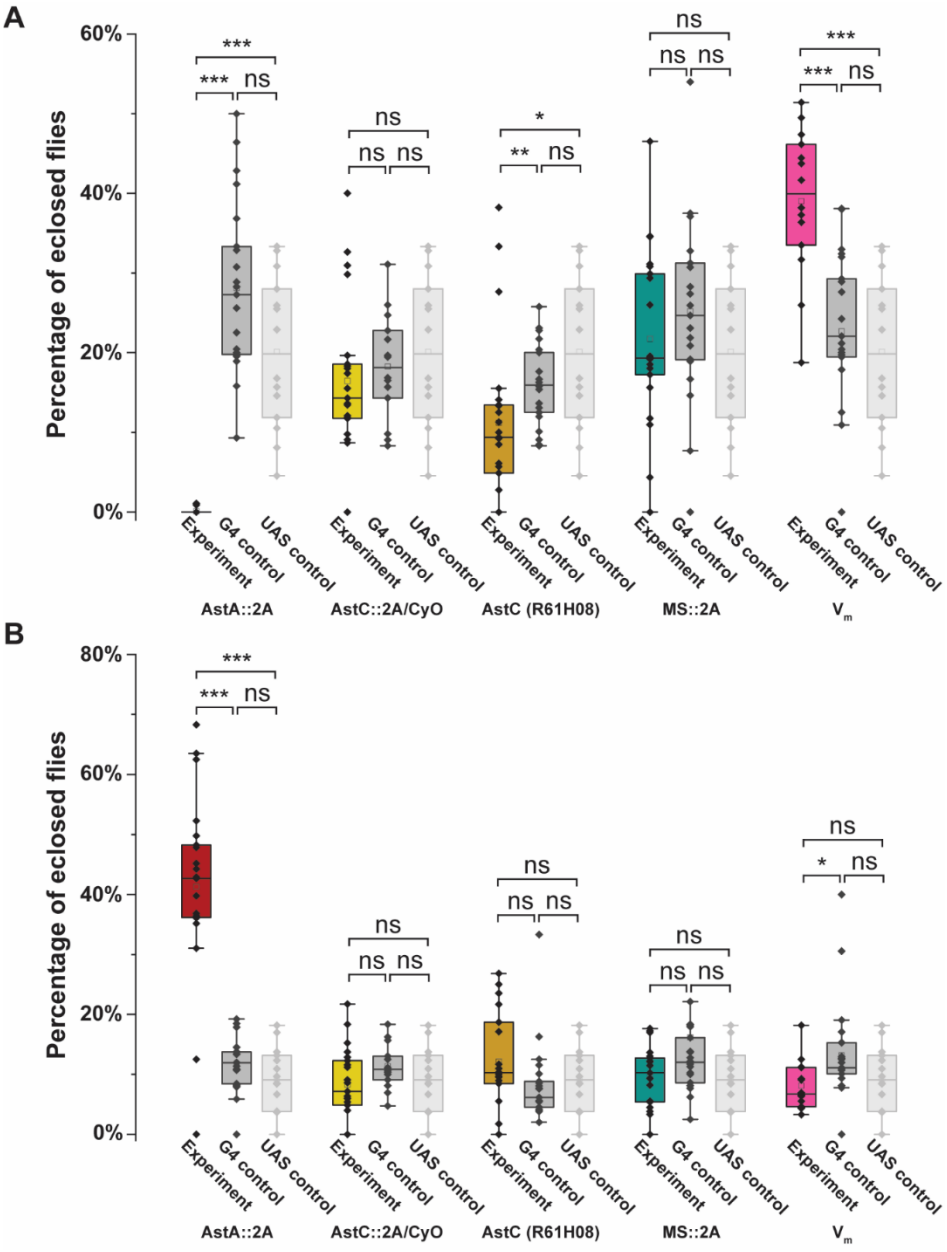

Figure 3.11. Summary: excitation of AstA and AstC neurons significantly decrease the light-induced premature eclosion rate. A The results of the Opto-DEM experiments for AstA, AstC (two different driver lines), Ms, and V_m neurons at ZT18 (during blue light pulse) are summarized. Evidently, during the light pulse, the AstA neurons excitation highly suppressed light-induced premature eclosion compared to its controls ($p < 0.0001$). Also, AstC neurons excitation driven by *R61H08-Gal4* significantly reduced the premature eclosion rate ($p < 0.001$ for Gal4 control and $p < 0.01$ for UAS control). Despite showing a lower eclosion rate compared to their controls, the *AstC::2A> ChR2-XXL* showed no significant decrease in premature eclosion rate. Ms showed no significant difference between the experiment and control group eclosion rates either. Simultaneous excitation of V_m neurons while inducing premature eclosion significantly boosted the eclosion rate ($p < 0.0001$). **B** One hour later at ZT19 when the light pulse was over, significantly more *AstA> ChR2-XXL* flies eclose. It seems that these were the flies that could not eclose during light pulse, perhaps because of the strong inhibitory effects of AstA neurons. Hence, they eclosed only after the light pulse was over. At ZT19 *Eh (C21)> ChR2-XXL* flies compared to their Gal4 control showed lower eclosion rate. ($p < 0.01$). * = $p \leq 0.05$, ** = $p < 0.001$, and *** = $p < 0.0001$. ns = not significantly different.

6. Anatomical characterization of synaptic and peptidergic connections from peptidergic neurons involved in modulating eclosion to the PTTH neurons

Results in III.1 and III.2 showed that the PTTHn express AstA-R1, AstA-R2, AstC-R1, AstC-R2, MsR1, and MsR2, while the V_m neurons express only AstA-R1, AstA-R2, and MsR1 receptors. It was also shown that AstA and AstC negatively affect premature eclosion. In Chapter II, it was shown that some of the clock neurons were presynaptic to the PTTHn and V_m. Most of the clock neurons are peptidergic (Abruzzi et al., 2017; Ma et al., 2021; Reinhard et al., 2023). AstA expressed in $DN1_p$s and LPN neurons (Reinhard et al., 2023, 2022a), AstC from LPNs, DN2s, $DN1_p$s, and many DN3 (Abruzzi et al., 2017; Reinhard et al., 2023). Ms is predicted by single-cell transcriptomics to be expressed by LN_ds (Abruzzi et al., 2017; Reinhard et al., 2023), but this is not supported by immunostainings. Besides peptide-expressing clock neurons, other peptidergic neurons may provide synaptic or peptidergic (through volume transmission) input to PTTHns and V_m neurons. To check whether PTTHns and V_m neurons receive synaptic input from neighboring peptidergic neurons expressing Ms, AstA, or AstC, we used syb-GRASP and trans-synaptic staining methods. The driver lines used for the Opto-DEM experiments above mark many neurons expressing the same peptide. Not all of these neurons are necessarily presynaptic to PTTHn or V_m neurons, but BAcTrace can identify the ones that provide the synaptic input. Complementary to BAcTrace, a positive *trans*-Tango signal shows whether PTTHn and V_m neurons receive synaptic input from neurons with a given chemical identity.

a. Myosuppressin

The *Ms::2A-Gal4* driver line drove GFP expression in around 180 neurons (See Appendix 6). To check for the possibility of synaptic connectivity between PTTHn and their neighboring Ms neurons, double staining was performed. mCD::GFP was expressed in PTTHn while rCD2::RFP was expressed in Ms neurons. The PTTHn and Ms neurons that reside in superior neuropils (superior lateral protocerebrum neuropil (SLP), superior intermediate protocerebrum neuropil (SIP), and superior medial protocerebrum neuropil (SMP) were close to each other. Therefore, possible synaptic connections between Ms neurons and PTTHn were formed in the superior protocerebrum (Figure 3.12 A'). The strong syb-GRASP in the SMP and around the esophageal orifice in the prow neuropil (where PTTHns exit the brain through nervi corporis cardiacii to PG) showed that these neurons form synaptic connections (Figure 3.12 B). *Ptth::2A-Gal4; Ms::2A-LexA> BAcTrace* showed that from a total of 180 Ms neurons in the brain, only a few are presynaptic to the PTTH neurons (Figure 3.12 C-C'). A group of five to six neurons with cells in the PI send down their processes to the SMP and through the MBDL to the prow and showed the strongest BAcTrace signal (Figure 3.12 D-D"). These large cell-bodied neurons were previously described as Taotie neurons (Hadjieconomou et al., 2020; Zhan et al., 2016). The second strong signal was made by two lateral Ms neurons projecting to the SLP (Figure 3.12 G-G"). Other presynaptic Ms neurons were two anteriorly located neurons that projected to the antennal lobe (Figure 3.12 E-E"), four-five medial neurons that projected to bulb neuropil (Figure 3.12 F-F"), and a single posteriorly located neuron that projected to the lateral horn, clamp and the pedunculus of the mushroom bodies (Figure 3.12 H-H"). Unfortunately, the tdTomato signal expressed by BAcTrace did not show the complete neuronal morphology. Therefore, BAcTrace was limited in anatomically depicting single

neuronal arborizations. Individual morphology of single Ms neurons has not yet been described. Therefore, it is not exactly clear where the posteriorly located Ms neuron (projecting to the lateral horn, clamp, and pedunculus) processes overlapped with PTTHn. *Ms::2A> trans-Tango* showed that both PTTHn receive synaptic input from the Ms neurons (Figure 3.12 I').

To summarize PTTHn neurons received both peptidergic (by expressing MsR1 and MsR2) and synaptic input from Ms neurons. These Ms neurons were five-six Taotie, two SLP projecting, two antennal lobe projecting, four-five bulb projecting, and a single Ms neuron whose cell body was located at the posterior cell body rind.

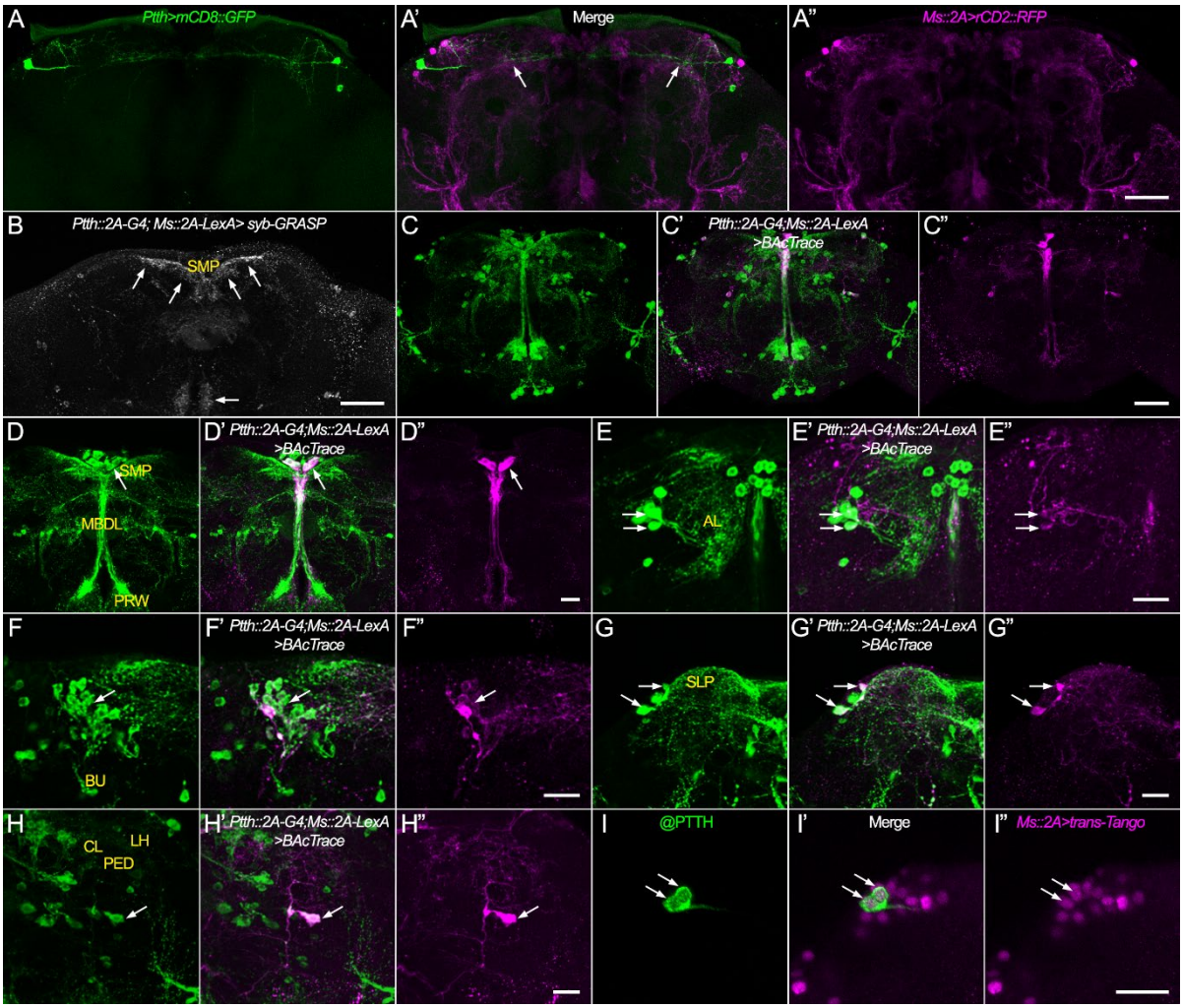

Figure 3.12. The PTTHn received synaptic input from Ms neurons at the superior neuropils and esophagus orifice regions. A-A" Double labeling PTTHn (using *Ptth::2A-Gal4> UAS-mCD8::GFP*) and Ms neurons (using *Ms::2A-LexA> LexAop-rCD2::RFP*). **A** mCD8::GFP (green) was expressed in PTTHn. **A'** In the superior neuropils region of the brain (arrows) PTTHn and the Ms neurons were close to each other. **A"** Expression of rCD2::RFP (magenta) in Ms neurons showed that Ms neurons heavily arborized in the brain, especially in the superior protocerebrum and optic lobes. **B** Synaptic connections between PTTHn and Ms neurons were checked with syb-GRASP. A syb-GRASP signal between PTTHn and Ms neurons was visible at the medial superior medial protocerebrum (SMP; top arrows) and prow (PRW; bottom arrow). **C** *Ptth::2A-Gal4; Ms::2A-LexA> BAcTrace* expresses GFP (green) in nearly 180 Ms neurons. **C'** BAcTrace GFP and tdTomato colocalized only in a few Ms neurons. **C"** The overall image of the Ms neurons that expressed positive BAcTrace signal (tdTomato; magenta)

showed only a few of Ms neurons provided synaptic input to PTTHn. **D-H** BAcTrace showed the Ms neurons providing synaptic input to PTTH. **D-D"** Five-six Ms neurons with cell bodies in the PI that projected to the SMP and through the median bundle (MBDL) to the PRW were presynaptic to PTTHns. **E-E"** Two antennal lobe-projecting (AL) Ms neurons were also presynaptic to PTTHns. **F-F"** Other Ms neurons presynaptic to PTTHn were four to five bulb (BU) projecting neurons. **G-G"** Two lateral neurons that projected to the superior lateral protocerebrum (SLP) provided PTTHn with synaptic input. **H-H"** And only one posterior Ms neuron projecting to the clamp (CL), pedunculus of mushroom body (PED), and lateral horn (LH) was upstream of the PTTHns. **I-I"** *trans*-Tango showed that both PTTHns received synaptic input from Ms neurons. **I** PTTHn were identified using anti-PTTH (arrows). **I'** The nuclear RFP signal of *trans*-Tango was visible in both PTTHn. **I"** *Ms::2A> trans-Tango* drove nuclear RFP expression in all neurons postsynaptic to Ms neurons (arrows point to PTTHn). The names of the neuropils were indicated with yellow letters. *Scale bars*: A-C 50 μm and D-I 20 μm.

b. Allatostatin A

The experiments dissecting the connections of AstA and AstC neurons to PTTHn and AstA and AstC neurons to EH neurons were performed by Abdullah Sert (part of his BSc thesis supervised by Emad Amini) and Emad Amini (Sert, 2022). Their data acquisition and analysis were performed by Emad Amini.

The possibility of synaptic input from AstA neurons to PTTHn was checked using immunostaining-based techniques. First, to check if there are possible overlaps between the processes of AstA neurons and PTTHn, double staining was performed. Using *Ptth::2A-Gal4> UAS-mCD8::GFP* the PTTHn and using *AstA::2A-LexA> LexAop-rCD2::RFP* AstA neurons were marked. *AstA::2A-LexA* driver line marked ~400 neurons in the brain. Different subsets of these neurons heavily arborize different neuropils such as SMP, SIP, SLP, optic lobes, central complex, and dorsal fan-shaped body (see Appendix 7). Many AstA neurons reside or arborize in the superior protocerebrum, and therefore represent potential synaptic partners of the PTTHn (Figure 3.13 A'-A"). However, unlike what was shown for PTTHn and Ms neurons (Figure 3.12 B), the GRASP signal between the AstA and PTTHn was sparse and mainly limited to the SLP and SMP (Figure 3.13 B). BAcTrace showed that a small portion of the AstA neurons were presynaptic to the PTTHn (Figure 3.13 C-C"). More precisely, five distinctive neuronal groups were involved in signaling to PTTHn. Four neurons with cell bodies residing at the lobula rim and projecting to the lobula and SLP make up the first group (Figure 3.13 D-D"). A pair of neurons with large cell bodies in the SEZ that project to the prow, flange neuropil, and via the MBDL to the SMP showing the strongest BAcTrace signal (Figure 3.13 E-E"). As previously described (Figure 1.3 I-I") two of the LPN clock neurons provide input to the PTTHn (Figure 3.13 F-F"). A pair of neurons with cell bodies located at the SMP cell body rim and projecting to the SMP and clamp (Figure 3.13 G-G"), and an AstA neuron that projected to the SLP that has been previously described to be important for sleep regulation (Ni et al., 2019; Figure 3.13 H-H"). *AstA> trans-Tango* confirmed that both PTTHn are postsynaptic partners of the AstA neurons (Figure 3.13 I-I").

In conclusion, both PTTHn received synaptic and peptidergic (through expression of AstA-R1 and AstA-R2) input from AstA neurons. The sparse and limited GRASP signal between AstA and PTTHn in SLP and SMP indicated that AstA mainly provides peptidergic input to PTTHn. BAcTrace showed in each hemisphere one large cell-bodied AstA neuron sitting at SEZ and projecting through MBDL to SMP, four lobula projecting neurons, two LPN clock neurons,

and one SMP and clamp projecting neuron (in total eight AstA neurons) were presynaptic to PTTHn. Finally, colocalization of PTTH and RFP derived by *AstA> trans-Tango* in PTTHn showed that both PTTHn receive synaptic input from AstA neurons.

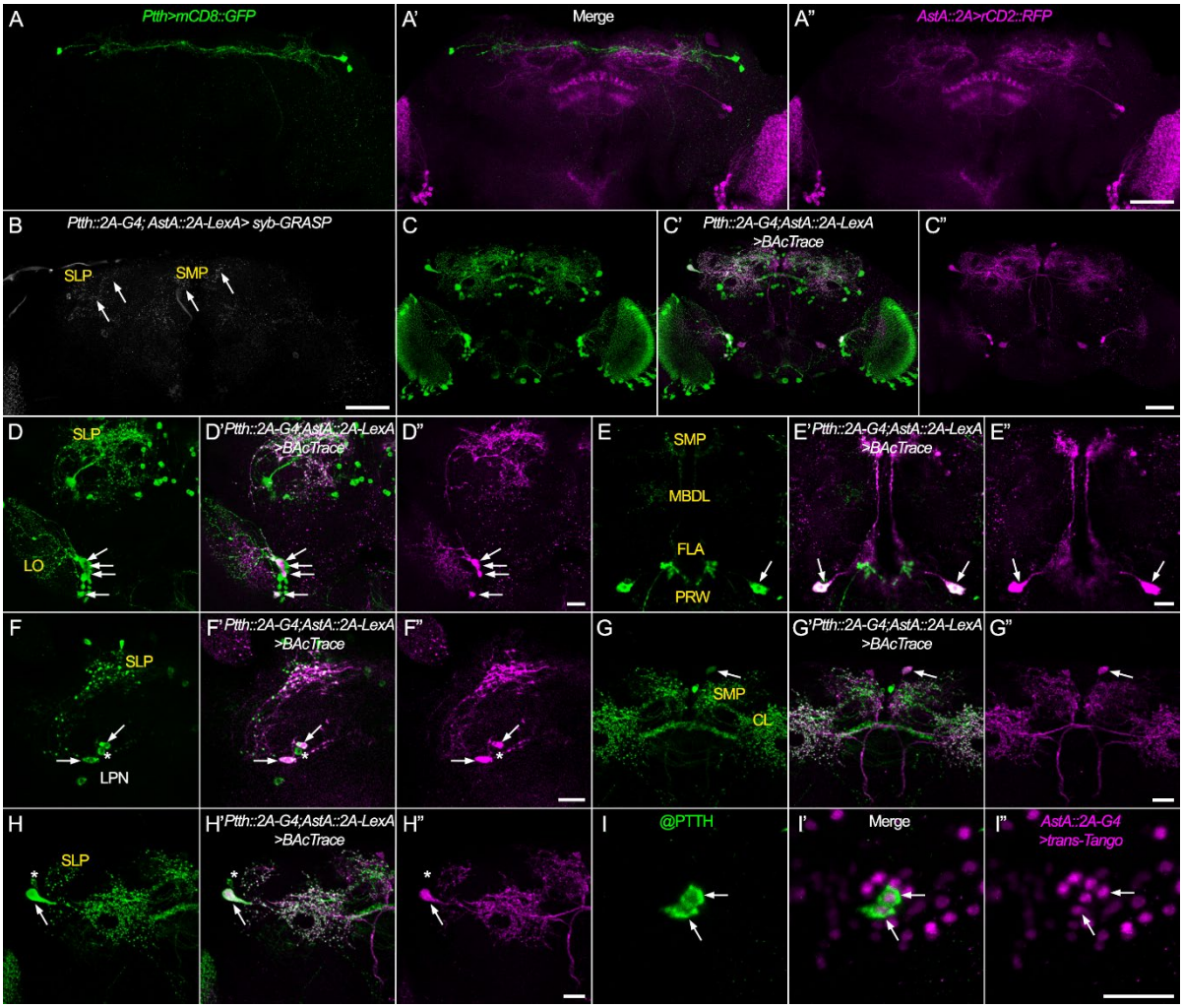

Figure 3.13. AstA neurons provided synaptic input to the PTTHn. A-A" Double labeling PTTHn (using *Ptth::2A-Gal4> UAS-mCD8::GFP*) and AstA neurons (using *AstA::2A-LexA> LexAop-rCD2::RFP*). **A** mCD8::GFP (green) was expressed in PTTHn. **A'** In the superior neuropils region of the brain (arrows) PTTHn and AstA neurons were adjacent to each other. **A"** Expression of rCD2::RFP (magenta) in AstA neurons showed that AstA neurons heavily arborized in different brain regions, especially in the superior protocerebrum (superior medial protocerebrum (SMP), superior intermediate protocerebrum (SIP), and superior lateral protocerebrum (SLP), dorsal fan-shaped body, and optic lobes. **B** To check for the synaptic connections between PTTHn and AstA neurons syb-GRASP was used. The GRASP signal between PTTHn and AstA neurons only showed a weak and sparse signal in SLP and SMP (arrows). **C** *Ptth::2A-Gal4; AstA::2A-LexA> BAcTrace* expressed GFP (green) in nearly 400 AstA neurons. **C'** GFP and tdTomato fluorescent proteins only colocalized in about 18 AstA neurons. **C"** The overall image of the AstA neurons that expressed tdTomato (magenta) showed only a few of AstA neurons provided synaptic input to PTTHn. **D-H** Using BAcTrace AstA neurons presynaptic to PTTH were marked. **D-D"** Four neurons from a group of AstA neurons that projected to lobula (LO) and SLP were upstream of PTTHns. **E-E"** The strongest BAcTrace signal was detected in a pair of large cell-bodied AstA-SEZ neurons projecting to the prow (PRW), flange (FLA), and through the median bundle (MBDL) to the SMP. **F-F"** Two LPN clock neurons were found to be presynaptic to PTTHns. **G-G"** One medial AstA neuron projecting to the SMP and clamp (CL) was presynaptic to

PTTHns. **H-H"** Finally BAcTrace marked one large SLP projecting AstA neuron presynaptic to PTTHns. **I-I"** *trans*-Tango showed that both PTTHns received synaptic input from AstA neurons. **I** PTTHn were identified using anti-PTTH (arrows). **I'** The nuclear RFP signal of *trans*-Tango was visible in both PTTHn. **I"** *AstA::2A> trans-Tango* drove nuclear RFP expression in all neurons postsynaptic to AstA neurons (arrows point to PTTHn). Neuropils were indicated with yellow letters. *Scale bars*: A-C 50 μm and D-I 20 μm.

c. Allatostatin C

As shown in III.1, PTTHn expressed both AstC receptors, suggesting that PTTHns receive peptidergic input from AstC neurons. To check for the possibility of synaptic input from AstC neurons to PTTHn, immunostaining-based anatomical approaches were used. To demonstrate the morphology of the AstC neurons, two driver lines were used, *AstC::2A-Gal*4 and *R61H08-Gal4*. For BAcTrace, only *R61H08-LexA* was available. Double staining using *Ptth::2A-LexA>LexAop-rCD2::RFP* and *R61H08-Gal4>UAS-mCD8::GFP*, showed that AstC neurons in the superior protocerebrum came close to PTTHn (Figure 3.14 A-A"). *Ptth::2A-LexA; R61H08-Gal4> syb-GRASP* flies showed a syb-GFP signal only in the lateral SMP (Figure 3.14 B-B') and nowhere else. *R61H08-LexA; Ptth-Gal4* flies were used for BAcTrace, but this did not identify any AstC neurons presynaptic to PTTHn (Figure 3.14 C-C"). This lack of signal might be due to the weakness of the *R61H08-LexA* driver. Therefore, the BAcTrace results are inconclusive. *AstC::2A> trans-Tango* showed that all PTTHns are postsynaptic to the AstC neurons (Figure 3.14 D-D").

Taken together, it is evident that AstC modulates the PTTHns by AstC receptors through volume transmission. AstC neurons in the SMP provide synaptic input to PTTHn but to identify the upstream AstC neurons will require more investigation with better driver lines or other techniques in the future.

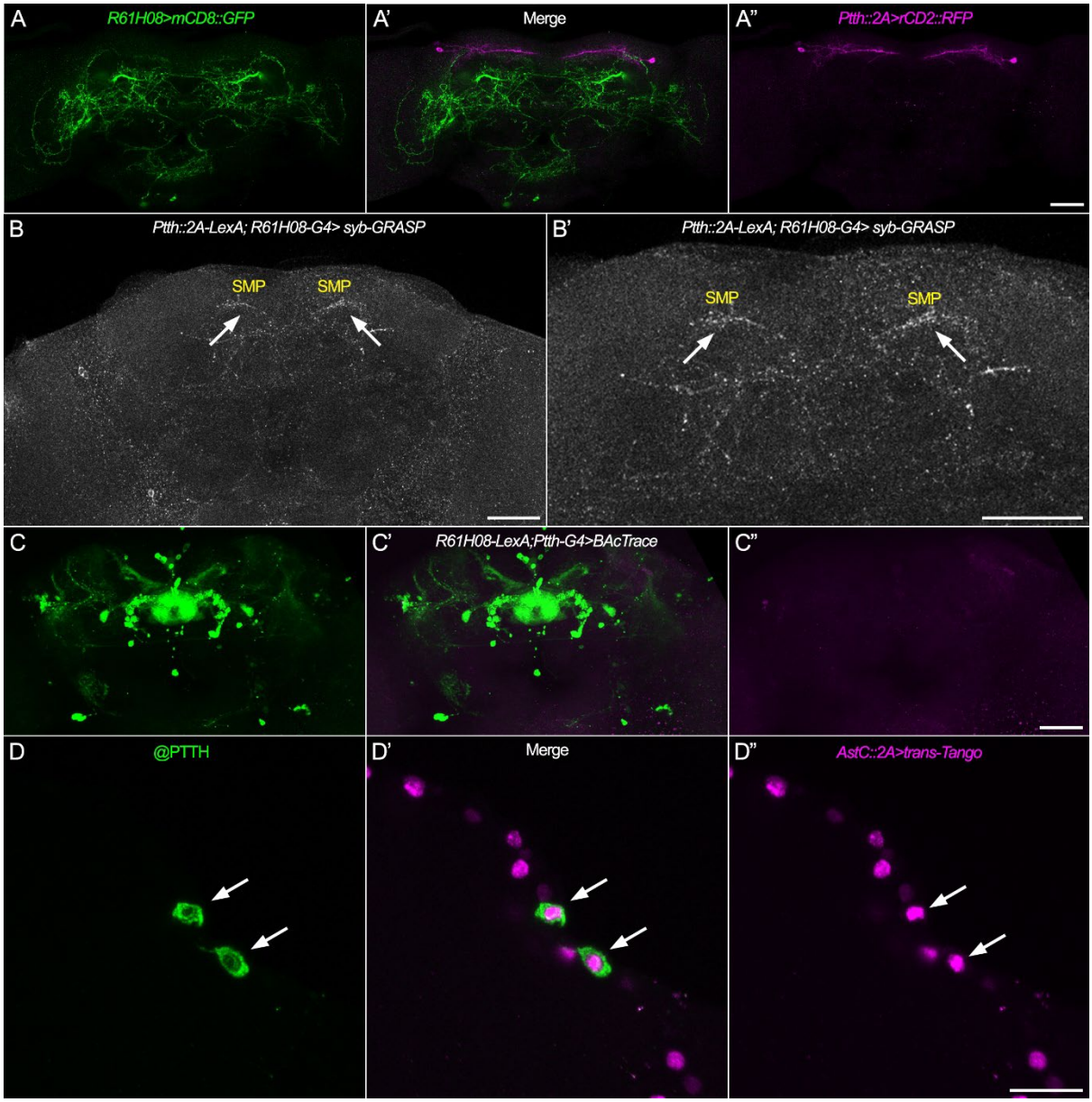

Figure 3.14. The PTTHn received synaptic input from AstC neurons. A-A" Double labeling AstC neurons (using *R61H08-Gal4> UAS-mCD8::GFP*) and PTTHns (using *Ptth::2A-LexA> LexAop-rCD2::RFP*). **A** mCD8::GFP (green) expression in AstC neurons showed AstC neurons projections in the superior protocerebrum, SEZ, lobula plate, and posterior lateral protocerebrum. **A'** The processes of the PTTHn and the AstC neurons overlapped in the superior protocerebrum. **A"** rCD2::RFP (magenta) was expressed in PTTHn. **B-B'** Synaptic connectivity between PTTHns and AstA neurons was checked using syb-GRASP. *Ptth::2A-LexA; R61H08-Gal4> syb-GRASP* signal showed overlap between PTTHn and AstC resulting in synaptic connections between them in the lateral part of superior medial protocerebrum (SMP; arrows). **C-C"** To identify presynaptic AstC neurons to PTTHns, BAcTrace was used. *R61H08-LexA; Ptth-Gal4> BAcTrace* only showed the GFP signal (**C-C'** green) and not the tdTomato (**C"**) meaning BAcTrace failed to identify the presynaptic AstC neurons to PTTHn perhaps due to weakness of driver line. **D-D"** *trans*-Tango showed that both PTTHns received synaptic input from AstC neurons. **D** PTTHns were stained using anti-PTTH (arrows). **D'** The colocalization of nuclear RFP and PTTH (arrows) showed that both PTTHns were postsynaptic to AstC neurons. **D"** *AstC::2A> trans-Tango* drove nuclear RFP expression in all neurons postsynaptic to AstC neurons (arrows marked PTTHn). *Scale bars*: A-C 50 µm and D 20 µm.

7. Connections from peptidergic neurons involved in modulating eclosion to the EH neurons

Part III.2 showed that the V_m neurons express receptors for Ms and AstA, suggesting that V_m neurons are modulated by these two neuropeptides. On the other hand, D_{ls} mainly expressed AstC receptors. Like what was shown in part III.6, here the immunostaining-based approach was used to identify the Ms, AstA, and AstC neurons presynaptic to the V_m neurons as well.

a. Myosuppressin

In part III.2 it was shown that MsR1 is expressed by the V_m neurons. Therefore, Ms possibly plays a role in modulating the V_m neurons. To test for synaptic connections between the Ms and EH neurons and identify the presynaptic partners, we again used an anatomic approach. The first step was to double-stain EH and Ms neurons. For that, *Ms::2A-Gal4> UAS-mCD8::GFP* was used to label Ms neurons and *Eh::2A-LexA> rCD2::RFP* labeled the EH neurons. The V_m neurons were closely located to Taotie Ms neurons. Taotie cell bodies were located in the PI and projected to the SMP and through the MBDL to the peri-esophageal neuropil prow. Around the esophagus orifice, V_m neurons were neighbors to another group of Ms neurons with cell bodies residing in the SEZ that projected to the saddle neuropil (Figure 3.15 A-A"). The D_{ls} also came in close contact with the Ms neurons at the SLP (Figure 3.15 B-B"). To check for synaptic connections between Ms and EH neurons syb-GRASP was used. *Ms::2A-Gal4/Eh::2A-LexA> syb-GRASP* showed a strong signal in the SMP and SLP. Most connections between the V_m and the Ms neurons were made in the SMP and around the MBDL and the esophagus orifice, while D_{ls} formed synaptic connections to Ms neurons in the SLP (Figure 3.15 C-C' and D-D'). BAcTrace showed that some of the Ms neurons previously found to be presynaptic to PTTHn were also presynaptic to the V_m neurons. The strongest BAcTrace signal was from the Taotie neurons and the pair of neurons that projected to the saddle (Figure 3.15 F-F"). Two other groups were the lateral horn-projecting neurons (Figure 3.15 H-H") and some of the neurons of the bulb-projecting cluster (Figure 3.15 I-I"). The positive BAcTrace signal was visible in neurons projection to the antennal lobe (Figure 3.15 E-E") and clamp (Figure 3.15 G-G"), and in a posterior neuron with unidentifiable projections (Figure 3.15 J-J"). For *trans*-Tango, the EH neurons were marked by expressing myr::GFP due to the lack of an antibody against EH. Surprisingly, the *Ms::2A> trans-Tango* did not mark any of the EH neurons (Figure 3.15 K-K" and L-L").

Taken together, our data suggest that V_m neurons are modulated by Ms as they express MsR1. Moreover, based on the strong syb-GRASP and BAcTrace signal, V_m neurons seem to be postsynaptic to Ms neurons. However, the lack of *trans*-Tango-driven RFP expression in V_m neurons seems to contradict this conclusion. Except for the GRASP signal, there is no other evidence that D_{ls} receive input from the Ms neurons and a connection therefore is unlikely.

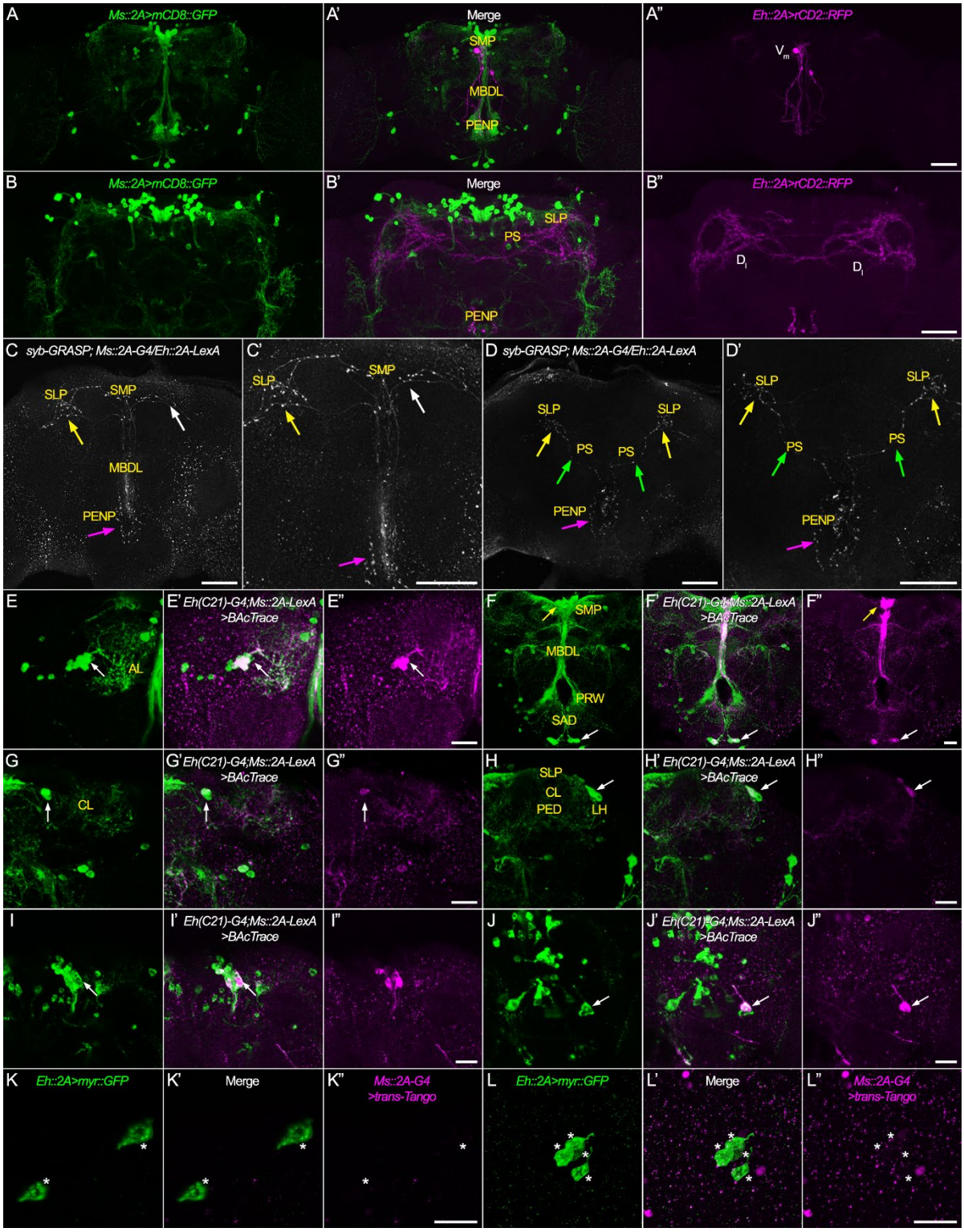

Figure 3.15. V_m neurons received synaptic input from the Ms neurons. A-A" Double labeling Ms (using *Ms::2A-Gal4> UAS-mCD8::GFP*) and V_m neurons (using *Eh::2A-LexA> LexAop-rCD2::RFP*). **A** mCD8::GFP (green) was expressed in Ms neurons and showed Ms neurons projecting through the median bundle (MBDL) and suboesophageal zone (SEZ), and Ms neurons that projected to the esophagus orifice (anterior view plane). **A'** The arborizations of V_m neurons and Ms neurons were adjacent to each other at MBDL. **A"** To label the V_m neurons, rCD2::RFP (magenta) was expressed in V_m neurons. **B-B"** Double labeling Ms (using *Ms::2A-Gal4> UAS-mCD8::GFP*) and D_l neurons (using *Eh::2A-LexA> LexAop-rCD2::RFP*). **B** mCD8::GFP (green) expression showed Ms neurons arborized

superior protocerebrum (posterior view plane). **B'** The arborizations of D_l neurons and Ms neurons overlapped in the superior lateral protocerebrum (SLP). **B"** rCD2::RFP (magenta) was expressed in D_l neurons and showed their arborization morphology in the posterior slope, SLP, and lateral horn. **C-C'** The V_m and Ms neurons made synaptic connections around the superior medial protocerebrum (SMP) and SLP (white arrows), MBDL, and the esophagus foramen (magenta arrow). **D-D'** The D_ls and Ms neurons made synaptic connections at the SLP (white) and posterior slope (PS; green arrows). The signal around the esophagus orifice (magenta arrow) was from the V_m and Ms connections. **E-J** *Eh (C21)-Gal4; Ms::LexA> BAcTrace* showed that the Ms neurons were presynaptic to V_ms (neurons expressing both GFP and tdTomato were marked by arrows): **E-E"** BacTrace showed three antennal lobe projecting (AL) Ms neurons were presynaptic to the V_m neurons. **F-F"** The strongest BAcTrace signal belonged to four to five Taotie neurons projecting to the SMP and through MBDL to the prow (PRW) and a pair of saddle-projecting (SAD) neurons with cell bodies located in the SEZ. **G-G"** BAcTrace marked Ms neurons projecting to the clamp (CL) to be presynaptic to V_m neurons. **H-H"** Other Ms neurons presynaptic to V_m projected to the lateral horn (LH), SLP, CL, and pedunculus of mushroom bodies (PED). **I-I"** BAcTrace showed a group of three to four Ms neurons possibly projecting to the bulb (BU) to be also presynaptic to V_ms. **J-J"** Finally with BAcTrace a posteriorly located neuron with an unknown arborization pattern was shown to be upstream partner of V_m neurons. **K-K"** Surprisingly, *Ms::2A> trans-Tango* showed neither V_m neurons **L-L"** nor D_ls were postsynaptic to Ms neurons (the lack of colocalization of GFP and nuclear RFP signal of *trans*-Tango is marked by asterisks). The names of the neuropils are indicated with yellow letters. *Scale bars*: A-D 50 μm and E-L 20 μm.

b. Allatostatin A

The V_m neurons express both AstA receptors as shown in part III.2. Double stainings of AstA and EH neurons, however, showed that not many AstA neurons were in close contact with arborization of the V_m neurons in the antennal lobe, SMP, and MBDL (Figure 3.16 A-A"). On the other hand, many AstA neuronal processes overlapped with the arborizations of the D_ls (Figure 3.16 B-B"). Nevertheless, the GRASP signal between EH and AstA neurons was very faint (Figure 3.16 C-C" and D-D"). The V_m and AstA neuron-associated syb-GRASP signal was limited to a small region of the medial SMP (Figure 3.16 C-C"), while the D_ls and AstA neuron GRASP signal was limited to the SLP (Figure 3.16 D-D"). Both signals were sparse, faint, and limited to small regions. Again, BAcTrace was used to identify whether AstA neurons were presynaptic to the V_m neurons. Some of the identified neurons were the same AstA neurons that provided synaptic input to PTTHn (see III.6.b): the PI neurons projecting to the SMP and clamp (Figure 3.16 H-H"), the large MBDL passing neurons that project to the prow, flange, and SMP (Figure 3.16 I-I"), two of the LPNs (Figure 3.16 J-J"), and one SLP-projecting neuron. The SLP-projecting neuron along with the LPNs are known to regulate sleep (Figure 3.16 G-G"; Ni et al., 2019). Other neurons that showed a positive BAcTrace-driven tdTomato signal were one AstA neuron projecting to the anterior ventrolateral protocerebrum neuropil (Figure 3.16 F-F") and one SMP projecting AstA neuron that showed faint expression of tdTomato (Figure 3.16 E-E"). Complementary to BAcTrace, *trans*-Tango labeled the V_m neurons (Figure 3.16 K-K") and three of four D_ls (Figure 3.16 L-L") to be postsynaptic to AstA neurons.

To summarize, the EH neurons (both V_ms and most D_ls) seem to receive synaptic as well as peptidergic input from AstA neurons. The weak and sparse GRASP signal suggested that the connections between the AstA and EH neurons are mainly peptidergic. In total, from about 400 AstA neurons in the brain, only seven neurons in each hemisphere appear to provide synaptic

input to EH neurons. Five groups of these AstA neurons (AstA neurons located at PI, the large MBDL passing AstA neurons, two of the LPNs, one SLP-projecting AstA neuron, and one AstA neuron projecting to the anterior ventrolateral protocerebrum neuropil) provided input to both PTTHn and EH neurons.

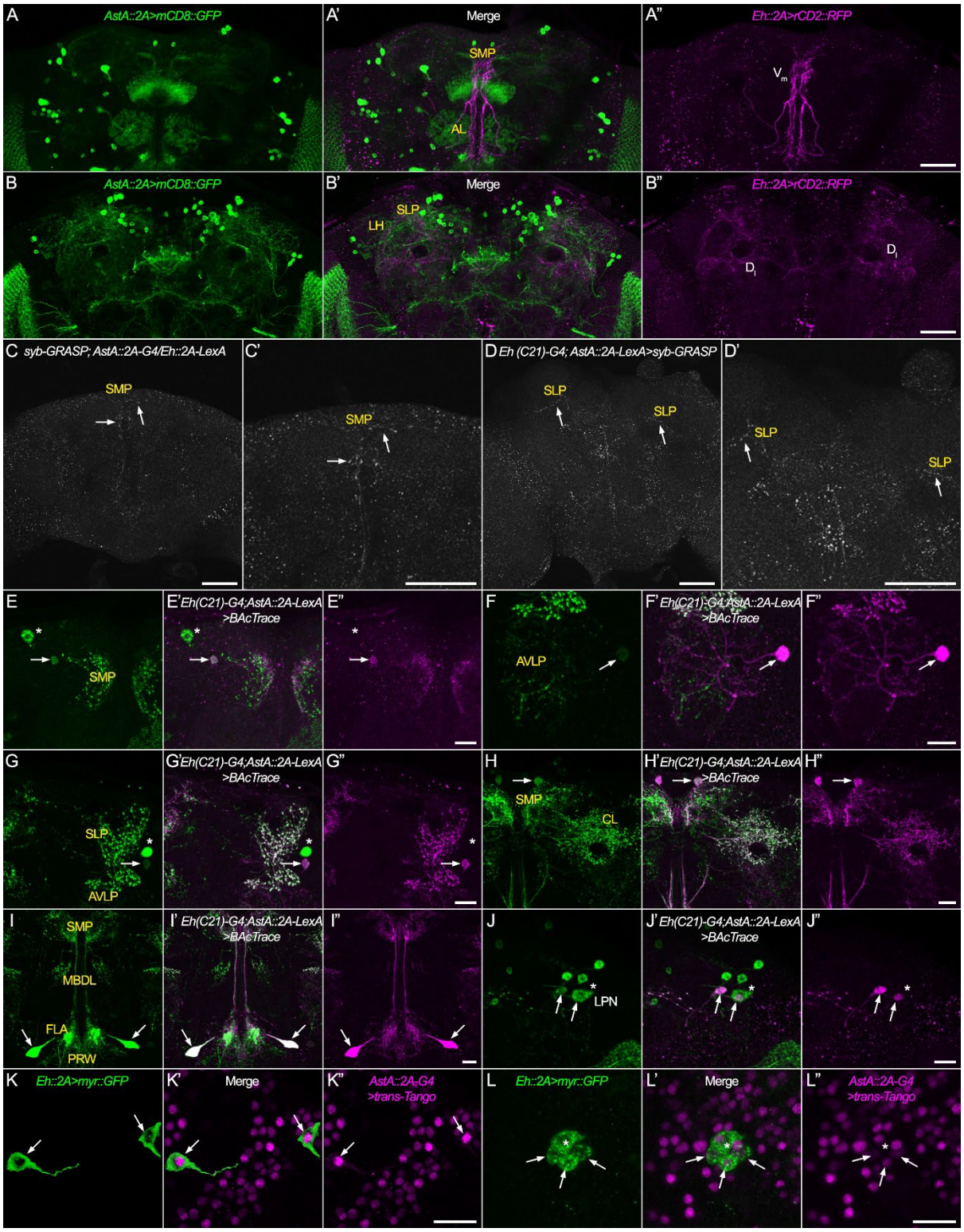

Figure 3.16. EH neurons were postsynaptic partners of the AstA neurons. A-A" Double labeling AstA (using *AstA::2A-Gal4> UAS-mCD8::GFP*) and V_m neurons (using *Eh::2A-LexA> LexAop-*

rCD2::RFP). **A** mCD8::GFP (green) was expressed in AstA neurons and showed AstA neurons projecting to the median bundle, antennal lobe (AL), fan-shaped body, and suboesophageal zone (SEZ; anterior view plane). **A'** The arborization of the V_m and AstA neurons met at medial superior medial protocerebrum (SMP), median bundle, and AL. **A"** rCD2::RFP (magenta) was expressed in V_m neurons. **B-B"** Double labeling AstA (using *AstA::2A-Gal4> UAS-mCD8::GFP*) and D_l neurons (using *Eh::2A-LexA> LexAop-rCD2::RFP*). **B** mCD8::GFP (green) expression showed AstA neurons that arborized in the superior lateral protocerebrum (SLP), lateral horn (LH), dorsal fan-shaped body, and posterior slope (posterior view plane). **B'** D_l and AstA neuron processes overlapped at the SLP, LH, and posterior slope. **B"** rCD2::RFP (magenta) is expressed in D_l neurons. **C-D** syb-GRASP was used to check synaptic connectivity between AstA and EH neurons. **C-C"** The syb-GRASP signal between the V_m and AstA was weak and limited to a small region of the SMP. **D-D"** The GRASP signal for D_ls and AstA neurons was also weak and limited to the posterior SLP. **E-J** To identify the AstA neurons upstream of V_m neurons BAcTrace (*Eh (C21)-Gal4; AstA::2A-LexA> BAcTrace*) was used (arrows). **E-E"** BAcTrace showed one SMP projecting AstA neuron presynaptic to the V_m neurons. **F-F"** One anterior ventrolateral protocerebrum projecting (AVLP) AstA neurons was identified to be presynaptic to V_ms. **G-G"** BAcTrace showed one SLP projecting AstA neurons upstream of V_m. **H-H"** A pair of SMP and clamp projecting (CL) AstA neurons were also identified by BAcTrace. **I-I"** The strongest BAcTrace signal was detected in a pair of large cell-bodied AstA neurons projecting to prow (PRW), Flange (FLA), and via median bundle (MBDL) to SMP. **J-J"** And finally two LPN clock neurons were identified to be presynaptic to the V_m neurons. The four latter groups (**G'**, **H'**, **I'**, and **J'**) were the same neurons that provided input to PTTHn as well. **K-L** *trans*-Tango showed nearly all EH neurons were postsynaptic to AstA neurons. **K-K"** *AstA::2A> trans-Tango* showed both V_m neurons and **L-L"** three out of four D_ls are postsynaptic to the AstA neurons (colocalization of GFP and nuclear RFP signal of *trans*-Tango was marked by arrows and their lack of colocalization by asterisks). Names of the neuropils were indicated with yellow letters. *Scale bars*: A-D 50 μm and E-L 20 μm.

c. Allatostatin C

AstC receptors were the most broadly expressed receptors by the D_ls (see III.2). Using opto-DEM, it was shown in part III.5 that exciting AstC neurons with *R61H08-Gal4* driver while inducing premature eclosion with blue light lowered eclosion rate. Nevertheless, this eclosion suppression was not as strong as AstA excitation (see III.5). Therefore, the question was whether EH^+ neurons received any direct synaptic input from AstC neurons. To check for overlap between EH and AstC neurons as potential sites of synaptic connections, double staining was performed. *AstC::2A-Gal4> UAS-mCD8::GFP* expression in AstC neurons and *Eh::2A-LexA> rCD2::RFP* expression in EH neurons showed two sites of overlap. Overlap between AstC and V_m neuronal processes was limited to the medial SMP and MBDL (Figure 3.17 A-A"). The D_ls and AstC arborizations also met in the superior protocerebrum from the SMP to the SLP and lateral horn (Figure 3.17 B-B"). *AstC::2A; Eh::2A-LexA> syb-GRASP* showed GFP signals limited to medial SMP and SLP neuropils (Figure 3.17 C-C') suggesting synaptic connections between the V_m-AstC and D_ls-AstC pairs respectively. Unfortunately, the only available Gal4-LexA line to study the presynaptic partners with BAcTrace was *R61H08-LexA; Eh::2A-Gal4.* The offspring of *R61H08-LexA; Eh::2A-Gal4> BAcTrace* were not viable and never hatched from eggs. Therefore, information on which AstC neuron signals to EH was not obtainable. *AstC::2A> trans-Tango* showed that all V_ms (Figure 3.17 D-D") and D_ls (Figure 3.17 E-E") were postsynaptic to AstC neurons.

To summarize, the results from double staining, syb-GRASP, and *trans*-Tango showed that all EH^+ neurons receive synaptic input from AstC neurons arborizing in the superior

protocerebrum. Unfortunately, due to the failure of BAcTrace, the identities of these AstC neurons were not identified.

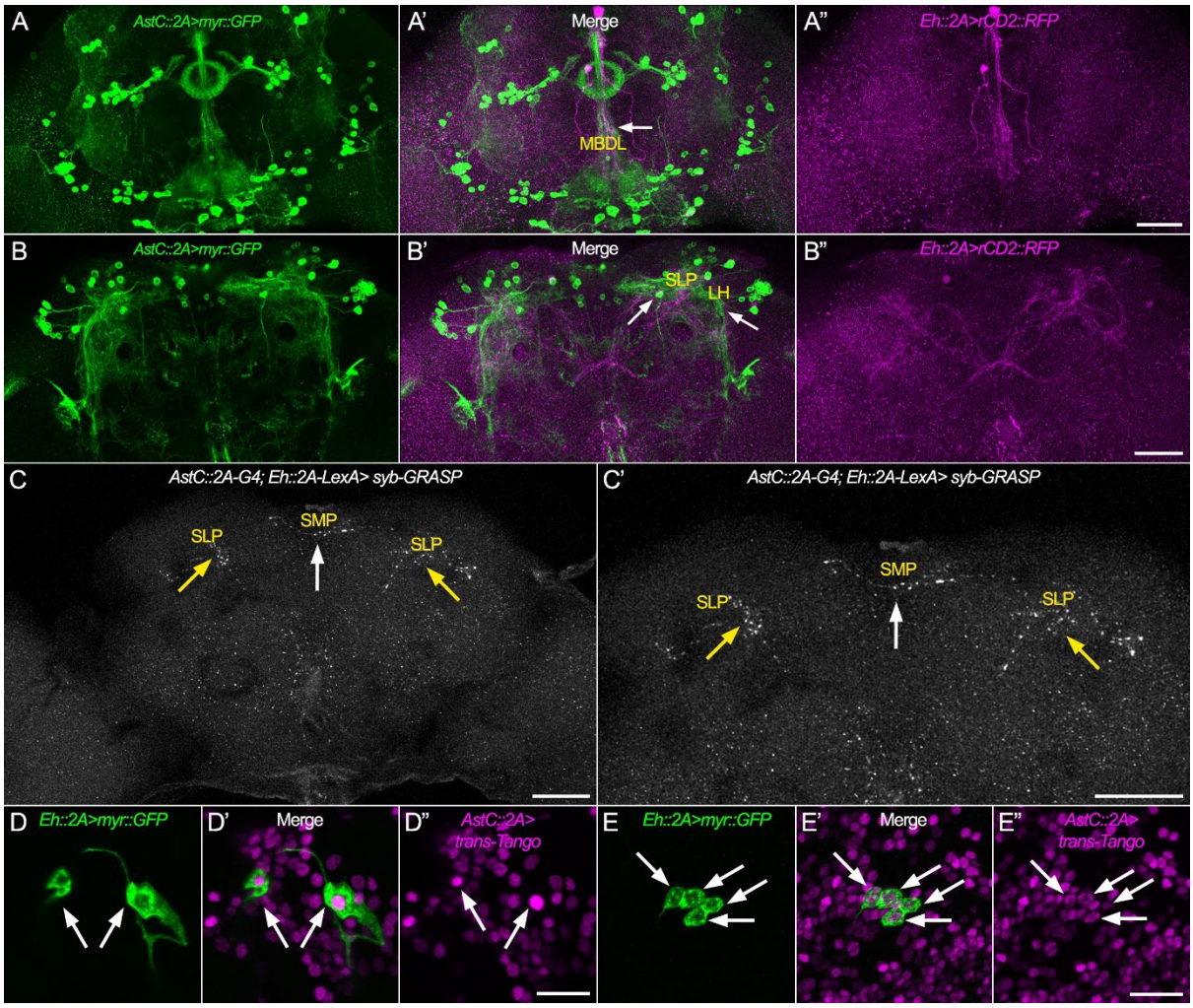

Figure 3.17. All EH neurons were postsynaptic to AstC neurons. A-A" Double labeling AstC (using *AstC::2A-Gal4> UAS-mCD8::GFP*) and V_m neurons (using *Eh::2A-LexA> LexAop-rCD2::RFP*). **A** mCD8::GFP (green) was expressed in AstC neurons and showed AstC neurons in superior medial protocerebrum projecting via median bundle (MBDL) to periesophageal neuropils, and ellipsoid body projecting AstC neurons (anterior view plane). **A'** The arborization of the V_m and AstC neurons overlapped in the medial part of superior medial protocerebrum and MBDL (arrow). **A"** rCD2::RFP (magenta) was expressed in V_m neurons and showed their morphology. **B-B"** Double labeling AstC (using *AstC::2A-Gal4> UAS-mCD8::GFP*) and D_l neurons (using *Eh::2A-LexA> LexAop-rCD2::RFP*). **B** mCD8::GFP (green) expression showed AstC neurons arborizing superior protocerebrum in superior medial protocerebrum, superior intermediate protocerebrum, superior lateral protocerebrum (SLP), and lateral horn (LH; posterior view plane). **B'** The D_ls and AstC neurons processes met at the SLP, LH, and clamp (arrows). **B"** rCD2::RFP (magenta) was expressed in D_l neurons. **C-C"** Using syb-GRASP the synaptic connectivity between AstC and EH neurons was investigated. V_m neurons at the superior medial protocerebrum (SMP; white arrow), and the D_ls at anterior lateral SLP (yellow arrows) made synaptic connections to the AstC neurons. **D-E** *trans*-Tango showed that all EH neurons were postsynaptic to the AstC neurons. **D-D"** *AstC::2A> trans-Tango* showed that both V_m (arrows) and **E-E"** all D_ls were receiving synaptic input from the AstC neurons (arrows show colocalization of GFP and nuclear RFP signal of *trans*-Tango). *Scale bars*: A-C 50 µm and D-E 20 µm.

8. The predictions of the role of the receptors and how they might modulate the PTTH and V_m neurons activity

Much of the complexity in peptide signaling arises from the various peptides and their respective receptors (mostly G protein-coupled receptors (GPCRs) that are involved in the signaling process (Bauknecht and Jékely, 2015; Hewes and Taghert, 2001; Jékely, 2013; Nässel and Winther, 2010). All GPCRs have seven-membrane passing α-helix domains and bind to guanosine triphosphate-binding proteins (G proteins). The G proteins are heterotrimeric proteins made of Gα, Gβ, and Gγ subunits (Simon et al., 1991; Weis and Kobilka, 2018). Peptide binding to the GPCR changes the spatial conformation that causes G protein activation to start different intracellular cascades depending on the type of G protein (Neves et al., 2002; Weis and Kobilka, 2018). Here, the Gα subunit signaling is important to determine which intracellular cascade becomes activated. $G\alpha_{i/o}$ and $G\alpha_s$ respectively inhibit or stimulate adenylate cyclases that catalyze the production of cyclic-adenosine monophosphate (cAMP) from ATP. The $G\alpha_{q/11}$ subunit activates phospholipase C which leads to inositol trisphosphate/diacylglycerol ($InsP_3$/DAG) signaling that increases intracellular Ca^{2+} levels (Neves et al., 2002; Weis and Kobilka, 2018; Wettschureck and Offermanns, 2005). Therefore, based on which Gα subunit can bind to a given GPCR, it is possible to predict the second messenger cascade downstream of that GPCR.

sNPF inhibits the PTTH neurons (Selcho et al., 2017). The modulatory effect of the AstA, AstC, and Ms on PTTHn activity is however unknown. Therefore, we used PRED-COUPLE 2.00 to predict which Gα subunit binds to the respective receptor (Sgourakis et al., 2005b, 2005a). The prediction scores for the receptors expressed by PTTHn and EH neurons in P14 pharate adults are presented in Table 3.3. The results suggest that the sNPF-R, AstA-R1, AstA-$R2^{AC}$, $MsR1^{B,}$ and $MsR2^{C}$ most likely signal via $G\alpha_{i/o}$ which decreases cytoplasmic cAMP and typically causes neuronal inhibition. On the other hand, AstC-R1 and AstC-R2 probably act through $G\alpha_{q/11}$ which increases the cytoplasmic level of free Ca^{2+} and typically causes neuronal excitation. Even though these predictions might be incorrect, they suggest that genetically encoded sensors for both cAMP and Ca^{2+} are required to investigate the functionality of peptide signaling to PTTHn or V_m neurons.

Table 3.3. Summary of Gα subunit scores predicted with PRED-COUPLE 2.00 system. More than 0.5 is considered prominent and shown in bold.

Prediction score for Gα	PDFR	sNPF-R	AstA-R1	AstA-$R2^{C}$	AstC-R1	AstC-R2	Dh31-R^{C}	$MsR1^{B}$	$MsR2^{C}$
$G\alpha_{i/o}$	**0.96**	**0.99**	**0.92**	**0.83**	0.19	0.11	**0.94**	**0.96**	**0.99**
$G\alpha_s$	**0.65**	0	0.01	0.07	0.02	0.01	**0.91**	0.08	0.12
$G\alpha_{q/11}$	0.08	0.56	0	0.21	**0.95**	**0.92**	0.04	0.02	0.05

Chapter IV: Testing the role of the periphery in modulating eclosion

As outlined in the introduction and chapter II, the role of PTTH in timing eclosion is well understood (Cavieres-Lepe et al., 2023; Mark et al., 2021; Selcho et al., 2017). Now it is evident that PTTH itself does not gate eclosion, but rather the final steps of pupal development (Mark et al., 2021). On the other hand, it is very well shown that the neuroendocrine EH/ETH feedback loop initiates ecdysis/eclosion (see Ewer, 2007a; Zitnan and Adams, 2012). Ecdysone signaling is important to activate the EH/ETH feedback loop (Cho et al., 2014; D Zitnan et al., 2007). However, the signals starting the EH/ETH feedback loop and ecdysis/eclosion are not known. PTTH signaling does not seem to directly be involved here, because TORSO is not expressed in the CNS or Inka cells (own results; Bossen et al., 2023).

In this chapter, two hypotheses were tested: 1. Peripheral sensory neurons that potentially sense changes in gas composition during tracheal collapse (v'Td neurons), or mechanical changes during molting (C4da multidendritic neurons on the body wall) sense the progress of molting and trigger eclosion. 2. PTTH signaling to peripheral *torso*-expressing cells (trophocytes in the fat body, C4da neurons) activates signaling from these cells which subsequently activates the EH/ETH feedback loop.

1. The peripheral v'Td neurons provide synaptic input to V_m neurons but are not involved in the rhythmicity of the eclosion

In the larval connectome, it has been shown that peripheral gas-sensing neurons provide synaptic input to larval V_m neurons (Hückesfeld et al., 2021). These neurons are named ventral' Tracheal dendrite neurons (v'Td) based on their location and morphology in larval PNS (Qian et al., 2018; Singhania and Grueber, 2014). The morphology of the two subtypes of v'Td neurons in the larval PNS is well described. In larval abdominal hemisegments A1 to A6, one v'Td1 and one v'Td2 neurons are located. In A7 abdominal hemisegment, only one v'Td2 is present. v'Td neurons are missing altogether in abdominal hemisegments 8/9. The v'Td cell bodies are located next to the larval ganglionic branch of the larval trachea. The v'Td1 cell bodies are located dorsal to those of v'Td2. Both v'Td neurons dendrites branch out dorsally along the ganglionic branch, then bifurcate and extend along the lateral trunk of the trachea and terminate either on the lateral trunk or lateral group branch of the trachea. v'Td axons enter the VNC to their corresponding abdominal neuromere and project through the ventral lateral tract to the thoracic neuromeres. The axons of v'Td2 neurons originating from A4 to A7 abdominal hemisegments terminate in the third thoracic neuromere while A1-A3 v'Td2 and all v'Td1 axons continue through the dorsomedial fascicle at the midline of VNC to the brain and terminate in SEZ (Qian et al., 2018). The presynaptic protein Bruchpilot is expressed in the axons of SEZ projecting v'Td1 neurons. Therefore, v'Td1 neurons can form *en passant* connections (Qian et al., 2018).

The organization of v'Td neurons in adult PNS and CNS is not yet described. Whether these neurons maintain the larval synaptic contact with V_m neurons is not known. Whether they play a role in eclosion rhythmicity or initiation of eclosion is also unknown. Therefore, here first the possibility of synaptic connectivity between adult v'Td and V_m neurons was tested using

genetic trans-synaptic tools. Then their role in maintaining eclosion gating and triggering premature eclosion was assessed using eclosion assays.

a. The arborizations of the V_m neurons and the v'Td neurons are closely situated at the midline of the VNC

Four previously described driver lines, three Janelia GMR lines (Jenett et al., 2012), and one from InSite (Gohl et al., 2011) were used to drive mCD8::GFP expression in the v'Td neurons to assess their morphology in the adult CNS. The neurons labeled by these lines have been previously described for the larval nervous system (Hückesfeld et al., 2021; Imambocus et al., 2022; Qian et al., 2018). The *R35B01-GAL4* line labeled broadly in A1 to A5 of v'Td1 neurons also the A1 v'Td2 neuron (Jenett et al., 2012; Qian et al., 2018). The *R31D10-Gal4* labeled the larval A4 to A6 v'Td1 neurons (Qian et al., 2018). Another GMR line, *R73B01-Gal4*, along with the InSITE line, *0260-Gal4*, were used as v'Td2 targeting driver lines (Gohl et al., 2011; Hückesfeld et al., 2021; Qian et al., 2018). *R73B01-Gal4* driver broadly labeled A1 to A7 v'Td2 neurons while the *0260-Gal4* line (also described as the Td-CO_2 neurons driver) labeled larval A1 to A6 v'Td2 neurons (Hückesfeld et al., 2021; Qian et al., 2018). In adults, the cell bodies and dendrites of v'Tds were located near the trachea, and expression of mCD8::GFP using these driver lines (Figure 4.1 A-H) revealed axonal projections inside the CNS. All driver lines showed a similar GFP expression pattern in the abdominal neuromeres of the VNC. This expression created a ladder-like structure in the abdominal ganglia with projections that converged in the metathoracic neuromere and projected through the median dorsal abdominal tract (MDT) in the midline of the VNC to the cervical connective and SEZ region of the brain (Figure 4.1 B, D, F, and H). All drivers drove GFP expression in SEZ neuropils such as the prow and flange (Figure 4.1 A, C, E, and G). This distribution was very similar to the larval expression patterns described above. This suggests that these lines can be used to drive expression in the v'Td neurons of not only in larvae, but also in adult flies. In addition, all driver lines showed ectopic expression in the VNC and the brain. *R35B01> mCD8::GFP* showed the broadest ectopic expression in every VNC neuromeres including cell bodies in metathoracic and abdominal neuromeres and dense neuronal processes that passed through intermediate tract of dorsal cervical fasciculus, ventral lateral tract, and ventral median tract of ventral cervical fasciculus of VNC. However, it seemed that none of the ectopically labeled projections passed through MTD and close the V_m axons (Figure 4.1 D). In the brain *R35B01> mCD8::GFP* showed ectopic expression in optic lobes and brain neuropils (antennal lobe, anterior ventrolateral protocerebrum, flange, lateral horn, clamp, saddle, prow, antennal mechanosensory and motor center, and posterior slope; Figure 4.1 C). Also for *R31D10> mCD8::GFP* very weak GFP expression was present in every VNC neuromere. However, strong ectopic expression was present in neurons located in the mesothoracic neuromere (Figure 4.1 B). However, these neurons did not project into MDT. In the brain, the flange, saddle, and antennal lobes showed the strongest GFP expression (Figure 4.1 A). *R73B01> mCD8::GFP* showed no ectopic GFP expression in the VNC, and GFP expression was limited to v'Td2 axons in the abdominal neuromere and MDT (Figure 4.1 H). In the brain, expression was limited to prow and flange and ectopically and weakly in two neurons located at SMP (Figure 4.1 G). Therefore, *R73B01-Gal4* was the specific v'Td2 driver line. *0260> mCD8::GFP* showed an expression pattern similar to *R73B01> mCD8::GFP* except for ectopic expression in neurons and neuronal processes confined to the prothoracic neuromere of VNC and weaker GFP expression in two neurons located at meso- and metathoracic

neuromeres (Figure 4.1 F) and in antennal lobe (Figure 4.1 E). All the cell bodies within the VNC that expressed mCD8::GFP with either of the driver lines were not part of v'Tds but represented ectopic expression. On the other hand, all afferent neurites clearly identified the projections of the v'Tds. None of the neurites of non-v'Td neurons marked by GFP passed through MDT. Yet, due to the compact structure of the abdominal ganglia, it was not possible to morphologically differentiate between the individual axonal projections of v'Tds entering VNC. Therefore, and despite the considerable ectopic expression, the expression pattern of R31D10 is regarded as v'Td1^{A4-6}, R35B01 as v'Td1^{A1-5}, R73B01 as v'Td2^{A1-7}, and 0260 as v'Td2^{A1-6}.

rCD2::RFP expression showed superficial cell bodies of the V_m neurons at the anterior cell body rind of the SMP, each of which with bifurcated arborization in the MBDL in the brain (Figure 4.1 A", C", E", and G"). The axonal projections of V_ms descended through the cervical connective and via the MDT to the abdominal neuromeres in the VNC (Figure 4.1 B, D, F, and H). The double stainings showed that neurites GFP-labeled by all v'Td Gal4 drivers in the SEZ. These processes were close to V_m processes in SEZ (Figure 4.1 A', C', E', and G'). In the VNC, axons of V_ms and v'Tds were close to each other along the MDT (Figure 4.1 B''', D''', F''', and H''').

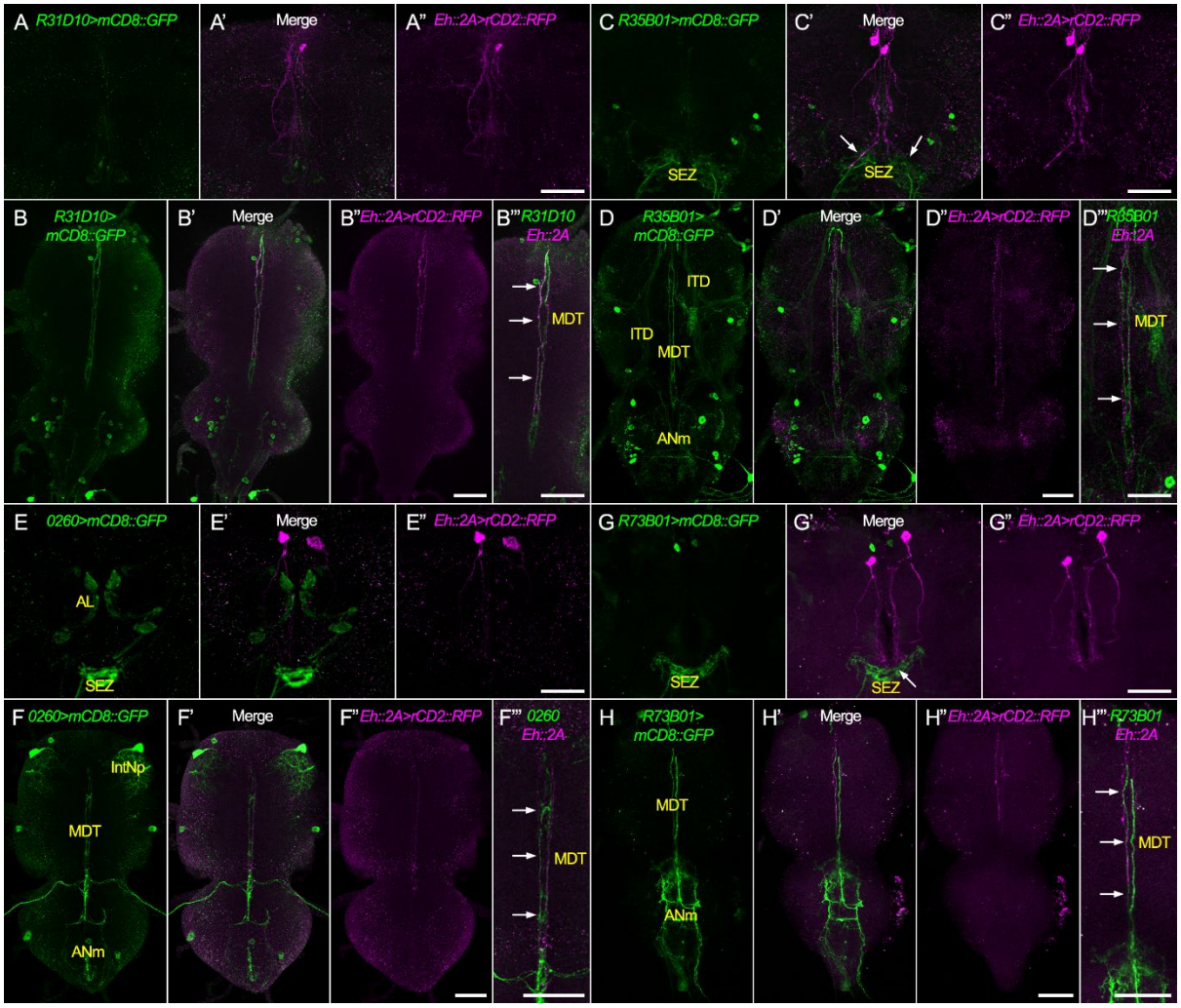

Figure 4.1. v'Td neurons and V_m neurons were closely contacting each other in the suboesophageal zone (SEZ) and at the VNC midline. A-A" Double labeling of v'Td1^{A4-6} and V_m neurons in the brain. **A** *R31D10-Gal4> UAS-mCD8::GFP* was used to express GFP in v'Td1^{A4-6} neurons. The expression pattern was shown in the brain without the optic lobes. GFP was only expressed in processes located at the SEZ (green). **A'** Overlap between the processes of V_m neurons in the brain (magenta) and R31D10-driven GFP expression (green) was observable at SEZ. **A"** *Eh::2-LexA> LexAop-rCD2::RFP* expressed RFP in V_m neurons (magenta). **B-B"** Double labeling of v'Td1^{A4-6} and V_m neurons in the VNC. **B** mCD8::GFP expression showed the axons of v'Td1^{A4-6} neurons in VNC (green). The neurons entered the VNC from the abdominal neuromeres and ascended through the median dorsal abdominal tract (MDT) to the brain. The present cell bodies in the metathoracic neuromere did not belong to v'Td1 neurons. **B'** v'Td1^{A4-6} axons (green) passed by V_m axons (magenta) in the MDT. **B"** The axons of V_m neurons in the VNC were marked by rCD2::RFP (magenta). The V_m axons passed through MDT. **B"'** The axons of V_m neurons (magenta) and v'Td1^{A4-6} neurons (green) were near in MDT fascicle (arrows) located at the VNC midline. **C-C"** Double labeling of v'Td1^{A1-5} and V_m neurons in the brain. **C** *R35B01-Gal4> UAS-mCD8::GFP* expressed GFP in the axonal projections of v'Td1^{A1-5} neurons in the SEZ (green). However, ectopic expression of non-v'Td1 neurons in the SEZ and anterior ventrolateral protocerebrum was present. **C'** In the SEZ, axonal projection of the SEZ-projecting v'Td1^{A1-5} neurons and V_m projections came very close to each other. **C"** *Eh::2-LexA> LexAop-rCD2::RFP* expressed RFP in V_m neurons in the brain (magenta). **D-D"** Double labeling of v'Td1^{A1-5} and V_m neurons in the VNC. **D** mCD8::GFP labeled the axons of v'Td1^{A1-5} neurons in the VNC (green) and many other non-v'Td1 neurons. This driver line expressed ectopically in nearly every VNC ganglion. The present cell bodies in metathoracic and abdominal neuromeres and dense arborization patterns passed through the intermediate tract of dorsal cervical fasciculus (ITD) of VNC were not from v'Td1 neurons. **D'** In VNC v'Td1^{A1-5} axons (green) passed by V_m axons (magenta) in the MDT fascicle. **D"** The MDT passing axons of V_m neurons were labeled by rCD2::RFP expression (magenta). **D"'** Proximity of v'Td1^{A1-5} axons and V_m axons were marked by arrows. **E-E"** Double labeling of v'Td2^{A1-6} and V_m neurons in the brain. **E** *0260-Gal4> UAS-mCD8::GFP* expressed GFP in the axonal projections of v'Td2^{A1-6} neurons at SEZ (green) and ectopically expressed in non-v'Td2 neurons at the antennal lobe. **E'** Again, in the SEZ the v'Td2^{A1-6} axons and V_m processes were closely located to each other. **E"** *Eh::2-LexA> LexAop-rCD2::RFP* expressed RFP in V_m neurons (magenta). **F-F"** Double labeling of v'Td2^{A1-6} and V_m neurons in the VNC. **F** mCD8::GFP showed expression in the axons of v'Td2^{A1-6} neurons in VNC (green). The neurons entered the VNC from the abdominal neuromere and ascended through MDT to the brain. The present cell bodies in thoracic neuromeres and dense neuronal arborization in prothoracic neuromere were not related to v'Td2 neurons. **F'** In the MDT, the v'Td2^{A1-6} axons (green) came in contact with the V_m axons (magenta). **F"** V_m axons (magenta) descending through the MDT. **F"'** Close-up view of axons of V_m (magenta) and v'Td2^{A1-6} neurons (green) in the MDT fascicle showing their proximity (arrows). **G-G"** Double labeling of v'Td2^{A1-7} and V_m neurons in the brain. **G** *73B01> mCD8::GFP* expressed GFP in the axonal projections of v'Td2^{A1-7} neurons in the SEZ (green). GFP was ectopically expressed in two non-v'Td2 neurons in the superior medial protocerebrum. **G'** In the SEZ, v'Td2^{A1-7} axons (green) and V_m processes (magenta) were close to each other (arrows). **G"** *Eh::2-LexA> LexAop-rCD2::RFP* expressed RFP in V_m neurons (magenta). **H-H"** Double labeling of v'Td2^{A1-7} and V_m neurons in the VNC. **H** mCD8::GFP showed the expression in the axons of v'Td2^{A1-7} neurons in the VNC (green). This driver line specifically labeled v'Td2^{A1-7} axons in the VNC. The v'Td2^{A1-7} neurons entered the VNC from the abdominal neuromere and ascended to the mesothoracic neuromere and through MDT to the brain. **H'** In the MDT, the v'Td2^{A1-7} axons (green) were close to V_m axons (magenta). **H"** Descending V_m axons (magenta) were labeled by RFP. **H"'** Close-up view showing v'Td2^{A1-6} axons (green) were close to axons of V_m (magenta) in the MDT fascicle (arrows). *Scale bars*: 50 μm.

b. The v'Td neurons provide synaptic input to the V_m neurons

To check for the possibility of synaptic connections between the V_ms and the v'Tds, syb-GRASP was performed (Macpherson et al., 2015). The syb-GRASP results showed that there are synaptic connections between all v'Td neurons and the V_m neurons in the VNC at MDT (Figure 4.2 A-D) but no reconstruction of GFP was observed in the brain. *R35B01-Gal4; Eh::2A-LexA> syb-GRASP* (Figure 4.2 B) showed the strongest GFP signal in the VNC between V_m and v'Td1^{A1-5} while the *73B01-Gal4; Eh::2A-LexA> syb-GRASP* (Figure 4.2 D) showed the weakest signal between V_m and v'Td2^{A1-7}. The GRASP signal along the MDT was also present for v'Td1^{A4-6} and V_m (*R31D10-Gal4; Eh::2A-LexA> syb-GRASP*; Figure 4.2 A) and v'Td^{A1-6} and V_m (*0260-Gal4; Eh::2A-LexA> syb-GRASP*; Figure 4.2 C) neurons.

Since both v'Td1 and -2 neurons and the V_m neurons send their axons into the VNC through the MDT, the presence of synaptic connections between them in this area states the possibility of *en passant* axo-axonic synapses (Qian et al., 2018). In Chapter II using the DenMark and syt-eGFP (see II.1) it was shown that the dendrites of V_m were mostly limited to the brain while the axon branches travel down to the VNC with mixed arbors containing dendritic parts not entirely covered with boutons (Figure 2.1 B). Qian et al. (2018) showed that at least the larval axonal projections of v'Td1^{A4-6} neurons that ascend to the SEZ (labeled by *R31D10-Gal4*) contain Bruchpilot and form presynaptic sites. Therefore, the connections in the VNC may be classic axodendritic synapses and not *en passant* axo-axonic structures.

To confirm that the v'Td neurons are presynaptic partners of the V_m neurons, *trans*-Tango MkII was used. To mark the V_m neurons, myr::GFP was expressed in the V_m neurons using the LexA/LexAop2 expression system. *trans*-Tango with driver lines for v'Td1^{A4-6} (*R31D10-Gal4*) and v'Td1^{A1-5} (*R35B01-Gal4*) confirmed that V_m neurons are postsynaptic to the v'Td1 neurons (Figure 4.2 E-F). Both *0260> trans-Tango* and *R73B01> trans-Tango* showed RFP expression in V_m cell bodies as well (Figure 4.2 G-H) meaning V_ms are postsynaptically connected to v'Td2^{A1-6} and v'Td2^{A1-7}, respectively.

To conclude, the results of double staining with syb-GRASP and *trans*-Tango showed that V_m neurons receive synaptic input from both v'Td1 and -2 neurons at VNC and not the brain. *R35B01-Gal4; Eh::2A-LexA> syb-GRASP* showed the strongest GRASP signal at the MDT among the lines. It is thus likely that v'Td1^{A1-5} made more synaptic connections with V_m compared to v'Td2^{A1-7} neurons.

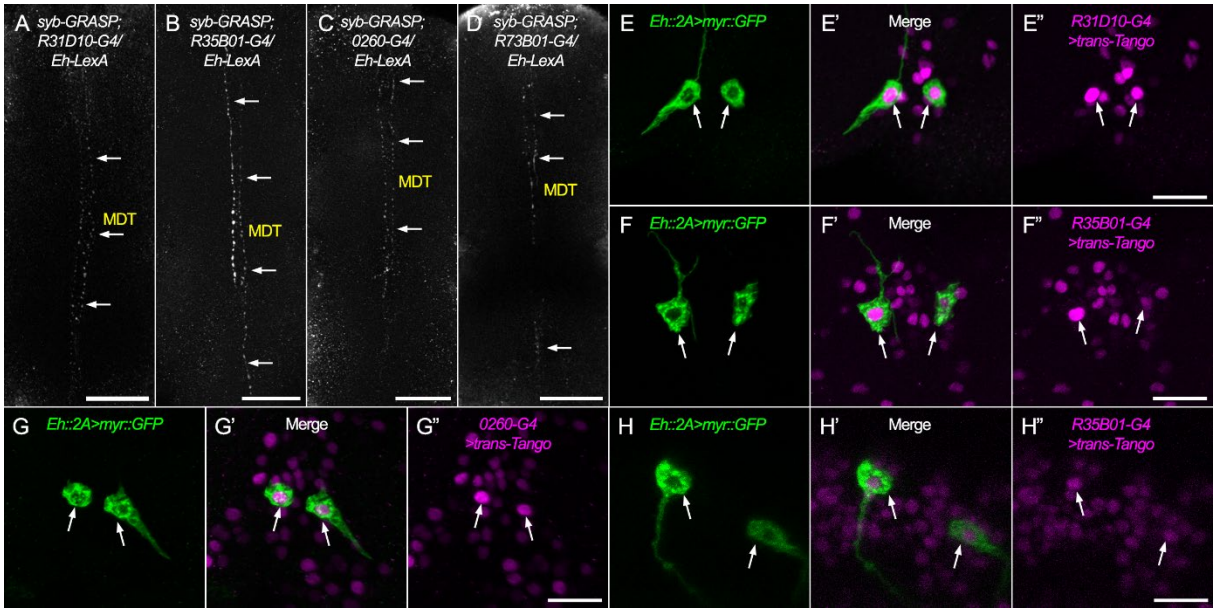

Figure 4.2. v'Td neurons made synaptic connections to the V_m neurons at the midline of VNC. A-D Synaptic connectivity between v'Td and V_m neurons was checked by syb-GRASP. **A** *R31D10-Gal4; Eh::2A-LexA> syb-GRASP* (arrows) signal was present along the median dorsal abdominal tract (MDT) at the midline of VNC, indicating synaptic connection between v'Td1^{A4-6} and V_m neurons. **B** Similarly, *R35B01-Gal4; Eh::2A-LexA> syb-GRASP* (arrows, dense and strong signal) showed connections between v'Td1^{A1-5} and V_m. **C** *0260-Gal4; Eh::2A-LexA> syb-GRASP* (arrows) showed synaptic connection between v'Td2^{A1-6} and V_m neurons. **D** *R73B01-Gal4; Eh::2A-LexA> syb-GRASP* (arrows, sparse and weak signal) showed reconstituted GFP signals between v'Td2^{A1-7} and V_m neurons. **E-H** *trans*-Tango showed that V_m neurons were postsynaptic to v'Td neurons. **E** *Eh::2A-LexA>LexAop-myr::GFP* labeled V_m neurons (arrows). **E'** Colocalization of GFP and *trans*-Tango-driven nuclear RFP in V_m neurons showed that V_m neurons were postsynaptic to v'Td1^{A4-6} neurons (arrows). **E"** *R31D10> trans-Tango* drove nuclear RFP expression in neurons postsynaptic to v'Td1^{A4-6} neurons. Arrows showed the nuclei of V_m neurons. **F** *LexAop-myr::GFP* labeled V_m neurons (arrows). **F'** Colocalization of GFP and nuclear RFP from *trans*-Tango in V_m neurons showed V_m received synaptic input from v'Td1^{A1-5} neurons (arrows). **F"** *R35B01> trans-Tango* drove nuclear RFP expression in postsynaptic neurons of v'Td1^{A1-5} neurons. The nuclei of V_m neurons were indicated by arrows. **G** Expression of *myr::GFP* in V_m neurons (arrows). **G'** Nuclear RFP driven by *trans*-Tango in V_m neurons showed they were postsynaptically connected to v'Td2^{A1-6} neurons (arrows). **G"** *0260> trans-Tango* labeled all neurons postsynaptic to v'Td1^{A4-6} neurons including V_m (arrows) with nuclear RFP expression. **H** V_m neurons marked by myr::GFP expression (arrows). **H'** Colocalization of GFP and *trans*-Tango signal in V_m neurons showed they were postsynaptic to v'Td2^{A1-7} neurons (arrows). **H"** *R73B01> trans-Tango* drove nuclear RFP expression in neurons postsynaptic to v'Td2^{A1-7} neurons including V_m neurons (arrows). *Scale bars*: A-D 50 µm, E-H 20 µm.

c. Optogenetic activation of the v'Td neurons increases the free Ca^{2+} levels of the V_m neurons

To assess the functionality of the synaptic connection between the v'Tds and the V_m neurons, a combination of optogenetic activation with the blue light-activated ChR2-XXL and Ca^{2+} imaging in the V_m neurons in the intact fly with the red-shifted Ca^{2+} indicator jRCaMP1a was used. The v'Td neurons were excited with intense blue LED light for 0.5 seconds at 200 seconds of Ca^{2+} imaging. A second pulse to activate the neurons was given at 1200 seconds

(1000 seconds after the first pulse). The entire recording timespan was 1800 seconds (30 minutes).

For negative control the *w*; UAS-ChR2-XXL/LexAop-jRCaMP1a; +/Eh::2A-LexA* flies were used (Figure 4.3 A and D). Ten V_m neurons from eight flies were recorded. All neurons showed a clear jRCaMP signal. After the light pulses, the neurons showed no significant changes in the Ca^{2+} levels in the controls (Figure 4.3 A); their average activity remained unchanged (Figure 4.3 D). This result shows that the blue light itself does not affect the jRCaMP signal in the V_m neurons.

For the v'Td1^{A1-5} neurons, six flies (10 V_m neurons) of the *w*; UAS-ChR2-XXL/LexAop-jRCaMP1a; R35B01-Gal4/Eh::2A-LexA* genotype were tested. Four out of the ten neurons did not show changes in the fluorescence after optogenetic activation of v'Td1^{A1-5} neurons. The other six neurons also showed no immediate change in cytoplasmic Ca^{2+} level. Yet, starting about 500 seconds after activation, the Ca^{2+} level of 60% of the neurons (three flies) increased and remained high for 50 to 200 seconds and then gradually dropped back to the baseline (Figure 4.3 B). For one of the flies, 400 seconds after the second activation the Ca^{2+} levels rose, and induced Ca^{2+} oscillations in the V_m neurons. The average activity of the V_m neurons after exciting the v'Td1^{A1-5} neurons showed an increased free Ca^{2+} concentration ($\Delta F/F \approx 0.2$). This delayed increase was about ten minutes after excitation, mostly due to the activity of four out of 10 neurons. This increased Ca^{2+} level lasted about three minutes and then dropped to baseline (Figure 4.3 E). The second activation affected the activity of only one V_m neuron.

To measure the influence of the v'Td2^{A1-7} neurons on the intracellular Ca^{2+} level of the V_m neurons, *w*; UAS-ChR2-XXL/LexAop-jRCaMP1a; R73B01-Gal4/Eh::2A-LexA* flies were used. The fluorescence of 12 neurons from seven flies was measured. In nearly all cases, the V_m neurons responded with a slow Ca^{2+} increase after the first but not second light pulse. The level and temporal cause of the Ca^{2+} signal increase was, however, very variable. In most neurons shortly (within one minute) after the first light pulse, the neurons showed increasing Ca^{2+} levels (Figure 4.3 C). In one neuron, the second pulse seemed to induce Ca2+ oscillations indicative of a strong activation favoring EH release. The average activity showed increased activity of the V_m neurons after v'Td2^{A1-7} activation (Figure 4.3 F). This high Ca^{2+} level remained high ($\Delta F/F \approx 0.25$) for about 15 minutes but in individual cases, lasted not more than six to seven minutes.

Taken together, optogenetic activation of both v'Td1^{A1-5} and v'Td2^{A1-7} neurons had either no effect or slowly increased the intracellular Ca^{2+} level in V_m neurons. As recording was not from the VNC but from the V_m cell bodies in the brain, the optogenetic activation of v'Td1 neurons leads to stronger local Ca^{2+} increases in the descending V_m neurites cannot be excluded. Nevertheless, the lack of a consistent, strong, and fast Ca^{2+} response in the V_m cell bodies upon optogenetic activation of the v'Td1 and v'Td2 neurons suggests that the synaptic input via v'Td neurons was not enough to trigger a strong activation and EH release from the V_m neurons. It seems therefore unlikely that the v'Td neurons are able to initiate eclosion via activation of EH release from the V_m neurons.

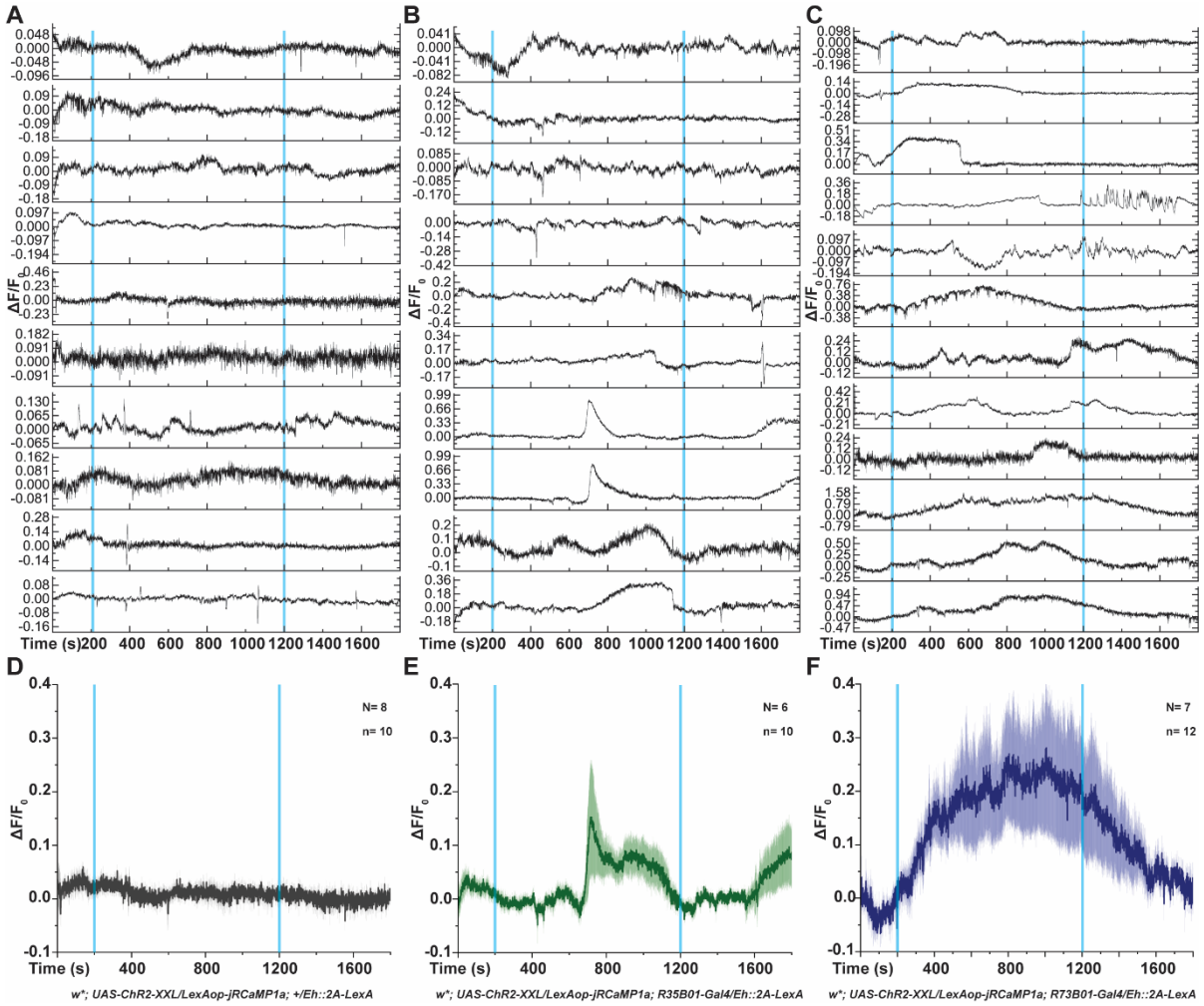

Figure 4.3. Intracellular Ca^{2+} levels in V_m cell bodies upon optogenetic activation of the v'Td neurons. The imaging lasted for 30 min (1800 seconds). Two bright blue light pulses (0.5s duration at 200s and 1200s, blue lines) were used to activate ChR2-XXL. **A** Ten V_m neurons of eight flies were imaged without the Gal4 driver line as control (*w*; UAS-ChR2-XXL/LexAop-jRCaMP1a; +/Eh::2A-LexA*). The control flies showed no significant change in intracellular Ca^{2+} levels. **B** To test if v'Td1^{A1-5} could excite the V_m neurons, ten neurons from eight flies were imaged (*w*; UAS-ChR2-XXL/LexAop-jRCaMP1a; R35B01-Gal4/Eh::2A-LexA*). Six V_m neurons showed increased Ca^{2+} levels. However, the increase was delayed by about ten minutes. **C** Optogenetic activation of the v'Td2^{A1-7} neurons did not cause consistent Ca^{2+} responses in the V_m neurons (*w*; UAS-ChR2-XXL/LexAop-jRCaMP1a; R73B01-Gal4/Eh::2A-LexA*), although most V_m neurons (12 neurons of seven brains) showed a slow and delayed Ca^{2+} increase. One V_m neuron showed strong Ca^{2+} oscillations after the second optogenetic stimulation. **D** The average jRCaMP1a signal of the control flies remained at the baseline ($\Delta F/F = 0$) indicating no effect on the Ca^{2+} level in V_m neurons. **E** The average fluorescence of V_m neurons in the v'Td1^{A1-5} experiment group showed an overall slow and delayed Ca^{2+} increase ($\Delta F/F \approx 0.2$). The delayed increase of the average Ca^{2+} signal after the second activation was due to only two neurons, while the others did not respond. **F** The average Ca^{2+} signal of the V_m neurons after activation of the v'Td2^{A1-7} neurons ($\Delta F/F \approx 0.25$) indicated a slow and longer-lasting Ca^{2+} increase of V_m neurons. As for the v'Td1 neurons, the average curve did not reflect a typical response of a single neuron.

d. The v'Td neurons are not required for the eclosion rhythmicity

To test whether v'Td neurons were required for eclosion rhythmicity, eclosion assays with v'Td ablated neurons were essential. However, ablating v'Td1 and v'Td2 neurons using *UAS-RA* was not possible. When *UAS-RA* flies were crossed to v'Td1^{A4-6}, v'Td1^{A1-5}, v'Td2^{A1-6}, or v'Td2^{A1-7} driver lines, the offspring never reached the L2 stage and, therefore did not pupariate. The v'Td neurons are required during development and a previous study also showed ablating them caused ecdysis failure and lethality (Morton et al., 2008). Ablating the O_2-sensing v'Td neurons using tetanus toxin expression (*UAS-TNTi*) led to lethality by drowning larvae that burrowed inside food (Morton et al., 2008). Therefore, to perform eclosion assays, it was decided to conditionally ablate these neurons during the final pupal stages using cold-sensitive ricin (*UAS-RA^{CS2}.CC*; Chen et al., 2012). *v'Td1^{A4-6}-Gal4*, *v'Td1^{A1-5}-Gal4*, *v'Td2^{A1-6}-Gal4*, or *v'Td2^{A1-7}-Gal4* driver lines were crossed to *UAS-RA^{CS2}.CC* flies (experimental groups) This way, a sufficient number of flies passed the larval stages and pupariated. Eclosion assays were performed as explained in Materials and Methods 5.e. This time v'Td1^{A4-6}, v'Td1^{A1-5}, v'Td2^{A1-6}, or v'Td2^{A1-7} driver flies were crossed to *UAS-RA^{CS2}.CC* flies (experimental groups) or *w^{1118}* (controls). The efficiency of *UAS-RA^{CS2}.CC* in ablating v'Td1 neurons was tested by *v'Td1^{A1-5}-Gal4> UAS-mCD8::GFP; UAS-RA^{CS2}.CC* flies (see Appendix 2).

v'Td1^{A4-6}> RA^{CS2}.CC flies and their respective Gal4 control showed rhythmic eclosion patterns, and autocorrelation, LS, and eJTK analyses revealed a significant rhythmicity. Noteworthy, the control group showed a broad MESA peak with a period of 20.7h (Figure 4.4 A and Table 4.1). Also the flies with ablated v'Td1^{A1-5} neurons and their controls showed rhythmic eclosion patterns, even though the autocorrelation for the *v'Td1^{A1-5}> w^{1118}* showed arrhythmicity in autocorrelation analysis and a two MESA peaks and a period of 28.4 hours. Yet, LS and eJTK revealed significant rhythmicity for both experiment and controls (Figure 4.4 A and Table 4.1). *v'Td2^{A1-6}> RA^{CS2}.CC* and their controls both showed rhythmic eclosion patterns (Figure 4.4 A and Table 4.1). Again, autocorrelation indicated arrhythmicity and MESA analysis revealed two peaks. However, both LS and eJTK analysis revealed a significant rhythmicity. Finally, after ablating all v'Td2 neurons (*v'Td2^{A1-7}> RA^{CS2}.CC*) eclosion remained rhythmic. Both the experiment and Gal4 control group showed rhythmic eclosion patterns, single MESA peaks with periods around 23 hours, and rhythmic autocorrelation RI, LS, and eJTK values. The UAS control group (*w^{1118}> RA^{CS2}.CC*) showed rhythmic eclosion, with a single-peaked sharp MESA peak with a period of 28.3 hours and rhythmic RI and LS values. However, eJTK analysis of this control group showed arrhythmicity (Table 4.1). Taken together, the results show that ablating v'Tds did not affect eclosion rhythmicity. The arrhythmic values for single analysis methods were likely due to temperature changes necessary for activating and deactivating cold-sensitive ricin.

Next, the v'Td neurons were silenced with Kir2.1. Strikingly, after silencing v'Td2 neurons using *v'Td2^{A1-6}> Kir2.1* or *v'Td2^{A1-7}> Kir2.1,* only very few flies pupariated. Therefore, performing eclosion assays was not possible. Using *v'Td1^{A4-6}> Kir2.1* led to complete pupariation failure. Apparently by silencing v'Td2 and v'Td1^{A4-6} neurons the majority of larvae could not pass through the first ecdysis and died. However, silencing v'Td1 neurons using *v'Td1^{A1-5}> Kir2.1* was more tolerable, and flies were able to pupariate and eclosion assays were performed on these flies (Figure 4.4 B and Table 4.1). *v'Td1^{A1-5}> Kir2.1* flies and both Gal4 and UAS control groups showed rhythmic eclosion patterns, with strong rhythmicity (RI ≥

0.46), and single MESA peaks with periods close to 24 hours. Also, eJTK and LS analyses showed rhythmic values. Therefore, electrically silencing the v'Td1^{A1-5} neurons did not cause arrhythmic eclosion, in line with the results from neuronal ablation.

In conclusion, conditional ablation of v'Td1^{A4-6}, v'Td1^{A1-5}, v'Td2^{A1-6}, and v'Td2^{A1-7} neurons, and electrical silencing of v'Td1^{A1-5} did not impair eclosion rhythmicity, suggesting that neither v'Td1 nor v'Td2 neurons are required to maintain eclosion rhythmicity. However, they were required during development, and silencing or ablating them led to no pupariation.

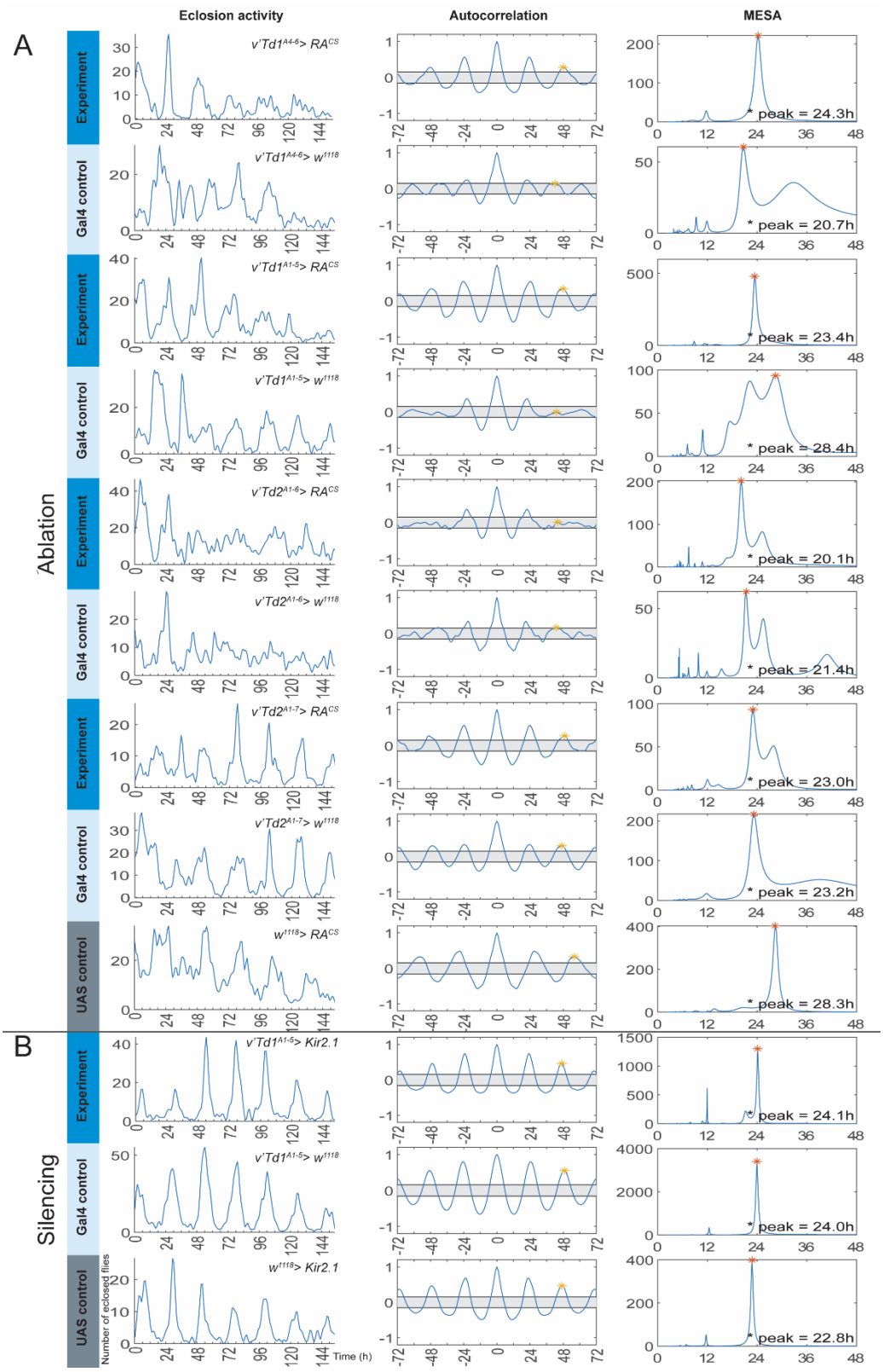

Figure 4.4. Conditional ablation or silencing v'Td neurons did not impair rhythmic eclosion. A After conditional ablation of the v'Td1^{A4-6} using RA^{CS} (*R31D10> RA^{CS2}.CC*) the eclosion pattern remained rhythmic (RI=0.28; Table 4.1). Also, *v'Td1^{A4-6}> w^{1118}* flies eclosed rhythmically, but less rhythmic (RI=0.14) compared to the experiment group. However, the Gal4 control group showed a broader MESA peak with a period close to 21h. Flies with ablated v'Td1^{A1-5} neurons (*R35B01> RA^{CS2}.CC*) showed a highly rhythmic eclosion pattern (RI=0.34) with a period close to 24h. In contrast,

the autocorrelation analysis for *v'Td1*$^{A1\text{-}5}$> w^{1118} showed arrhythmicity (RI=0). The period analyzed by MESA was more than 28h. Ablating v'Td2$^{A1\text{-}6}$ neurons (*0260> RA*^{CS2}*.CC*) also led to arrhythmicity after autocorrelation analysis (RI=0.01). Both experiment and Gal4 control showed rhythmic eclosion patterns. However, after the second day the amplitude of eclosion peaks for each day in both experiment and control group became lower (lowered eclosion peaks) and this might be the reason for causing a low RI. Finally ablating v'Td2$^{A1\text{-}7}$ neurons with RA^{CS} (*R73B01> RA*^{CS2}*.CC*) did not impair rhythmic eclosion in the experiment and Gal4 control group with rhythmic RI values (RI=0.27 and =0.31 respectively). w^{1118}> *RA*^{CS2}*.CC* controls showed a very rhythmic eclosion (RI=0.33) with a period of 28h according to MESA analysis. The probable reason for the low RIs (for v'Td1$^{A1\text{-}5}$ control and v'Td2$^{A1\text{-}6}$ experiment group) was the temperature changes before the eclosion assays for activating and deactivating RA^{CS}. **B** Electrical silencing of v'Td1$^{A1\text{-}5}$ neurons (*R35B01> Kir2.1*) showed a rhythmic eclosion pattern with a very rhythmic RI value (0.46). Both Gal4 and control groups showed strong rhythmicity as well. Taken together, conditional ablation of the v'Td neurons and silencing of v'Td1$^{A1\text{-}5}$ neurons did not impair eclosion rhythmicity.

Table 4.1. Rhythmicity analysis of the eclosion in time-restricted ablation and silencing of v'Td neurons eclosion assays (see figure 4.4). The arrhythmic values are shown in red. These arrhythmic values were probably a result of temperature shocks for activating and deactivating RA^{CS}.

	Neurons	Genotype	Number of flies	Error	Period	Rhythmicity index	Lomb-Scargle	eJTK BH bf corrected p
Ablation	v' Td1$^{A4\text{-}6}$	*R31D10> RA*^{CS2}*.CC*	1057	5.0%	24.3h	0.28	17.3	$1.3*10^{-10}$
		R31D10> w^{1118}	1430	2.4%	20.7h	0.14	2.6	0.07
	v' Td1$^{A1\text{-}5}$	*R35B01> RA*^{CS2}*.CC*	1695	3.1%	23.4h	0.34	15.4	$5.4*10^{-14}$
		R35B01> w^{1118}	1536	4.4%	28.4h	0.00	6.6	$7.4*10^{-8}$
	v' Td2$^{A1\text{-}6}$	*0260> RA*^{CS2}*.CC*	2122	6.9%	20.1h	0.01	11.5	$6.1*10^{-4}$
		0260> w^{1118}	1382	3.6%	21.4h	0.17	3.1	0.07
	v' Td2$^{A1\text{-}7}$	*R73B01> RA*^{CS2}*.CC*	993	0%	23.0h	0.27	15.9	$4.1*10^{-17}$
		R73B01> w^{1118}	1843	3.9%	23.2h	0.31	20.0	$6.0*10^{-19}$
	UAS Control	w^{1118}> *RA*^{CS2}*.CC*	2639	7.2%	28.3h	0.33	16.6	1
Silencing	v' Td1$^{A1\text{-}5}$	*R35B01>* w^{1118}	2245	6.8%	24.1h	0.55	40.9	$7.3*10^{-33}$
		R35B01> Kir2.1	1291	5.7%	24.0h	0.46	28.7	$1.5*10^{-25}$
	UAS control	w^{1118}> *Kir2.1*	895	4.1%	22.8h	0.47	29.1	$6.9*10^{-29}$

e. Activation of all v'Td1 but not the v'Td2 neurons promotes premature eclosion

In part III.5, the Opto-DEM method was used to assess the role of neurons in promoting or impeding premature eclosion. While Opto-DEM records the eclosion activity of flies entrained by temperature cycles, six hours before cold to warm temperature transition (during ZT18) a blue light pulse activates neurons expressing ChR2-XXL and prematurely induces eclosion. Here, Opto-DEM was used to test whether v'Td neurons affect premature eclosion. Activating v'Td1^{A4-6} neurons using *R31D10> ChR2-XXL* at ZT18 did not affect the eclosion rate compared to controls (*R31D10> w^{1118}*, *w^{1118} >ChR2-XXL*). However, at ZT16 and ZT17 (two and one hours before light pulse) significantly fewer experimental flies eclosed compared to the controls (Figure 4.5 A). When nv'Td1^{A1-5} neurons were optogenetically activated using *R35B01> ChR2-XXL*, significantly more experiment flies eclosed compared to Gal4 ($p < 0.01$) and UAS control groups at ZT 18 ($p < 0.001$; Figure 4.5 B). Activation of v'Td2^{A1-6} neurons using *0260> ChR2-XXL* compared to both Gal4 and UAS controls did neither change the eclosion rate at ZT18 nor at other ZTs (Figure 4.5 C). Activation of v'Td2^{A1-7} neurons using *R73B01> ChR2-XXL* compared to both controls only showed a small significant increase compared to the UAS- ($p < 0.05$; Figure 4.5 D) but not the Gal4 control (Figure 4.5 D). For comparison, Opto-DEM data for V_m neurons (see III.5) were charted along with the data for v'Td1 and v'Td2 (Figure 4.5 E). Activation of V_m neurons (*Eh (C21)> ChR2-XXL*) during ZT18 significantly increased the premature eclosion rate ($p < 0.0001$; Figure 4.5 E). In comparison to V_m neuron activation, the v'Td1^{A1-5} experiment group (*R35B01> ChR2-XXL*) showed lower eclosion rates (Figure 4.5 B). Thus, optogenetic activation of *R35B01> ChR2-XXL* flies, despite being able to increase the rate of premature eclosion, was not as effective as the direct activation of V_m neurons.

Collectively, only the activation of v'Td1^{A1-5} neurons significantly increased the premature eclosion rate. However, this increase is not as pronounced as activating V_m neurons while inducing premature eclosion with light.

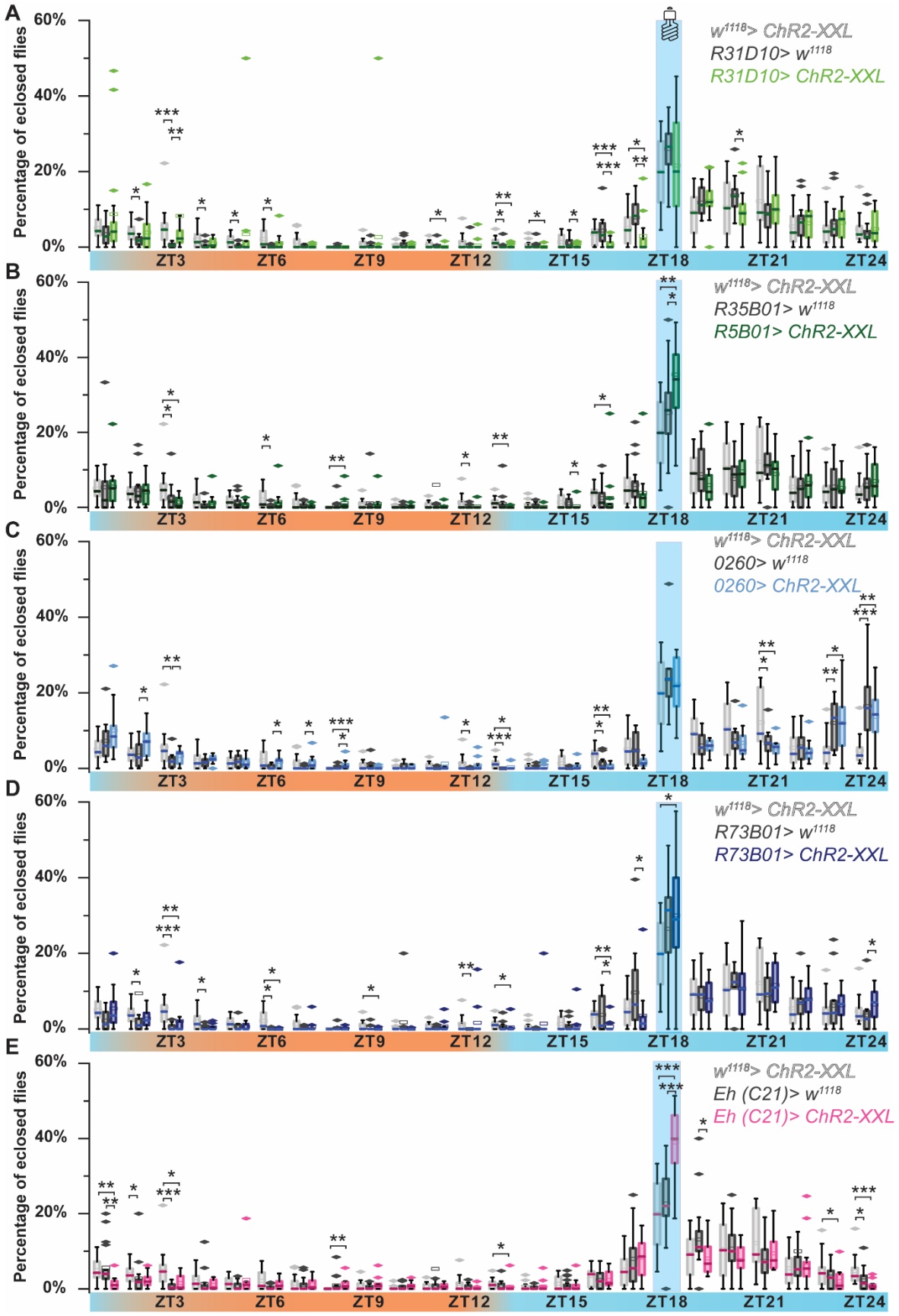

Figure 4.5. Blue Light-induced premature eclosion and simultaneous optogenetic activation of v'Td neurons. The flies were entrained to temperature changes (WC, indicated by an orange-blue

gradient). Using Opto-DEM, six hours before subjective morning (ZT24-1 when the temperature changes from cold to warm) at ZT18 one one-hour pulse of intense blue light was shone on the flies (blue bars). The percentage of eclosed flies per hour compared to the entire day is plotted on the y-axis. **A** At ZT18 (during blue light pulse) the eclosion rate of *v'Td1^{A4-6}> ChR2-XXL* flies showed no significant difference compared to both controls. **B** Activation of v'Td1^{A1-5} at ZT18 while inducing premature eclosion significantly increased the eclosion rate compared to controls. **C** *v'Td2^{A1-6}> ChR2-XXL* flies did not show an altered eclosion rate after optogenetic activation at ZT18. **D** Activation of all v'Td2 neurons (*v'Td2^{A1-7}> ChR2-XXL*) significantly increased the eclosion rate compared to the UAS control ($p \leq 0.05$) but not the Gal4 control. **E** For comparison, the eclosion assay with optogenetic activation of the V_m neurons. At ZT18, the highest eclosion rate for *Eh (C21)> ChR2-XXL* flies compared to both controls was recorded. Mann-Whitney *U* analysis followed by a one-sample Wilcoxon signed-rank test: * = $p \leq 0.05$, ** = $p < 0.001$, and *** = $p < 0.0001$.

2. Knock-down of *torso* in the fat body does not affect eclosion rhythmicity

The eclosion assays of *torso* knock-down plus their data collection were performed by Milena Sekulic (MSc student supervised by Emad Amini). Their data analysis was performed by Emad Amini.

According to the FlyAtlas 2 database (Leader et al., 2018), the adult fat body expresses *torso*. Therefore, the fat body seems downstream of PTTH, and PTTH to fat body signaling may potentially influence eclosion rhythmicity. To test whether the fat body indeed plays a role in maintaining the rhythmicity of eclosion, *torso* expression was downregulated in fat body cells RNAi, using two *UAS-RNA^i* lines with designed long hairpins (GD and KK lines from VDRC). *NP5253-Gal4* drives expression in adult fat body cells (Hayashi et al., 2002) and was chosen for RNAi. *NP5253> torso^i (GD)* flies showed a rhythmic eclosion pattern (Figure 4.6) with high RI (RI=0.38) after autocorrelation and a single MESA peak with a period of 19.9h (Table 4.2). In addition, RNAi using *NP5253> torso^i (KK)* did not impair rhythmicity (RI=0.29, p=22.9). Both controls showed rhythmic eclosion patterns and RIs of more than 0.3 which indicate strong rhythmicity (Figure 4.6 and Table 4.2). LS and eJTK analyses for all experiment and control groups confirmed the rhythmicity (Table 4.2).

In conclusion, the knock-down of *torso* in the fat body did not lead to arrhythmic eclosion. In other words, even though fat body likely is a downstream target of PTTH signaling, it seems not involved in maintaining eclosion rhythmicity.

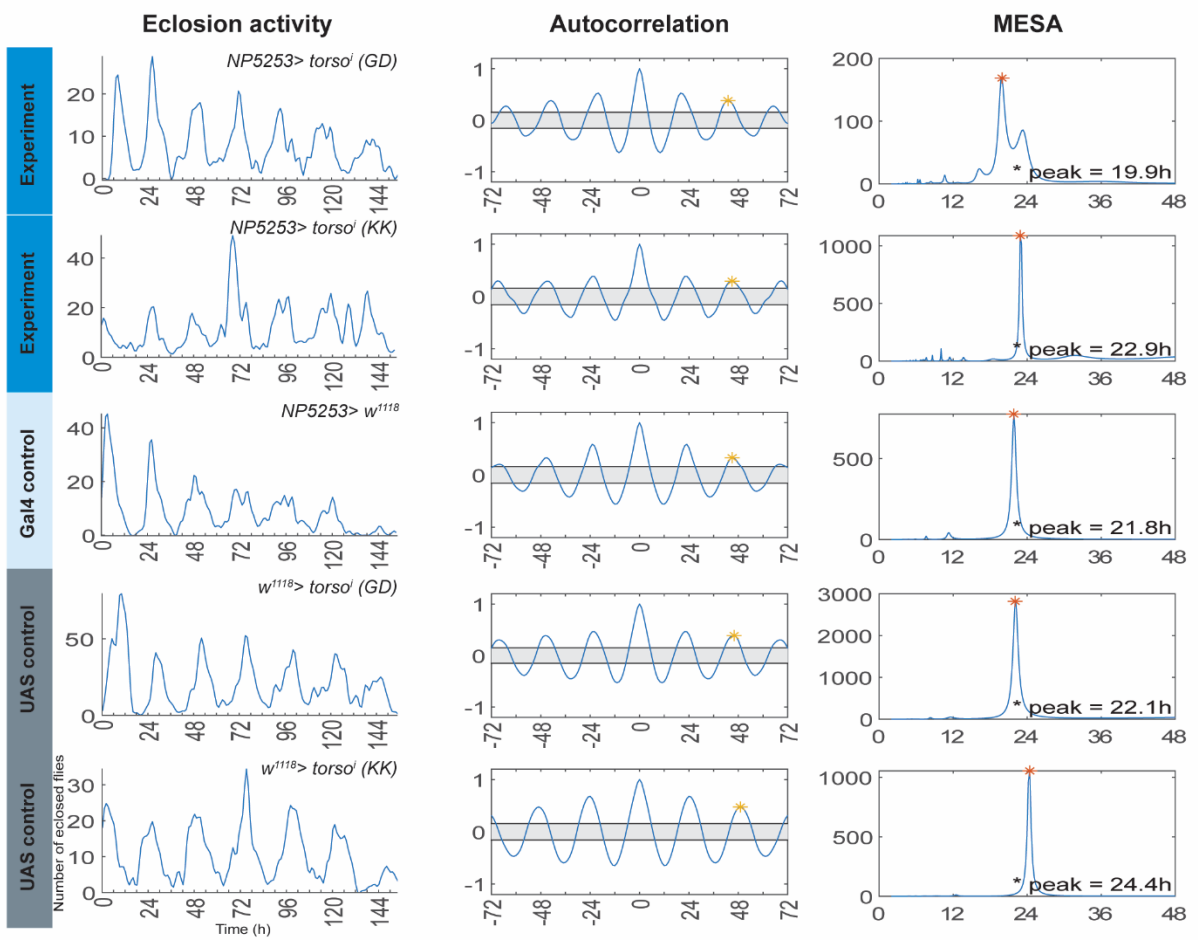

Figure 4.6. PTTH to fat body signaling was not necessary to maintain the rhythmic eclosion pattern. Knock-down of *torso* in the fat body by RNAi did not lead to an arrhythmic eclosion pattern. In all experiment and control groups, the eclosion patterns remained rhythmic. All experiment and control groups showed one MESA peak with a period close to 24h.

Table 4.2. Rhythmicity analysis of eclosion after *torso* knock-down in the fat body (see Figure 4.6).

Genotype	Number of flies	Error	Period	Rhythmicity index	Lomb-Scargle	eJTK BH bf corrected p
NP5253> torso^{i} (GD)	1220	0.1%	19.9h	0.38	27.5	$1.3*10^{-4}$
NP5253> torso^{i} (KK)	1825	5.7%	22.9h	0.29	22.4	$5.9*10^{-9}$
NP5253> w^{1118}	1496	4.9%	21.8h	0.33	24.4	$1.1*10^{-13}$
w^{1118}> torso^{i} (GD)	3546	0.6%	22.1h	0.39	34.4	$4.8*10^{-20}$
w^{1118}> torso^{i} (KK)	1678	2.3%	24.4h	0.47	36.3	$4.9*10^{-25}$

3. The C4da neurons are possible peripheral PTTH targets for eclosion timing

C4da neurons are peripheral sensory neurons with highly branched dendrites on the body wall. They belong to so-called class IV neurons and express the degenerin/epithelial sodium channel subunit *pickpocket1* (*ppk1* or *ppk*; Adams et al., 1998; Darboux et al., 1998). C4da are mainly nociceptive and respond to a variety of noxious (mechanical and/or heat) stimuli (Hwang et al., 2007; Robertson et al., 2013). They are also involved in larval light avoidance. This response is mediated by TORSO, and impairment of PTTH signaling renders the larvae indifferent to strong light stimuli (Xiang et al., 2010; Yamanaka et al., 2013).

The expression of *torso* makes C4da neurons a potential target in PTTH-dependent timing of eclosion. In the larva, C4da neurons can be subdivided into three subtypes that either branch in the dorsal dendritic arborization C (ddaC), ventral dendritic arborization B (vdaB), and ventrolateral dendritic arborization (v'ada) parts of the body wall of each hemisegment. All C4da neurons send their processes to the VNC (Grueber et al., 2002; Singhania and Grueber, 2014). As shown for v'Td neurons (see IV.1.a), C4da axonal projections pass through the midline of the VNC (Grueber et al., 2007) and there, they might pass close to V_m axons. This morphology combined with the presence of TORSO makes C4da a good candidate to neuroendocrinally connect the PTTHn to the V_m neurons. Hypothetically, they could sense hormonally released PTTH before eclosion and synaptically signal to V_m neurons. Therefore, it was interesting to test for their potential role in maintaining eclosion rhythmicity or in triggering the EH/ETH feedback loop.

a. The C4da neurons form synaptic connections with the V_m neurons

The morphology of the peripheral C4da neurons is well described in larvae (Grueber et al., 2007, 2002). There are three types of C4da neurons in each larval hemisegment vdaB, v'ada, and ddaC. C4da cell bodies and dendrites are located superficially at the body wall and attached to the epidermis. The C4da dendrites are space-filling and tile the body surface (Grueber et al., 2007, 2002). During metamorphosis, the dendrites of all C4da neurons are pruned and completely remodeled while the primary axon of each neuron remains unchanged (Kuo et al., 2005). The dendrites of ddaC and v'ada degrade and remodel and ddaB completely disappear (Kuo et al., 2005; Shimono et al., 2009; Yasunaga et al., 2010). Dorsal and ventral' C4da neurons project their axons to their respective hemisegment in the VNC. All afferent projections then pass through the midline of VNC (Grueber et al., 2007). Along the midline, the excessive branching of axons forms a ladder-like structure throughout the entire larval VNC (Ainsley et al., 2003; Grueber et al., 2007).

Since in the larvae, the C4da neurons branch along the VNC midline, it is possible that they form synapses there with the descending V_m neurons in pharate adults. This was checked using double immunostainings and the trans-synaptic anatomical approach used before. A *ppk-Gal4* driver line (Adams et al., 1998; Darboux et al., 1998; Grueber et al., 2002) was used to express mCD::GFP in adult PPK neurons including C4da neurons. In the pharate brain, the *ppk> mCD::GFP* showed two cell bodies in each hemisphere at SEZ and their projections remained in the SEZ (Figure 4.7 A). The line also labeled neurons projecting from the antennal nerve to the SEZ (Figure 4.7 A). Some brains showed inconsistent and faint GFP expression in three to

four additional neurons located in the superior protocerebrum neuropils (SMP to SLP) that also arborized in the posterior slope very close to the projections of D_l neurons (Figure 4.7 A). Because the dendrites and cell bodies of C4da neurons were located outside of the CNS, only axonal projections of C4da neurons were labeled with GFP in the VNC (Figure 4.7 B). Apparently, like in larvae (Grueber et al., 2007), the various C4da neurons projected to the VNC neuromere correlated with the segment the cell bodies were located in. Three pairs of C4da entered from the thoracic connectives and seven to eight pairs from the abdominal connective and joined the MDT. The axonal projections of the C4da neurons from the VNC ascended to the brain through MDT, the cervical connective, and ended in the SEZ close to the antennal nerve projecting and SEZ-located PPK neurons (Figure 4.7 A). In the VNC, the C4da axons projected through the abdominal and thoracic segmental nerves to the MDT. However, this needs to be investigated in detail with multicolor labeling methods. *ppk-Gal4* also drove GFP expression in two PPK neurons located at prothoracic neuromere and accessory metathoracic neuropil as well as neurites that passed through the dorsal lateral tract of ventral cervical fasciculus and ventral median tract of ventral cervical fasciculus at the midline of VNC, not coming into close contact with V_m neuron fibers. The PPK neuron axon endings in the SEZ overlapped with dendrites of the V_m neurons (Figure 4.7 A'), and in the superior protocerebrum neurons overlapped with the D_ls (Figure 4.7 A'). The C4da axonal projections located at the MDT were in proximity to the V_m axons (Figure 4.7 B' and B'''). Next, syb-GRASP was used to check if synaptic connections were formed at the sites of overlaps between EH neurons and PPK neurons (Figure 4.7 C-D). A strong syb-GRASP signal was found in the SMP and MBDL indicating synaptic connections between the V_m and PPK neurons. In addition, a strong syb-GRASP signal at the overlap between D_ls and PPK neurons in the superior protocerebrum and posterior slope was visible. However, the GRASP signal in the SEZ was weaker and sparser (Figure 4.7 C-C'). Again, syb-GRASP was used to check for synaptic contacts between C4da and V_m at MDT. A discernible yet weak and sparse GRASP signal was present in the MDT (Figure 4.7 D-D'). To check if C4da is upstream of the EH neurons, *trans*-Tango was performed. *ppk> trans-Tango* showed that the V_ms (Figure 4.7 E-E") but not the D_ls (Figure 4.7 F-F") are postsynaptic to the C4da neurons.

To summarize, PPK neurons including peripheral C4da neurons appear to be presynaptic to V_m neurons. The synaptic connections are made in the SEZ in the brain and along the MDT in the VNC.

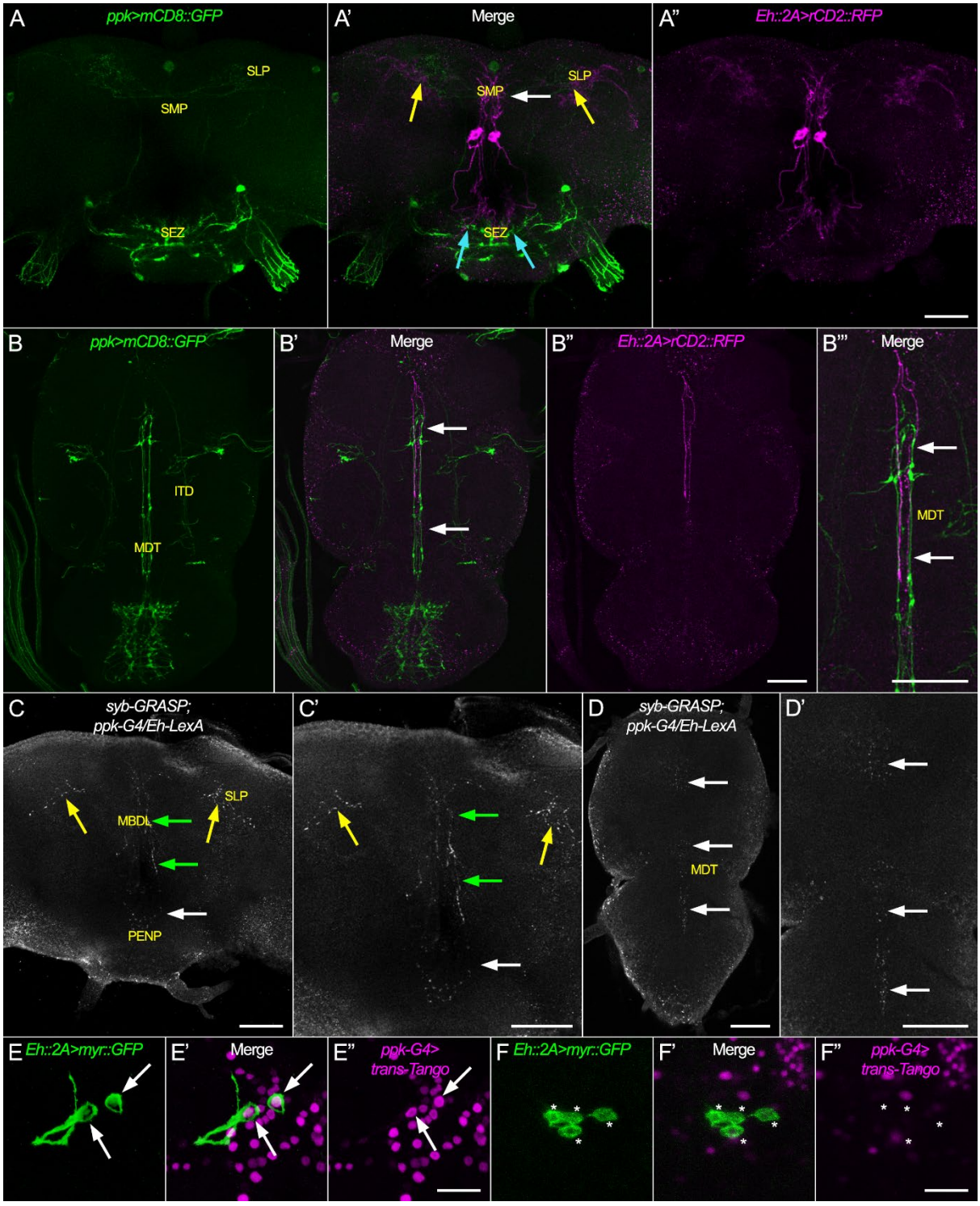

Figure 4.7. The C4da neurons were presynaptic to the V_m neurons. A-A" Double labeling *ppk* expressing neurons (PPK neurons) and V_m neurons in the brain. **A** *ppk-Gal4> UAS-mCD8::GFP* was used to express GFP in C4da neurons. In the brain, GFP was expressed in the axons of PPK neurons ascending from the VNC to the suboesophageal zone (SEZ; green). GFP was expressed in neurons located at the SEZ, in the antennal nerve (AN), and weakly was expressed in the superior medial protocerebrum (SMP) and superior lateral protocerebrum (SLP). **A'** Overlap between the processes of V_m neurons in the brain (magenta) and PPK neurons (green) was observable in the SEZ (cyan arrows) and at the MBDL between V_m and PPK neurons located at superior neuropils (white arrow). In addition, projections from the D_ls and PPK neurons located at superior neuropils overlapped in the posterior slope

(yellow arrows). **A"** *Eh::2A-LexA> LexAop-rCD2::RFP* expressed RFP in V_m neurons (magenta). **B-B"** Double labeling C4da and V_m neurons in the VNC. **B** mCD8::GFP was expressed in the neurites of PPK neurons in the VNC (green). The C4da neurons entered the VNC from the abdominal and thoracic nerves and ascended through the MDT to the brain. *ppk-Gal4> UAS-mCD8::GFP* labeled two PPK neurons in the prothoracic neuromere inside the VNC. GFP also labeled neurites passing through the intermediate tract of dorsal cervical fasciculus (ITD). **B'** C4da axons (green) passed by V_m axons (magenta) in the MDT (arrows). **B"** The axons of V_m neurons in the VNC were marked by rCD2::RFP (magenta). The V_m axons also passed through the MDT. **B"'** Close-up view of the axons of V_m neurons (magenta) and C4da (green) which come close together in the MDT (arrows) at the VNC midline. **C-C'** *ppk-Gal4; Eh::2A-LexA> syb-GRASP* showed synaptic contacts between V_m neurons and PPK neurons in the periesophageal neuropil (PENP; white arrow) and at median bundle (MBDL; green arrows). GRASP signals also showed connections between non-canonical D_ls and PPK neurons at SLP (yellow arrows). **D-D'** *ppk-Gal4; Eh::2A-LexA> syb-GRASP* showed synaptic contacts between V_m neurons and C4da neurons in the VNC. A GRASP signal was sparsely present at the midline of the VNC (white arrows), indicating synaptic connections between V_m and C4da neurons in the VNC. **E-F** *trans*-Tango showed that only V_ms were postsynaptic to PPK neurons. **E** Using *Eh::2A-LexA> LexAop-myr::GFP* V_m neurons were labeled (arrows). **E'** Colocalization of GFP and *trans*-Tango nuclear RFP signal in V_m neurons showed that the V_m neurons were postsynaptic to PPK neurons (arrows). **E"** *ppk> trans-Tango* drove nuclear RFP expression in neurons postsynaptic to PPK neurons including V_m neurons (arrows). **F** Non-canonical D_l neurons were labeled by GFP expression (asterisks). **F'** GFP and nuclear RFP signals were not colocalized in D_l neurons meaning D_ls were not postsynaptic to PPK neurons (asterisks). **F"** *ppk> trans-Tango* drove nuclear RFP expression in neurons postsynaptic to PPK neurons but not D_l neurons (asterisks). *Scale bars*: A-D 50 µm, E-F 20 µm.

b. The C4da neurons might be involved in sustaining the rhythmicity of eclosion

To check whether PTTH signals to C4da neurons in pharate adults were relevant to eclosion timing, eclosion assays were performed with a series of loss-of-function genotypes. Constitutive ablation of the C4da neurons using *ppk> RA* was lethal and drastically reduced the number of puparia. Therefore, for timed ablation of C4da neurons during the final pupal stages, *UAS-RA^{CS}* was used. Eclosion assays of the *ppk> RA^{CS}* showed weak rhythmicity (autocorrelation RI=0.13; Table 4.3), and the eclosion activity showed a distinctive peak on the first day (Figure 4.8). However, during the next six days, distinctive peaks and troughs separated by ~24h intervals were missing. Therefore, the rhythmicity of *ppk> RA^{CS}* flies was considerably lowered to their controls (RIs > 0.3). The MESA peak of the experiment group was broad with a period of 21.1 hours and showed a wide shoulder. Also, LS and eJTK analyses of experiment and control groups showed rhythmic values, which were again lower for the experimental flies. (Figure 4.8 and Table 4.3). To further assess the rhythmicity, the calculations were done for the final six days that showed the arrhythmic eclosion pattern. This time analyses resulted in an arrhythmic RI (RI=0.04; Table 4.3) however, the LS (Power > 0) and eJTK ($p < 0.05$) analyses again showed rhythmicity albeit reduced compared to the controls (Table 4.3). MESA showed a significantly dampened peak with a 19.5h period, compared to controls (Figure 4.8 and Table 4.3). Taken together, these results suggest that conditional ablation of C4da neurons reduces and destabilizes eclosion rhythmicity.

Next, C4da neurons were silenced using *UAS-Kir2.1*. In contrast to the results after C4da ablation, *ppk> Kir2.1* flies showed rhythmic eclosion patterns similar to their UAS and Gal4 controls (Figure 4.8, Table 4.3). Thus, electrically silencing the C4da neurons did not affect rhythmic eclosion.

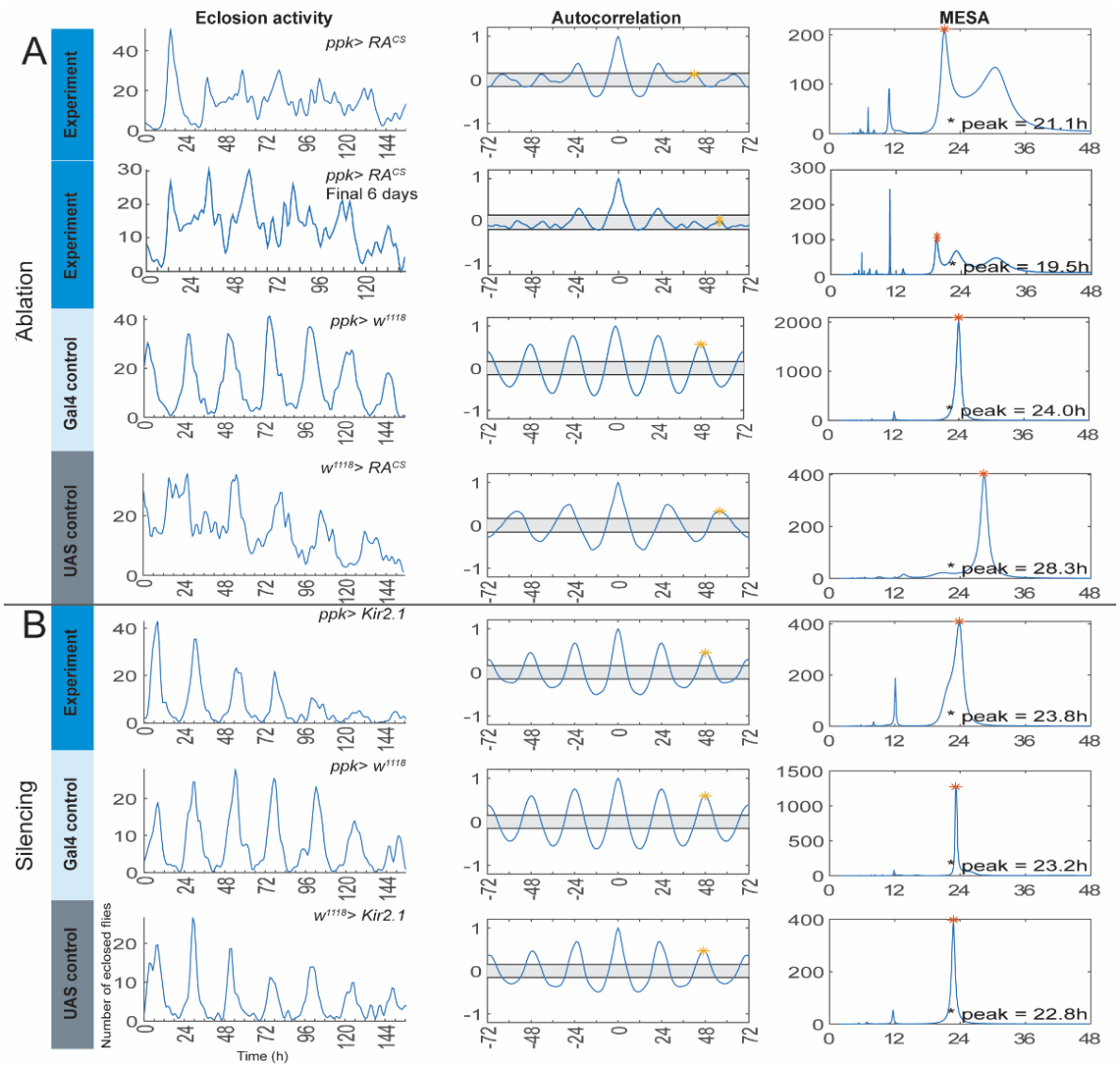

Figure 4.8. Effects of conditional killing and electrical silencing of C4da neurons on eclosion rhythmicity. A Ablating the C4da neurons at final pupal development (*ppk> UAS-RA^{CS2}.CC*) showed weak rhythmicity (for values see Table 4.3), while the controls were strongly rhythmic. By omitting the first day and only analyzing the final six days, autocorrelation resulted in an arrhythmic RI with rhythmic LS and eJTK values which suggested low rhythmicity. **B** In contrast, electrical silencing of the C4da neurons showed strongly rhythmic eclosion in both experiment and control groups.

Table 4.3. Eclosion rhythmicity analysis of flies with ablated or silenced C4da neurons (see Figure 4.8). Arrhythmic values are shown in red.

	Genotype	Number of flies	Error	Period	Rhythmicity index	Lomb-Scargle	eJTK BH bf corrected p
Ablation	*ppk> RA^{CS2}.CC* (7 days)	2390	6.5%	21.1h	0.13	8.0	$4.6*10^{-6}$
	ppk> RA^{CS2}.CC (Final 6 days)	1880	-	19.5h	0.04	4.6	$3.9*10^{-5}$
	ppk> w^{1118}	2223	5.5%	24.0h	0.57	47.2	$5.5*10^{-32}$
	w^{1118}> RA^{CS2}.CC	2639	7.2%	28.3h	0.33	16.6	0.06
Silencing	*ppk> Kir2.1*	1126	5.1%	23.8h	0.45	25.6	$2*10^{-26}$
	ppk> w^{1118}	1202	7.7%	23.2h	0.60	42.7	$1.3*10^{-34}$
	w^{1118}> Kir2.1	895	4.1%	22.8h	0.47	29.1	$6.9*10^{-29}$

Next, *torso* was knocked down in C4da neurons to impair PTTH signaling to C4da neurons. As previously was done for the fat body (see IV.2), two long hairpin *UAS-torso^{i} (GD)* and *UAS-torso^{i} (KK)* RNAi lines were used to downregulate *torso* mRNA in the C4da neurons. Both *ppk> torsoi (GD)* and *ppk> torso^{i} (KK)* flies as well as the controls showed a rhythmic eclosion pattern (Figure 4.9 A) with high rhythmicity (RIs ≥ 0.39; Table 4.4) and MESA peaks with periods around 24h (Figure 4.9 A and Table 4.4). LS and eJTK analyses also showed rhythmic values (Table 4.4).

The lack of effect of RNAi against *torso* may indicate that PTTH signaling to C4da neurons is not required for eclosion rhythmicity. Alternatively, not uncommon for receptors, the RNAi may have led to an insufficient knock-down of *torso* expression. To test for the latter alternative, *torso* was knocked out in C4da neurons using conditional CRISPR/Cas9 mutagenesis (Port et al., 2020). For this purpose, *UAS-uMCas9; ppk-Gal4* flies were crossed to *torso-gRNA* flies. *w^{1118}* flies were crossed to each of these lines to generate controls. For these eclosion assays, the parental flies were removed after egg laying. When pupariation started, the offspring were treated with a one-hour 37 °C heat shock to induce mutagenesis. Two days later the flies were transferred to DD and the rest of the eclosion assays were carried out as usual (see Materials and Methods 5.a). *UAS-uMCas9/torso-gRNA; ppk-Gal4/+* experiment flies showed an arrhythmic eclosion pattern (Figure 4.9 B) and all three analysis methods confirmed this arrhythmicity (Table 4.4). In contrast, *w^{1118}> torso-gRNA* control flies showed a rhythmic eclosion pattern, even though the rhythmic pattern was impaired during the first two days (Figure 4.9 B). Nevertheless, autocorrelation, LS, and eJTK analyses showed rhythmicity. However, while *w^{1118}> UAS-uMCas9; ppk-G4* control flies graphically showed rhythmic eclosion, autocorrelation indicated arrhythmicity (RI = 0.04). This is perhaps because most flies eclosed in the first three days, and the amplitude of eclosion was very low from day 4 on. In contrast, LS and eJTK analyses indicated rhythmicity.

Therefore, the result of the *torso* knock-out experiment is not entirely clear and should be repeated. It seems, however, possible that the knock-out of *torso* in C4da neurons strongly impairs eclosion rhythmicity.

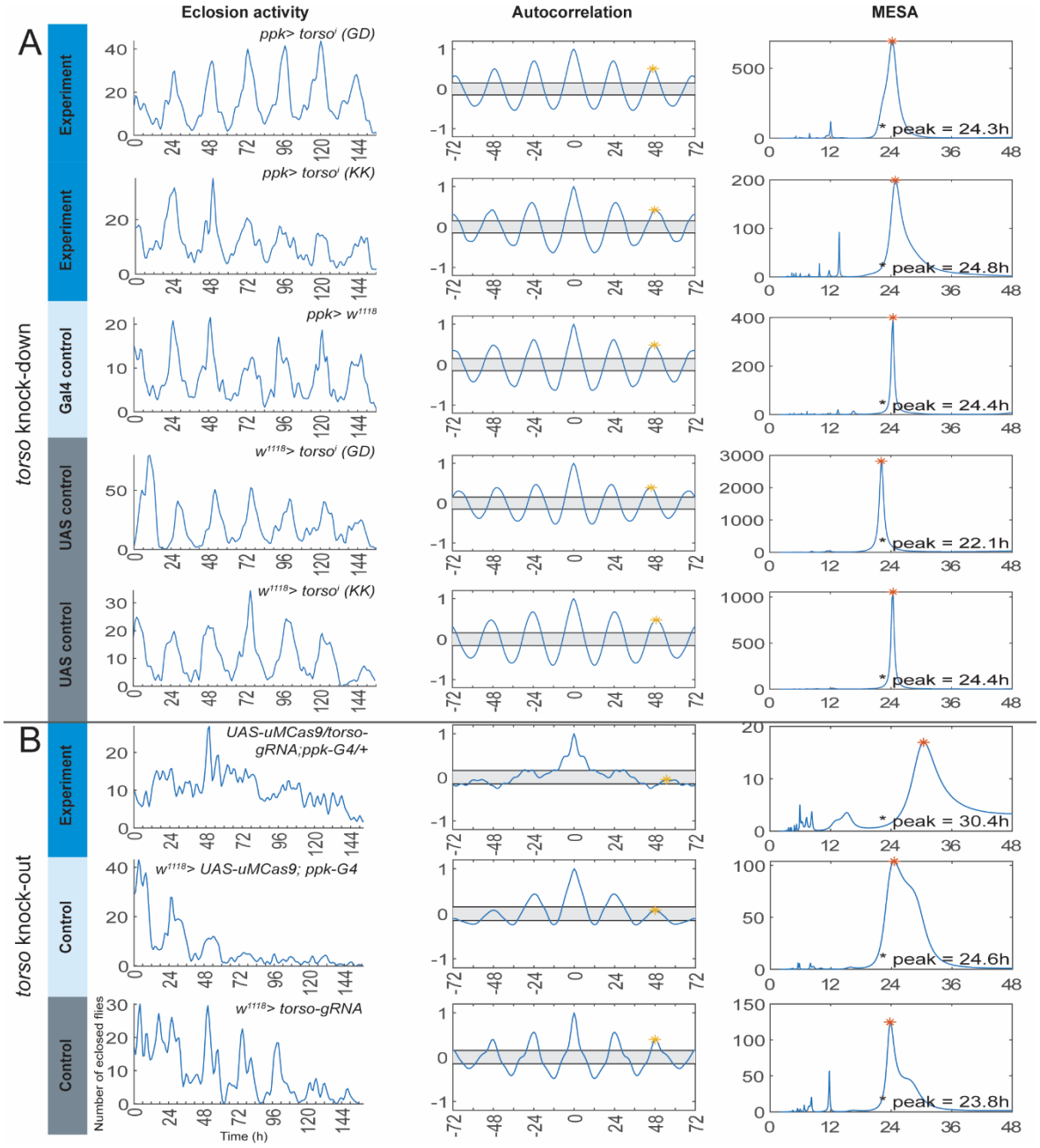

Figure 4.9. CRISPR/Cas-mediated *torso* knock-out in C4da neurons but not RNAi-mediated knock-down caused arrhythmic eclosion. A Knock-down of *torso* in C4da neurons using *UAS-torso^{i} (GD)* and *UAS-torso^{i} (GD)* did not impair eclosion rhythmicity which was similarly strong as in controls. **B** However, knock-out of *torso* in C4da neurons strongly impaired eclosion rhythmicity, while both *w^{1118}> UAS-uMCas9; ppk-Gal4* and *w^{1118}> torso-guide RNA* controls showed rhythmic eclosion.

Table 4.4. Rhythmicity analysis of the eclosion of flies with downregulated or knocked out *torso* in C4da neurons (see Figure 4.9). Arrhythmic values are shown in red.

	Genotype	Number of flies	Error	Period	Rhythmicity index	Lomb-Scargle	eJTK BH bf corrected p
***torso* downregulation**	*ppk> torso^{i} (GD)*	2607	6.7%	24.3h	0.51	34.2	$6*10^{-26}$
	ppk> torso^{i} (KK)	1986	5.6%	24.8h	0.42	35.9	$1.2*10^{-19}$
	ppk> w^{1118}	1331	1.7%	24.4h	0.49	36.2	$6*10^{-26}$
	w^{1118}>torso^{i} (GD)	3546	0.6%	22.1h	0.39	34.4	$4.8*10^{-20}$
	w^{1118}> torso^{i} (KK)	1678	2.3%	24.4h	0.47	36.3	$4.9*10^{-25}$
***torso* knock-out**	*UAS-uMCas9/torso-gRNA; ppk-G4/+*	1277	7.6%	30.4h	-0.05	0	1
	w^{1118}> UAS-uMCas9; ppk-G4	1726	8.1%	24.6h	0.08	2.9	$8.2*10^{-5}$
	w^{1118}> torso-gRNA	1689	7.3%	23.8h	0.40	2.6	$2.7*10^{-9}$

c. Optogenetical activation of C4da neurons while inducing premature eclosion with blue light reduces the eclosion rate

To further investigate whether C4da neurons may provide input to the V_m neurons, the effects of optogenetic activation of C4da neurons on the light-induced premature eclosion rate was tested, using Opto-DEM. During ZT18 (light pulse), significantly fewer *ppk> ChR2-XXL* flies eclosed ($p < 0.0001$; Figure 4.10 A) compared to the Gal4 control (*ppk> w^{1118}*). However, compared to the UAS control (*w^{1118}> ChR2-XXL*) the difference in eclosion rates was not significantly different. Interestingly, at ZT19 one hour after the light pulse, significantly more experiment flies emerged compared to both controls ($p < 0.001$; Figure 4.10 A). In comparison to the Opto-DEM eclosion pattern of V_m neurons at ZT18, it was evident that significantly fewer *ppk> ChR2-XXL* flies eclosed than *Eh (C21)> ChR2-XXL* ($p < 0.0001$; Figure 4.10 B). At ZT19, significantly more *ppk> ChR2-XXL* than *Eh (C21)> ChR2-XXL* emerged ($p < 0.001$; Figure 4.10 B). This rather remarkable increased eclosion rate at ZT19 after optogenetic activation of the C4da neurons suggested that activation of the C4da neurons decreased the premature eclosion rate and delayed it by one hour. The C4da neurons might thus modulate or inhibit the activity of the V_m neurons, thus reducing light-induced eclosion in *ppk> ChR2-XXL* flies.

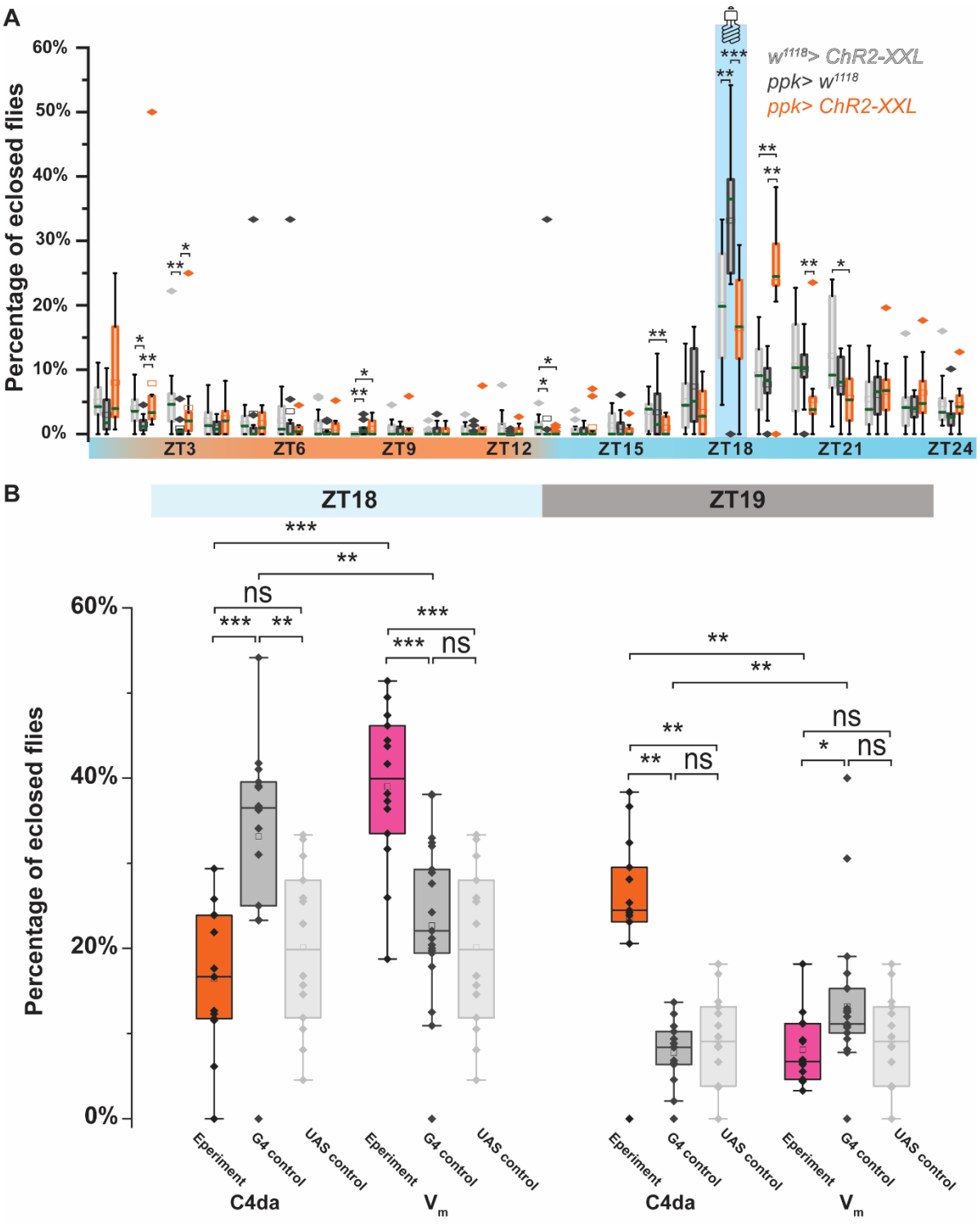

Figure 4.10. Blue light-induced premature eclosion and simultaneous optogenetic activation of the C4da neurons decreased the eclosion rate. A The flies were entrained to temperature changes (WC, indicated by an orange-blue gradient). Using Opto-DEM, six hours before subjective morning (ZT24-1 when the temperature changes from cold to warm) at ZT18 one one-hour pulse of intense blue light was shone on the flies (blue bars). The percentage of eclosed flies per hour compared to the entire day is plotted on the y-axis. During the light pulse at ZT18, fewer *ppk> ChR2-XXL* flies eclosed (~20 flies) than Gal4 control flies (*ppk> w*^{1118}; ~40 flies). However, the UAS control (*w*^{1118}*> ChR2-XXL*) was statistically not different from the experiment group (~20%). The eclosion rate of the Gal4 control was also significantly higher compared to the UAS control. At ZT19, significantly more experiment

flies eclosed compared to both control groups. **B** The eclosion rate upon optogenetic C4da neuron activation experiment and controls were compared to the activation of the V_m neurons (as positive control). At ZT18 both experimental groups (*ppk> ChR2-XXL* and *Eh (C21)> ChR2-XXL*) were significantly different from each other, with a higher eclosion rate for *Eh (C21)> ChR2-XXL* flies). When comparing the C4da neuron activation to V_m neuron activation at ZT19, the eclosion rates were significantly higher for the C4da neuron experiment (*ppk> ChR2-XXL*). Mann-Whitney *U* analysis followed by a one-sample Wilcoxon signed-rank test: * = $p \leq 0.05$, ** = $p < 0.001$, and *** = $p < 0.0001$. ns = not significantly different.

d. The *in vivo* activity of the PPK neurons correlates with PTTHn and V_m neurons activity

C4da neurons express TORSO and therefore may respond to PTTH signaling in the puparia and pharate adults. In addition, the findings above suggested that the C4da neurons may provide inhibitory synaptic input to the V_m neurons (see IV.3.a and IV.3.c). Therefore, the existence of a PTTH-C4da-V_m axis is in principle possible. Chapter I based on ARG-Luc imaging, described that PTTHn were active around 31 hours and six hours before eclosion (see I.1.c). If the activity of the PTTHns through C4da influences the activity of V_m neurons just prior to eclosion, one would therefore expect that the C4da neurons are also active at the time of PTTHn and V_m neuron activity.

To check for any temporal correlations between the activities of PTTHn, V_m, and C4da neurons, *ppk> ARG-luc* flies were used to record the activity of PPK neurons including C4da neurons during pupal development in the same way as done before for the PTTHn and V_m neurons. Unfortunately, however, due to technical problems, camera images to track down the eclosion activity of the tested flies could not be recorded. Therefore, to arrange the ARG-Luc data according to the time of eclosion, the artifact peak resulting from the flies leaving the puparia was used to indicate the time of eclosion (see Appendix 10). As the flies eclose, more photons reach the detector as fewer are absorbed by the puparium, creating this artifact peak. Therefore, the artifact peak should indicate eclosion very well. After finding the artifact peak and marking the datapoint before that as the moment of eclosion, the activity of C4da neurons during pupal development was plotted (Figure 4.11 A). All flies showed synchronized C4da activity around seven hours before eclosion. Some flies also showed synchronized C4da activity around -18 to -16 hours (Figure 4.11 A). C4da activity was also high the day after eclosion, yet this activity was not synchronized among the different flies. Around 48h after eclosion, a large seemingly synchronized ARG-Luc signal from many flies was recorded, for which we currently have no explanation.

PPK neurons within the first 24 hours after eclosion showed random and sharp peaks of activity in individual flies (*e.g.*, the blue line in Figure 4.11 A). To check if the activity of PPK neurons correlated with PTTHn and V_m activity, the average activity of *ppk> ARG-Luc* was plotted along with *ppk> ARG-Luc* and *ppk> ARG-Luc* averages (Figure 4.11 B). All three groups of neurons showed a peak of activity at around seven to six hours before eclosion. While both V_m and C4da showed narrow and sharp peaks, PTTHn showed a broader peak with lower amplitude (Figure 4.11 B).

These results suggested that around seven hours before eclosion, the PPK neurons including C4da neurons became active which resembled the activity of V_m neurons. However, if the

observed activity of the V_m neurons at the same time is influenced by PPK activity is not known and requires further research with functional imaging.

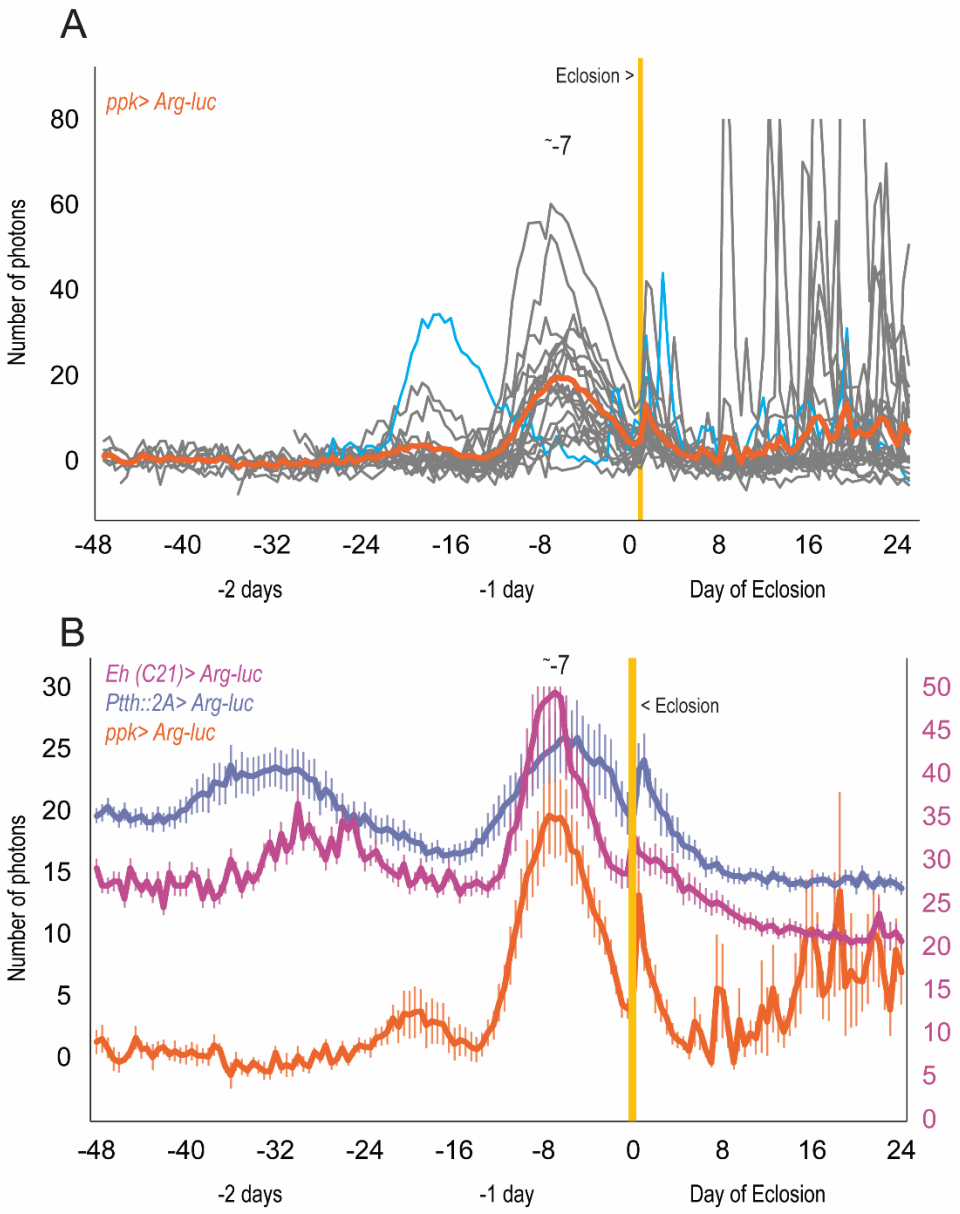

Figure 4.11. PPK neurons were active around seven hours before eclosion. A Using *ppk> ARG-Luc* the activity of PPK neurons of 23 flies during pupal development is measured and arranged according to the time of eclosion (yellow line). The data of each individual was shown in gray while the average activity was depicted in orange. Data from a single fly was shown in blue as an example. All flies showed a peak in activity around seven hours before eclosion. PPK neurons of four flies showed an earlier activity around 18 to 16 hours before eclosion. Within the first 24 hours after eclosion flies showed different activity patterns indicated by sharp and narrow peaks (see the example depicted in blue). Noteworthy, two days after eclosion all flies showed PPK activity that lasted for hours (depicted by continuous and large peaks); the underlying reason for this peak was unknown. **B** The average activity of C4da neurons (*ppk> ARG-Luc*; orange), V_m (*Eh (C21)> ARG-Luc*; orange), and PTTHn (*Ptth::2A> ARG-Luc*; blue) were plotted together (The number of photons for V_m activity is plotted on the right y-axis). At around seven hours before eclosion, all neuronal groups showed an increase in their activities. Error bars indicate SEM.

Discussion

Chapter I

A deeper insight into the timing of PTTH signaling

In Chapter I, the primary aim was to understand circadian eclosion gating when during development PTTH signaling is required. First TARGET was used to obtain a rough estimation of the timing of PTTH signaling. TARGET showed that the PTTH signaling was required in the second half of pupal development for eclosion gating. Then CaLexA was used as a proxy to measure the intracellular Ca^{2+} levels of PTTHn and their activity shortly before eclosion. CaLexA showed that Ca^{2+} levels of PTTHn were highest around lights on (ZT0). To obtain a deeper understanding of the timing of PTTHn activity, ARG-Luc imaging was used and showed that PTTHns are active only two times during the final pupal stages, once around 31 hours and the other time six hours prior to eclosion. Altogether, PTTH signaling to maintain eclosion rhythmicity is only required in the final pupal stages and the activity of PTTHn is confined to the day before and the day of eclosion.

Here, the TARGET technique (McGuire et al., 2003) was used to specifically silence the PTTHn at the first and second half of pupal development. The data confirmed previous studies that PTTH signaling is required for eclosion timing under constant conditions (Selcho et al., 2017). Unfortunately, however, TARGET required an increase in temperature that accelerated the speed of pupal development. The accelerated pupal development affected the data acquisition for silencing PTTHn in the second half or entire pupal development and caused a concentration of eclosion events to only three to four instead of five to seven days under our experimental conditions. This brought problems in the calculation of the rhythmicity index (RI) by autocorrelation analysis, the standard analysis method for eclosion rhythmicity. Therefore, two additional analysis methods typically used for the analysis of locomotor and molecular rhythmicity, Lomb-Scargle (LS) and eJTK (Ruf, 1999; Zielinski et al., 2014) were additionally utilized. Another study had a similar problem with the acceleration of development during TARGET experiments (Mark et al., 2021). Mark and colleagues used TARGET to knock-down the ecdysone receptor in the PG during the final pupal stages to see how it affects the developmental timing of eclosion. They found that the temperature change required to knock-down *EcR* in PG (about 24 hours) highly accelerated pupal development (Mark et al., 2021). In addition, following Mark et al. (2021), visual inspection of the temporal distance of eclosion peaks and throughs was used to evaluate circadian activity within the three to four days of data (Mark et al., 2021). To overcome the temperature-caused acceleration of development problem, in other chapters of this thesis, $RA^{CS2}.CC$ was used (Chen et al., 2012). A limited 12h temperature raise activated the cold-sensitive ricin and a follow-up temperature drop deactivated it. However, the temperature changes required to fully activate and deactivate ricin did not influence the development speed. Therefore, to efficiently and specifically limit neuronal ablation (see Appendix 2) to the final pupal stages $RA^{CS2}.CC$ was used (Chen et al., 2012).

A drop of ecdysteroid levels is necessary to allow eclosion (Schwartz and Truman, 1983; Sláma, 1980; Zitnan and Adams, 2012). In *Drosophila*, 20 hours before eclosion ecdysteroids levels are not detectable anymore (Handler, 1982; Lavrynenko et al., 2015). However, the

mechanism that clock uses to gate eclosion is downstream of 20-E regardless of ecdysteroid levels (Mark et al., 2021). Mark et al. (2021) showed that clock controls the final steps of metamorphosis and eclosion timing is affected at the level of EcR signaling, downstream of 20-E. Thus, the circadian clock gates the completion of metamorphosis around 14 hours before eclosion (Mark et al., 2021). In this thesis, using ARG-Luc imaging, two peaks of PTTHn activity are observed at around 31 and six hours before eclosion. These two peaks are nearly 24 hours apart. ARG-Luc imaging shows that the activity of the PG starts two days before eclosion, independent of the PTTHns which are still inactive at that time. Later, starting PTTHns activity seems to shift the phase of PG activity, compatible with the current model of PTTH signaling subserving synchronization of the central brain and peripheral PG clocks (Selcho et al. 2017). The -31h peak in PTTHn activity might be associated with the timing of the eclosion as it seems to shift the phase of the PG activity by 16 hours. After phase shifting PG shows two activities at -24h and at the time of eclosion. The ~24h intervals in PTTH and PG activity and the likely phase shift of PG activity by PTTH at the end of pupal development suggest that PTTH is a circadian timer as well as a developmental timer. This may underly the relation of the two pacemakers needed for rhythmic eclosion (Myers, 2003). However, further ARG-Luc experiments with disassociating PTTH to PG signaling (such as knock-down of *torso* in PG) are required to better characterize this PTTH-PG activity relationship. ARG-Luc might also provide a better insight into whether and how PG activity is driven by the PG clock. As an example, the pace of the PG molecular clock could be changed by over-expressing dbt^S and dbt^L (Selcho et al., 2017) and this can be used in combination with ARG-Luc to investigate how PG clock affects ecdysone production.

Temperature entrainment of eclosion

Temperature is a potent Zeitgeber that can entrain the clock and eclosion rhythmicity (Ruf et al., 2021; Wheeler et al., 1993; Zimmerman et al., 1968). Yet, the neuronal network underlying temperature entrainment of eclosion rhythmicity is uncharacterized. To assess whether clock-derived input to PTTHns is involved, we electrically silenced different combinations of clock neurons during temperature entrainment and then monitored eclosion rhythmicity. As expected, silencing all clock neurons and silencing PDF^+ neurons as major pacemaker clock neurons (Helfrich-Förster, 1995; Liang et al., 2017; Renn et al., 1999) caused arrhythmic eclosion after temperature entrainment. Therefore, PDF^+ LN_vs are required for temperature-entrained eclosion rhythmicity. The studies of daily locomotor activity rhythms showed that important temperature-perceiving clock neurons are DN1 and DN2 neurons (Guo et al., 2016; Kaneko et al., 2012; Y. Zhang et al., 2010). Remarkably, silencing $DN1_p$s or DN2s did not affect eclosion rhythmicity after temperature entrainment. However, when compared to their relative controls, flies with silenced $DN1_p$s or DN2s showed broader peaks and lower amplitudes. This opens the possibility that temperature-entrained rhythmicity is an outcome of several clock neuron groups that process the temperature information together or in parallel, with $DN1_p$s and DN2s being reciprocally redundant in this function. Therefore, perhaps, silencing individual clock clusters one by one did not impair eclosion rhythmicity because other clusters can compensate for and maintain rhythmicity. Therefore, more experiments using driver lines that silence more than two clock clusters need to be performed to clarify this issue. It is possible that silencing $DN1_p$s and DN2s together impairs eclosion rhythmicity. Moreover, due to the lack of a specific driver line for LN_ds, this thesis could not assess the role of LN_ds in temperature entrainment of eclosion. Finally, the expression strength and specificity of the

driver lines correlate with their effectiveness. Possibly some of the driver lines used in this study are not driving strong enough to silence the neurons efficiently or did not silence the entire subgroup efficiently. For example, drivers used for silencing DN2 (see Appendix 5 and Figure 6.5 C) and LPNs (see Appendix 5 and Figure 6.5 D) showed weak myr::GFP expression in DN2s and LPNs respectively. In conclusion, the results of the thesis demonstrate that the sLNv are required for temperature-entrained eclosion rhythmicity. The role of the dorsal neurons previously shown to be involved in temperature entrainment of locomotor activity (Guo et al., 2016; Kaneko et al., 2012; Y. Zhang et al., 2010) still remains to be resolved. However, the results of the thesis suggest that at least neither $DN1_{p}$s nor DN2s are strictly required, and it is possible that these dorsal clock neuron subsets are reciprocally redundant for temperature entrainment of eclosion.

Insulin signaling does not affect eclosion rhythmicity

InR-based insulin signaling to the PG promotes ecdysteroid production and represents a major endocrine axis that controls developmental timing (Boulan et al., 2013; Caldwell et al., 2005; Colombani et al., 2005; Mirth et al., 2005; Moeller et al., 2017). In contrast, ILP8 from damaged imaginal disks is sensed by LGR3 present in PG and represses ecdysone production (Jaszczak et al., 2016). Furthermore, *torso* expression in the PG is under the control of insulin signaling which influences PTTH signaling to the PG (Di Cara and King-Jones, 2016). All this suggests that insulin signaling might play an important role in regulating eclosion rhythmicity by controlling ecdysone production. A recent study looked at ILP2, -3, and -5 as the main growth regulating ILPs (Ikeya et al., 2002) and showed that *Ilp 2,3, 5* null mutants and flies with down-regulated InR have a rhythmic eclosion pattern (Cavieres-Lepe et al., 2023). In this thesis, eclosion assays of *Ilp7*, *Ilp8,* and *Lgr3* null mutants showed unimpaired rhythmicity. These results show that insulin signaling neither through InR nor *Lgr3*, ILP7, and ILP8 signaling pathways influences the timing of eclosion. This is remarkable, as PTTH and insulin signaling both act as developmental timers during larval and pupal development. This finding suggests that PTTH signaling is the key signaling pathway in circadian eclosion timing.

Chapter II

The EH^+ neurons receive synaptic input from the clock

As the name indicates, ETH from the Inka cells is thought to trigger ecdysis behavior (Ewer et al., 1997; Zitnan et al., 1996). Yet, it is currently unknown what causes the initial release of ETH. As eclosion rhythmicity is under the control of the circadian clock, it is possible that signaling from the central clock starts eclosion. Yet, the Inka cells are not innervated by clock neurons. The EH neurons are possible candidates that mediate clock input to the Inka cells, as EH is known to drive ETH release (reviewed in Zitnan and Adams, 2012). To test whether the clock is presynaptic to EH neurons, trans-synaptic anatomic methods were used. The anatomical connectomic analysis showed that several clock neuron subsets (sLN_vs, lLN_vs, LN_ds, $DN1_a$s, DN2s, LPNs) are presynaptic to EH neurons (summarized in Figure 5.2). Thus, clock neurons may fine-tune both the activity of the EH and PTTH neurons until eclosion. Another noteworthy point is finding anatomically stronger synaptic connections between the sLN_vs and the EH^+ neurons compared to the other connections. The proximity of the V_m neurons to PDF^+ neurons and the possibility of clock input to these neurons have been shown

and discussed before (Blanchardon et al., 2001). The syb-GRASP results in this thesis suggest that the connections of the sLN_vs to EH neurons are likely not peptidergic but synaptic and perhaps glycinergic (Frenkel et al., 2017). This would be in contrast to the connection between sLN_vs and PTTHn which is peptidergic (Cavieres-Lepe et al., 2023; Selcho et al., 2017).

The connectomics results of this thesis further suggest that both V_ms and non-canonical D_ls are postsynaptic to the sLN_vs. syb-GRASP, BAcTrace, and *trans*-Tango signals obtained by the *Pdf-Gal4* driver line are distinctly stronger compared to those obtained by the *Clk856-Gal4* line. This is likely caused by the stronger Gal4 expression of the *Pdf-Gal4* driver, a notion that is supported by the varying strength of the *trans*-Tango signal in V_m neurons between the drivers. Both *Pdf-Gal4* and *Clk856-Gal4* label sLN_vs, therefore both V_ms and D_ls are postsynaptic to the sLN_vs. However, in V_ms the *Pdf> trans-Tango* signal is distinctly stronger than the *Clk856> trans-Tango* signal. Further, while all D_l neurons show the *Pdf> trans-Tango* signal, none show a *Clk856> trans-Tango* signal. Therefore, D_ls receive input from PDF^+ neurons. Whether further clock neurons signal to D_ls through synaptic connections, unfortunately, cannot be determined with the available tools. The very low survival rate and poor health condition of the *Eh::2A-Gal4* flies especially in combinations with the other genetically inserted components made it hard to study non-canonical EH neurons. The *Eh::2A-LexA* flies are healthier and live longer. However, even with the *Eh::2A-LexA* line, the dense arborizations made it impossible to discern which of the non-canonical neurons is involved in the connections with the clock. Thus, whether clock neurons provide input to the D_ls must be investigated in the future. V_m neurons are important for the immediate light-on eclosion response (McNabb and Truman, 2008). This light input can be provided to the V_ms through the sLN_vs as described for PTTHn in the larval brain (see Discussion I; and Sorkaç et al., 2022). A recent study showed that the R8 photoreceptors are also important for this eclosion response (Bidell et al., 2023). The R8 photoreceptors are not directly connected to lLN_vs (Senthilan et al., 2019). Therefore, whether R8 provides the light input to the clock and then to the V_m neurons is unknown. The R8 neurons end in the M3 layer of the medulla (Hadjieconomou et al., 2011). This is close to the endings of the non-canonical D_l that ends in M7-8 layers of the medulla (Scott et al., 2020). If there is a connection between these neurons that triggers initial EH release from them is likely and worth investigating.

In Chapter III, the peptidergic connections from the clock to the EH^+ neurons are investigated and discussed in detail (see Results III.2 and Discussion III).

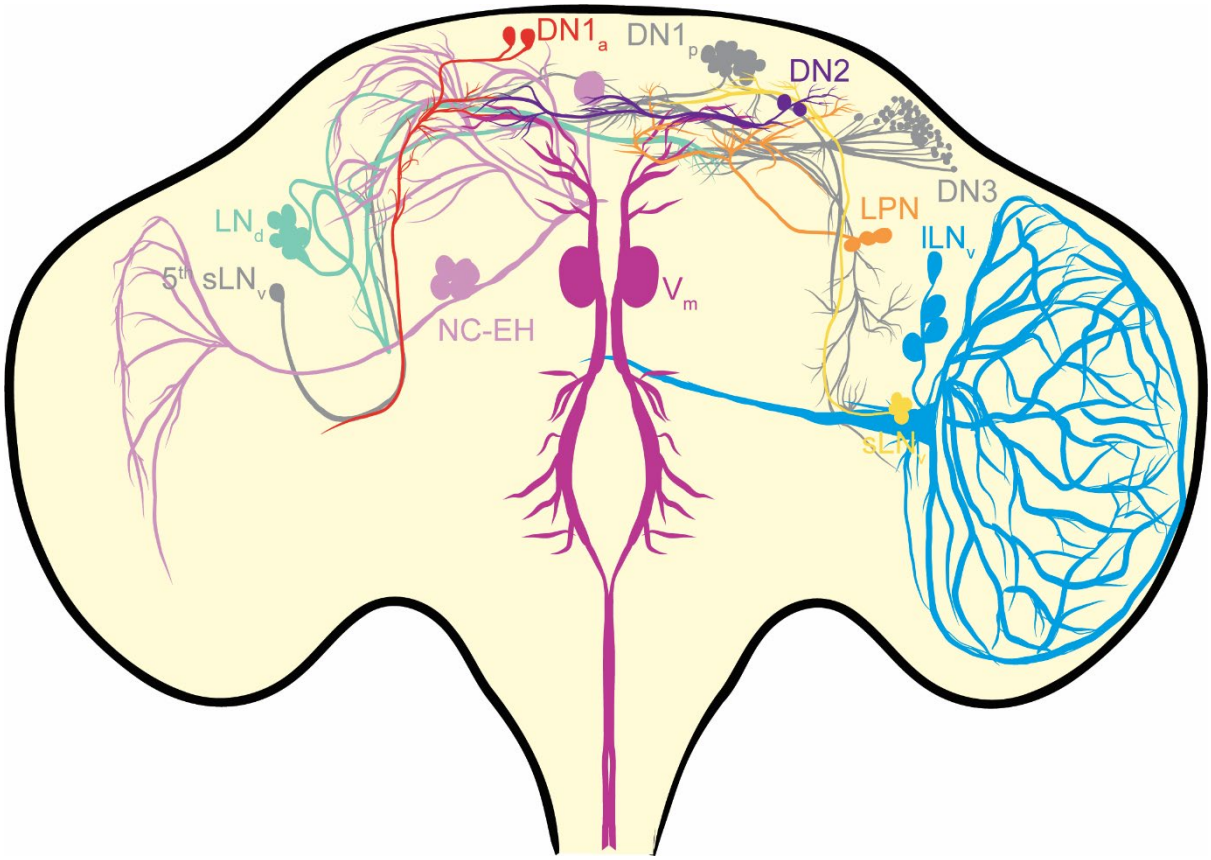

Figure 5.2. Schematic view of synaptic connections from clock neurons to EH neurons in the pharate brain of *Drosophila*. sLN_vs (yellow), lLN_vs (light blue), $DN1_as$ (red), DN2s (purple), LN_ds (green), and LPNs (orange) provide synaptic input to EH neurons (magenta and pink) while the 5^{th} sLN_v (gray) do not. Whether $DN1_ps$ and DN3 neurons are presynaptic to EH neurons is not investigated.

What starts eclosion, EH or ETH?

The timing and duration of the ETH release into the hemolymph is well described for *Drosophila* larva (Kim et al., 2006b). On average, 4.5 minutes before pre-ecdysis, ETH is released and is thought to activate the V_m neurons. However, due to the movement of the flies during ecdysis, the authors were unable to measure the chimeric ETH-EGFP fluorescence signal. The decrease in the ETH-EGFP signal was associated with ETH-releasing activity (Kim et al., 2006b). In this thesis, the non-invasive ARG-Luc imaging as a proxy for real-time cellular activity worked very well regardless of movement and provided stable continuous signaling that lasted for a week. The ARG-Luc data were obtained with a 30-minute resolution. This time resolution is suitable for monitoring long-term activity but does not reflect the exact temporal events of eclosion that span a few minutes. It is possible to record the ARG-Luc data (depending on the photon counting machine) with higher temporal resolution. However, there is a limit since the transcription factor Lola needs about one hour to decay (X. Chen et al., 2016), and this might affect data collection and the effective possible temporal resolution.

In *Drosophila*, so far it is not known whether the EH/ETH feedback is initially started by EH or ETH release. In *Manduca*, corazonin initiates the release of ETH (Kim et al., 2004), yet there is no evidence that corazonin is important for ETH release or effective in light-induced initiation of premature eclosion in *Drosophila* (Ruf et al., 2017). One of the differences between the pre-ecdysis procedure of *Manduca* and *Drosophila* is the initiation of the pre-

ecdysial motor program. While in *Manduca* ETH is in charge of this motor program (Kim et al., 2004), in *Drosophila*, EH prepares the CNS for the program (Krüger et al., 2015). Yet, the initial release of ETH is independent of EH release and happens on time even if the V_m neurons are ablated (McNabb et al., 1997). On the other hand, two different ETHR isoforms act on two distinctive neuronal populations. $ETHR^B$ is in charge of delaying the ecdysis/eclosion program while $ETHR^A$ is in charge of starting it (Daubnerová et al., 2021; Diao et al., 2016; Kim et al., 2006a, 2006b; Scott et al., 2020). Scott et al. (2020) showed that only the V_m neurons express both ETHR isoforms and the non-canonical neurons do not express any of the isoforms. EH may also be released from non-neural tissues during eclosion (Scott et al., 2020). The comparison between the Inka cell and V_m neurons ARG-Luc activity profile acquired during this thesis shows that indeed V_m neurons increase their activity (~-7h before eclosion) around one hour earlier than the Inka cells (~-6h before eclosion; Figure 2.1 C). In *Drosophila*, around half an hour after the beginning of pre-ecdysis, the Inka cells pick up the hemolymph EH signal and promote the EH/ETH feedback loop (Ewer et al., 1997). The ARG-Luc data agree with the finding from *Manduca sexta* that the Inka cells can respond to EH only during a limited time frame which is around eight hours before pupal ecdysis (Kingan et al., 1997).

A role for EH in adult flies?

In this thesis, it is shown that some D_l neurons expressed RFP days after eclosion. Therefore, at least non-canonical EH neurons survive into adulthood and hence they potentially could play roles in adult physiology and behavior that are not known yet. Here, in future studies, the expression pattern of the EH-R in adult flies could be studied to provide hints about the possible adult function of EH. Conditional genetic interference with EH signaling and observing changes in behavior and physiology could further be used to study the unknown adult roles of EH.

Interestingly, "new" adult-specific roles unrelated to ecdysis/eclosion have been discovered for ETH. ETH released from adult Inka cells acts as an allatotropin and promotes juvenile hormone production several days post-eclosion. This prepares the flies for egg production and sexual maturation (Meiselman et al., 2017, 2018). It also weakens the courtship short-term memory through juvenile hormone production (Lee et al., 2017). Therefore, the substantial activity of the Inka cells observed two to three days after eclosion may be due to the sexual maturation of the individual flies (Figure 2.4 B). However, the late post-eclosion activity of Inka cells reported in this thesis was found in both male and female flies. A sex-specific relation in the activity of Inka cells was not observed and both sexes showed this large activity peak. Therefore, ETH may also have yet undiscovered functions in adult male flies.

Chapter III

Chemoconnectomics: an approach to dissect non-synaptic peptidergic connections to eclosion-relevant neurons

Unlike synaptic neurotransmitter signaling, neuropeptide paracrine or volume transmission affects greater parts of the nervous system and lasts longer (Agnati et al., 1995; Kim et al., 2017; Nässel, 2018, 2009; van den Pol, 2012). Peptides can either act very generally and modulate many physiological and behavioral aspects, or be very specific and restricted to a

certain circuit (Nässel et al., 2019). The paracrine nature of neuropeptide signaling in the brain makes it impossible to trace their downstream partners by synaptic "connectomic" analysis (Nässel, 2018, 2009; Nässel and Winther, 2010; Nässel and Zandawala, 2019; Nusbaum et al., 2017). In 2019, the term “chemoconnectomics” was coined for an approach to identify the downstream targets of peptidergic neurons with the aid of highly specific intragenic driver lines that label the peptide receptor-expressing neurons (Deng et al., 2019). Here in this thesis, chemoconnectomics was used to identify the peptidergic input (especially ones mediated by the clock) affecting eclosion circuits.

Specifically, to assess the peptidergic influence of the clock on PTTHns and V_m neurons, the peptide receptors expressed by the PTTHn and EH neurons were investigated using chemoconnectomics (see Results III.1 and III.2). Close to eclosion time, receptors for sNPF, AstA, AstC, and Ms are expressed by the PTTHns. Importantly, we identified the expression of sNPF-R in PTTHn, which fully confirms the inhibitory effect of sNPF on the PTTHn found by calcium imaging (Selcho et al., 2017).

Most of the receptors expressed by PTTHn likely act inhibitory and seem to inhibit the activity of the PTTHn when necessary. To confirm whether the other identified receptors expressed by the PTTHn similarly cause inhibition could be investigated by peptide application on exposed brains and imaging PTTHn activity using Ca^{2+} or cAMP sensors. However, the predictions using the PRED-COUPLE 2.00 neural network (see Results III.8) suggest that most of these receptors have an inhibitory effect. For example, coupling to the inhibitory G protein subunit $G\alpha_{i/o}$ gained the highest score for AstA-R1 (see Table 3.3, and Appendix 9), and AstA-R1 has indeed been shown to inhibit neurons using $G\alpha_{i/o}$ (Birgül et al., 1999; Larsen et al., 2001; Ni et al., 2019; Yamagata et al., 2016). PRED-COUPLE 2.0 also predicts an inhibitory role for both MsRs through $G\alpha_{i/o}$. In *Drosophila* only the inhibitory role of MsRs on the visceral muscles is described so far (Hadjieconomou et al., 2020; Leander et al., 2015). In moth, only one MsR exists which acts inhibitory (Yamanaka et al., 2005). $G\alpha_{q/11}$ which increases the intracellular Ca^{2+} level and hence activates the neuron (Neves et al., 2002; Wettschureck and Offermanns, 2005), gained the highest prediction score for both AstC-Rs. This prediction contradicts experimental data that showed an inhibitory effect of AstC-R2 (Díaz et al., 2019).

For V_m neurons, Ms and AstA seem to play an important role as modulators. Based on the receptor profile both AstA receptors and only MsR1 but not MsR2 are expressed by pharate V_m neurons. Why both AstA-Rs are expressed by the V_ms is not yet known but should be investigated. Interestingly, in *Drosophila* (Larsen et al., 2001) and two different species of mosquitos (Christ et al., 2018), AstA-R2 is more sensitive to AstA than -R1. Therefore, AstA may act differentially in a concentration-dependent manner on V_m neurons. One eclosion-related example is two different isoforms of ETHR. $ETHR^B$ is much more sensitive to ETH than $ETHR^A$ (Park et al., 2003). While $ETHR^B$ is expressed by eclosion delay neurons and receives the primary small bout of hormonally released ETH, $ETHR^A$ is expressed by neurons initiating eclosion that sense the massive ETH bout of EH/ETH feedback (Diao et al., 2016; Kim et al., 2006a, 2006b).

Eclosion provides a nice model for studying neuronal modulation. EH and ETH reservoirs can only be used once and if depleted they cannot be refilled until a certain time has passed. This time for ETH is until the next ecdysteroid peak and for EH is the time vesicles are transferred from the V_m cell body to its axonal terminals (Ewer, 2007b). Therefore, inhibitory circuits may

be involved in gating of the EH/ETH feedback timing. This putative precise control could, for example, be achieved by changing the receptor expression profile of V_m neurons during pupal development. V_m neurons also showed lower expression frequency of sNPF-R, AstC-R1, and Dh31-R^C and higher expression of AstA-Rs and MsR1 in pharates. The developmental receptor expression profile can be tested at the beginning and in the middle of pupal development. Changes in the expression profile might show the modulation of different receptors is required during development to promote the arrest of V_m neuron activity. A prominent example in the context of ecdysis is the stage-specific PG inhibition in moths based on variable expression levels of MsR and sex peptide receptor in the PG (Yamanaka et al., 2010, 2006, 2005). PG inhibition in moths is under the influence of prothoracicostatic peptides, Ms, and other FMRFamides (Yamanaka et al., 2006, 2005). FMRFamides do not have a specific receptor in PG and are perceived by the sex peptide receptor and MsR. Prothoracicostatic peptides are only perceived by the sex peptide receptor (Yamanaka et al., 2010). It is shown that PG inhibition by Ms through MsR is much more effective than FMRFamides through MsR (Yamanaka et al., 2006, 2005). During the larval foraging stage, the FMRFamide neurons activity and MsR expression in PG are at their highest, and both decrease close to ecdysteroids peaking. Close to ecdysis, the Ms and FMRFamides production and MsR expression by PG decrease while the production of prothoracicostatic peptides and sex peptide receptor by PG highly increases. Therefore, complexity and sophistication in the timing of receptor expression and peptide release suggest stage-specific peptide control of the developmental timing of each ecdysis in moths (Yamanaka et al., 2010).

Differentiating between the dense D_{ls} arborizations from each other in the superior neuropils and posterior slope with single color staining was not possible. Therefore, all the D_l neurons together were considered as one population, which caused unclarity in receptor profiling for individual D_l neurons. For example, from the four D_{ls}, at least one of the D_{ls} always expressed the AstA-R1. And always one of them expressed AstC-R1 and -R2 but it was not possible to clearly distinguish which D_l neuron. Furthermore, it was not possible to tell if AstA-R1 and ActC-Rs were expressed by the same D_l neuron. Another problem was caused by the disability of the driver line in homogenously expressing RFP in the D_ms. Most of the time D_ms were not labeled. Because of these problems, the receptor expression profiles of individual non-canonical EH neurons (D_ms and D_{ls}) remained largely unknown.

After identifying the receptor expression profile of PTTHn and V_m neurons, the role of these peptides in maintaining eclosion rhythmicity was investigated with loss-of-function eclosion assays. None of the peptides alone was found to be required for maintaining eclosion gating or initiating eclosion. In the assays lacking a certain peptide signaling pathway, all flies successfully performed rhythmic eclosion behavior. This multi-peptide modulation mechanism as discussed above, might be ensuring the safe activation of the PTTHn or EH neurons at the correct moment. Therefore, each of these peptide signals acts as an auxiliary decision that summation of all of them ensures the correct moment of activity.

Peptidergic neurons upstream of eclosion-specific neurons

As mentioned above, peptides do not act on their downstream neurons through synaptic transmission. Even though they were mentioned as synaptic connections, the observed connections are possibly peptidergic. Trans-synaptic tools (syb-GRASP, BAcTrace, and *trans*-Tango) were able to identify these connections because of nSyb in the membrane of dense core

vesicles. Therefore, using trans-synaptic analyzing tools the upstream Ms, AstA, and AstC neurons of PTTHn and V_m neurons are identified. The strength and density of the syb-GRASP signal show whether the means of connections between upstream peptidergic neurons and PTTHn or V_m are peptidergic or synaptic. While both Ms and AstC show strong synaptic connections to both PTTHn and EH neurons, AstA neurons connections to these neurons are mainly peptidergic due to weak and sparse GRASP signals. The positive *trans*-Tango driven nuclear RFP signal in all PTTH and EH neurons was detected except for one surprising case. *Ms> trans-Tango* expressed no RFP in any of the EH neurons (see III.7.a and Figure 3.15 K-L). This was unexpected because the GRASP signal showed a strong synaptic connection from Ms to EH neurons. BAcTrace showed that nearly the same AstA and Ms neurons were upstream of both PTTHn and V_m. Interestingly, for both AstA and Ms neurons, neurons passing through MBDL showed the strongest BAcTrace-driven tdTomato signals suggesting they are strongly connected to PTTHn and V_m. Testing AstA and Ms roles in modulating the activity of PTTHn and V_m using specific driver lines that label these MBDL passing neurons would be interesting.

The PTTHn receive input from other clock neurons beyond the sLNv

A main finding in this chapter is that in the pharate adult brain, many clock neurons from different subsets provide input to the PTTHn (summarized in Figure 5.1). Until now, the connections from clock neurons to the PTTHns were comprehensively described in the larval brain, which however has a much-reduced set of clock neurons. GRASP signal between the larval PDF^+ LN_vs and PTTH neurons showed that they are possibly connected and suggested that the PTTHn receive light input from the LNvs (Gong et al., 2010). However, a later detailed analysis using specific driver lines and *trans*-Tango showed that the clock provides light input to the PTTHn but not through PDF^+ LN_vs. And since no trans-synaptic signal from the LN_vs was identified they rejected the LN_vs synaptic connection to PTTHn (Sorkaç et al., 2022). Sorkaç et al. (2022) showed that the 5^{th} sLN_v, $DN1_a$s, and DN2s are presynaptic to the PTTHn. They showed that bright light information is detected by the Bolwig organs through the 5^{th} sLN_v and is transmitted to the DN2 neurons which then excite PTTHn. They also showed that DN1s are important for larval light avoidance under dim light (Sorkaç et al., 2022).

In line with the larval findings, the combination of syb-GRASP and *trans*-Tango in this thesis suggests that the connection from the sLN_vs to the PTTHn is peptidergic in pharate adults. We here found connections from the sLN_vs, $DN1_a$s, and DN2s to the PTTHn in the pharate adult brain, similar to those described in the larval brain. This suggests that the larval connections are kept during metamorphosis. In addition, other adult-specific clock neurons (LPNs and $DN1_p$s) that do not exist in the larval brain were found to provide input to the PTTHn in this thesis. Yet, it is unknown what type of input these clock neurons provide to the PTTHn and whether they modulate PTTHn activity. Recently, specific driver lines that target specific subsets of clock neurons have been characterized (Sekiguchi et al., 2020). The combination of these driver lines with effectors that silence or activate neuronal activity along with functional connectivity studies can provide future insight into how the clock affects the PTTHns. The clock circuit of the adults compared to the larval brain is much more complex and the adult-specific neurons can affect the PTTHn differently. Therefore, the activation of different clock clusters in pharate brains may not necessarily influence PTTHn activity similar to the situation described in larval brains (Sorkaç et al., 2022).

Interestingly, the results of this chapter further show that the PDF-expressing non-clock PDF-tri neurons (Helfrich-Förster, 1997; Selcho et al., 2018) do not connect to the PTTHn. This implies that PDF-tri neurons do not play a role in regulating PTTHn and is in line with the lack of expression of the PDFR and PDF-sensitivity in the PTTHn (Selcho et al. 2017, this thesis).

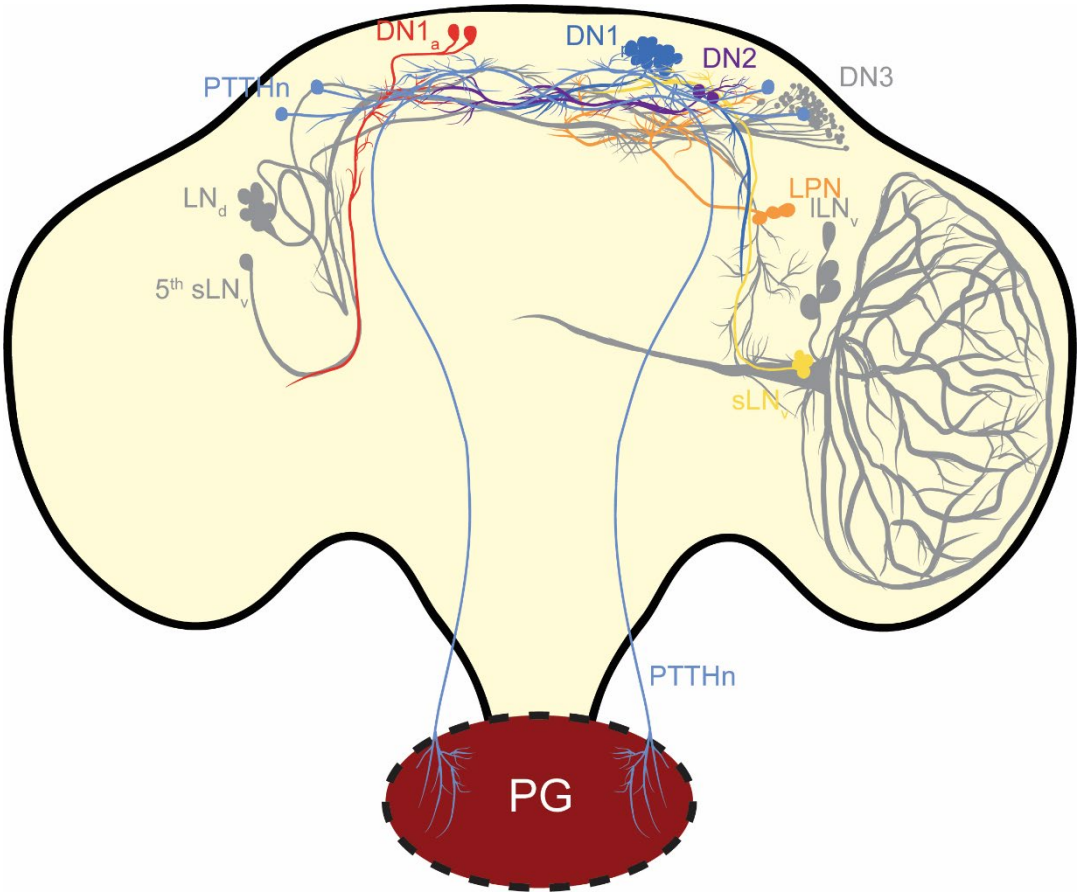

Figure 5.1. Schematic summary of the connections between clock neurons and the PTTHn in the *Drosophila* pharate brain. $DN1_a$s (red), $DN1_p$s (dark blue), DN2 (purple), and LPNs (orange) provide synaptic input and sLN_vs (yellow) provide peptidergic input to PTTHn (light blue) while lLN_vs, the 5th sLN_v, and LN_ds (gray) do not. Whether DN3 neurons are presynaptic to PTTHn is still unaddressed.

Allatostatin A effectively inhibits eclosion circuits

The AstA neurons upstream of both PTTHns and V_ms were mainly AstA-SEZ neurons (large cell-bodied projecting through MBDL to SMP), AstA-SLP (projecting to superior protocerebrum), and LPN neurons. Opto-DEM assay results (see Results III.5 and Figure 3.8) were consistent with AstA receptor expression by the V_m neurons. Heavy suppression of premature eclosion by AstA along with AstA-Rs expression in both V_m neurons suggests that AstA inhibited these neurons. AstA might also inhibit eclosion using similar pathways that promote sleep, as the identified AstA neurons, AstA-SLP and LPN neurons, are important for sleep in *Drosophila* (Ni et al., 2019). Simply put, during metamorphosis, the flies are put to sleep (a coma-like state) possibly by AstA, and they cannot eclose until this modulation is over. However, there is another more probable possibility that should be considered. The driver lines used for Opto-DEM assays label many neurons (see Appendix 6-8). Some AstA neurons possibly inhibit the motoneurons and prevent light-induced premature eclosion simply by paralyzing locomotion. To specifically confirm the role of AstA in preventing premature

eclosion, a good strategy is to use specific driver lines that drive sparsely in the AstA neurons. As an example, *AstA^{34}-Gal4* lines are described before that label fewer neurons (J. Chen et al., 2016). Other possibilities are provided by the new Flylight GMR, VT, and split driver lines (Dionne et al., 2018; Jenett et al., 2012; Meissner et al., 2023). Combined with the data obtained from the connectomics, the AstA-SEZ pair seems to be a promising candidate for suppressing eclosion that should be tested.

Myosuppressin possibly modulates PTTHn and V_m neurons

This thesis showed that Ms is not required for eclosion gating (see Results III.5). Using trans-synaptic methods, the Ms neurons providing input to both PTTHn and V_m neurons were identified. These include the Ms neurons projecting via the MBDL known as Taotie neurons (Zhan et al., 2016), Ms neurons projection to the AL, and Ms neurons projecting to the BU. Surprisingly, *Ms> trans-Tango* did not drive nuclear RFP expression in any of the EH neurons, despite the strong GRASP signal observed in the SMP and SLP, suggesting that both V_ms and D_ls are downstream of Ms neurons. Moreover, using chemoconnectomics, both Ms receptors were found to be expressed in PTTHn, and MsR1 in V_m neurons.

Expression of both MsRs by the PTTHn and synaptic connections of the PTTHn by various Ms neurons suggest that PTTHn activity is modulated by Ms. Probably, Ms indirectly controls ecdysone production by inhibiting the PTTHns and controlling the PTTH release. However, this needs to be functionally tested and shown. In moths, Ms directly inhibits ecdysone production via its receptor in the PG (Budd et al., 1993; Carlisle and Ellis, 1968; Hua et al., 1997; Malá et al., 1977; Yamanaka et al., 2010, 2006, 2005).

Recently, a study showed how Taotie neurons are an important part of an endocrine gut-brain axis (Hadjieconomou et al., 2020). After mating, the ecdysone levels rise to facilitate egg production in females (Harshman et al., 1999; Schwedes and Carney, 2012). Taotie neurons express EcR and sense the circulating ecdysone. Ms from Taotie neurons at the crop is sensed by MsR1 and increase the size of the crop (Hadjieconomou et al., 2020). Expression of EcR by Taotie neurons in the pharates can be investigated through chemoconnectomics. Then a hypothesis regarding the role of PTTH in the developmental timing of eclosion can be tested. If EcR is expressed in Ms neurons, a feedback loop that controls ecdysone production is possible. High levels of 20-E may increase Ms release and therefore inhibit the PTTH neurons.

Another important problem to address is how Ms modulates the activity of V_m neurons and initiates premature eclosion. Previous WEclMon assays showed that activation of Ms neurons triggers premature eclosion (Ruf et al., 2017). However, this thesis failed to confirm the role of Ms in triggering premature eclosion. Perhaps the difference between our results and Ruf et al. (2017) comes from the difference in used driver lines. In this thesis, a T2A driver line was used which is different from the P-element inserted driver line that Ruf et al. (2017) used. The P-element driver may include expression in non-Ms neurons that are not included by the T2A line. Repeating the Opto-DEM assays using specific *taotie-Gal4* that are expressed in the large Taotie neurons (Zhan et al., 2016) can also be very helpful in studying this signaling pathway.

Allatostatin C might play a role in eclosion

Unfortunately, the peptidergic connections of the AstC to PTTHn and V_m had to remain unexplored due to several reasons. First of all, the overall survival rate of *Eh::2A-Gal4* lines

was generally low. Moreover, *R61H08-LexA; Eh::2A-Gal4> BAcTrace* progeny never hatched, therefore identifying the AstC neurons upstream of EH neurons was not possible. The *R61H08-LexA; Ptth-Gal4> BAcTrace* progeny was viable. However, this BAcTrace experiment did not identify any AstC neuron upstream of PTTHns. Therefore, possibly PTTHns do not receive any synaptic input from AstC neurons. Since the AstC receptors are mainly expressed by the D_Is and less by V_ms, AstC inhibition might mostly affect the non-canonical EH neurons. The Opto-DEM of AstC neurons showed two different outcomes based on the driver line used. Using the intragenic *AstC::2A-Gal4* driver (see Results III.5 and Figure 3.9), no significant difference between the eclosion rates of the experimental group and the controls was observable. This is likely because the majority of *AstC::2A-Gal4* flies are heterozygous. Thus, in the experimental flies, many flies did not express *ChR2-XXL* and hence showed a wildtype-like phenotype. In addition, it is noteworthy that the rare homozygous *AstC::2A-Gal4* flies had wing expansion defects. The AstC gene in these flies may be negatively affected by the T2A insertion. Therefore, AstC might have an undescribed role in post-eclosion events such as wing expansion. Repeating Opto-DEM with the *R61H08-Gal4* line (see III.5 and Figure 3.10) showed a significantly decreased premature eclosion rate, yet not as drastic as AstA activation. All in all, more experiments are needed to identify the role of AstC in the control of eclosion.

Chapter IV

The v'Td neurons provide auxiliary input to the V_m neurons

It is not clear what initiates the EH/ETH feedback loop. Based on the larval connectome, synaptic connections between the v'Td neurons and V_m neurons in larval CNS were found (Hückesfeld et al., 2021). We hypothesized that such connections exist in pharates as well and might be required for initiating EH/ETH feedback. This prompted us to test whether the connections between v'Td neurons and V_m neurons exist in pharate CNS as well. This thesis also investigated the potential role of v'Td neurons in the initiation and timing of eclosion. In the *Drosophila* larvae, dendritic arborizations of v'Td neurons collect information from the trachea and send projections into the VNC (Qian et al., 2018). How these neurons are organized in the PNS and CNS of adult flies is still uncharacterized. While the morphology of v'Td dendrites and their distribution along the adult trachea was not addressed in this thesis, we characterized the v'Td axonal projections within the pharate VNC (see Results IV.1.a and Figure 4.1) based on four driver lines capable of driving GFP expression in the larval v'Td neurons: v'Td1$^{A1\text{-}5}$ (*R35B01-Gal4*), v'Td1$^{A4\text{-}6}$ (*R31D10-Gal4*), v'Td2$^{A1\text{-}6}$ (*0260-Gal4*), and v'Td2$^{A1\text{-}7}$ (*R73B01-Gal4*). Their connectivity with V_m neurons was assessed using trans-synaptic genetic tools. None of the four driver lines was specific for v'Td neurons; all showed ectopic expression in the VNC, brain, and especially optic lobes. The double labelings obtained with the help of these drivers and *Eh::2A-LexA* showed that V_m neurons are synaptically connected to the peripheral v'Td1 and -2 neurons. The V_m neurons project their descending axons along the MDT at the VNC midline, while the peripheral v'Td neurons collect the information from the trachea and project into the abdominal ganglia via the segmental nerves and ascend through the MDT to end in the SEZ. Both v'Td1 and -2 neurons are presynaptic to the V_m neurons, and the connections are made in the MDT where the axonal processes of v'Td and V_m are in close apposition (see Results IV.1.b and Figure 4.2). The v'Td neurons in the larval CNS were shown to make *en passant* axo-axonic connections (Qian et al., 2018). In the

pharate VNC, the v'Td1 neurons seem to be more strongly connected to the V_m neurons than the v'Td2 neurons. This assumption is based on the stronger syb-GRASP signals of v'Td1 compared to v'Td2. *trans*-Tango experiments also confirmed that v'Tds are presynaptic to V_m neurons and provide them with synaptic input, possibly O_2 and CO_2 gas information collected from the trachea (Hückesfeld et al., 2021; Morton, 2011, 2004; Morton et al., 2008; Qian et al., 2018).

The intracellular Ca^{2+} rising in V_ms in response to the activation of both v'Tds did not happen. Even though in some cases V_m neurons showed increased activity, this activity was not instantaneous and not consistent. Activation of the v'Td1 neurons increased the activity of V_m neurons in most experiments usually after a 10-minute delay. However, activation of v'Td2 neurons always caused V_m excitation but with various timings. While in some of the V_m neurons Ca^{2+} level rises immediately in others it increases after a delay. The increased Ca^{2+} level mostly does not lead to rapid and high amplitude Ca^{2+} signals, and most often, the V_m neurons became indifferent to the second input from the v'Td neurons. This suggests that the activity of v'Tds is not directly and strongly affecting the intracellular Ca^{2+} levels of the V_m neurons. It is therefore unlikely that the v'Td neurons start the EH/ETH feedback loop.

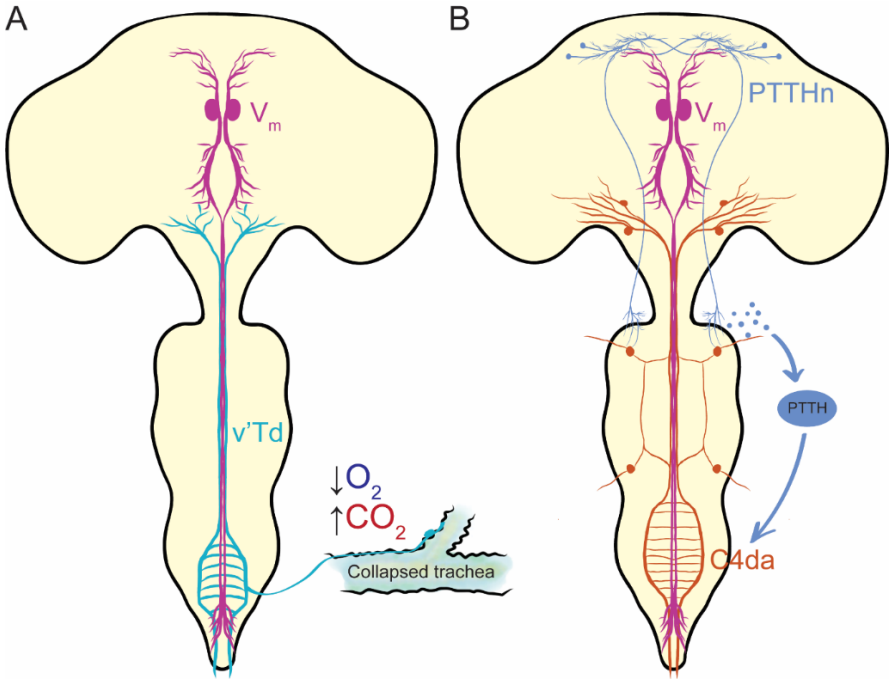

Figure 5.3. Working hypothesis of the role of peripheral neurons that provide synaptic input to V_m neurons during eclosion. Hypothetical model based on v'Td and PPK neurons (including C4da neurons) connection to V_m neurons. **A** Shortly before eclosion, during the tracheal collapse, dropping O2 and rising CO2 levels are sensed by v'Td neurons (turquoise). The axons of v'Td neurons in the VNC pass close to the axons of V_m neurons (magenta). Through synaptic input, the v'Td neurons provide auxiliary information to V_m neurons. **B** Before eclosion PTTHn (dark blue) release PTTH into the hemolymph. The peripheral C4da neurons (orange) express TORSO that perceives PTTH. Then C4da neurons in the midline of VNC provide synaptic input to V_m neurons. Whether C4da neurons perceive bloodborne PTTH in pharates and whether the activity of C4da excites or inhibits the V_m neurons are currently unknown.

The v'Td2 are necessary for successful eclosion/ecdysis but not required for rhythmic eclosion

Consecutive ablation of either v'Td1 and -2 leads to high early lethality during the first ecdyses (see Results IV.1.d; Morton et al., 2008). Also, consecutive silencing of the v'Td2 neurons with Kir2.1 led to high lethality and nearly no flies pupariated. This suggests that v'Td neurons, especially v'Td2 are necessary for successful ecdysis. This confirms former experiments by Morton et al. (2008) that showed ablating O_2 sensing v'Td1 neurons causes larval death by suffocation in food.

To test whether the v'Td neurons have any role in eclosion rhythmicity or initiation, a cold-sensitive form of ricin, RA^{CS2}.CC was therefore used to conditionally ablate the v'Td neurons close to eclosion (see Results IV.1.d). After conditional ablation of v'Td neurons, flies eclosed rhythmically. Hence, ablation of the v'Td neurons does not affect the rhythmicity of eclosion. In addition, silencing v'$Td1^{A1\text{-}5}$ neurons also did not impair rhythmicity, confirming that v'Td1 neurons do not participate in the control of eclosion rhythmicity. As projections of the v'Td neurons are not coming in close contact with arborizations of the PTTHn, there is no possibility of a synaptic connection between v'Tds and PTTHn. So far, there is also no evidence suggesting the presence of the PTTH receptor, TORSO, on any of the v'Td neurons. Therefore, the v'Td neurons seem to be neither directly upstream or downstream of PTTH signaling.

Using Opto-DEM, however, optogenetic activation of v'$Td1^{A1\text{-}5}$ neurons significantly increased the light-induced premature eclosion rate, while activation of v'$Td1^{A4\text{-}6}$, v'$Td2^{A1\text{-}6}$, and v'$Td2^{A1\text{-}7}$ neurons had no effect. The v'$Td1^{A1\text{-}5}$ neuron-dependent increase of the premature eclosion rate was modest, compared to direct optogenetic activation of the V_m neurons. Thus, it seems possible that v'Td1 but not the v'Td2 neurons facilitate premature eclosion, but only when most of them are activated (Figure 5.3 A).

Due to the quite broad ectopic expression pattern of the v'Td driver lines, we did not perform ARG-Luc imaging. In the future, specific v'Td drivers will allow ARG-Luc imaging and will inform whether the v'Td neurons are active in the same time windows as the V_m and Inka cells.

The C4da neurons might indirectly mediate the PTTHn and V_m connection

Whether in the pharate brain, PTTHn and V_m neurons are directly connected was not known. syb-GRASP in the pharate brain did not indicate any synaptic connections between the PTTHn and V_m (data not shown in this thesis). A study worked on the PTTHn-V_m connections in the larval brain and described their effects on each other (Gong et al., 2019). Gong et al. (2019) based on the GRASP signal in larval brains showed that overlapping PTTHn and V_m neurons processes make dendrodendritic synaptic connections. Such a GRASP signal was not observed in the ring gland. Authors showed optogenetic activation of the PTTHn increases the intracellular Ca^{2+} level inside V_m cell bodies, while optogenetic exciting of the V_ms inhibits PTTHn. However, Gong et al. (2019) did not show any details about the directionality of the connection or if any interneurons were involved. The connection found by GRASP in the larval brain is most likely due to proximity during development and is not a real connection. This is similar to LN_vs and PTTHn connections found by GRASP (Gong et al., 2010) that Sorkaç et al. (2022) showed to be an artifact of proximity. Besides, the possibility of dendrodendritic connections between PTTHn and V_ms seems to be not supported by previous data. First of all,

previous attempts to find classic neurotransmitters in V_ms showed that V_m neurons are exclusively peptidergic (Selcho et al., 2018). In this thesis it was also shown that V_m are peptidergic (see Results II.2). Moreover, our data suggest that PTTHn are purely peptidergic (see Results I.4), and the EH neurons do not express TORSO. Therefore, a valid hypothesis in connecting PTTH and V_m neurons is the PTTH-C4da-V_m (Figure 5.3 B).

The trans-synaptic tracing stainings show that PPK neurons including C4da neurons are indeed presynaptic to the V_m neurons (see Results IV.3.a), with synaptic connections in both VNC and the brain. To test whether C4da neurons may provide input to the V_m neurons, light-induced premature eclosion assays with the Opto-DEM were conducted (see Results IV.3.c). While optogenetic activation of the C4da neurons did not significantly increase the rate of light-induced premature eclosion, we found a significantly increased eclosion rate directly after the light pulse was over. This suggests that activation of the C4da neurons may inhibit the V_m neurons, therefore the eclosion initiating system is temporarily stopped. Nevertheless, it remains unclear whether optogenetic activation of C4da neurons inhibits or excites the V_m neurons.

To investigate further a connection between C4da neurons and PTTH/V_m neuron activity, ARG-Luc imaging was used to see when during pupal development the C4da neurons are active and whether this activity correlates with PTTHn and V_m activity. Unfortunately, due to technical problems, the data acquisition had to be performed without camera photographs of the eclosing flies. To be able to still analyze the data, the eclosion peak artifact was used to indicate the moment of eclosion (see Results IV.3.d and Appendix 10). This showed a sharp peak in the PPK neurons activity diagram at around -7h, which is around the activity time of the V_m neurons. The peak maximum of the PTTHn activity was around -6h. However, the -6h PTTHn peak is broader, suggesting that PTTHns start their activity earlier and stay active longer than PPK and V_m neurons. Yet more data is required to draw a conclusion based on the observed coincided ARG-Luc activities at around -7 hours.

Unfortunately, this thesis did not have the chance to perform functional connectivity between the C4da and V_m neurons. It is important to show how activation of the C4da neurons influences the activity of the V_ms. Like v'Td neurons, C4da neurons might not affect the Ca^{2+} levels of V_m neurons and simply have modulatory effects. This might provide insight into why the activation of the C4da prevents eclosion and how the eclosion rhythmicity generation and eclosion initiation are coordinated.

The significance of C4da neurons for eclosion regulation needs further investigation

A day before eclosion, the ecdysone level drops below the threshold to allow eclosion (Kingan and Adams, 2000; Truman et al., 1983), and PG starts to degenerate 30-40 hours after pupariation (Dai and Gilbert, 1991). Therefore, the activity of PTTHn right before eclosion does not seem to increase ecdysone production by signaling to PG. TORSO is not expressed by the neurons of the CNS (own data). However, larval C4da neurons and photoreceptors express TORSO and are capable of receiving PTTH signaling (Gong et al., 2010; Xiang et al., 2010; Yamanaka et al., 2013) required for larval light avoidance (Gong et al., 2010; Yamanaka et al., 2013). Removing the PTTH signaling either by silencing the PTTHn or knocking down *Ptth* strongly impairs light avoidance (Yamanaka et al., 2013). Therefore, we hypothesized that

the clock-PTTH-C4da pathway described before in the larval light avoidance and here in eclosion rhythm maintenance is a developmentally conserved neuronal pathway. Simply, the brain and neuroendocrine system instead of creating a new pathway reused an already existing circuit. In this thesis, the possibility of C4da involvement in eclosion gating is tested using loss-of-function eclosion assays (see Results IV.3.b).

In line with this hypothesis, flies with conditionally ablated C4da neurons showed arrhythmic eclosion from day 2 on. Similarly, knock-out of *torso* in the C4da neurons resulted in arrhythmic eclosion. Yet, in contrast, genetic silencing of C4da neurons did not impair eclosion rhythmicity. In addition, rhythmic eclosion was also observed in flies with *torso*-knock-down in the C4da neurons.

The contradicting findings made during this thesis do not allow us to draw a firm conclusion on the role of C4da neurons for eclosion rhythmicity, and further experiments will be required in the future. The discrepancy in the results so far may be related to developmental effects or insufficient knock-down efficiency. Future experiments thus may include *Dicer* to improve RNAi efficiency and should be carried out conditionally. PTTH signaling to C4da neurons and its association with eclosion rhythmicity can also be addressed by ARG-Luc combined with RNAi. This can be done by blocking PTTH signaling to the C4da neurons and ARG-Luc imaging from these neurons using *ppk-Gal4> ARG-Luc; torso*^{i} flies. This ARG-Luc data might show whether the final PTTHn activity is associated with the -7h activity of the C4da neurons.

General discussion

1. PTTH acts as a circadian as well as a developmental timer

PTTH controls developmental timing by controlling ecdysone production from PG (McBrayer et al., 2007). However, the results of this thesis also suggest that PTTH is a circadian timer as well. CaLexA showed that Ca^{2+} levels of PTTHn increase near dawn. ARG-Luc data showed that the PTTHns are active two times close to the eclosion. These two activities are around 24 hours apart and seem to be a circadian rhythmicity since the experiment was done under constant temperature and darkness. ARG-Luc experiment showed a correlation between PTTHn and PG activity. It seems that PG activity is shifted by PTTHns activity and observed peaks of PG activity after being shifted by PTTHns activity are also ~24h apart. However, this idea should be tested by blocking PTTH signaling to PG and observing the autonomous PG activity.

Besides, here we showed that PTTHns receive many synaptic inputs from the clock neurons. Among these neurons are sLN_vs, $DN1_as$, and one of DN2s. This can again point to the circadian nature of PTTH signaling under clock influence. However, what type of circadian input (light, temperature, …) clock neurons for PTTHn is still unknown and needs to be investigated. For example, Sorkaç et al. (2022) showed in larval brains that sLN_vs, DN1, and DN2s clock neurons provide PTTHn with different light inputs. According to Sorkaç et al. (2022) and Selcho et al. (2017) experimental confirmations, the sLN_vs input has inhibitory effects on PTTHn. While DNs have excitatory effects on the PTTHn (Sorkaç et al., 2022). The effect of dorsal clock neurons on PTTHn has yet to be tested for the pharate adult brain and a plausible way to test it is Opto-DEM assays combined with functional connectivity using specific clock driver lines. Based on previous research assumptions about the outcome of the future Opto-DEM assays can be made. For example, by comparing larval light preference to positive light on response, activation of sLN_vs probably promotes premature eclosion (Gong et al., 2010; Sorkaç et al., 2022). Similarly, activation of the 5^{th} sLN_v and DNs are likely to restrain premature eclosion as they promote larval light avoidance (Sorkaç et al., 2022).

Whether PTTHns in the pharate adult brain are connected to V_m neurons and whether PTTH signaling contributes to initiating eclosion behavior by starting EH/ETH feedback loop is unknown. However, in the larval brain, paracrine and endocrine PTTH signaling serves different purposes. The paracrine signaling of the PTTHn to PG is important for the timing of pupariation (Rewitz et al., 2009; Yamanaka et al., 2013). The endocrine PTTH signaling in larvae is only important for larval light avoidance and does not affect pupariation timing (Yamanaka et al., 2013). Feeding *Drosophila* larvae burrow inside the food and prefer darkness. On the contrary, at the wandering stage this darkness preference is reduced (Mazzoni et al., 2005; Sawin et al., 1994; Sawin-McCormack et al., 1995). Increasing 20-E levels initiates wandering behavior (Dominick and Truman, 1986a, 1986b, 1985; Miller and Levine, 2006). Therefore, PTTH as the peptide that regulates ecdysone production indirectly controls wandering behavior. Since PTTHns receive input from the clock, switching the light preference for wandering might also be influenced by the clock. However, the transition between the feeding and wandering stages can be affected by manipulating the C4da neurons. Peripheral C4da neurons are downstream of PTTH (Yamanaka et al., 2013). Before crawling out of the food, wandering L3 fly larvae appear more frequently on the food surface. Genetic disruption

of the *ppk* gene causes defects in this behavior (Ainsley et al., 2008; Wegman et al., 2010). Frequent surfacing is absent in the *ppk* null mutants or flies with silenced C4da neurons, and these flies spend more time feeding leading to larger wandering larvae (Wegman et al., 2010). These large larvae highly resemble the ones having PTTH signaling defects (McBrayer et al., 2007; Rewitz et al., 2009). In contrast, hyperactivation of the C4da neurons causes a premature wandering stage with smaller larvae (Wegman et al., 2010).

With insights from larval light avoidance and PTTH-related light preference shifting, the role of C4da neurons in maintaining eclosion rhythmicity was tested in this thesis. However, we could not show that C4da neurons are required for eclosion rhythmicity. Despite, finding connections between C4da and V_m neurons, we could not show that C4da neurons are important for starting eclosion behavior either. Another reason to test the role of C4da neurons in eclosion gating was previous research by Mark et al. (2021). They showed that the eclosion gating is not influenced by 20-E levels but is controlled downstream of 20-E and at the level of EcR. It has been shown that larval C4da neurons also express EcR (Kuo et al., 2005). A recent study showed that the ecdysone signaling to C4da neurons during L2 to L3 transition is necessary for regulating the nociceptive activity of these neurons. Ecdysone signaling to C4da neurons may control the developmental timing of eclosion. Therefore, checking adult C4da neurons for EcR and TORSO expression and conditional knock-out of *EcR* in C4da neurons is recommended. Conditional knock-out of *EcR* in C4da neurons might cause an arrhythmic eclosion pattern.

2. The clock might influence the EH/ETH feedback loop by direct signaling to V_m neurons or indirect endocrine signaling to Inka cells

This thesis showed that many clock neurons provide input to the V_m neurons. Unfortunately, this thesis did not have the chance to functionally test whether the clock provides time, light, or temperature input to the V_m neurons. However, based on previous research and data presented in this thesis, speculations can be made for future research. Clock input might be important for the initial EH release from the V_ms and for starting the EH/ETH feedback loop. The PDF^+ sLN_vs and lLN_vs are presynaptic to V_m neurons. Since PDFR was not found to be expressed in the V_ms, the PDF^+ sLN_vs may use either the classic neurotransmitter glycine (Frenkel et al., 2017) or sNPF (Abruzzi et al., 2017; Liang et al., 2017; Reinhard et al., 2023) to inhibit V_ms. However, it seems that sNPF-R shortly before eclosion is not expressed by V_m neurons anymore. Since the inhibitory role of sNPF on the PTTHn and clock neurons has been shown before (Liang et al., 2017; Selcho et al., 2017), it is a possibility that during metamorphosis the V_m neurons are under constant inhibition by sNPF from the sLN_vs, and close to eclosion this inhibition is removed to allow V_m neuron activity. On the other hand, lLN_vs receive light and temperature input and are very important for entrainment (Dubowy and Sehgal, 2017; Schlichting et al., 2016). Light is an important factor in initiating eclosion. Most flies eclose in the morning (Bunning, 1935; Kalmus, 1935; Pittendrigh, 1954). And of course, the light masking effect before subjective morning and when the eclosion gate is opened can induce premature eclosion (Pittendrigh, 1954). For masking light input from compound eyes and ocelli and V_m neurons are required (Bidell et al., 2023; McNabb and Truman, 2008). Clock may mediate the connection between V_m and photoreceptors.

3. Various peptides modulate eclosion circuits

In the third chapter of this thesis, the expression profile of different GPCRs responding to some of the clock-released neuropeptides and Ms in PTTHn and EH neurons was investigated. This identified receptors of sNPF, AstA, AstC, and Ms to be expressed in these neurons. However, mutant flies lacking either of these peptide signaling pathways not only eclosed normally but also rhythmically. This means none of these peptides are required for normal eclosion behavior and eclosion rhythmicity. And most likely these peptides only modulate PTTHn and V_m neurons (Figure 5.4).

PTTHn that are involved in eclosion gating, express sNPF, AstA, AstC, and Ms receptors. It seems none of the peptides alone is required for modulating the PTTHn activity regarding eclosion timing. The loss of signaling pathways for each of these peptides alone did not render an arrhythmic eclosion pattern. Therefore, it seems that the loss of each peptide signaling to PTTHn is compensated by other peptides. Therefore, the summation of peptidergic input to PTTHns finetunes the overall PTTHn activity required for eclosion gating. Or simply these peptides do not modulate PTTHn activity within eclosion timing. For example, it has been shown that blocking AstA signaling to PTTHn delays the pupariation (Deveci et al., 2019; Pan and O'Connor, 2019). Therefore, AstA receptors (or other mentioned receptors) may be expressed by PTTHn for purposes other than maintaining eclosion rhythmicity. The effects of these peptides in modulating PTTHn activity can be investigated by synaptically isolating the PTTHn and measuring PTTHn activity (using genetically encoded voltage or Ca^{2+} indicators) after applying the peptides. Future eclosion assays with flies lacking multiple peptide signaling pathways (if applicable) might show whether peptides are required for modulating PTTHn activity regarding eclosion rhythmicity.

Ruf et al. (2017) designed the WEclMon system and studied whether optogenetic activation of various peptidergic neurons affects premature light-induced eclosion. They checked peptidergic neurons capable of releasing Corazonin, EH, Ms, PTTH, Hugin, Dh31, Dh44, and sNPF along with octopaminergic and tyraminergic neurons and Inka cells but only optogenetic activation of EH neurons, Ms neurons, and Inka cells significantly increased premature eclosion (Ruf et al., 2017). Therefore, we investigated the possibility of synaptic connections between AstA, AstC, and Ms neurons and eclosion-related PTTHn and V_m neurons. Based on the work of Ruf et al. (2017), using Opto-DEM, the possible effect of these peptidergic neurons in eclosion was also explored. Unlike WEclMon experiments, we could not show Ms neurons activation to effectively trigger premature eclosion. Opto-DEM experiments showed that AstA and AstC neurons can reduce premature eclosion. EH and ETH are directly involved in the EH/ETH positive feedback loop (Ewer et al., 1997). Therefore, direct optogenetic activation of V_ms and Inka cells triggered premature eclosion (see Results III.5; Ruf et al., 2017). The strong effect of eclosion prevention by AstA activation might be caused by direct inhibition of motoneurons. Therefore, repeating Opto-DEM with specific AstA driver lines is necessary. AstA-Rs and MsR1 are expressed by V_m neurons. Showing how Ms and AstA influence the activity of V_m neurons is the next step. Also, checking the receptor expression profile of Inka cells using chemoconnectomics or single-cell RNA sequencing will provide more insight into the neuropeptide modulation of eclosion initiation.

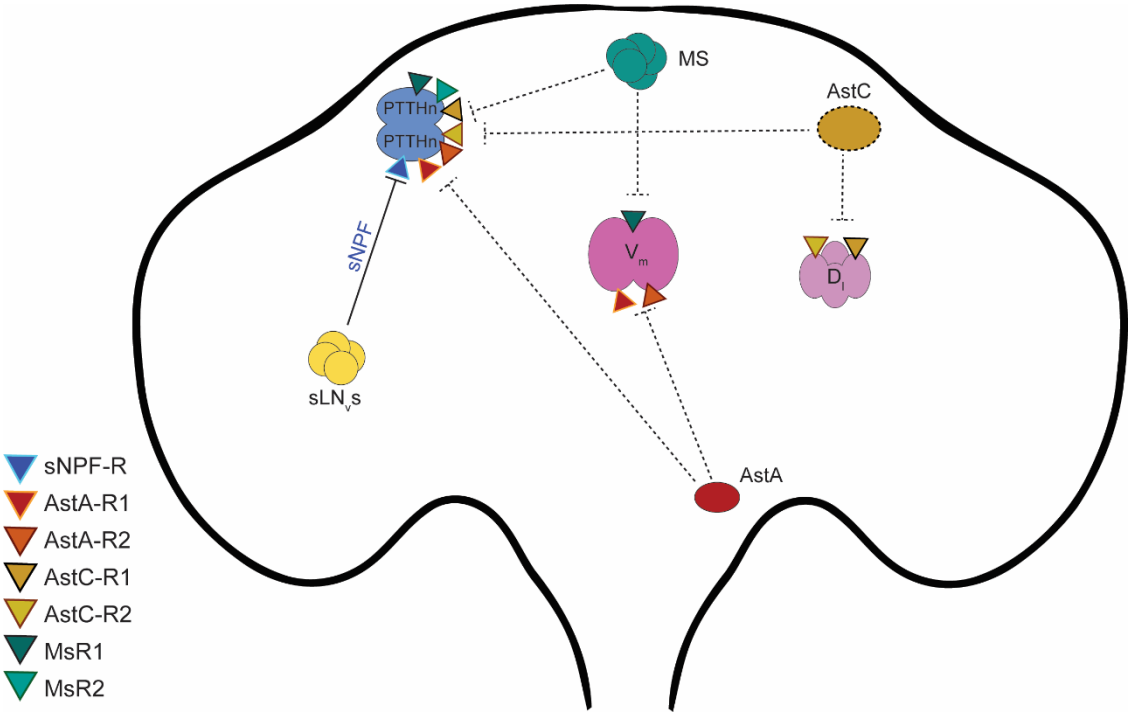

Figure 5.4. Schematic diagram of peptidergic input to PTTHn and V_m neurons in pharate *Drosophila*. Previously, it has been shown that sNPF from sLN_vs inhibits PTTHn. Peptidergic neurons that release AstA, AstC, and Ms possibly inhibit PTTHn through their respective GPCRs. V_m neurons mainly receive peptidergic input from AstA (through both AstA receptors) and Ms (through MsR1). Possibly AstA inhibits the V_m neurons while Ms excites them. The non-canonical EH neurons (D_ls) express both AstC receptors. However, what these neurons do and how AstC influences D_ls is not known. The dashed lines represent hypothesized modulation pathways and are not functionally shown.

4. The possible role of v'Td neurons in modulating V_m neurons and tracheal air filling during ecdysis

The v'Td1 and v'Td2 neurons are special somatosensory neurons that express different types of gaseous, chemical, and light receptors. The presence of the O_2-sensing atypical guanylyl cyclases receptors Gyc-89Da, Gyc-89Db, and Gyc-88E is confirmed on some of the v'Td neurons (Langlais et al., 2004; Morton et al., 2008). These receptors are active under low O_2 conditions (Morton, 2004). Also, the CO_2 receptor Gr28a is found on some v'Td neurons (Qian et al., 2018; Xiang et al., 2010). It seems thus possible that during molting when the trachea is filled with molting fluid, the v'Td neurons sense the decreased O_2 and increased CO_2 levels in the trachea and relay this information to the V_m neurons.

Both EH and ETH neuropeptides are essential for tracheal air filling and clearance. The increased level of EH can push forward the molting and facilitate the molting fluid reabsorption and the tracheal air filling since most of the V_m ablated flies or *ETH* knock-out mutants fail at tracheal air filling and die during each ecdysis (Baker et al., 1999; Clark et al., 2004; McNabb et al., 1997; Park et al., 2002). Today, it is known that EH released from the non-canonical EH neurons helps the surviving flies to inflate their trachea and reach adulthood (Scott et al., 2020). Interestingly, an ETH injection cannot restore the tracheal inflation in the V_m ablated flies (Clark et al., 2004). The completion of tracheal clearance requires leucokinin released in

response to ETH (Kim et al., 2018). Therefore, the EH/ETH feedback can push forward the airway cleaning and remove the remainder of the molting fluid.

A look into the timing of the pupal ecdysis provides insight into the eclosion events. The pre-ecdysis program lasts about ten minutes while the duration of the ecdysis itself is around five minutes (Kim et al., 2006b; Park et al., 2002). The tracheal collapse and air filling are a response to ETH and leucokinin through water reabsorption by Degenerin/Epithelial sodium channel (Kim et al., 2018; Park et al., 2002). This process takes two to five minutes and happens before pre-ecdysis. About 20 minutes later the ecdysis is initiated (Park et al., 2002). During the tracheal collapse, the animals briefly experience O_2 loss and an abundance of CO_2. V_m neurons probably receive O_2 and CO_2 gas input from the v'Td neurons as an auxiliary signal. However, with the data from this thesis, a firm conclusion cannot be drawn. The synaptic connection between v'Td and V_m neurons suggests that activation of v'Td neurons might activate V_m neurons. However, activation of neither of v'Tds caused Ca^{2+} increase in the V_m cell bodies. This problem might be associated with a second chromosome balancer which is not morphologically detectable in puparia. Therefore, possibly some of the flies tested for v'Td-V_m connectivity did not contain ChR2-XXL and this caused inconsistency in the data. This problem can be solved by replacing the second chromosome balancer with a detectable fluorescent balancer and repeating the experiments. Besides, including a positive control test (optogenetic activating of the V_ms and measuring their Ca^{2+} signal) is necessary.

This research could not find any functional role for direct or indirect light-induced premature eclosion triggering or modulation of the V_m neurons activity via the v'Td neurons. Larval v'Td2 neurons like C4da neurons also express Gr28b, known to be sensitive to ultraviolet and violet light (Keene and Sprecher, 2012; Qian et al., 2018; Xiang et al., 2010). Recently, it has been shown that v'Td2 neurons are presynaptic to ILP7 neurons and important for light-mediated nociception and triggering the escape response in the larvae (Imambocus et al., 2022). Whether v'Td2 neurons are also light sensitive in adults and whether this light sensitivity is required for eclosion or not, calls for more investigation. One possibility is that these neurons might perceive the morning light as an additional pathway and signal to the V_m neurons and prepare eclosion.

References

Abruzzi, K.C., Zadina, A., Luo, W., Wiyanto, E., Rahman, R., Guo, F., Shafer, O., Rosbash, M., 2017. RNA-seq analysis of Drosophila clock and non-clock neurons reveals neuron-specific cycling and novel candidate neuropeptides. PLOS Genetics 13, e1006613. https://doi.org/10.1371/journal.pgen.1006613

Adams, C.M., Anderson, M.G., Motto, D.G., Price, M.P., Johnson, W.A., Welsh, M.J., 1998. Ripped Pocket and Pickpocket, Novel Drosophila DEG/ENaC Subunits Expressed in Early Development and in Mechanosensory Neurons. Journal of Cell Biology 140, 143–152. https://doi.org/10.1083/jcb.140.1.143

Agnati, L.F., Zoli, M., Strömberg, I., Fuxe, K., 1995. Intercellular communication in the brain: Wiring versus volume transmission. Neuroscience 69, 711–726. https://doi.org/10.1016/0306-4522(95)00308-6

Agui, N., Bollenbacher, W.E., Granger, N.A., Gilbert, L.I., 1980. Corpus allatum is release site for insect prothoracicotropic hormone. Nature 285, 669–670. https://doi.org/10.1038/285669a0

Agui, N., Granger, N.A., Gilbert, L.I., Bollenbacher, W.E., 1979. Cellular localization of the insect prothoracicotropic hormone: In vitro assay of a single neurosecretory cell. Proceedings of the National Academy of Sciences 76, 5694–5698. https://doi.org/10.1073/pnas.76.11.5694

Aguinaldo, A.M.A., Turbeville, J.M., Linford, L.S., Rivera, M.C., Garey, J.R., Raff, R.A., Lake, J.A., 1997. Evidence for a clade of nematodes, arthropods and other moulting animals. Nature 387, 489–493. https://doi.org/10.1038/387489a0

Ahmad, M., Li, W., Top, D., 2021. Integration of Circadian Clock Information in the Drosophila Circadian Neuronal Network. J Biol Rhythms 36, 203–220. https://doi.org/10.1177/0748730421993953

Ainsley, J.A., Kim, M.J., Wegman, L.J., Pettus, J.M., Johnson, W.A., 2008. Sensory mechanisms controlling the timing of larval developmental and behavioral transitions require the Drosophila DEG/ENaC subunit, Pickpocket1. Dev Biol 322, 46–55. https://doi.org/10.1016/j.ydbio.2008.07.003

Ainsley, J.A., Pettus, J.M., Bosenko, D., Gerstein, C.E., Zinkevich, N., Anderson, M.G., Adams, C.M., Welsh, M.J., Johnson, W.A., 2003. Enhanced locomotion caused by loss of the Drosophila DEG/ENaC protein Pickpocket1. Curr Biol 13, 1557–1563. https://doi.org/10.1016/s0960-9822(03)00596-7

Akerboom, J., Carreras Calderón, N., Tian, L., Wabnig, S., Prigge, M., Tolö, J., Gordus, A., Orger, M., Severi, K., Macklin, J., Patel, R., Pulver, S., Wardill, T., Fischer, E., Schüler, C., Chen, T.-W., Sarkisyan, K., Marvin, J., Bargmann, C., Kim, D., Kügler, S., Lagnado, L., Hegemann, P., Gottschalk, A., Schreiter, E., Looger, L., 2013. Genetically encoded calcium indicators for multi-color neural activity imaging and combination with optogenetics. Frontiers in Molecular Neuroscience 6.

Allada, R., White, N.E., So, W.V., Hall, J.C., Rosbash, M., 1998. A mutant Drosophila homolog of mammalian Clock disrupts circadian rhythms and transcription of period and timeless. Cell 93, 791–804. https://doi.org/10.1016/s0092-8674(00)81440-3

Allen, M.J., O'Kane, C.J., Moffat, K.G., 2002. Cell ablation using wild-type and cold-sensitive ricin-A chain in Drosophila embryonic mesoderm. Genesis 34, 132–134. https://doi.org/10.1002/gene.10129

Alpert, M.H., Frank, D.D., Kaspi, E., Flourakis, M., Zaharieva, E.E., Allada, R., Para, A., Gallio, M., 2020. A Circuit Encoding Absolute Cold Temperature in Drosophila. Curr Biol 30, 2275-2288.e5. https://doi.org/10.1016/j.cub.2020.04.038

Axelrod, S., Saez, L., Young, M.W., 2015. Studying circadian rhythm and sleep using genetic screens in Drosophila. Methods Enzymol 551, 3–27. https://doi.org/10.1016/bs.mie.2014.10.026

Bae, K., Lee, C., Sidote, D., Chuang, K.Y., Edery, I., 1998. Circadian regulation of a Drosophila homolog of the mammalian Clock gene: PER and TIM function as positive regulators. Mol Cell Biol 18, 6142–6151. https://doi.org/10.1128/MCB.18.10.6142

Bainbridge, S.P., Bownes, M., 1981. Staging the metamorphosis of Drosophila melanogaster. Development 66, 57–80. https://doi.org/10.1242/dev.66.1.57

Baines, R.A., Uhler, J.P., Thompson, A., Sweeney, S.T., Bate, M., 2001. Altered electrical properties in Drosophila neurons developing without synaptic transmission. J Neurosci 21, 1523–1531. https://doi.org/10.1523/JNEUROSCI.21-05-01523.2001

Baker, J.D., McNabb, S.L., Truman, J.W., 1999. The hormonal coordination of behavior and physiology at adult ecdysis in Drosophila melanogaster. Journal of Experimental Biology 202, 3037–3048. https://doi.org/10.1242/jeb.202.21.3037

Barber, A.F., Erion, R., Holmes, T.C., Sehgal, A., 2016. Circadian and feeding cues integrate to drive rhythms of physiology in Drosophila insulin-producing cells. Genes Dev 30, 2596–2606. https://doi.org/10.1101/gad.288258.116

Bargiello, T.A., Jackson, F.R., Young, M.W., 1984. Restoration of circadian behavioural rhythms by gene transfer in Drosophila. Nature 312, 752–754. https://doi.org/10.1038/312752a0

Barth, A.L., Gerkin, R.C., Dean, K.L., 2004. Alteration of neuronal firing properties after in vivo experience in a FosGFP transgenic mouse. J Neurosci 24, 6466–6475. https://doi.org/10.1523/JNEUROSCI.4737-03.2004

Bauknecht, P., Jékely, G., 2015. Large-Scale Combinatorial Deorphanization of Platynereis Neuropeptide GPCRs. Cell Rep 12, 684–693. https://doi.org/10.1016/j.celrep.2015.06.052

Beckwith, E.J., Ceriani, M.F., 2015. Communication between circadian clusters: The key to a plastic network. FEBS Lett 589, 3336–3342. https://doi.org/10.1016/j.febslet.2015.08.017

Berndt, A., Kottke, T., Breitkreuz, H., Dvorsky, R., Hennig, S., Alexander, M., Wolf, E., 2007. A novel photoreaction mechanism for the circadian blue light photoreceptor Drosophila cryptochrome. J Biol Chem 282, 13011–13021. https://doi.org/10.1074/jbc.M608872200

Bestman, J.E., Booker, R., 2003. Modulation of foregut synaptic activity controls resorption of molting fluid during larval molts of the moth Manduca sexta. Journal of Experimental Biology 206, 1207–1220. https://doi.org/10.1242/jeb.00237

Bidell, D., Feige, N.-D., Triphan, T., Pauls, D., Helfrich-Förster, C., Selcho, M., 2023. Immediate effects of light on circadian eclosion and locomotor activity depend on distinct sensory input pathways. https://doi.org/10.1101/2023.04.21.537872

Birgül, N., Weise, C., Kreienkamp, H.J., Richter, D., 1999. Reverse physiology in drosophila: identification of a novel allatostatin-like neuropeptide and its cognate receptor structurally related to the mammalian somatostatin/galanin/opioid receptor family. EMBO J 18, 5892–5900. https://doi.org/10.1093/emboj/18.21.5892

Blanchardon, E., Grima, B., Klarsfeld, A., Chélot, E., Hardin, P.E., Préat, T., Rouyer, F., 2001. Defining the role of Drosophila lateral neurons in the control of circadian rhythms in motor activity and eclosion by targeted genetic ablation and PERIOD protein overexpression. European Journal of Neuroscience 13, 871–888. https://doi.org/10.1046/j.0953-816x.2000.01450.x

Blau, J., Young, M.W., 1999. Cycling vrille expression is required for a functional Drosophila clock. Cell 99, 661–671. https://doi.org/10.1016/s0092-8674(00)81554-8

Bodmer, R., Jan, Y.N., 1987. Morphological differentiation of the embryonic peripheral neurons in Drosophila. Roux's Arch Dev Biol 196, 69–77. https://doi.org/10.1007/BF00402027

Bollenbacher, W.E., Agui, N., Granger, N.A., Gilbert, L.I., 1979. In vitro activation of insect prothoracic glands by the prothoracicotropic hormone. Proceedings of the National Academy of Sciences 76, 5148–5152. https://doi.org/10.1073/pnas.76.10.5148

Bollenbacher, W.E., Smith, S.L., Goodman, W., Gilbert, L.I., 1981. Ecdysteroid titer during larval-pupal-adult development of the tobacco hornworm, Manduca sexta. General and Comparative Endocrinology 44, 302–306. https://doi.org/10.1016/0016-6480(81)90005-8

Bossen, J., Prange, R., Kühle, J.-P., Künzel, S., Niu, X., Hammel, J.U., Krieger, L., Knop, M., Ehrhardt, B., Uliczka, K., Krauss-Etschmann, S., Roeder, T., 2023. Adult and Larval Tracheal Systems Exhibit Different Molecular Architectures in Drosophila. Int J Mol Sci 24, 5628. https://doi.org/10.3390/ijms24065628

Boulan, L., Martín, D., Milán, M., 2013. bantam miRNA Promotes Systemic Growth by Connecting Insulin Signaling and Ecdysone Production. Current Biology 23, 473–478. https://doi.org/10.1016/j.cub.2013.01.072

Boulan, L., Milán, M., Léopold, P., 2015. The Systemic Control of Growth. Cold Spring Harb Perspect Biol 7, a019117. https://doi.org/10.1101/cshperspect.a019117

Brett, W.J., 1955. Persistent Diurnal Rhythmicity in Drosophila Emergence1. Annals of the Entomological Society of America 48, 119–131. https://doi.org/10.1093/aesa/48.3.119

Brogiolo, W., Stocker, H., Ikeya, T., Rintelen, F., Fernandez, R., Hafen, E., 2001. An evolutionarily conserved function of the Drosophila insulin receptor and insulin-like peptides in growth control. Current Biology 11, 213–221. https://doi.org/10.1016/S0960-9822(01)00068-9

Budd, E., Käuser, G., Koolman, J., 1993. On the control of ecdysone biosynthesis by the central nervous system of blowfly larvae. Arch Insect Biochem Physiol 23, 181–197. https://doi.org/10.1002/arch.940230405

Bunning, E., 1935. Zur Kenntnis der endonomen Tagesrhythmik bei Insekten und bei Pflanzen. Ber Deut Bot Ges 53, 594–623.

Busza, A., Emery-Le, M., Rosbash, M., Emery, P., 2004. Roles of the two Drosophila CRYPTOCHROME structural domains in circadian photoreception. Science 304, 1503–1506. https://doi.org/10.1126/science.1096973

Cachero, S., Gkantia, M., Bates, A.S., Frechter, S., Blackie, L., McCarthy, A., Sutcliffe, B., Strano, A., Aso, Y., Jefferis, G.S.X.E., 2020. BAcTrace, a tool for retrograde tracing of neuronal circuits in Drosophila. Nature Methods 17, 1254–1261. https://doi.org/10.1038/s41592-020-00989-1

Caldwell, P.E., Walkiewicz, M., Stern, M., 2005. Ras Activity in the Drosophila Prothoracic Gland Regulates Body Size and Developmental Rate via Ecdysone Release. Current Biology 15, 1785–1795. https://doi.org/10.1016/j.cub.2005.09.011

Carlisle, D.B., Ellis, P.E., 1968. Hormonal inhibition of the prothoracic gland by the brain in locusts. Nature 220, 706–707. https://doi.org/10.1038/220706a0

Cavanaugh, D.J., Geratowski, J.D., Wooltorton, J.R.A., Spaethling, J.M., Hector, C.E., Zheng, X., Johnson, E.C., Eberwine, J.H., Sehgal, A., 2014. Identification of a Circadian Output Circuit for Rest:Activity Rhythms in Drosophila. Cell 157, 689–701. https://doi.org/10.1016/j.cell.2014.02.024

Cavieres-Lepe, J., Amini, E., Nässel, D.R., Stanewsky, R., Wegener, C., Ewer, J., 2023. Timed receptor tyrosine kinase signaling couples the central and a peripheral circadian clock in Drosophila. https://doi.org/10.1101/2023.05.14.540706

Chang, J.-C., Yang, R.-B., Adams, M.E., Lu, K.-H., 2009. Receptor guanylyl cyclases in Inka cells targeted by eclosion hormone. Proc Natl Acad Sci U S A 106, 13371–13376. https://doi.org/10.1073/pnas.0812593106

Chávez, V.M., Marqués, G., Delbecque, J.P., Kobayashi, K., Hollingsworth, M., Burr, J., Natzle, J.E., O'Connor, M.B., 2000. The Drosophila disembodied gene controls late embryonic morphogenesis and codes for a cytochrome P450 enzyme that regulates embryonic ecdysone levels. Development 127, 4115–4126. https://doi.org/10.1242/dev.127.19.4115

Chen, C., Buhl, E., Xu, M., Croset, V., Rees, J.S., Lilley, K.S., Benton, R., Hodge, J.J., Stanewsky, R., 2015. Drosophila Ionotropic Receptor 25a mediates circadian clock resetting by temperature. Nature 527, 516–520.

Chen, C.-C., Wu, J.-K., Lin, H.-W., Pai, T.-P., Fu, T.-F., Wu, C.-L., Tully, T., Chiang, A.-S., 2012. Visualizing Long-Term Memory Formation in Two Neurons of the Drosophila Brain. Science 335, 678–685. https://doi.org/10.1126/science.1212735

Chen, J., Reiher, W., Hermann-Luibl, C., Sellami, A., Cognigni, P., Kondo, S., Helfrich-Förster, C., Veenstra, J.A., Wegener, C., 2016. Allatostatin A Signalling in Drosophila Regulates Feeding and Sleep and Is Modulated by PDF. PLoS Genet 12, e1006346. https://doi.org/10.1371/journal.pgen.1006346

Chen, W., Liu, Z., Li, T., Zhang, R., Xue, Y., Zhong, Y., Bai, W., Zhou, D., Zhao, Z., 2014. Regulation of Drosophila circadian rhythms by miRNA let-7 is mediated by a regulatory cycle. Nat Commun 5, 5549. https://doi.org/10.1038/ncomms6549

Chen, X., Rahman, R., Guo, F., Rosbash, M., 2016. Genome-wide identification of neuronal activity-regulated genes in Drosophila. eLife 5, e19942. https://doi.org/10.7554/eLife.19942

Chen, X., Rosbash, M., 2016. mir-276a strengthens Drosophila circadian rhythms by regulating timeless expression. Proc Natl Acad Sci U S A 113, E2965-2972. https://doi.org/10.1073/pnas.1605837113

Cho, K.-H., Daubnerová, I., Park, Y., Zitnan, D., Adams, M.E., 2014. Secretory competence in a gateway endocrine cell conferred by the nuclear receptor βFTZ-F1 enables stage-specific ecdysone responses throughout development in Drosophila. Developmental Biology 385, 253–262. https://doi.org/10.1016/j.ydbio.2013.11.003

Christ, P., Hill, S.R., Schachtner, J., Hauser, F., Ignell, R., 2018. Functional characterization of the dual allatostatin-A receptors in mosquitoes. Peptides 99, 44–55. https://doi.org/10.1016/j.peptides.2017.10.016

Christensen, C.F., Koyama, T., Nagy, S., Danielsen, E.T., Texada, M.J., Halberg, K.A., Rewitz, K., 2020. Ecdysone-dependent feedback regulation of prothoracicotropic hormone controls the timing of developmental maturation. Development 147, dev188110. https://doi.org/10.1242/dev.188110

Clark, A.C., del Campo, M.L., Ewer, J., 2004. Neuroendocrine Control of Larval Ecdysis Behavior in Drosophila: Complex Regulation by Partially Redundant Neuropeptides. J Neurosci 24, 4283–4292. https://doi.org/10.1523/JNEUROSCI.4938-03.2004

Colombani, J., Andersen, D.S., Boulan, L., Boone, E., Romero, N., Virolle, V., Texada, M., Léopold, P., 2015. Drosophila Lgr3 Couples Organ Growth with Maturation and Ensures Developmental Stability. Curr Biol 25, 2723–2729. https://doi.org/10.1016/j.cub.2015.09.020

Colombani, J., Andersen, D.S., Léopold, P., 2012. Secreted Peptide Dilp8 Coordinates Drosophila Tissue Growth with Developmental Timing. Science 336, 582–585. https://doi.org/10.1126/science.1216689

Colombani, J., Bianchini, L., Layalle, S., Pondeville, E., Dauphin-Villemant, C., Antoniewski, C., Carré, C., Noselli, S., Léopold, P., 2005. Antagonistic Actions of Ecdysone and

Insulins Determine Final Size in Drosophila. Science 310, 667–670. https://doi.org/10.1126/science.1119432
Copenhaver, P.F., Truman, J.W., 1986a. Identification of the cerebral neurosecretory cells that contain eclosion hormone in the moth Manduca sexta. J Neurosci 6, 1738–1747. https://doi.org/10.1523/JNEUROSCI.06-06-01738.1986
Copenhaver, P.F., Truman, J.W., 1986b. Control of neurosecretion in the moth Manduca sexta: physiological regulation of the eclosion hormone cells. Journal of Comparative Physiology A 158, 445–455.
Court, R., Namiki, S., Armstrong, J.D., Börner, J., Card, G., Costa, M., Dickinson, M., Duch, C., Korff, W., Mann, R., Merritt, D., Murphey, R.K., Seeds, A.M., Shirangi, T., Simpson, J.H., Truman, J.W., Tuthill, J.C., Williams, D.W., Shepherd, D., 2020. A Systematic Nomenclature for the Drosophila Ventral Nerve Cord. Neuron 107, 1071-1079.e2. https://doi.org/10.1016/j.neuron.2020.08.005
Cyran, S.A., Buchsbaum, A.M., Reddy, K.L., Lin, M.-C., Glossop, N.R.J., Hardin, P.E., Young, M.W., Storti, R.V., Blau, J., 2003. vrille, Pdp1, and dClock form a second feedback loop in the Drosophila circadian clock. Cell 112, 329–341. https://doi.org/10.1016/s0092-8674(03)00074-6
Dai, J.D., Gilbert, L.I., 1991. Metamorphosis of the corpus allatum and degeneration of the prothoracic glands during the larval-pupal-adult transformation of Drosophila melanogaster: a cytophysiological analysis of the ring gland. Dev Biol 144, 309–326. https://doi.org/10.1016/0012-1606(91)90424-2
Dana, H., Mohar, B., Sun, Y., Narayan, S., Gordus, A., Hasseman, J.P., Tsegaye, G., Holt, G.T., Hu, A., Walpita, D., Patel, R., Macklin, J.J., Bargmann, C.I., Ahrens, M.B., Schreiter, E.R., Jayaraman, V., Looger, L.L., Svoboda, K., Kim, D.S., 2016. Sensitive red protein calcium indicators for imaging neural activity. eLife 5, e12727. https://doi.org/10.7554/eLife.12727
Darboux, I., Lingueglia, E., Pauron, D., Barbry, P., Lazdunski, M., 1998. A New Member of the Amiloride-Sensitive Sodium Channel Family inDrosophila melanogasterPeripheral Nervous System. Biochemical and Biophysical Research Communications 246, 210–216. https://doi.org/10.1006/bbrc.1998.8183
Darlington, T.K., Wager-Smith, K., Ceriani, M.F., Staknis, D., Gekakis, N., Steeves, T.D., Weitz, C.J., Takahashi, J.S., Kay, S.A., 1998. Closing the circadian loop: CLOCK-induced transcription of its own inhibitors per and tim. Science 280, 1599–1603. https://doi.org/10.1126/science.280.5369.1599
Daubnerová, I., Roller, L., Satake, H., Zhang, C., Kim, Y.-J., Žitňan, D., 2021. Identification and function of ETH receptor networks in the silkworm Bombyx mori. Sci Rep 11, 11693. https://doi.org/10.1038/s41598-021-91022-8
Davis, N.T., Blackburn, M.B., Golubeva, E.G., Hildebrand, J.G., 2003. Localization of myoinhibitory peptide immunoreactivity in Manduca sexta and Bombyx mori, with indications that the peptide has a role in molting and ecdysis. J Exp Biol 206, 1449–1460. https://doi.org/10.1242/jeb.00234
Dawydow, A., Gueta, R., Ljaschenko, D., Ullrich, S., Hermann, M., Ehmann, N., Gao, S., Fiala, A., Langenhan, T., Nagel, G., Kittel, R.J., 2014. Channelrhodopsin-2–XXL, a powerful optogenetic tool for low-light applications. Proceedings of the National Academy of Sciences 111, 13972–13977. https://doi.org/10.1073/pnas.1408269111
de Azevedo, R.V.D.M., Hansen, C., Chen, K.-F., Rosato, E., Kyriacou, C.P., 2020. Disrupted Glutamate Signaling in Drosophila Generates Locomotor Rhythms in Constant Light. Front Physiol 11, 145. https://doi.org/10.3389/fphys.2020.00145
de Velasco, B., Erclik, T., Shy, D., Sclafani, J., Lipshitz, H., McInnes, R., Hartenstein, V., 2007. Specification and development of the pars intercerebralis and pars lateralis,

neuroendocrine command centers in the Drosophila brain. Developmental Biology 302, 309–323. https://doi.org/10.1016/j.ydbio.2006.09.035
Deng, B., Li, Q., Liu, X., Cao, Y., Li, B., Qian, Y., Xu, R., Mao, R., Zhou, E., Zhang, W., Huang, J., Rao, Y., 2019. Chemoconnectomics: Mapping Chemical Transmission in Drosophila. Neuron 101, 876-893.e4. https://doi.org/10.1016/j.neuron.2019.01.045
Deveci, D., Martin, F.A., Leopold, P., Romero, N.M., 2019. AstA Signaling Functions as an Evolutionary Conserved Mechanism Timing Juvenile to Adult Transition. Current Biology 29, 813-822.e4. https://doi.org/10.1016/j.cub.2019.01.053
Dewey, E.M., McNabb, S.L., Ewer, J., Kuo, G.R., Takanishi, C.L., Truman, J.W., Honegger, H.-W., 2004. Identification of the gene encoding bursicon, an insect neuropeptide responsible for cuticle sclerotization and wing spreading. Curr Biol 14, 1208–1213. https://doi.org/10.1016/j.cub.2004.06.051
Diao, Feici, Elliott, A.D., Diao, Fengqiu, Shah, S., White, B.H., 2017. Neuromodulatory connectivity defines the structure of a behavioral neural network. Elife 6, e29797. https://doi.org/10.7554/eLife.29797
Diao, Feici, Mena, W., Shi, J., Park, D., Diao, Fengqiu, Taghert, P., Ewer, J., White, B.H., 2016. The Splice Isoforms of the Drosophila Ecdysis Triggering Hormone Receptor Have Developmentally Distinct Roles. Genetics 202, 175–189. https://doi.org/10.1534/genetics.115.182121
Díaz, M.M., Schlichting, M., Abruzzi, K.C., Long, X., Rosbash, M., 2019. Allatostatin-C/AstC-R2 Is a Novel Pathway to Modulate the Circadian Activity Pattern in Drosophila. Curr Biol 29, 13-22.e3. https://doi.org/10.1016/j.cub.2018.11.005
Di Cara, F., King-Jones, K., 2016. The Circadian Clock Is a Key Driver of Steroid Hormone Production in Drosophila. Current Biology 26, 2469–2477. https://doi.org/10.1016/j.cub.2016.07.004
Dietzl, G., Chen, D., Schnorrer, F., Su, K.-C., Barinova, Y., Fellner, M., Gasser, B., Kinsey, K., Oppel, S., Scheiblauer, S., Couto, A., Marra, V., Keleman, K., Dickson, B.J., 2007. A genome-wide transgenic RNAi library for conditional gene inactivation in Drosophila. Nature 448, 151–156. https://doi.org/10.1038/nature05954
Dionne, H., Hibbard, K.L., Cavallaro, A., Kao, J.-C., Rubin, G.M., 2018. Genetic Reagents for Making Split-GAL4 Lines in Drosophila. Genetics 209, 31–35. https://doi.org/10.1534/genetics.118.300682
Dircksen, H., Tesfai, L.K., Albus, C., Nässel, D.R., 2008. Ion transport peptide splice forms in central and peripheral neurons throughout postembryogenesis of Drosophila melanogaster. Journal of Comparative Neurology 509, 23–41. https://doi.org/10.1002/cne.21715
Dominick, O.S., Truman, J.W., 1986a. The physiology of wandering behaviour in Manduca sexta: III. Organization of wandering behaviour in the larval nervous system. Journal of experimental biology 121, 115–132.
Dominick, O.S., Truman, J.W., 1986b. The Physiology of Wandering Behaviour in Manduca Sexta: IV. Hormonal Induction of Wandering Behaviour from the Isolated Nervous System. Journal of Experimental Biology 121, 133–151.
Dominick, O.S., Truman, J.W., 1985. The physiology of wandering behaviour in Manduca sexta. II. The endocrine control of wandering behaviour. J Exp Biol 117, 45–68. https://doi.org/10.1242/jeb.117.1.45
Dubowy, C., Sehgal, A., 2017. Circadian Rhythms and Sleep in Drosophila melanogaster. Genetics 205, 1373–1397. https://doi.org/10.1534/genetics.115.185157
Egerod, K., Reynisson, E., Hauser, F., Cazzamali, G., Williamson, M., Grimmelikhuijzen, C.J.P., 2003. Molecular cloning and functional expression of the first two specific insect

myosuppressin receptors. Proc Natl Acad Sci U S A 100, 9808–9813. https://doi.org/10.1073/pnas.1632197100
Elliott, A.D., Berndt, A., Houpert, M., Roy, S., Scott, R.L., Chow, C.C., Shroff, H., White, B.H., 2021. Pupal behavior emerges from unstructured muscle activity in response to neuromodulation in Drosophila. Elife 10, e68656. https://doi.org/10.7554/eLife.68656
Emery, I.F., Noveral, J.M., Jamison, C.F., Siwicki, K.K., 1997. Rhythms of Drosophila period gene expression in culture. Proc Natl Acad Sci U S A 94, 4092–4096.
Emery, P., So, W.V., Kaneko, M., Hall, J.C., Rosbash, M., 1998. CRY, a Drosophila clock and light-regulated cryptochrome, is a major contributor to circadian rhythm resetting and photosensitivity. Cell 95, 669–679. https://doi.org/10.1016/s0092-8674(00)81637-2
Emery, P., Stanewsky, R., Helfrich-Förster, C., Emery-Le, M., Hall, J.C., Rosbash, M., 2000. Drosophila CRY is a deep brain circadian photoreceptor. Neuron 26, 493–504. https://doi.org/10.1016/s0896-6273(00)81181-2
Ewer, J., 2007a. Neuroendocrinology of Eclosion, in: Invertebrate Neurobiology. Cold Spring Harbor Laboratory Press, Cold Spring Harbor, p. Chapter 25.
Ewer, J., 2007b. 21 Neuroendocrinology of Eclosion. Cold Spring Harbor Monograph Archive 49, 555–579. https://doi.org/10.1101/0.555-579
Ewer, J., 2005a. Behavioral actions of neuropeptides in invertebrates: Insights from Drosophila. Hormones and Behavior, Special Issue on Behavioral Neuroendocrinology Evolving: Contributions of Comparative and Field Studies 48, 418–429. https://doi.org/10.1016/j.yhbeh.2005.05.018
Ewer, J., 2005b. How the Ecdysozoan Changed Its Coat. PLOS Biology 3, e349. https://doi.org/10.1371/journal.pbio.0030349
Ewer, J., Gammie, S.C., Truman, J.W., 1997. Control of insect ecdysis by a positive-feedback endocrine system: roles of eclosion hormone and ecdysis triggering hormone. Journal of Experimental Biology 200, 869–881. https://doi.org/10.1242/jeb.200.5.869
Ewer, J., Reynolds, S., 2002. 35 - Neuropeptide Control of Molting in Insects, in: Pfaff, D.W., Arnold, A.P., Fahrbach, S.E., Etgen, A.M., Rubin, R.T. (Eds.), Hormones, Brain and Behavior. Academic Press, San Diego, pp. 1–XVI. https://doi.org/10.1016/B978-012532104-4/50037-8
Feinberg, E.H., VanHoven, M.K., Bendesky, A., Wang, G., Fetter, R.D., Shen, K., Bargmann, C.I., 2008. GFP Reconstitution Across Synaptic Partners (GRASP) Defines Cell Contacts and Synapses in Living Nervous Systems. Neuron 57, 353–363. https://doi.org/10.1016/j.neuron.2007.11.030
Fellner, S.K., Rybczynski, R., Gilbert, L.I., 2005. Ca2+ signaling in prothoracicotropic hormone-stimulated prothoracic gland cells of Manduca sexta: Evidence for mobilization and entry mechanisms. Insect Biochemistry and Molecular Biology 35, 263–275. https://doi.org/10.1016/j.ibmb.2004.11.006
Feng, G., Reale, V., Chatwin, H., Kennedy, K., Venard, R., Ericsson, C., Yu, K., Evans, P.D., Hall, L.M., 2003. Functional characterization of a neuropeptide F-like receptor from Drosophila melanogaster. European Journal of Neuroscience 18, 227–238. https://doi.org/10.1046/j.1460-9568.2003.02719.x
Feng, Y., Ueda, A., Wu, C.-F., 2004. A modified minimal hemolymph-like solution, HL3.1, for physiological recordings at the neuromuscular junctions of normal and mutant Drosophila larvae. J Neurogenet 18, 377–402. https://doi.org/10.1080/01677060490894522
Fernandez, R., Tabarini, D., Azpiazu, N., Frasch, M., Schlessinger, J., 1995. The Drosophila insulin receptor homolog: a gene essential for embryonic development encodes two receptor isoforms with different signaling potential. The EMBO Journal 14, 3373–3384. https://doi.org/10.1002/j.1460-2075.1995.tb07343.x

Förster, T.D., Woods, H.A., 2013. Mechanisms of tracheal filling in insects. Biological Reviews 88, 1–14. https://doi.org/10.1111/j.1469-185X.2012.00233.x

Fowler, T., Sen, R., Roy, A.L., 2011. Regulation of Primary Response Genes. Molecular Cell 44, 348–360. https://doi.org/10.1016/j.molcel.2011.09.014

Frenkel, L., Muraro, N.I., Beltrán González, A.N., Marcora, M.S., Bernabó, G., Hermann-Luibl, C., Romero, J.I., Helfrich-Förster, C., Castaño, E.M., Marino-Busjle, C., Calvo, D.J., Ceriani, M.F., 2017. Organization of Circadian Behavior Relies on Glycinergic Transmission. Cell Reports 19, 72–85. https://doi.org/10.1016/j.celrep.2017.03.034

Fucile, S., 2004. Ca2+ permeability of nicotinic acetylcholine receptors. Cell Calcium 35, 1–8. https://doi.org/10.1016/j.ceca.2003.08.006

Gammie, S.C., Truman, J.W., 1999. Eclosion hormone provides a link between ecdysis-triggering hormone and crustacean cardioactive peptide in the neuroendocrine cascade that controls ecdysis behavior. Journal of Experimental Biology 202, 343–352. https://doi.org/10.1242/jeb.202.4.343

Gammie, S.C., Truman, J.W., 1997. Neuropeptide Hierarchies and the Activation of Sequential Motor Behaviors in the Hawkmoth, Manduca sexta. J. Neurosci. 17, 4389–4397. https://doi.org/10.1523/JNEUROSCI.17-11-04389.1997

Garelli, A., Gontijo, A.M., Miguela, V., Caparros, E., Dominguez, M., 2012. Imaginal Discs Secrete Insulin-Like Peptide 8 to Mediate Plasticity of Growth and Maturation. Science 336, 579–582. https://doi.org/10.1126/science.1216735

Garelli, A., Heredia, F., Casimiro, A.P., Macedo, A., Nunes, C., Garcez, M., Dias, A.R.M., Volonte, Y.A., Uhlmann, T., Caparros, E., Koyama, T., Gontijo, A.M., 2015. Dilp8 requires the neuronal relaxin receptor Lgr3 to couple growth to developmental timing. Nat Commun 6, 8732. https://doi.org/10.1038/ncomms9732

Gatto, C.L., Broadie, K., 2011. Fragile X mental retardation protein is required for programmed cell death and clearance of developmentally-transient peptidergic neurons. Dev Biol 356, 291–307. https://doi.org/10.1016/j.ydbio.2011.05.001

Gekakis, N., Saez, L., Delahaye-Brown, A.M., Myers, M.P., Sehgal, A., Young, M.W., Weitz, C.J., 1995. Isolation of timeless by PER protein interaction: defective interaction between timeless protein and long-period mutant PERL. Science 270, 811–815. https://doi.org/10.1126/science.270.5237.811

Ghosh, A., McBrayer, Z., O'Connor, M.B., 2010. The Drosophila gap gene giant regulates ecdysone production through specification of the PTTH-producing neurons. Developmental Biology 347, 271–278. https://doi.org/10.1016/j.ydbio.2010.08.011

Gibbens, Y.Y., Warren, J.T., Gilbert, L.I., O'Connor, M.B., 2011. Neuroendocrine regulation of Drosophila metamorphosis requires TGFβ/Activin signaling. Development 138, 2693–2703. https://doi.org/10.1242/dev.063412

Gilbert, L.I., 2004. Halloween genes encode P450 enzymes that mediate steroid hormone biosynthesis in Drosophila melanogaster. Molecular and Cellular Endocrinology, Proceedings of the Serono Foundation for the Advancement of Medical Science Workshop on Molecular Steroidogenesis 215, 1–10. https://doi.org/10.1016/j.mce.2003.11.003

Gilbert, L.I., Rybczynski, R., Warren, J.T., 2002. Control and Biochemical Nature of the Ecdysteroidogenic Pathway. Annual Review of Entomology 47, 883–916. https://doi.org/10.1146/annurev.ento.47.091201.145302

Giribet, G., Edgecombe, G.D., 2017. Current Understanding of Ecdysozoa and its Internal Phylogenetic Relationships. Integrative and Comparative Biology 57, 455–466. https://doi.org/10.1093/icb/icx072

Glaser, F.T., Stanewsky, R., 2005. Temperature synchronization of the Drosophila circadian clock. Curr Biol 15, 1352–1363. https://doi.org/10.1016/j.cub.2005.06.056

Gohl, D.M., Silies, M.A., Gao, X.J., Bhalerao, S., Luongo, F.J., Lin, C.-C., Potter, C.J., Clandinin, T.R., 2011. A versatile in vivo system for directed dissection of gene expression patterns. Nat Methods 8, 231–237. https://doi.org/10.1038/nmeth.1561

Gong, C., Ouyang, Z., Zhao, W., Wang, J., Li, K., Zhou, P., Zhao, T., Zheng, N., Gong, Z., 2019. A Neuronal Pathway that Commands Deceleration in Drosophila Larval Light-Avoidance. Neurosci Bull 35, 959–968. https://doi.org/10.1007/s12264-019-00349-w

Gong, Z., Liu, J., Guo, C., Zhou, Y., Teng, Y., Liu, L., 2010. Two Pairs of Neurons in the Central Brain Control Drosophila Innate Light Preference. Science 330, 499–502. https://doi.org/10.1126/science.1195993

Gontijo, A.M., Garelli, A., 2018. The biology and evolution of the Dilp8-Lgr3 pathway: A relaxin-like pathway coupling tissue growth and developmental timing control. Mechanisms of Development 154, 44–50. https://doi.org/10.1016/j.mod.2018.04.005

Green, E.W., Fedele, G., Giorgini, F., Kyriacou, C.P., 2014. A Drosophila RNAi collection is subject to dominant phenotypic effects. Nat Methods 11, 222–223. https://doi.org/10.1038/nmeth.2856

Greenlee, K.J., Harrison, J.F., 2005. Respiratory changes throughout ontogeny in the tobacco hornworm caterpillar, Manduca sexta. Journal of Experimental Biology 208, 1385–1392. https://doi.org/10.1242/jeb.01521

Grima, B., Chélot, E., Xia, R., Rouyer, F., 2004. Morning and evening peaks of activity rely on different clock neurons of the Drosophila brain. Nature 431, 869–873. https://doi.org/10.1038/nature02935

Grima, B., Lamouroux, A., Chélot, E., Papin, C., Limbourg-Bouchon, B., Rouyer, F., 2002. The F-box protein slimb controls the levels of clock proteins period and timeless. Nature 420, 178–182. https://doi.org/10.1038/nature01122

Grimm, S., 2023. Inputs from Clock Neurons to the Eclosion Hormone Neurons and the Influence of Temperature on Eclosion.

Grönke, S., Clarke, D.-F., Broughton, S., Andrews, T.D., Partridge, L., 2010. Molecular Evolution and Functional Characterization of Drosophila Insulin-Like Peptides. PLOS Genetics 6, e1000857. https://doi.org/10.1371/journal.pgen.1000857

Grueber, W.B., Jan, L.Y., Jan, Y.N., 2002. Tiling of the Drosophila epidermis by multidendritic sensory neurons. Development 129, 2867–2878. https://doi.org/10.1242/dev.129.12.2867

Grueber, W.B., Ye, B., Yang, C.-H., Younger, S., Borden, K., Jan, L.Y., Jan, Y.-N., 2007. Projections of Drosophila multidendritic neurons in the central nervous system: links with peripheral dendrite morphology. Development 134, 55–64. https://doi.org/10.1242/dev.02666

Gummadova, J.O., Coutts, G.A., Glossop, N.R.J., 2009. Analysis of the Drosophila Clock Promoter Reveals Heterogeneity in Expression between Subgroups of Central Oscillator Cells and Identifies a Novel Enhancer Region. J Biol Rhythms 24, 353–367. https://doi.org/10.1177/0748730409343890

Guo, F., Holla, M., Díaz, M.M., Rosbash, M., 2018. A Circadian Output Circuit Controls Sleep-Wake Arousal in Drosophila. Neuron 100, 624-635.e4. https://doi.org/10.1016/j.neuron.2018.09.002

Guo, F., Yu, J., Jung, H.J., Abruzzi, K.C., Luo, W., Griffith, L.C., Rosbash, M., 2016. Circadian neuron feedback controls the Drosophila sleep–activity profile. Nature 536, 292–297. https://doi.org/10.1038/nature19097

Hadjieconomou, D., King, G., Gaspar, P., Mineo, A., Blackie, L., Ameku, T., Studd, C., de Mendoza, A., Diao, F., White, B.H., Brown, A.E.X., Plaçais, P.-Y., Préat, T., Miguel-Aliaga, I., 2020. Enteric neurons increase maternal food intake during reproduction. Nature 587, 455–459. https://doi.org/10.1038/s41586-020-2866-8

Hadjieconomou, D., Timofeev, K., Salecker, I., 2011. A step-by-step guide to visual circuit assembly in Drosophila. Current Opinion in Neurobiology, Developmental neuroscience 21, 76–84. https://doi.org/10.1016/j.conb.2010.07.012
Handler, A.M., 1982. Ecdysteroid titers during pupal and adult development in Drosophila melanogaster. Dev Biol 93, 73–82. https://doi.org/10.1016/0012-1606(82)90240-8
Hardin, P.E., Hall, J.C., Rosbash, M., 1990. Feedback of the Drosophila period gene product on circadian cycling of its messenger RNA levels. Nature 343, 536–540. https://doi.org/10.1038/343536a0
Harper, R.E.F., Dayan, P., Albert, J.T., Stanewsky, R., 2016. Sensory Conflict Disrupts Activity of the Drosophila Circadian Network. Cell Rep 17, 1711–1718. https://doi.org/10.1016/j.celrep.2016.10.029
Harshman, L.G., Loeb, A.M., Johnson, B.A., 1999. Ecdysteroid titers in mated and unmated Drosophila melanogaster females. J Insect Physiol 45, 571–577. https://doi.org/10.1016/s0022-1910(99)00038-4
Hayashi, S., Ito, K., Sado, Y., Taniguchi, M., Akimoto, A., Takeuchi, H., Aigaki, T., Matsuzaki, F., Nakagoshi, H., Tanimura, T., Ueda, R., Uemura, T., Yoshihara, M., Goto, S., 2002. GETDB, a database compiling expression patterns and molecular locations of a collection of gal4 enhancer traps. genesis 34, 58–61. https://doi.org/10.1002/gene.10137
Hazelrigg, T., Levis, R., Rubin, G.M., 1984. Transformation of white locus DNA in Drosophila: Dosage compensation, zeste interaction, and position effects. Cell 36, 469–481. https://doi.org/10.1016/0092-8674(84)90240-X
Helfrich-Förster, C., 2020. Light input pathways to the circadian clock of insects with an emphasis on the fruit fly Drosophila melanogaster. J Comp Physiol A 206, 259–272. https://doi.org/10.1007/s00359-019-01379-5
Helfrich-Förster, C., 2017. The Drosophila Clock System, in: Kumar, V. (Ed.), Biological Timekeeping: Clocks, Rhythms and Behaviour. Springer India, New Delhi, pp. 133–176. https://doi.org/10.1007/978-81-322-3688-7_6
Helfrich-Förster, C., 2005. Neurobiology of the fruit fly's circadian clock. Genes, Brain and Behavior 4, 65–76. https://doi.org/10.1111/j.1601-183X.2004.00092.x
Helfrich-Förster, C., 2004. The circadian clock in the brain: a structural and functional comparison between mammals and insects. Journal of Comparative Physiology A 190, 601–613.
Helfrich-Förster, C., 2003. The neuroarchitecture of the circadian clock in the brain of Drosophila melanogaster. Microsc Res Tech 62, 94–102. https://doi.org/10.1002/jemt.10357
Helfrich-Förster, C., 1998. Robust circadian rhythmicity of Drosophila melanogaster requires the presence of lateral neurons: a brain-behavioral study of disconnected mutants. J Comp Physiol A 182, 435–453. https://doi.org/10.1007/s003590050192
Helfrich-Förster, C., 1997. Development of pigment-dispersing hormone-immunoreactive neurons in the nervous system of Drosophila melanogaster. J Comp Neurol 380, 335–354. https://doi.org/10.1002/(sici)1096-9861(19970414)380:3<335::aid-cne4>3.0.co;2-3
Helfrich-Förster, C., 1995. The period clock gene is expressed in central nervous system neurons which also produce a neuropeptide that reveals the projections of circadian pacemaker cells within the brain of Drosophila melanogaster. Proceedings of the National Academy of Sciences 92, 612–616. https://doi.org/10.1073/pnas.92.2.612
Helfrich-Förster, C., Shafer, O.T., Wülbeck, C., Grieshaber, E., Rieger, D., Taghert, P., 2007. Development and morphology of the clock-gene-expressing lateral neurons of

Drosophila melanogaster. Journal of Comparative Neurology 500, 47–70. https://doi.org/10.1002/cne.21146
Helfrich-Förster, C., Winter, C., Hofbauer, A., Hall, J.C., Stanewsky, R., 2001. The circadian clock of fruit flies is blind after elimination of all known photoreceptors. Neuron 30, 249–261. https://doi.org/10.1016/s0896-6273(01)00277-x
Henrich, V.C., Rybczynski, R., Gilbert, L.I., 1999. Peptide hormones, steroid hormones, and puffs: mechanisms and models in insect development. Vitam Horm 55, 73–125. https://doi.org/10.1016/s0083-6729(08)60934-6
Hentze, J.L., Carlsson, M.A., Kondo, S., Nässel, D.R., Rewitz, K.F., 2015. The Neuropeptide Allatostatin A Regulates Metabolism and Feeding Decisions in Drosophila. Sci Rep 5, 11680. https://doi.org/10.1038/srep11680
Hermann-Luibl, C., Helfrich-Förster, C., 2015. Clock network in Drosophila. Curr Opin Insect Sci 7, 65–70. https://doi.org/10.1016/j.cois.2014.11.003
Hermann-Luibl, C., Yoshii, T., Senthilan, P.R., Dircksen, H., Helfrich-Förster, C., 2014. The Ion Transport Peptide Is a New Functional Clock Neuropeptide in the Fruit Fly Drosophila melanogaster. J. Neurosci. 34, 9522–9536. https://doi.org/10.1523/JNEUROSCI.0111-14.2014
Hewes, R., Truman, J., 1994. Steroid regulation of excitability in identified insect neurosecretory cells. J Neurosci 14, 1812–1819. https://doi.org/10.1523/JNEUROSCI.14-03-01812.1994
Hewes, R.S., Taghert, P.H., 2001. Neuropeptides and Neuropeptide Receptors in the Drosophila melanogaster Genome. Genome Res. 11, 1126–1142. https://doi.org/10.1101/gr.169901
Hewes, R.S., Truman, J.W., 1991. The roles of central and peripheral eclosion hormone release in the control of ecdysis behavior in Manduca sexta. J Comp Physiol A 168, 697–707. https://doi.org/10.1007/BF00224359
Hill, R.J., Billas, I.M.L., Bonneton, F., Graham, L.D., Lawrence, M.C., 2013. Ecdysone Receptors: From the Ashburner Model to Structural Biology. Annual Review of Entomology 58, 251–271. https://doi.org/10.1146/annurev-ento-120811-153610
Hökfelt, T., Millhorn, D., Seroogy, K., Tsuruo, Y., Ceccatelli, S., Lindh, B., Meister, B., Melander, T., Schalling, M., Bartfai, T., 1987. Coexistence of peptides with classical neurotransmitters. Experientia 43, 768–780. https://doi.org/10.1007/BF01945354
Horodyski, F.M., Ewer, J., Riddiford, L.M., Truman, J.W., 1993. Isolation, characterization and expression of the eclosion hormone gene of Drosophila melanogaster. European Journal of Biochemistry 215, 221–228. https://doi.org/10.1111/j.1432-1033.1993.tb18026.x
Hua, Y.-J., Jiang, R.-J., Koolman, J., 1997. Multiple control of ecdysone biosynthesis in blowfly larvae: Interaction of ecdysiotropins and ecdysiostatins. Archives of Insect Biochemistry and Physiology 35, 125–134. https://doi.org/10.1002/(SICI)1520-6327(1997)35:1/2<125::AID-ARCH11>3.0.CO;2-D
Huang, X., Warren, J.T., Gilbert, L.I., 2008. New players in the regulation of ecdysone biosynthesis. Journal of Genetics and Genomics 35, 1–10. https://doi.org/10.1016/S1673-8527(08)60001-6
Hückesfeld, S., Schlegel, P., Miroschnikow, A., Schoofs, A., Zinke, I., Haubrich, A.N., Schneider-Mizell, C.M., Truman, J.W., Fetter, R.D., Cardona, A., Pankratz, M.J., 2021. Unveiling the sensory and interneuronal pathways of the neuroendocrine connectome in Drosophila. eLife 10, e65745. https://doi.org/10.7554/eLife.65745
Hwang, R.Y., Zhong, L., Xu, Y., Johnson, T., Zhang, F., Deisseroth, K., Tracey, W.D., 2007. Nociceptive Neurons Protect Drosophila Larvae from Parasitoid Wasps. Current Biology 17, 2105–2116. https://doi.org/10.1016/j.cub.2007.11.029

Ikeya, T., Galic, M., Belawat, P., Nairz, K., Hafen, E., 2002. Nutrient-Dependent Expression of Insulin-like Peptides from Neuroendocrine Cells in the CNS Contributes to Growth Regulation in Drosophila. Current Biology 12, 1293–1300. https://doi.org/10.1016/S0960-9822(02)01043-6

Imambocus, B.N., Zhou, F., Formozov, A., Wittich, A., Tenedini, F.M., Hu, C., Sauter, K., Macarenhas Varela, E., Herédia, F., Casimiro, A.P., Macedo, A., Schlegel, P., Yang, C.-H., Miguel-Aliaga, I., Wiegert, J.S., Pankratz, M.J., Gontijo, A.M., Cardona, A., Soba, P., 2022. A neuropeptidergic circuit gates selective escape behavior of Drosophila larvae. Current Biology 32, 149-163.e8. https://doi.org/10.1016/j.cub.2021.10.069

Ito, K., Shinomiya, K., Ito, M., Armstrong, J.D., Boyan, G., Hartenstein, V., Harzsch, S., Heisenberg, M., Homberg, U., Jenett, A., Keshishian, H., Restifo, L.L., Rössler, W., Simpson, J.H., Strausfeld, N.J., Strauss, R., Vosshall, L., Insect Brain Name Working Group, 2014. A systematic nomenclature for the insect brain. Neuron 81, 755–765.

Iversen, A., Cazzamali, G., Williamson, M., Hauser, F., Grimmelikhuijzen, C.J.P., 2002. Molecular identification of the first insect ecdysis triggering hormone receptors. Biochem Biophys Res Commun 299, 924–931. https://doi.org/10.1016/s0006-291x(02)02798-5

Jaszczak, J.S., Wolpe, J.B., Bhandari, R., Jaszczak, R.G., Halme, A., 2016. Growth Coordination During Drosophila melanogaster Imaginal Disc Regeneration Is Mediated by Signaling Through the Relaxin Receptor Lgr3 in the Prothoracic Gland. Genetics 204, 703–709. https://doi.org/10.1534/genetics.116.193706

Jaumouillé, E., Koch, R., Nagoshi, E., 2021. Uncovering the Roles of Clocks and Neural Transmission in the Resilience of Drosophila Circadian Network. Front Physiol 12, 663339. https://doi.org/10.3389/fphys.2021.663339

Jékely, G., 2013. Global view of the evolution and diversity of metazoan neuropeptide signaling. Proceedings of the National Academy of Sciences 110, 8702–8707. https://doi.org/10.1073/pnas.1221833110

Jenett, A., Rubin, G.M., Ngo, T.-T.B., Shepherd, D., Murphy, C., Dionne, H., Pfeiffer, B.D., Cavallaro, A., Hall, D., Jeter, J., Iyer, N., Fetter, D., Hausenfluck, J.H., Peng, H., Trautman, E.T., Svirskas, R.R., Myers, E.W., Iwinski, Z.R., Aso, Y., DePasquale, G.M., Enos, A., Hulamm, P., Lam, S.C.B., Li, H.-H., Laverty, T.R., Long, F., Qu, L., Murphy, S.D., Rokicki, K., Safford, T., Shaw, K., Simpson, J.H., Sowell, A., Tae, S., Yu, Y., Zugates, C.T., 2012. A GAL4-driver line resource for Drosophila neurobiology. Cell Rep 2, 991–1001. https://doi.org/10.1016/j.celrep.2012.09.011

Jiang, C., Lamblin, A.-F.J., Steller, H., Thummel, C.S., 2000. A Steroid-Triggered Transcriptional Hierarchy Controls Salivary Gland Cell Death during Drosophila Metamorphosis. Molecular Cell 5, 445–455. https://doi.org/10.1016/S1097-2765(00)80439-6

Johard, H.A.D., Yoishii, T., Dircksen, H., Cusumano, P., Rouyer, F., Helfrich-Förster, C., Nässel, D.R., 2009. Peptidergic clock neurons in Drosophila: Ion transport peptide and short neuropeptide F in subsets of dorsal and ventral lateral neurons. Journal of Comparative Neurology 516, 59–73. https://doi.org/10.1002/cne.22099

Johnson, E.C., Shafer, O.T., Trigg, J.S., Park, J., Schooley, D.A., Dow, J.A., Taghert, P.H., 2005. A novel diuretic hormone receptor in Drosophila: evidence for conservation of CGRP signaling. Journal of Experimental Biology 208, 1239–1246. https://doi.org/10.1242/jeb.01529

Juarez-Carreño, S., Morante, J., Dominguez, M., n.d. Systemic signalling and local effectors in developmental stability, body symmetry, and size. Cell Stress 2, 340–361. https://doi.org/10.15698/cst2018.12.167

Jungreis, A.M., 1978. The composition of larval-pupal moulting fluid in the tobacco hornworm, Manduca sexta. Journal of Insect Physiology 24, 65–73. https://doi.org/10.1016/0022-1910(78)90013-6

Kadener, S., Menet, J.S., Schoer, R., Rosbash, M., 2008. Circadian transcription contributes to core period determination in Drosophila. PLoS Biol 6, e119. https://doi.org/10.1371/journal.pbio.0060119

Kadener, S., Stoleru, D., McDonald, M., Nawathean, P., Rosbash, M., 2007. Clockwork Orange is a transcriptional repressor and a new Drosophila circadian pacemaker component. Genes Dev 21, 1675–1686. https://doi.org/10.1101/gad.1552607

Kahsai, L., Kapan, N., Dircksen, H., Winther, A.M.E., Nässel, D.R., 2010. Metabolic stress responses in Drosophila are modulated by brain neurosecretory cells that produce multiple neuropeptides. PLoS One 5, e11480. https://doi.org/10.1371/journal.pone.0011480

Kalmus, H., 1935. Periodizität und autochronie (ideochronie) als zeitregelnde eigenschaffen der organismen. Biologia generalis 11, 93–114.

Kamiyama, T., Niwa, R., 2022. Transcriptional Regulators of Ecdysteroid Biosynthetic Enzymes and Their Roles in Insect Development. Frontiers in Physiology 13.

Kaneko, H., Head, L.M., Ling, J., Tang, X., Liu, Y., Hardin, P.E., Emery, P., Hamada, F.N., 2012. Circadian rhythm of temperature preference and its neural control in Drosophila. Curr Biol 22, 1851–1857. https://doi.org/10.1016/j.cub.2012.08.006

Kaneko, M., Hall, J.C., 2000. Neuroanatomy of cells expressing clock genes in Drosophila: transgenic manipulation of the period and timeless genes to mark the perikarya of circadian pacemaker neurons and their projections. J Comp Neurol 422, 66–94. https://doi.org/10.1002/(sici)1096-9861(20000619)422:1<66::aid-cne5>3.0.co;2-2

Kaneko, M., Helfrich-Förster, C., Hall, J.C., 1997. Spatial and temporal expression of the period and timeless genes in the developing nervous system of Drosophila: newly identified pacemaker candidates and novel features of clock gene product cycling. J Neurosci 17, 6745–6760. https://doi.org/10.1523/JNEUROSCI.17-17-06745.1997

Kataoka, H., Nagasawa, H., Isogai, A., Ishizaki, H., Suzuki, A., 1991. Prothoracicotropic hormone of the silkworm, Bombyx mori: amino acid sequence and dimeric structure. Agric Biol Chem 55, 73–86.

Kataoka, H., Troetschler, R.G., Kramer, S.J., Cesarin, B.J., Schooley, D.A., 1987. Isolation and primary structure of the eclosion hormone of the tobacco hornworm, Manduca sexta. Biochem Biophys Res Commun 146, 746–750. https://doi.org/10.1016/0006-291x(87)90592-4

Kawakami, A., Kataoka, H., Oka, T., Mizoguchi, A., Kimura-Kawakami, M., Adachi, T., Iwami, M., Nagasawa, H., Suzuki, A., Ishizaki, H., 1990. Molecular Cloning of the Bombyx mori Prothoracicotropic Hormone. Science 247, 1333–1335. https://doi.org/10.1126/science.2315701

Keene, A.C., Sprecher, S.G., 2012. Seeing the light: photobehavior in fruit fly larvae. Trends Neurosci 35, 104–110. https://doi.org/10.1016/j.tins.2011.11.003

Keister, M.L., 1948. The morphogenesis of the tracheal system of Sciara. Journal of Morphology 83, 373–423. https://doi.org/10.1002/jmor.1050830304

Kim, D.-H., Kim, Y.-J., Adams, M.E., 2018. Endocrine regulation of airway clearance in Drosophila. Proceedings of the National Academy of Sciences 115, 1535–1540. https://doi.org/10.1073/pnas.1717257115

Kim, S.M., Su, C.-Y., Wang, J.W., 2017. Neuromodulation of Innate Behaviors in Drosophila. Annual Review of Neuroscience 40, 327–348. https://doi.org/10.1146/annurev-neuro-072116-031558

Kim, Y.-J., Spalovská-Valachová, I., Cho, K.-H., Zitnanova, I., Park, Y., Adams, M.E., Žitňan, D., 2004. Corazonin receptor signaling in ecdysis initiation. Proceedings of the National Academy of Sciences 101, 6704–6709. https://doi.org/10.1073/pnas.0305291101

Kim, Y.-J., Žitňan, D., Cho, K.-H., Schooley, D.A., Mizoguchi, A., Adams, M.E., 2006a. Central peptidergic ensembles associated with organization of an innate behavior. Proceedings of the National Academy of Sciences 103, 14211–14216. https://doi.org/10.1073/pnas.0603459103

Kim, Y.-J., Žitňan, D., Galizia, C.G., Cho, K.-H., Adams, M.E., 2006b. A Command Chemical Triggers an Innate Behavior by Sequential Activation of Multiple Peptidergic Ensembles. Current Biology 16, 1395–1407. https://doi.org/10.1016/j.cub.2006.06.027

Kimura, K.I., Truman, J.W., 1990. Postmetamorphic cell death in the nervous and muscular systems of Drosophila melanogaster. J. Neurosci. 10, 403–411. https://doi.org/10.1523/JNEUROSCI.10-02-00403.1990

King, A.N., Sehgal, A., 2020. Molecular and circuit mechanisms mediating circadian clock output in the Drosophila brain. Eur J Neurosci 51, 268–281. https://doi.org/10.1111/ejn.14092

Kingan, T.G., Adams, M.E., 2000. Ecdysteroids regulate secretory competence in Inka cells. Journal of Experimental Biology 203, 3011–3018. https://doi.org/10.1242/jeb.203.19.3011

Kingan, T.G., Gray, W., Zitnan, D., Adams, M.E., 1997. Regulation of ecdysis-triggering hormone release by eclosion hormone. Journal of Experimental Biology 200, 3245–3256. https://doi.org/10.1242/jeb.200.24.3245

King-Jones, K., Thummel, C.S., 2005. Nuclear receptors — a perspective from Drosophila. Nat Rev Genet 6, 311–323. https://doi.org/10.1038/nrg1581

Klarsfeld, A., Malpel, S., Michard-Vanhée, C., Picot, M., Chélot, E., Rouyer, F., 2004. Novel features of cryptochrome-mediated photoreception in the brain circadian clock of Drosophila. J Neurosci 24, 1468–1477. https://doi.org/10.1523/JNEUROSCI.3661-03.2004

Kloss, B., Price, J.L., Saez, L., Blau, J., Rothenfluh, A., Wesley, C.S., Young, M.W., 1998. The Drosophila clock gene double-time encodes a protein closely related to human casein kinase Iepsilon. Cell 94, 97–107. https://doi.org/10.1016/s0092-8674(00)81225-8

Ko, H.W., Jiang, J., Edery, I., 2002. Role for Slimb in the degradation of Drosophila Period protein phosphorylated by Doubletime. Nature 420, 673–678. https://doi.org/10.1038/nature01272

Koelle, M.R., Talbot, W.S., Segraves, W.A., Bender, M.T., Cherbas, P., Hogness, D.S., 1991. The drosophila EcR gene encodes an ecdysone receptor, a new member of the steroid receptor superfamily. Cell 67, 59–77. https://doi.org/10.1016/0092-8674(91)90572-G

Kono, T., Nagasawa, H., Kataoka, H., Isogai, A., Fugo, H., Suzuki, A., 1990. Eclosion hormone of the silkworm Bombyx mori. Expression in Escherichia coli and location of disulfide bonds. FEBS Lett 263, 358–360. https://doi.org/10.1016/0014-5793(90)81413-i

Konopka, R.J., Benzer, S., 1971. Clock Mutants of Drosophila melanogaster. Proceedings of the National Academy of Sciences 68, 2112–2116. https://doi.org/10.1073/pnas.68.9.2112

Kopeć, S., 1922. Studies on the necessity of the brain for the inception of insect metamorphosis. The Biological Bulletin 42, 323–342. https://doi.org/10.2307/1536759

Kopec, S., 1917. Experiments on metamorphosis of insects. Bull. Int. Acad. Sci. Cracovie (B) 57–60.

Kreienkamp, H.-J., Larusson, H.J., Witte, I., Roeder, T., Birgül, N., Hönck, H.-H., Harder, S., Ellinghausen, G., Buck, F., Richter, D., 2002. Functional Annotation of Two Orphan G-protein-coupled Receptors, Drostar1 and -2, from Drosophila melanogaster and Their Ligands by Reverse Pharmacology*. Journal of Biological Chemistry 277, 39937–39943. https://doi.org/10.1074/jbc.M206931200

Kristensen, N.P., 1999. Phylogeny of endopteryygote insects, the most successful lineage of living organisms. European Journal of Entomology 96, 237–254.

Krüger, E., Mena, W., Lahr, E.C., Johnson, E.C., Ewer, J., 2015. Genetic analysis of Eclosion hormone action during Drosophila larval ecdysis. Development 142, 4279–4287. https://doi.org/10.1242/dev.126995

Kubrak, O., Koyama, T., Ahrentløv, N., Jensen, L., Malita, A., Naseem, M.T., Lassen, M., Nagy, S., Texada, M.J., Halberg, K.V., Rewitz, K., 2022. The gut hormone Allatostatin C/Somatostatin regulates food intake and metabolic homeostasis under nutrient stress. Nat Commun 13, 692. https://doi.org/10.1038/s41467-022-28268-x

Kunst, M., Hughes, M.E., Raccuglia, D., Felix, M., Li, M., Barnett, G., Duah, J., Nitabach, M.N., 2014. Calcitonin Gene-Related Peptide Neurons Mediate Sleep-Specific Circadian Output in Drosophila. Current Biology 24, 2652–2664. https://doi.org/10.1016/j.cub.2014.09.077

Kuo, C.T., Jan, L.Y., Jan, Y.N., 2005. Dendrite-specific remodeling of Drosophila sensory neurons requires matrix metalloproteases, ubiquitin-proteasome, and ecdysone signaling. Proc Natl Acad Sci U S A 102, 15230–15235. https://doi.org/10.1073/pnas.0507393102

Lamaze, A., Krätschmer, P., Chen, K.-F., Lowe, S., Jepson, J.E.C., 2018. A Wake-Promoting Circadian Output Circuit in Drosophila. Curr Biol 28, 3098-3105.e3. https://doi.org/10.1016/j.cub.2018.07.024

Langlais, K.K., Stewart, J.A., Morton, D.B., 2004. Preliminary characterization of two atypical soluble guanylyl cyclases in the central and peripheral nervous system of Drosophila melanogaster. J Exp Biol 207, 2323–2338. https://doi.org/10.1242/jeb.01025

Larsen, M.J., Burton, K.J., Zantello, M.R., Smith, V.G., Lowery, D.L., Kubiak, T.M., 2001. Type A Allatostatins from Drosophila melanogaster and Diplotera puncata Activate Two Drosophila Allatostatin Receptors, DAR-1 and DAR-2, Expressed in CHO Cells. Biochemical and Biophysical Research Communications 286, 895–901. https://doi.org/10.1006/bbrc.2001.5476

Lavrynenko, O., Rodenfels, J., Carvalho, M., Dye, N.A., Lafont, R., Eaton, S., Shevchenko, A., 2015. The ecdysteroidome of Drosophila: influence of diet and development. Development 142, 3758–3768. https://doi.org/10.1242/dev.124982

Leader, D.P., Krause, S.A., Pandit, A., Davies, S.A., Dow, J.A.T., 2018. FlyAtlas 2: a new version of the Drosophila melanogaster expression atlas with RNA-Seq, miRNA-Seq and sex-specific data. Nucleic Acids Research 46, D809–D815. https://doi.org/10.1093/nar/gkx976

Leander, M., Bass, C., Marchetti, K., Maynard, B.F., Wulff, J.P., Ons, S., Nichols, R., 2015. Cardiac contractility structure-activity relationship and ligand-receptor interactions; the discovery of unique and novel molecular switches in myosuppressin signaling. PLoS One 10, e0120492. https://doi.org/10.1371/journal.pone.0120492

Lee, C., Parikh, V., Itsukaichi, T., Bae, K., Edery, I., 1996. Resetting the Drosophila clock by photic regulation of PER and a PER-TIM complex. Science 271, 1740–1744. https://doi.org/10.1126/science.271.5256.1740

Lee, P.-T., Zirin, J., Kanca, O., Lin, W.-W., Schulze, K.L., Li-Kroeger, D., Tao, R., Devereaux, C., Hu, Y., Chung, V., Fang, Y., He, Y., Pan, H., Ge, M., Zuo, Z., Housden, B.E., Mohr, S.E., Yamamoto, S., Levis, R.W., Spradling, A.C., Perrimon, N., Bellen, H.J., 2018. A

gene-specific T2A-GAL4 library for Drosophila. eLife 7, e35574. https://doi.org/10.7554/eLife.35574
Lee, S.S., Ding, Y., Karapetians, N., Rivera-Perez, C., Noriega, F.G., Adams, M.E., 2017. Hormonal Signaling Cascade during an Early-Adult Critical Period Required for Courtship Memory Retention in Drosophila. Curr Biol 27, 2798-2809.e3. https://doi.org/10.1016/j.cub.2017.08.017
Levine, J.D., Funes, P., Dowse, H.B., Hall, J.C., 2002. Signal analysis of behavioral and molecular cycles. BMC Neurosci 3, 1. https://doi.org/10.1186/1471-2202-3-1
Li, M.-T., Cao, L.-H., Xiao, N., Tang, M., Deng, B., Yang, T., Yoshii, T., Luo, D.-G., 2018. Hub-organized parallel circuits of central circadian pacemaker neurons for visual photoentrainment in Drosophila. Nat Commun 9, 4247. https://doi.org/10.1038/s41467-018-06506-5
Liang, X., Holy, T.E., Taghert, P.H., 2017. A Series of Suppressive Signals within the Drosophila Circadian Neural Circuit Generates Sequential Daily Outputs. Neuron 94, 1173-1189.e4. https://doi.org/10.1016/j.neuron.2017.05.007
Lim, C., Chung, B.Y., Pitman, J.L., McGill, J.J., Pradhan, S., Lee, J., Keegan, K.P., Choe, J., Allada, R., 2007. clockwork orange encodes a transcriptional repressor important for circadian clock amplitude in Drosophila. Curr Biol 17, 1082–1089. https://doi.org/10.1016/j.cub.2007.05.039
Lin, X., Smagghe, G., 2019. Roles of the insulin signaling pathway in insect development and organ growth. Peptides 122, 169923. https://doi.org/10.1016/j.peptides.2018.02.001
Lindsley, D.L., 1968. Genetic variations of Drosophila melanogaster. Carnegie Inst. 627, 472.
Liu, Y., Liao, S., Veenstra, J.A., Nässel, D.R., 2016. Drosophila insulin-like peptide 1 (DILP1) is transiently expressed during non-feeding stages and reproductive dormancy. Sci Rep 6, 26620. https://doi.org/10.1038/srep26620
Locke, M., Huie, P., 1979. Apolysis and the turnover of plasma membrane plaques during cuticle formation in an insect. Tissue and Cell 11, 277–291.
Luo, C.-W., Dewey, E.M., Sudo, S., Ewer, J., Hsu, S.Y., Honegger, H.-W., Hsueh, A.J.W., 2005. Bursicon, the insect cuticle-hardening hormone, is a heterodimeric cystine knot protein that activates G protein-coupled receptor LGR2. Proceedings of the National Academy of Sciences 102, 2820–2825. https://doi.org/10.1073/pnas.0409916102
Ma, D., Przybylski, D., Abruzzi, K.C., Schlichting, M., Li, Q., Long, X., Rosbash, M., 2021. A transcriptomic taxonomy of Drosophila circadian neurons around the clock. eLife 10, e63056. https://doi.org/10.7554/eLife.63056
Macpherson, L.J., Zaharieva, E.E., Kearney, P.J., Alpert, M.H., Lin, T.-Y., Turan, Z., Lee, C.-H., Gallio, M., 2015. Dynamic labelling of neural connections in multiple colours by trans-synaptic fluorescence complementation. Nat Commun 6, 10024. https://doi.org/10.1038/ncomms10024
Malá, J., Granger, N.A., Sehnal, F., 1977. Control of prothoracic gland activity in larvae of Galleria mellonella. Journal of Insect Physiology 23, 309–316. https://doi.org/10.1016/0022-1910(77)90267-0
Mark, B., Bustos-González, L., Cascallares, G., Conejera, F., Ewer, J., 2021. The circadian clock gates Drosophila adult emergence by controlling the timecourse of metamorphosis. Proc Natl Acad Sci U S A 118, e2023249118. https://doi.org/10.1073/pnas.2023249118
Masuyama, K., Zhang, Y., Rao, Y., Wang, J.W., 2012. Mapping Neural Circuits with Activity-Dependent Nuclear Import of a Transcription Factor. J Neurogenet 26, 89–102. https://doi.org/10.3109/01677063.2011.642910
Matsumoto, A., Ukai-Tadenuma, M., Yamada, R.G., Houl, J., Uno, K.D., Kasukawa, T., Dauwalder, B., Itoh, T.Q., Takahashi, K., Ueda, R., Hardin, P.E., Tanimura, T., Ueda,

H.R., 2007. A functional genomics strategy reveals clockwork orange as a transcriptional regulator in the Drosophila circadian clock. Genes Dev 21, 1687–1700. https://doi.org/10.1101/gad.1552207

Mazzoni, E.O., Desplan, C., Blau, J., 2005. Circadian pacemaker neurons transmit and modulate visual information to control a rapid behavioral response. Neuron 45, 293–300. https://doi.org/10.1016/j.neuron.2004.12.038

McBrayer, Z., Ono, H., Shimell, M., Parvy, J.-P., Beckstead, R.B., Warren, J.T., Thummel, C.S., Dauphin-Villemant, C., Gilbert, L.I., O'Connor, M.B., 2007. Prothoracicotropic Hormone Regulates Developmental Timing and Body Size in Drosophila. Developmental Cell 13, 857–871. https://doi.org/10.1016/j.devcel.2007.11.003

McGuire, S.E., Le, P.T., Osborn, A.J., Matsumoto, K., Davis, R.L., 2003. Spatiotemporal rescue of memory dysfunction in Drosophila. Science 302, 1765–1768. https://doi.org/10.1126/science.1089035

McNabb, S.L., Baker, J.D., Agapite, J., Steller, H., Riddiford, L.M., Truman, J.W., 1997. Disruption of a Behavioral Sequence by Targeted Death of Peptidergic Neurons in Drosophila. Neuron 19, 813–823. https://doi.org/10.1016/S0896-6273(00)80963-0

McNabb, S.L., Truman, J.W., 2008. Light and peptidergic eclosion hormone neurons stimulate a rapid eclosion response that masks circadian emergence in Drosophila. J Exp Biol 211, 2263–2274. https://doi.org/10.1242/jeb.015818

Meiselman, M., Lee, S.S., Tran, R.-T., Dai, H., Ding, Y., Rivera-Perez, C., Wijesekera, T.P., Dauwalder, B., Noriega, F.G., Adams, M.E., 2017. Endocrine network essential for reproductive success in Drosophila melanogaster. Proceedings of the National Academy of Sciences 114, E3849–E3858. https://doi.org/10.1073/pnas.1620760114

Meiselman, M.R., Kingan, T.G., Adams, M.E., 2018. Stress-induced reproductive arrest in Drosophila occurs through ETH deficiency-mediated suppression of oogenesis and ovulation. BMC Biology 16, 18. https://doi.org/10.1186/s12915-018-0484-9

Meissner, G.W., Nern, A., Dorman, Z., DePasquale, G.M., Forster, K., Gibney, T., Hausenfluck, J.H., He, Y., Iyer, N.A., Jeter, J., Johnson, L., Johnston, R.M., Lee, K., Melton, B., Yarbrough, B., Zugates, C.T., Clements, J., Goina, C., Otsuna, H., Rokicki, K., Svirskas, R.R., Aso, Y., Card, G.M., Dickson, B.J., Ehrhardt, E., Goldammer, J., Ito, M., Kainmueller, D., Korff, W., Mais, L., Minegishi, R., Namiki, S., Rubin, G.M., Sterne, G.R., Wolff, T., Malkesman, O., FlyLight Project Team, 2023. A searchable image resource of Drosophila GAL4 driver expression patterns with single neuron resolution. eLife 12, e80660. https://doi.org/10.7554/eLife.80660

Menet, J.S., Abruzzi, K.C., Desrochers, J., Rodriguez, J., Rosbash, M., 2010. Dynamic PER repression mechanisms in the Drosophila circadian clock: from on-DNA to off-DNA. Genes Dev 24, 358–367. https://doi.org/10.1101/gad.1883910

Merritt, D.J., Whitington, P.M., 1995. Central projections of sensory neurons in the Drosophila embryo correlate with sensory modality, soma position, and proneural gene function. J. Neurosci. 15, 1755–1767. https://doi.org/10.1523/JNEUROSCI.15-03-01755.1995

Mertens, I., Meeusen, T., Huybrechts, R., De Loof, A., Schoofs, L., 2002. Characterization of the short neuropeptide F receptor from Drosophila melanogaster. Biochemical and Biophysical Research Communications 297, 1140–1148. https://doi.org/10.1016/S0006-291X(02)02351-3

Mesce, K.A., Fahrbach, S.E., 2002. Integration of Endocrine Signals That Regulate Insect Ecdysis. Frontiers in Neuroendocrinology 23, 179–199. https://doi.org/10.1006/frne.2002.0228

Millard, C.J., Watson, P.J., Fairall, L., Schwabe, J.W.R., 2013. An evolving understanding of nuclear receptor coregulator proteins. Journal of Molecular Endocrinology 51, T23–T36. https://doi.org/10.1530/JME-13-0227

Miller, J.E., Levine, R.B., 2006. Steroid hormone activation of wandering in the isolated nervous system of Manduca sexta. J Comp Physiol A Neuroethol Sens Neural Behav Physiol 192, 1049–1062. https://doi.org/10.1007/s00359-006-0143-4

Mirth, C., Truman, J.W., Riddiford, L.M., 2005. The Role of the Prothoracic Gland in Determining Critical Weight for Metamorphosis in Drosophila melanogaster. Current Biology 15, 1796–1807. https://doi.org/10.1016/j.cub.2005.09.017

Mirth, C.K., Riddiford, L.M., 2007. Size assessment and growth control: how adult size is determined in insects. BioEssays 29, 344–355. https://doi.org/10.1002/bies.20552

Moeller, M.E., Nagy, S., Gerlach, S.U., Soegaard, K.C., Danielsen, E.T., Texada, M.J., Rewitz, K.F., 2017. Warts Signaling Controls Organ and Body Growth through Regulation of Ecdysone. Current Biology 27, 1652-1659.e4. https://doi.org/10.1016/j.cub.2017.04.048

Mongeau, R., Miller, G.A., Chiang, E., Anderson, D.J., 2003. Neural correlates of competing fear behaviors evoked by an innately aversive stimulus. J Neurosci 23, 3855–3868. https://doi.org/10.1523/JNEUROSCI.23-09-03855.2003

Morioka, E., Matsumoto, A., Ikeda, M., 2012. Neuronal influence on peripheral circadian oscillators in pupal Drosophila prothoracic glands. Nat Commun 3, 909. https://doi.org/10.1038/ncomms1922

Morton, D.B., 2011. Behavioral responses to hypoxia and hyperoxia in Drosophila larvae. Fly 5, 119–125. https://doi.org/10.4161/fly.5.2.14284

Morton, D.B., 2004. Atypical Soluble Guanylyl Cyclases in Drosophila Can Function as Molecular Oxygen Sensors *. Journal of Biological Chemistry 279, 50651–50653. https://doi.org/10.1074/jbc.C400461200

Morton, D.B., Stewart, J.A., Langlais, K.K., Clemens-Grisham, R.A., Vermehren, A., 2008. Synaptic transmission in neurons that express the Drosophila atypical soluble guanylyl cyclases, Gyc-89Da and Gyc-89Db, is necessary for the successful completion of larval and adult ecdysis. J Exp Biol 211, 1645–1656. https://doi.org/10.1242/jeb.014472

Morton, D.B., Truman, J.W., 1988. The EGPs: the eclosion hormone and cyclic GMP-regulated phosphoproteins. II. Regulation of appearance by the steroid hormone 20-hydroxyecdysone in Manduca sexta. J. Neurosci. 8, 1338–1345. https://doi.org/10.1523/JNEUROSCI.08-04-01338.1988

Murad, A., Emery-Le, M., Emery, P., 2007. A subset of dorsal neurons modulates circadian behavior and light responses in Drosophila. Neuron 53, 689–701. https://doi.org/10.1016/j.neuron.2007.01.034

Myers, E.M., 2003. The Circadian Control of Eclosion. Chronobiology International 20, 775–794. https://doi.org/10.1081/CBI-120024214

Myers, E.M., Yu, J., Sehgal, A., 2003. Circadian Control of Eclosion: Interaction between a Central and Peripheral Clock in Drosophila melanogaster. Current Biology 13, 526–533. https://doi.org/10.1016/S0960-9822(03)00167-2

Myers, M.P., Wager-Smith, K., Rothenfluh-Hilfiker, A., Young, M.W., 1996. Light-induced degradation of TIMELESS and entrainment of the Drosophila circadian clock. Science 271, 1736–1740. https://doi.org/10.1126/science.271.5256.1736

Nakagawa, Y., Henrich, V.C., 2009. Arthropod nuclear receptors and their role in molting. The FEBS Journal 276, 6128–6157. https://doi.org/10.1111/j.1742-4658.2009.07347.x

Nässel, D.R., 2018. Substrates for Neuronal Cotransmission With Neuropeptides and Small Molecule Neurotransmitters in Drosophila. Frontiers in Cellular Neuroscience 12.

Nässel, D.R., 2009. Neuropeptide signaling near and far: how localized and timed is the action of neuropeptides in brain circuits? Invert Neurosci 9, 57. https://doi.org/10.1007/s10158-009-0090-1

Nässel, D.R., Broeck, J.V., 2016. Insulin/IGF signaling in Drosophila and other insects: factors that regulate production, release and post-release action of the insulin-like peptides. Cell. Mol. Life Sci. 73, 271–290. https://doi.org/10.1007/s00018-015-2063-3

Nässel, D.R., Pauls, D., Huetteroth, W., 2019. Neuropeptides in modulation of Drosophila behavior: how to get a grip on their pleiotropic actions. Curr Opin Insect Sci 36, 1–8. https://doi.org/10.1016/j.cois.2019.03.002

Nässel, D.R., Winther, Å.M.E., 2010. Drosophila neuropeptides in regulation of physiology and behavior. Progress in Neurobiology 92, 42–104. https://doi.org/10.1016/j.pneurobio.2010.04.010

Nässel, D.R., Zandawala, M., 2019. Recent advances in neuropeptide signaling in Drosophila, from genes to physiology and behavior. Progress in Neurobiology 179, 101607. https://doi.org/10.1016/j.pneurobio.2019.02.003

Neves, S.R., Ram, P.T., Iyengar, R., 2002. G Protein Pathways. Science 296, 1636–1639. https://doi.org/10.1126/science.1071550

Ni, J.D., Gurav, A.S., Liu, W., Ogunmowo, T.H., Hackbart, H., Elsheikh, A., Verdegaal, A.A., Montell, C., 2019. Differential regulation of the Drosophila sleep homeostat by circadian and arousal inputs. Elife 8, e40487. https://doi.org/10.7554/eLife.40487

Nicolaï, L.J.J., Ramaekers, A., Raemaekers, T., Drozdzecki, A., Mauss, A.S., Yan, J., Landgraf, M., Annaert, W., Hassan, B.A., 2010. Genetically encoded dendritic marker sheds light on neuronal connectivity in Drosophila. Proceedings of the National Academy of Sciences 107, 20553–20558. https://doi.org/10.1073/pnas.1010198107

Nitabach, M.N., Taghert, P.H., 2008. Organization of the Drosophila Circadian Control Circuit. Current Biology 18, R84–R93. https://doi.org/10.1016/j.cub.2007.11.061

Nusbaum, M.P., Blitz, D.M., Marder, E., 2017. Functional consequences of neuropeptide and small-molecule co-transmission. Nat Rev Neurosci 18, 389–403. https://doi.org/10.1038/nrn.2017.56

Okamoto, N., Yamanaka, N., Yagi, Y., Nishida, Y., Kataoka, H., O'Connor, M.B., Mizoguchi, A., 2009. A Fat Body-Derived IGF-like Peptide Regulates Postfeeding Growth in Drosophila. Developmental Cell 17, 885–891. https://doi.org/10.1016/j.devcel.2009.10.008

Ono, H., Rewitz, K.F., Shinoda, T., Itoyama, K., Petryk, A., Rybczynski, R., Jarcho, M., Warren, J.T., Marqués, G., Shimell, M.J., Gilbert, L.I., O'Connor, M.B., 2006. Spook and Spookier code for stage-specific components of the ecdysone biosynthetic pathway in Diptera. Developmental Biology 298, 555–570. https://doi.org/10.1016/j.ydbio.2006.07.023

Pan, X., Connacher, R.P., O'Connor, M.B., 2021. Control of the insect metamorphic transition by ecdysteroid production and secretion. Current Opinion in Insect Science, Insect genomics * Development and regulation 43, 11–20. https://doi.org/10.1016/j.cois.2020.09.004

Pan, X., O'Connor, M.B., 2019. Developmental Maturation: Drosophila AstA Signaling Provides a Kiss to Grow Up. Current Biology 29, R161–R164. https://doi.org/10.1016/j.cub.2019.01.040

Panda, S., Hogenesch, J.B., Kay, S.A., 2002. Circadian rhythms from flies to human. Nature 417, 329–335. https://doi.org/10.1038/417329a

Park, J.H., Schroeder, A.J., Helfrich-Förster, C., Jackson, F.R., Ewer, J., 2003. Targeted ablation of CCAP neuropeptide-containing neurons of Drosophila causes specific defects in execution and circadian timing of ecdysis behavior. Development 130, 2645–2656. https://doi.org/10.1242/dev.00503

Park, Y., Filippov, V., Gill, S.S., Adams, M.E., 2002. Deletion of the ecdysis-triggering hormone gene leads to lethal ecdysis deficiency. Development 129, 493–503. https://doi.org/10.1242/dev.129.2.493

Park, Y., Zitnan, D., Gill, S.S., Adams, M.E., 1999. Molecular cloning and biological activity of ecdysis-triggering hormones in Drosophila melanogaster. FEBS Lett 463, 133–138. https://doi.org/10.1016/s0014-5793(99)01622-1

Patke, A., Young, M.W., Axelrod, S., 2020. Molecular mechanisms and physiological importance of circadian rhythms. Nat Rev Mol Cell Biol 21, 67–84. https://doi.org/10.1038/s41580-019-0179-2

Peabody, N.C., Diao, F., Luan, H., Wang, H., Dewey, E.M., Honegger, H.-W., White, B.H., 2008. Bursicon Functions within the Drosophila CNS to Modulate Wing Expansion Behavior, Hormone Secretion, and Cell Death. J Neurosci 28, 14379–14391. https://doi.org/10.1523/JNEUROSCI.2842-08.2008

Perry, S., Goel, P., Tran, N.L., Pinales, C., Buser, C., Miller, D.L., Ganetzky, B., Dickman, D., 2020. Developmental arrest of Drosophila larvae elicits presynaptic depression and enables prolonged studies of neurodegeneration. Development 147, dev186312. https://doi.org/10.1242/dev.186312

Peters, R.S., Meusemann, K., Petersen, M., Mayer, C., Wilbrandt, J., Ziesmann, T., Donath, A., Kjer, K.M., Aspöck, U., Aspöck, H., Aberer, A., Stamatakis, A., Friedrich, F., Hünefeld, F., Niehuis, O., Beutel, R.G., Misof, B., 2014. The evolutionary history of holometabolous insects inferred from transcriptome-based phylogeny and comprehensive morphological data. BMC Evol Biol 14, 52. https://doi.org/10.1186/1471-2148-14-52

Petryk, A., Warren, J.T., Marqués, G., Jarcho, M.P., Gilbert, L.I., Kahler, J., Parvy, J.-P., Li, Y., Dauphin-Villemant, C., O'Connor, M.B., 2003. Shade is the Drosophila P450 enzyme that mediates the hydroxylation of ecdysone to the steroid insect molting hormone 20-hydroxyecdysone. Proceedings of the National Academy of Sciences 100, 13773–13778. https://doi.org/10.1073/pnas.2336088100

Pfeiffer, B.D., Ngo, T.-T.B., Hibbard, K.L., Murphy, C., Jenett, A., Truman, J.W., Rubin, G.M., 2010. Refinement of Tools for Targeted Gene Expression in Drosophila. Genetics 186, 735–755. https://doi.org/10.1534/genetics.110.119917

Picot, M., Klarsfeld, A., Chélot, E., Malpel, S., Rouyer, F., 2009. A role for blind DN2 clock neurons in temperature entrainment of the Drosophila larval brain. J Neurosci 29, 8312–8320. https://doi.org/10.1523/JNEUROSCI.0279-08.2009

Pittendrigh, C.S., 1967. Circadian systems. I. The driving oscillation and its assay in Drosophila pseudoobscura. Proceedings of the National Academy of Sciences 58, 1762–1767. https://doi.org/10.1073/pnas.58.4.1762

Pittendrigh, C.S., 1959. Daily rhythms as coupled oscillator systems and their relation to thermoperiodsm and photoperiodism. Phatoperiodism and Related Phenomena in Plants and Animals 475–505.

Pittendrigh, C.S., 1958. Perspective in the study of biological clocks. Perspectives in marine biology 239–268.

Pittendrigh, C.S., 1957. An oscillator model for biological clocks. Rhythmic and synthetic processes in growth 75–109.

Pittendrigh, C.S., 1954. On temperature independence in the clock system controlling emergence time in drosophila*†. Proceedings of the National Academy of Sciences 40, 1018–1029. https://doi.org/10.1073/pnas.40.10.1018

Pittendrigh, C.S., Daan, S., 1976. A functional analysis of circadian pacemakers in nocturnal rodents: V. Pacemaker structure: A clock for all seasons. Journal of comparative physiology 106, 333–355.

Pittendrigh, C.S., Skopik, S.D., 1970. Circadian Systems, V. The Driving Oscillation and the Temporal Sequence of Development*. Proceedings of the National Academy of Sciences 65, 500–507. https://doi.org/10.1073/pnas.65.3.500

Port, F., Chen, H.-M., Lee, T., Bullock, S.L., 2014. Optimized CRISPR/Cas tools for efficient germline and somatic genome engineering in Drosophila. Proceedings of the National Academy of Sciences 111, E2967–E2976. https://doi.org/10.1073/pnas.1405500111

Port, F., Strein, C., Stricker, M., Rauscher, B., Heigwer, F., Zhou, J., Beyersdörffer, C., Frei, J., Hess, A., Kern, K., Lange, L., Langner, N., Malamud, R., Pavlović, B., Rädecke, K., Schmitt, L., Voos, L., Valentini, E., Boutros, M., 2020. A large-scale resource for tissue-specific CRISPR mutagenesis in Drosophila. eLife 9, e53865. https://doi.org/10.7554/eLife.53865

Price, J.L., Blau, J., Rothenfluh, A., Abodeely, M., Kloss, B., Young, M.W., 1998. double-time Is a Novel Drosophila Clock Gene that Regulates PERIOD Protein Accumulation. Cell 94, 83–95. https://doi.org/10.1016/S0092-8674(00)81224-6

Qian, C.S., Kaplow, M., Lee, J.K., Grueber, W.B., 2018. Diversity of Internal Sensory Neuron Axon Projection Patterns Is Controlled by the POU-Domain Protein Pdm3 in Drosophila Larvae. J. Neurosci. 38, 2081–2093. https://doi.org/10.1523/JNEUROSCI.2125-17.2018

Qiu, J., Hardin, P.E., 1996. Developmental State and the Circadian Clock Interact to Influence the Timing of Eclosion in Drosophila melanogaster. J Biol Rhythms 11, 75–86. https://doi.org/10.1177/074873049601100108

Reddy, P., Zehring, W.A., Wheeler, D.A., Pirrotta, V., Hadfield, C., Hall, J.C., Rosbash, M., 1984. Molecular analysis of the period locus in Drosophila melanogaster and identification of a transcript involved in biological rhythms. Cell 38, 701–710. https://doi.org/10.1016/0092-8674(84)90265-4

Reinhard, N., Bertolini, E., Saito, A., Sekiguchi, M., Yoshii, T., Rieger, D., Helfrich-Förster, C., 2022a. The lateral posterior clock neurons of Drosophila melanogaster express three neuropeptides and have multiple connections within the circadian clock network and beyond. J Comp Neurol 530, 1507–1529. https://doi.org/10.1002/cne.25294

Reinhard, N., Fukuda, A., Manoli, G., Derksen, E., Saito, A., Möller, G., Sekiguchi, M., Rieger, D., Helfrich-Förster, C., Yoshii, T., Zandawala, M., 2023. Synaptic and peptidergic connectomes of the Drosophila circadian clock. https://doi.org/10.1101/2023.09.11.557222

Reinhard, N., Schubert, F.K., Bertolini, E., Hagedorn, N., Manoli, G., Sekiguchi, M., Yoshii, T., Rieger, D., Helfrich-Förster, C., 2022b. The Neuronal Circuit of the Dorsal Circadian Clock Neurons in Drosophila melanogaster. Front Physiol 13, 886432. https://doi.org/10.3389/fphys.2022.886432

Ren, Q., Awasaki, T., Huang, Y.-F., Liu, Z., Lee, T., 2016. Cell Class-Lineage Analysis Reveals Sexually Dimorphic Lineage Compositions in the Drosophila Brain. Current Biology 26, 2583–2593. https://doi.org/10.1016/j.cub.2016.07.086

Renn, S.C.P., Park, J.H., Rosbash, M., Hall, J.C., Taghert, P.H., 1999. A pdf Neuropeptide Gene Mutation and Ablation of PDF Neurons Each Cause Severe Abnormalities of Behavioral Circadian Rhythms in Drosophila. Cell 99, 791–802. https://doi.org/10.1016/S0092-8674(00)81676-1

Rewitz, K.F., O'Connor, M.B., Gilbert, L.I., 2007. Molecular evolution of the insect Halloween family of cytochrome P450s: Phylogeny, gene organization and functional conservation. Insect Biochemistry and Molecular Biology, Special Issue in Honour of Lynn M. Riddiford 37, 741–753. https://doi.org/10.1016/j.ibmb.2007.02.012

Rewitz, K.F., Rybczynski, R., Warren, J.T., Gilbert, L.I., 2006. Developmental expression of Manduca shade, the P450 mediating the final step in molting hormone synthesis.

Molecular and Cellular Endocrinology 247, 166–174. https://doi.org/10.1016/j.mce.2005.12.053
Rewitz, K.F., Yamanaka, N., Gilbert, L.I., O'Connor, M.B., 2009. The insect neuropeptide PTTH activates receptor tyrosine kinase torso to initiate metamorphosis. Science 326, 1403–1405. https://doi.org/10.1126/science.1176450
Rewitz, K.F., Yamanaka, N., O'Connor, M.B., 2013. Chapter One - Developmental Checkpoints and Feedback Circuits Time Insect Maturation, in: Shi, Y.-B. (Ed.), Current Topics in Developmental Biology, Animal Metamorphosis. Academic Press, pp. 1–33. https://doi.org/10.1016/B978-0-12-385979-2.00001-0
Richier, B., Michard-Vanhée, C., Lamouroux, A., Papin, C., Rouyer, F., 2008. The Clockwork Orange Drosophila Protein Functions as Both an Activator and a Repressor of Clock Gene Expression. J Biol Rhythms 23, 103–116. https://doi.org/10.1177/0748730407313817
Riddiford, L.M., 2009. Chapter 170 - Molting, in: Resh, V.H., Cardé, R.T. (Eds.), Encyclopedia of Insects (Second Edition). Academic Press, San Diego, pp. 649–654. https://doi.org/10.1016/B978-0-12-374144-8.00179-X
Riddiford, L.M., 1993. Hormone receptors and the regulation of insect metamorphosis. Receptor 3, 203–209.
Riddiford, L.M., Cherbas, P., Truman, J.W., 2000. Ecdysone receptors and their biological actions, in: Vitamins & Hormones. Academic Press, pp. 1–73. https://doi.org/10.1016/S0083-6729(00)60016-X
Rieger, D., Shafer, O.T., Tomioka, K., Helfrich-Förster, C., 2006. Functional analysis of circadian pacemaker neurons in Drosophila melanogaster. J Neurosci 26, 2531–2543. https://doi.org/10.1523/JNEUROSCI.1234-05.2006
Rieger, D., Stanewsky, R., Helfrich-Förster, C., 2003. Cryptochrome, Compound Eyes, Hofbauer-Buchner Eyelets, and Ocelli Play Different Roles in the Entrainment and Masking Pathway of the Locomotor Activity Rhythm in the Fruit Fly Drosophila Melanogaster. J Biol Rhythms 18, 377–391. https://doi.org/10.1177/0748730403256997
Robertson, F.W., 1966. The ecological genetics of growth in Drosophila 8. Adaptation to a New Diet. Genetics Research 8, 165–179. https://doi.org/10.1017/S0016672300010028
Robertson, J.L., Tsubouchi, A., Tracey, W.D., 2013. Larval Defense against Attack from Parasitoid Wasps Requires Nociceptive Neurons. PLOS ONE 8, e78704. https://doi.org/10.1371/journal.pone.0078704
Rothenfluh, A., Abodeely, M., Young, M.W., 2000. Short-period mutations of per affect a double-time-dependent step in the Drosophila circadian clock. Curr Biol 10, 1399–1402. https://doi.org/10.1016/s0960-9822(00)00786-7
Roy, S., Saha, T.T., Zou, Z., Raikhel, A.S., 2018. Regulatory Pathways Controlling Female Insect Reproduction. Annual Review of Entomology 63, 489–511. https://doi.org/10.1146/annurev-ento-020117-043258
Ruf, F., Fraunholz, M., Öchsner, K., Kaderschabek, J., Wegener, C., 2017. WEclMon – A simple and robust camera-based system to monitor Drosophila eclosion under optogenetic manipulation and natural conditions. PLOS ONE 12, e0180238. https://doi.org/10.1371/journal.pone.0180238
Ruf, F., Mitesser, O., Mungwa, S.T., Horn, M., Rieger, D., Hovestadt, T., Wegener, C., 2021. Natural Zeitgebers Under Temperate Conditions Cannot Compensate for the Loss of a Functional Circadian Clock in Timing of a Vital Behavior in Drosophila. J Biol Rhythms 36, 271–285. https://doi.org/10.1177/0748730421998112

Ruf, T., 1999. The Lomb-Scargle Periodogram in Biological Rhythm Research: Analysis of Incomplete and Unequally Spaced Time-Series. Biological Rhythm Research 30, 178–201. https://doi.org/10.1076/brhm.30.2.178.1422

Rutila, J.E., Suri, V., Le, M., So, W.V., Rosbash, M., Hall, J.C., 1998. CYCLE is a second bHLH-PAS clock protein essential for circadian rhythmicity and transcription of Drosophila period and timeless. Cell 93, 805–814. https://doi.org/10.1016/s0092-8674(00)81441-5

Sathyanarayanan, S., Zheng, X., Kumar, S., Chen, C.-H., Chen, D., Hay, B., Sehgal, A., 2008. Identification of novel genes involved in light-dependent CRY degradation through a genome-wide RNAi screen. Genes Dev 22, 1522–1533. https://doi.org/10.1101/gad.1652308

Saunders, D.S., 2002. Insect clocks. Elsevier.

Sawin, E.P., Harris, L.R., Campos, A.R., Sokolowski, M.B., 1994. Sensorimotor transformation from light reception to phototactic behavior inDrosophila larvae (Diptera: Drosophilidae). J Insect Behav 7, 553–567. https://doi.org/10.1007/BF02025449

Sawin-McCormack, E.P., Sokolowski, M.B., Campos, A.R., 1995. Characterization and Genetic Analysis of Drosophila Melanogaster Photobehavior During Larval Development. Journal of Neurogenetics 10, 119–135. https://doi.org/10.3109/01677069509083459

Schindelin, J., Arganda-Carreras, I., Frise, E., Kaynig, V., Longair, M., Pietzsch, T., Preibisch, S., Rueden, C., Saalfeld, S., Schmid, B., Tinevez, J.-Y., White, D.J., Hartenstein, V., Eliceiri, K., Tomancak, P., Cardona, A., 2012. Fiji: an open-source platform for biological-image analysis. Nat Methods 9, 676–682. https://doi.org/10.1038/nmeth.2019

Schlichting, M., Menegazzi, P., Lelito, K.R., Yao, Z., Buhl, E., Benetta, E.D., Bahle, A., Denike, J., Hodge, J.J., Helfrich-Förster, C., Shafer, O.T., 2016. A Neural Network Underlying Circadian Entrainment and Photoperiodic Adjustment of Sleep and Activity in Drosophila. J. Neurosci. 36, 9084–9096. https://doi.org/10.1523/JNEUROSCI.0992-16.2016

Schmid, B., Helfrich-Förster, C., Yoshii, T., 2011. A New ImageJ Plug-in "ActogramJ" for Chronobiological Analyses. J Biol Rhythms 26, 464–467. https://doi.org/10.1177/0748730411414264

Schubert, F.K., Hagedorn, N., Yoshii, T., Helfrich-Förster, C., Rieger, D., 2018. Neuroanatomical details of the lateral neurons of Drosophila melanogaster support their functional role in the circadian system. J Comp Neurol 526, 1209–1231. https://doi.org/10.1002/cne.24406

Schwartz, L.M., Truman, J.W., 1983. Hormonal control of rates of metamorphic development in the tobacco hornworm Manduca sexta. Developmental Biology 99, 103–114. https://doi.org/10.1016/0012-1606(83)90257-9

Schwedes, C.C., Carney, G.E., 2012. Ecdysone signaling in adult Drosophila melanogaster. J Insect Physiol 58, 293–302. https://doi.org/10.1016/j.jinsphys.2012.01.013

Scott, R.L., Diao, F., Silva, V., Park, S., Luan, H., Ewer, J., White, B.H., 2020. Non-canonical Eclosion Hormone-Expressing Cells Regulate Drosophila Ecdysis. iScience 23, 101108. https://doi.org/10.1016/j.isci.2020.101108

Sehgal, A., Price, J.L., Man, B., Young, M.W., 1994. Loss of Circadian Behavioral Rhythms and per RNA Oscillations in the Drosophila Mutant timeless. Science 263, 1603–1606. https://doi.org/10.1126/science.8128246

Sekiguchi, M., Inoue, K., Yang, T., Luo, D.-G., Yoshii, T., 2020. A Catalog of GAL4 Drivers for Labeling and Manipulating Circadian Clock Neurons in Drosophila melanogaster. J Biol Rhythms 35, 207–213. https://doi.org/10.1177/0748730419895154

Selcho, M., Millán, C., Palacios-Muñoz, A., Ruf, F., Ubillo, L., Chen, J., Bergmann, G., Ito, C., Silva, V., Wegener, C., Ewer, J., 2017. Central and peripheral clocks are coupled by a neuropeptide pathway in Drosophila. Nature Communications 8, 15563. https://doi.org/10.1038/ncomms15563

Selcho, M., Mühlbauer, B., Hensgen, R., Shiga, S., Wegener, C., Yasuyama, K., 2018. Anatomical characterization of PDF-tri neurons and peptidergic neurons associated with eclosion behavior in Drosophila. Journal of Comparative Neurology 526, 1307–1328. https://doi.org/10.1002/cne.24408

Senthilan, P.R., Grebler, R., Reinhard, N., Rieger, D., Helfrich-Förster, C., 2019. Role of Rhodopsins as Circadian Photoreceptors in the Drosophila melanogaster. Biology 8, 6. https://doi.org/10.3390/biology8010006

Sert, A., 2022. The effect of Allatostatin-C on eclosion rhythmicity and its role in eclosion behavior (BSc). Julius-Maximilians-Universität Würzburg.

Sgourakis, N.G., Bagos, P.G., Hamodrakas, S.J., 2005a. Prediction of the coupling specificity of GPCRs to four families of G-proteins using hidden Markov models and artificial neural networks. Bioinformatics 21, 4101–4106. https://doi.org/10.1093/bioinformatics/bti679

Sgourakis, N.G., Bagos, P.G., Papasaikas, P.K., Hamodrakas, S.J., 2005b. A method for the prediction of GPCRs coupling specificity to G-proteins using refined profile Hidden Markov Models. BMC Bioinformatics 6, 104. https://doi.org/10.1186/1471-2105-6-104

Shafer, O.T., Helfrich-Förster, C., Renn, S.C.P., Taghert, P.H., 2006. Reevaluation of Drosophila melanogaster's neuronal circadian pacemakers reveals new neuronal classes. Journal of Comparative Neurology 498, 180–193. https://doi.org/10.1002/cne.21021

Shimell, M., Pan, X., Martin, F.A., Ghosh, A.C., Leopold, P., O'Connor, M.B., Romero, N.M., 2018. Prothoracicotropic hormone modulates environmental adaptive plasticity through the control of developmental timing. Development 145, dev159699. https://doi.org/10.1242/dev.159699

Shimono, K., Fujimoto, A., Tsuyama, T., Yamamoto-Kochi, M., Sato, M., Hattori, Y., Sugimura, K., Usui, T., Kimura, K., Uemura, T., 2009. Multidendritic sensory neurons in the adult Drosophila abdomen: origins, dendritic morphology, and segment- and age-dependent programmed cell death. Neural Dev 4, 37. https://doi.org/10.1186/1749-8104-4-37

Siegmund, T., Korge, G., 2001. Innervation of the ring gland of Drosophila melanogaster. Journal of Comparative Neurology 431, 481–491. https://doi.org/10.1002/1096-9861(20010319)431:4<481::AID-CNE1084>3.0.CO;2-7

Simon, M.I., Strathmann, M.P., Gautam, N., 1991. Diversity of G proteins in signal transduction. Science 252, 802–808. https://doi.org/10.1126/science.1902986

Simpson, J.H., 2009. Chapter 3 Mapping and Manipulating Neural Circuits in the Fly Brain, in: Advances in Genetics, Genetic Dissection of Neural Circuits and Behavior. Academic Press, pp. 79–143. https://doi.org/10.1016/S0065-2660(09)65003-3

Singhania, A., Grueber, W.B., 2014. Development of the embryonic and larval peripheral nervous system of Drosophila. WIREs Developmental Biology 3, 193–210. https://doi.org/10.1002/wdev.135

Siwicki, K.K., Eastman, C., Petersen, G., Rosbash, M., Hall, J.C., 1988. Antibodies to the period gene product of Drosophila reveal diverse tissue distribution and rhythmic

changes in the visual system. Neuron 1, 141–150. https://doi.org/10.1016/0896-6273(88)90198-5
Skopik, S.D., Pittendrigh, C.S., 1967. Circadian systems, II. The oscillation in the individual Drosophila pupa; its independence of developmental stage. Proc Natl Acad Sci U S A 58, 1862–1869.
Sláma, K., 1980. Homeostatic functions of ecdysteroid in ecdysis and oviposition. Acta ent. bohem. 77, 145–168.
Small, S., Arnosti, D.N., 2020. Transcriptional Enhancers in Drosophila. Genetics 216, 1–26. https://doi.org/10.1534/genetics.120.301370
Snell, N.J., Fisher, J.D., Hartmann, G.G., Zolyomi, B., Talay, M., Barnea, G., 2022. Complex representation of taste quality by second-order gustatory neurons in Drosophila. Curr Biol 32, 3758-3772.e4. https://doi.org/10.1016/j.cub.2022.07.048
Song, B.J., Sharp, S.J., Rogulja, D., 2021. Daily rewiring of a neural circuit generates a predictive model of environmental light. Sci Adv 7, eabe4284. https://doi.org/10.1126/sciadv.abe4284
Sorkaç, A., Savva, Y.A., Savaş, D., Talay, M., Barnea, G., 2022. Circuit analysis reveals a neural pathway for light avoidance in Drosophila larvae. Nat Commun 13, 5274. https://doi.org/10.1038/s41467-022-33059-5
Stanewsky, R., Kaneko, M., Emery, P., Beretta, B., Wager-Smith, K., Kay, S.A., Rosbash, M., Hall, J.C., 1998. The cryb mutation identifies cryptochrome as a circadian photoreceptor in Drosophila. Cell 95, 681–692. https://doi.org/10.1016/s0092-8674(00)81638-4
Stieper, B.C., Kupershtok, M., Driscoll, M.V., Shingleton, A.W., 2008. Imaginal discs regulate developmental timing in Drosophila melanogaster. Developmental Biology 321, 18–26. https://doi.org/10.1016/j.ydbio.2008.05.556
Stoleru, D., Peng, Y., Agosto, J., Rosbash, M., 2004. Coupled oscillators control morning and evening locomotor behaviour of Drosophila. Nature 431, 862–868. https://doi.org/10.1038/nature02926
Sullivan, A.A., Thummel, C.S., 2003. Temporal profiles of nuclear receptor gene expression reveal coordinate transcriptional responses during Drosophila development. Mol Endocrinol 17, 2125–2137. https://doi.org/10.1210/me.2002-0430
Sullivan, L.F., Barker, M.S., Felix, P.C., Vuong, R.Q., White, B.H., 2020. Neuromodulation and the toolkit for behavioural evolution: can ecdysis shed light on an old problem? The FEBS Journal n/a. https://doi.org/10.1111/febs.16650
Sun, L., Jiang, R.H., Ye, W.J., Rosbash, M., Guo, F., 2022. Recurrent circadian circuitry regulates central brain activity to maintain sleep. Neuron 110, 2139-2154.e5. https://doi.org/10.1016/j.neuron.2022.04.010
Taghert, P.H., Nitabach, M.N., 2012. Peptide Neuromodulation in Invertebrate Model Systems. Neuron 76, 82–97. https://doi.org/10.1016/j.neuron.2012.08.035
Takahashi, J.S., 2017. Transcriptional architecture of the mammalian circadian clock. Nat Rev Genet 18, 164–179. https://doi.org/10.1038/nrg.2016.150
Talay, M., Richman, E.B., Snell, N.J., Hartmann, G.G., Fisher, J.D., Sorkaç, A., Santoyo, J.F., Chou-Freed, C., Nair, N., Johnson, M., Szymanski, J.R., Barnea, G., 2017. Transsynaptic Mapping of Second-Order Taste Neurons in Flies by trans-Tango. Neuron 96, 783-795.e4. https://doi.org/10.1016/j.neuron.2017.10.011
Talbot, W.S., Swyryd, E.A., Hogness, D.S., 1993. Drosophila tissues with different metamorphic responses to ecdysone express different ecdysone receptor isoforms. Cell 73, 1323–1337. https://doi.org/10.1016/0092-8674(93)90359-x

Tanaka, K., Watari, Y., 2003. Adult eclosion timing of the onion fly, Delia antiqua, in response to daily cycles of temperature at different soil depths. Naturwissenschaften 90, 76–79. https://doi.org/10.1007/s00114-002-0390-3

Tanoue, S., Krishnan, P., Krishnan, B., Dryer, S.E., Hardin, P.E., 2004. Circadian clocks in antennal neurons are necessary and sufficient for olfaction rhythms in Drosophila. Curr Biol 14, 638–649. https://doi.org/10.1016/j.cub.2004.04.009

Telford, M.J., Bourlat, S.J., Economou, A., Papillon, D., Rota-Stabelli, O., 2008. The evolution of the Ecdysozoa. Philosophical Transactions of the Royal Society B: Biological Sciences. https://doi.org/10.1098/rstb.2007.2243

Texada, M.J., Koyama, T., Rewitz, K., 2020. Regulation of Body Size and Growth Control. Genetics 216, 269–313. https://doi.org/10.1534/genetics.120.303095

Texada, M.J., Malita, A., Christensen, C.F., Dall, K.B., Faergeman, N.J., Nagy, S., Halberg, K.A., Rewitz, K., 2019. Autophagy-Mediated Cholesterol Trafficking Controls Steroid Production. Developmental Cell 48, 659-671.e4. https://doi.org/10.1016/j.devcel.2019.01.007

Thummel, C.S., 2002. Ecdysone-regulated puff genes 2000. Insect Biochemistry and Molecular Biology 32, 113–120. https://doi.org/10.1016/S0965-1748(01)00112-6

Thummel, C.S., 1996. Flies on steroids — Drosophila metamorphosis and the mechanisms of steroid hormone action. Trends in Genetics 12, 306–310. https://doi.org/10.1016/0168-9525(96)10032-9

Top, D., Young, M.W., 2018. Coordination between Differentially Regulated Circadian Clocks Generates Rhythmic Behavior. Cold Spring Harb Perspect Biol 10, a033589. https://doi.org/10.1101/cshperspect.a033589

Truman, J.W., 2005. Hormonal Control of Insect Ecdysis: Endocrine Cascades for Coordinating Behavior with Physiology, in: Vitamins & Hormones, Insect Hormones. Academic Press, pp. 1–30. https://doi.org/10.1016/S0083-6729(05)73001-6

Truman, J.W., 1992. The eclosion hormone system of insects. Prog Brain Res 92, 361–374. https://doi.org/10.1016/s0079-6123(08)61189-9

Truman, J.W., 1984. Physiological Aspects of the Two Oscillators That Regulate the Timing of Eclosion in Moths, in: Ciba Foundation Symposium 104 - Photoperiodic Regulation of Insect and Molluscan Hormones. John Wiley & Sons, Ltd, pp. 221–239. https://doi.org/10.1002/9780470720851.ch14

Truman, J.W., 1981. Interaction Between Ecdysteroid, Eclosion Hormone, and Bursicon Titers inManduca sexta1. American Zoologist 21, 655–661. https://doi.org/10.1093/icb/21.3.655

Truman, J.W., 1972. Physiology of Insect Rhythms: I. Circadian Organization of the Endocrine Events Underlying the Moulting Cycle of Larval Tobacco Hornworms. Journal of Experimental Biology 57, 805–820. https://doi.org/10.1242/jeb.57.3.805

Truman, J.W., 1971. Physiology of Insect Ecdysis: I. The Eclosion Behaviour of Saturniid Moths and Its Hormonal Release. Journal of Experimental Biology 54, 805–814. https://doi.org/10.1242/jeb.54.3.805

Truman, J.W., Riddiford, L.M., 1974. Physiology of Insect Rhythms: III. The Temporal Organization of the Endocrine Events Underlying Pupation of the Tobacco Hornworm. Journal of Experimental Biology 60, 371–382. https://doi.org/10.1242/jeb.60.2.371

Truman, J.W., Riddiford, L.M., 1970. Neuroendocrine Control of Ecdysis in Silkmoths. Science 167, 1624–1626. https://doi.org/10.1126/science.167.3925.1624

Truman, J.W., Rountree, D.B., Reiss, S.E., Schwartz, L.M., 1983. Ecdysteroids regulate the release and action of eclosion hormone in the tobacco hornworm, Manduca sexta (L.). Journal of Insect Physiology 29, 895–900. https://doi.org/10.1016/0022-1910(83)90052-5

Vafopoulou, X., Steel, C.G.H., 1996. Circadian Regulation of a Daily Rhythm of Release of Prothoracicotropic Hormone from the Brain-Retrocerebral Complex ofRhodnius prolixus(Hemiptera) during Larval-Adult Development. General and Comparative Endocrinology 102, 123–129. https://doi.org/10.1006/gcen.1996.0053

Vallejo, D.M., Juarez-Carreño, S., Bolivar, J., Morante, J., Dominguez, M., 2015. A brain circuit that synchronizes growth and maturation revealed through Dilp8 binding to Lgr3. Science 350, aac6767. https://doi.org/10.1126/science.aac6767

van den Pol, A.N., 2012. Neuropeptide Transmission in Brain Circuits. Neuron 76, 98–115. https://doi.org/10.1016/j.neuron.2012.09.014

Vollborn, L., 2011. Ein interner Promotor im Drosophila-Gen Start1, dem Homolog von MLN64, generiert ein StAR-homologes Protein. Mensch & Buch.

Wang, J.W., Wong, A.M., Flores, J., Vosshall, L.B., Axel, R., 2003. Two-photon calcium imaging reveals an odor-evoked map of activity in the fly brain. Cell 112, 271–282. https://doi.org/10.1016/s0092-8674(03)00004-7

Wang, K.H., Majewska, A., Schummers, J., Farley, B., Hu, C., Sur, M., Tonegawa, S., 2006. In Vivo Two-Photon Imaging Reveals a Role of Arc in Enhancing Orientation Specificity in Visual Cortex. Cell 126, 389–402. https://doi.org/10.1016/j.cell.2006.06.038

Warren, J.T., Gilbert, L.I., 1986. Ecdysone metabolism and distribution during the pupal-adult development of Manduca sexta. Insect Biochemistry 16, 65–82. https://doi.org/10.1016/0020-1790(86)90080-6

Warren, J.T., Yerushalmi, Y., Shimell, M.J., O'Connor, M.B., Restifo, L., Gilbert, L.I., 2006. Discrete Pulses of Molting Hormone, 20-Hydroxyecdysone, During Late Larval Development of Drosophila melanogaster: Correlations With Changes in Gene Activity. Dev Dyn 235, 315–326. https://doi.org/10.1002/dvdy.20626

Weeks, J.C., Truman, J.W., 1984. Neural organization of peptide-activated ecdysis behaviors during the metamorphosis of Manduca sexta. J. Comp. Physiol. 155, 407–422. https://doi.org/10.1007/BF00610594

Wegman, L.J., Ainsley, J.A., Johnson, W.A., 2010. Developmental timing of a sensory-mediated larval surfacing behavior correlates with cessation of feeding and determination of final adult size. Developmental Biology 345, 170–179. https://doi.org/10.1016/j.ydbio.2010.07.004

Weis, W.I., Kobilka, B.K., 2018. The Molecular Basis of G Protein–Coupled Receptor Activation. Annual Review of Biochemistry 87, 897–919. https://doi.org/10.1146/annurev-biochem-060614-033910

Weiss, R., Bartok, O., Mezan, S., Malka, Y., Kadener, S., 2014. Synergistic interactions between the molecular and neuronal circadian networks drive robust behavioral circadian rhythms in Drosophila melanogaster. PLoS Genet 10, e1004252. https://doi.org/10.1371/journal.pgen.1004252

Westbrook, A.L., Bollenbacher, W.E., 1990. The development of identified neurosecretory cells in the tobacco hornworm, Manduca sexta. Developmental Biology 140, 291–299. https://doi.org/10.1016/0012-1606(90)90079-X

Wettschureck, N., Offermanns, S., 2005. Mammalian G Proteins and Their Cell Type Specific Functions. Physiological Reviews 85, 1159–1204. https://doi.org/10.1152/physrev.00003.2005

Wheeler, D.A., Hamblen-Coyle, M.J., Dushay, M.S., Hall, J.C., 1993. Behavior in light-dark cycles of Drosophila mutants that are arrhythmic, blind, or both. J Biol Rhythms 8, 67–94. https://doi.org/10.1177/074873049300800106

White, B.H., Ewer, J., 2014. Neural and Hormonal Control of Postecdysial Behaviors in Insects. Annual Review of Entomology 59, 363–381. https://doi.org/10.1146/annurev-ento-011613-162028

Xiang, Y., Yuan, Q., Vogt, N., Looger, L.L., Jan, L.Y., Jan, Y.N., 2010. Light-avoidance-mediating photoreceptors tile the Drosophila larval body wall. Nature 468, 921–926. https://doi.org/10.1038/nature09576

Yamagata, N., Hiroi, M., Kondo, S., Abe, A., Tanimoto, H., 2016. Suppression of Dopamine Neurons Mediates Reward. PLOS Biology 14, e1002586. https://doi.org/10.1371/journal.pbio.1002586

Yamanaka, N., Hua, Y.-J., Mizoguchi, A., Watanabe, K., Niwa, R., Tanaka, Y., Kataoka, H., 2005. Identification of a novel prothoracicostatic hormone and its receptor in the silkworm Bombyx mori. J Biol Chem 280, 14684–14690. https://doi.org/10.1074/jbc.M500308200

Yamanaka, N., Hua, Y.-J., Roller, L., Spalovská-Valachová, I., Mizoguchi, A., Kataoka, H., Tanaka, Y., 2010. Bombyx prothoracicostatic peptides activate the sex peptide receptor to regulate ecdysteroid biosynthesis. Proceedings of the National Academy of Sciences 107, 2060–2065. https://doi.org/10.1073/pnas.0907471107

Yamanaka, N., Marqués, G., O'Connor, M.B., 2015. Vesicle-Mediated Steroid Hormone Secretion in Drosophila melanogaster. Cell 163, 907–919. https://doi.org/10.1016/j.cell.2015.10.022

Yamanaka, N., Romero, N.M., Martin, F.A., Rewitz, K.F., Sun, M., O'Connor, M.B., Léopold, P., 2013. Neuroendocrine Control of Drosophila Larval Light Preference. Science 341, 1113–1116. https://doi.org/10.1126/science.1241210

Yamanaka, N., Žitňan, D., Kim, Y.-J., Adams, M.E., Hua, Y.-J., Suzuki, Y., Suzuki, M., Suzuki, A., Satake, H., Mizoguchi, A., Asaoka, K., Tanaka, Y., Kataoka, H., 2006. Regulation of insect steroid hormone biosynthesis by innervating peptidergic neurons. Proceedings of the National Academy of Sciences 103, 8622–8627. https://doi.org/10.1073/pnas.0511196103

Yao, Z., Shafer, O.T., 2014. The Drosophila circadian clock is a variably coupled network of multiple peptidergic units. Science 343, 1516–1520. https://doi.org/10.1126/science.1251285

Yasuda, R., Nimchinsky, E.A., Scheuss, V., Pologruto, T.A., Oertner, T.G., Sabatini, B.L., Svoboda, K., 2004. Imaging calcium concentration dynamics in small neuronal compartments. Sci STKE 2004, pl5. https://doi.org/10.1126/stke.2192004pl5

Yasunaga, K., Kanamori, T., Morikawa, R., Suzuki, E., Emoto, K., 2010. Dendrite reshaping of adult Drosophila sensory neurons requires matrix metalloproteinase-mediated modification of the basement membranes. Dev Cell 18, 621–632. https://doi.org/10.1016/j.devcel.2010.02.010

Yoshii, T., Heshiki, Y., Ibuki-Ishibashi, T., Matsumoto, A., Tanimura, T., Tomioka, K., 2005. Temperature cycles drive Drosophila circadian oscillation in constant light that otherwise induces behavioural arrhythmicity. Eur J Neurosci 22, 1176–1184. https://doi.org/10.1111/j.1460-9568.2005.04295.x

Yoshii, T., Sakamoto, M., Tomioka, K., 2002. A temperature-dependent timing mechanism is involved in the circadian system that drives locomotor rhythms in the fruit fly Drosophila melanogaster. Zoolog Sci 19, 841–850. https://doi.org/10.2108/zsj.19.841

Yoshiyama, T., Namiki, T., Mita, K., Kataoka, H., Niwa, R., 2006. Neverland is an evolutionally conserved Rieske-domain protein that is essential for ecdysone synthesis and insect growth. Development 133, 2565–2574. https://doi.org/10.1242/dev.02428

Yu, W., Zheng, H., Price, J.L., Hardin, P.E., 2009. DOUBLETIME plays a noncatalytic role to mediate CLOCK phosphorylation and repress CLOCK-dependent transcription within

the Drosophila circadian clock. Mol Cell Biol 29, 1452–1458. https://doi.org/10.1128/MCB.01777-08

Zehring, W.A., Wheeler, D.A., Reddy, P., Konopka, R.J., Kyriacou, C.P., Rosbash, M., Hall, J.C., 1984. P-element transformation with period locus DNA restores rhythmicity to mutant, arrhythmic Drosophila melanogaster. Cell 39, 369–376. https://doi.org/10.1016/0092-8674(84)90015-1

Zhan, Y.P., Liu, L., Zhu, Y., 2016. Taotie neurons regulate appetite in Drosophila. Nat Commun 7, 13633. https://doi.org/10.1038/ncomms13633

Zhang, L., Chung, B.Y., Lear, B.C., Kilman, V.L., Liu, Y., Mahesh, G., Meissner, R.-A., Hardin, P.E., Allada, R., 2010. DN1(p) circadian neurons coordinate acute light and PDF inputs to produce robust daily behavior in Drosophila. Curr Biol 20, 591–599. https://doi.org/10.1016/j.cub.2010.02.056

Zhang, Y., Liu, Y., Bilodeau-Wentworth, D., Hardin, P.E., Emery, P., 2010. Light and Temperature Control the Contribution of Specific DN1 Neurons to Drosophila Circadian Behavior. Current Biology 20, 600–605. https://doi.org/10.1016/j.cub.2010.02.044

Zhao, J., Kilman, V.L., Keegan, K.P., Peng, Y., Emery, P., Rosbash, M., Allada, R., 2003. Drosophila clock can generate ectopic circadian clocks. Cell 113, 755–766. https://doi.org/10.1016/s0092-8674(03)00400-8

Zhao, Y., Araki, S., Wu, J., Teramoto, T., Chang, Y.-F., Nakano, M., Abdelfattah, A.S., Fujiwara, M., Ishihara, T., Nagai, T., Campbell, R.E., 2011. An Expanded Palette of Genetically Encoded Ca2+ Indicators. Science 333, 1888–1891. https://doi.org/10.1126/science.1208592

Zielinski, T., Moore, A.M., Troup, E., Halliday, K.J., Millar, A.J., 2014. Strengths and Limitations of Period Estimation Methods for Circadian Data. PLOS ONE 9, e96462. https://doi.org/10.1371/journal.pone.0096462

Zimmerman, W., 1971. Some photophysiological aspects of circadian rhythmicity in Drosophila. Biochronometry 381–391.

Zimmerman, W.F., Pittendrigh, C.S., Pavlidis, T., 1968. Temperature compensation of the circadian oscillation in Drosophila pseudoobscura and its entrainment by temperature cycles. Journal of Insect Physiology 14, 669–684. https://doi.org/10.1016/0022-1910(68)90226-6

Zitnan, D., Adams, M.E., 2012. 7 - Neuroendocrine Regulation of Ecdysis, in: Gilbert, L.I. (Ed.), Insect Endocrinology. Academic Press, San Diego, pp. 253–309. https://doi.org/10.1016/B978-0-12-384749-2.10007-X

Zitnan, D., Adams, M.E., 2000. Excitatory and inhibitory roles of central ganglia in initiation of the insect ecdysis behavioural sequence. Journal of Experimental Biology 203, 1329–1340. https://doi.org/10.1242/jeb.203.8.1329

Zitnan, D., Hollar, L., Spalovská, I., Takác, P., Zitnanová, I., Gill, S.S., Adams, M.E., 2002. Molecular cloning and function of ecdysis-triggering hormones in the silkworm Bombyx mori. J Exp Biol 205, 3459–3473. https://doi.org/10.1242/jeb.205.22.3459

Zitnan, D., Kim, Y.-J., Žitňanová, I., Roller, L., Adams, M.E., 2007. Complex steroid–peptide–receptor cascade controls insect ecdysis. General and Comparative Endocrinology, Proceedings of the 23rd Conference of European Comparative Endocrinologists: Part 2 153, 88–96. https://doi.org/10.1016/j.ygcen.2007.04.002

Zitnan, D, Kim, Y.-J., Zitnanová, I., Roller, L., Adams, M.E., 2007. Complex steroid-peptide-receptor cascade controls insect ecdysis. Gen. Comp. Endocrinol. 153, 88–96. https://doi.org/10.1016/j.ygcen.2007.04.002

Zitnan, D., Kingan, T.G., Hermesman, J.L., Adams, M.E., 1996. Identification of Ecdysis-Triggering Hormone from an Epitracheal Endocrine System. Science 271, 88–91. https://doi.org/10.1126/science.271.5245.88

Publications

Habenstein, J.*, **Amini, E.***, Grübel, K., El Jundi, B., Rössler, W., 2020. The brain of *Cataglyphis* ants: Neuronal organization and visual projections. J. Comp. Neurol. 528, 3479–3506. https://doi.org/10.1002/cne.24934

Cavieres-Lepe, J.*, **Amini, E.***, Nässel, R.D., Stanewsky, R., Wegener, C., Ewer, J., 2023. Timed receptor tyrosine kinase signaling couples the central and the peripheral circadian clock in *Drosophila*. Under revision. BioRxiv. https://doi.org/10.1101/2023.05.14.540706

* Shared first-authorship

Acknowledgments

Here I want to thank many people without whom I could have never accomplished this thesis. I want to thank my great mentor Prof. Dr. Christian Wegener who was outstandingly patient and supportive. Without his guidance and his honest comments, I could have never grown up as a young scientist. I want to thank my second supervisor, Prof. Dr. John Ewer, and my third supervisor Prof. Dr. Keram Pfeifer who also guided me through the projects. Dr. Meet Zandawala and Prof. Dr. Ralf Stanewsky were not my supervisors but their scientific insights and providing me with the necessary reagents and equipment were undeniably important in improving my research. I would like to thank Mr. Konrad Öchsner and Mr. Oliver Schön from the Biocenter workshop who helped with their creative ideas and technical support in building up the setups made for my research. Also, I thank Mr. Andreas Eckart for writing the Arduino program used in our functional connectivity setup.

Also, I want to thank every nice person working at the Chair of Neurobiology and Genetics of the JMU such as principal investigators, lab technicians (Gertrud Gramlich, Susanne Klühspies, Sylwia Febocolon, Maria Gallant, and Barbara Mühlbauer), and Ph.D. or master students who helped me in this project. My special thanks to our beloved secretary Ms. Irina Wenzel who patiently and single-handedly fought my bureaucratic problems. From the students, I especially thank Ms. Sina Grimm, Mr. Abdullah Sert, Mr. Emanuel Schirm, Ms. Milena Sekulic, and Mr. Alexander Veh who were great helping hands.

I thank other kind academic people who also provided me with fly lines or helped in any way such as Prof. Dr. Yi Rao, Dr. Bowen Deng (chemmoconnectomic flies), Dr. Matthias Schlichting (ARG-Luc flies), Dr. Carlotta Martelli (functional connectivity), Prof. Dr. Peter Soba (syb-GRASP, C4da, and v'Td neurons), Dr. Sebastian Cachero (BAcTrace), Dr. Sebastian Hückesfeld (v'Td neurons), Dr. Francisco A Martin (PTTHn), Prof. Dr. Dick Nässel (PTTH antibody), and Dr. Takashi Koyama (AstC flies).

I would like to thank the Graduate School of Life Sciences (GSLS) of the University of Würzburg, especially Dr. Stephan Schröder-Köhne for supporting this PhD project and providing me with guidelines and necessities. And special thanks to the Deutsche Forschungsgemeinschaft initiative (DFG WE 2652/7-1) for funding this project for more than five years.

In the end, I want to thank my parents who have been supportive (financially and emotionally) throughout my entire life. Especially my late father, who never had the chance to see me finish my Doctorate thesis. My wife was with me every step of the way, helped me, and tolerated my absence while I was working in the laboratory even at late night or on the weekends and holidays.

Appendix

1. Downregulation of *Ptth* in the fat body

Ptth is *expressed* in adult fly fat body (Thomas Roeder, personal communication). To check if PTTH from fat body is required for rhythmic eclosion RNAi was used. Therefore, *Ptth* was knocked down (*UAS-Ptth^{i} (KK)*) in the pharates adults using two specific fat body driver lines *NP5253-Gal4* and *lsp-Gal4*. The *NP5253> Ptth^{i} (KK)* and *lsp> Ptth^{i} (KK)* eclosion assays showed rhythmic eclosion, similar to their controls (Figure 6.1). All experimented groups showed rhythmic RI (RI > 0.03), as well as rhythmic LS, and eJTK values (Table 6.1). These results suggested that PTTH from fat body was not involved in eclosion gating.

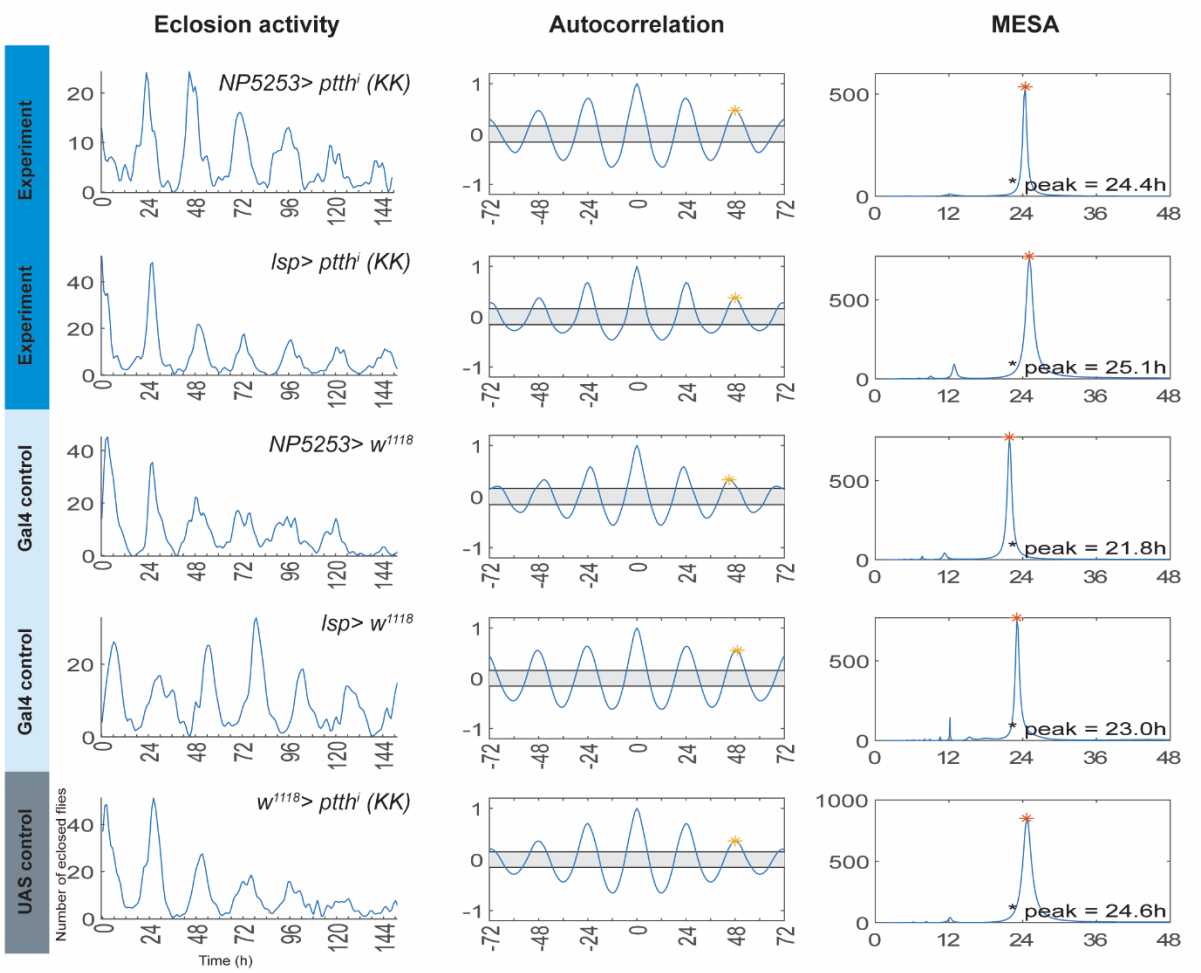

Figure 6.1. Knock-down of *ptth* in the fat body does not cause arrhythmic eclosion. The *Ptth* gene downregulation using two lines specific for the adult fat body (*lsp-Gal4* and *NP5253-Gal4*) does not lead to arrhythmic eclosion pattern. Neither the experiments (*lsp> Ptth (KK)* and *NP5253> Ptth (KK)*) nor Gal4 (*lsp> w^{1118}* and *NP5253> w^{1118}*) and UAS (*w^{1118}> Ptth^{i} (KK)*) controls show an arrhythmic eclosion pattern. The Autocorrelation and MESA, LS and eJTK analysis (Table 6.1) confirm this rhythmicity.

Table 6.1. Rhythmicity analysis of eclosion in flies with downregulated *Ptth* in the fat body (see Figure 6.1).

Genotype	Number of flies	Error	Period	Rhythmicity index	Lomb-Scargle	eJTK BH bf corrected p
NP5253> Ptth^{i} (KK)	1019	4.4%	24.0h	0.47	31.4	$3.5*10^{-21}$
lsp> Ptth^{i} (KK)	1446	7.3%	24.0h	0.37	24.6	$4.5*10^{-28}$
NP5253> w^{1118}	1496	4.9%	22.5h	0.33	24.4	$1.1*10^{-13}$
lsp> w^{1118}	1519	8.2%	24.5h	0.55	41.3	$2.5*10^{-30}$
w^{1118}> Ptth^{i} (KK)	1755	1.3%	24.0h	0.36	21.8	$7.1*10^{-23}$

2. Cold-sensitive Ricin as a potent and regulatable cell-killing agent

It was not possible to ablate v'Td, C4da, and Ms neurons using *UAS-RA* because flies never hatched from the eggs or died during the first ecdysis. Therefore, cold-sensitive ricin (*UAS-RA^{CS2}.CC*) was used to limit cell killing to the final pupal stages. To check if RA^{CS2}.CC is effective in ablating targeted neurons, it was expressed along with mCD8::GFP in v'Td1^{A1-5} neurons (*R35B01-Gal4> UAS-mCD8::GFP*; *UAS-RA^{CS2}.CC*). Three conditions were chosen and were compared together. In the control condition, the animals were raised at 20 °C and did not experience any temperature shocks necessary for RA^{CS2}.CC activation. The first experimental group was put for twelve hours at 30 °C and dissected immediately after the heat shock. The second experimental group was treated with twelve hours of 30 °C heat shock and dissected two days later. The VNCs of the adult flies (where the processes of v'Td1 neurons are mainly located) were dissected and stained for the GFP. To correctly quantify the results, the staining and the confocal imaging were done with the same settings. For each condition, six VNCs were imaged with the confocal microscope. The number of cell bodies inside the VNC (labeled by ectopic expression of GFP in non-v'Td neurons; see Results IV.1.a), their surface area (μm^2), and their mean fluorescence (mean gray value after background subtraction; arbitrary unit) were measured using Fiji (Figure 6.2 D, E, F). Since the distribution of the data points was not normal, the Mann-Whitney *U* test and pairwise Wilcoxon test were done to identify the significant differences between the control and experiment groups. In control, all the cell bodies and their processes were stained with anti-GFP staining (Figure 6.2 A). In contrast, in both experimental conditions, the processes were largely absent. In the immediately dissected after ablation group, many cell bodies and processes were still visible (Figure 6.2 B), while in VNCs dissected after 48 hours, the cell bodies and processes were nearly completely absent (Figure 6.2 C). On average the number of cell bodies between the control and the first experimental condition (dissected immediately after ablation) was not different. However, the second experimental condition compared to the control, or the first experimental condition had significantly fewer cell bodies (Figure 6.2 D; $p \geq 0.001$). The immediately dissected after ablation VNCs showed on average significantly increased surface area of the cell bodies ($p = 0.01$), but after two days the surface area of cell bodies effectively decreased compared to other experiment and control groups (Figure 6.2 E; $p \geq 0.0001$). The average fluorescence of the cell bodies GFP in the immediately dissected after ablation group compared to the control was nearly the same (Figure 6.2 F; $p \leq 0.05$). However, this fluorescence level dropped largely after two days (Figure 6.2 F; $p \geq 0.0001$). Taken together *UAS-RA^{CS2}.CC* effectively ablates the

neurons. However, it is possible that some neurons survive and the passage of time is necessary to see its full effects.

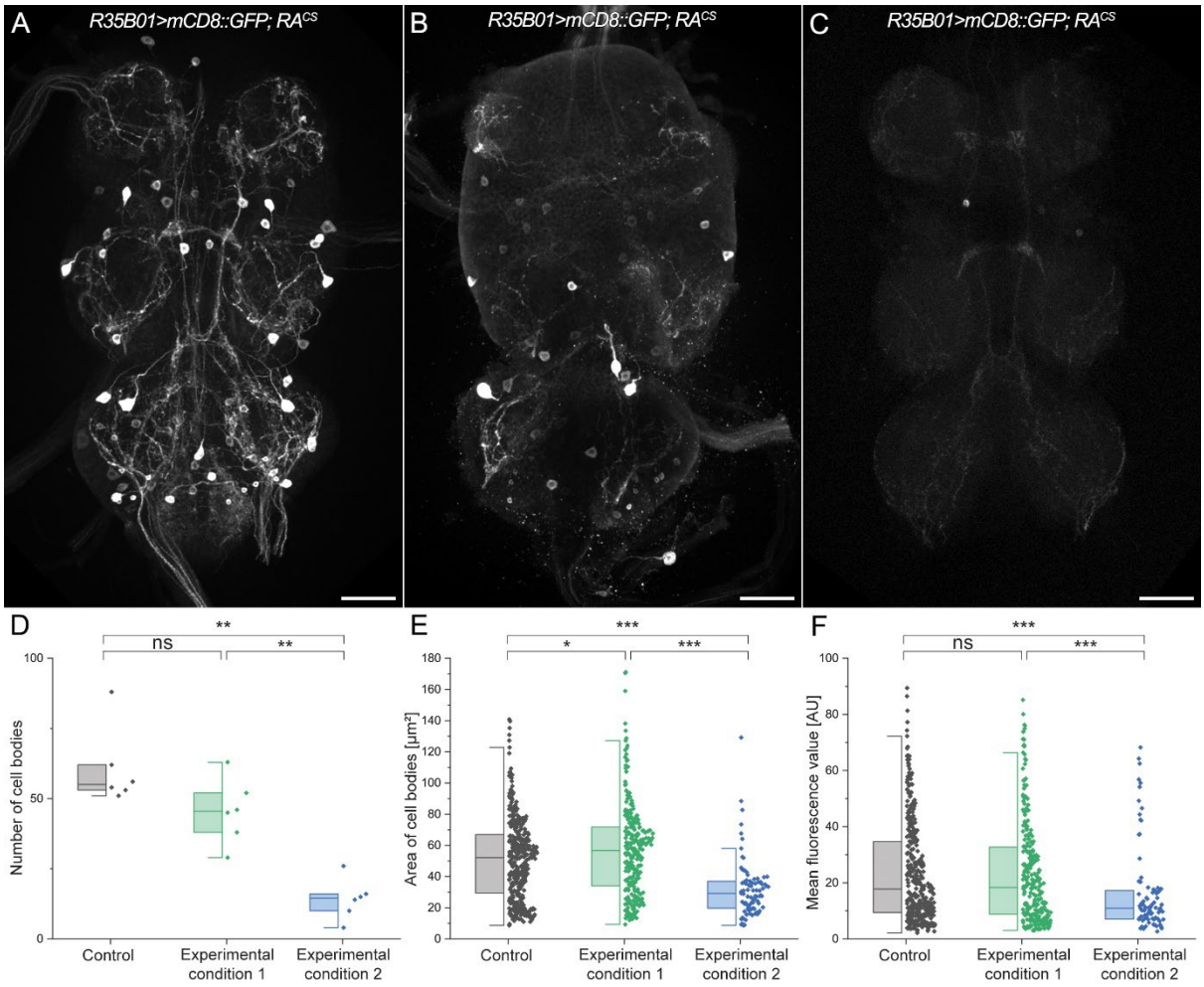

Figure 6.2. *UAS-RA^{CS2}.CC* can effectively ablate neurons. A The simultaneous expression of the GFP and RA^{CS2}.CC (ricin not activated as control) in the v'Td1^{A1-5} neurons (*R35B01-Gal4> UAS-mCD8::GFP; UAS-RA^{CS2}.CC*) labels all non-v'Td1 neurons plus the axonal processes of v'Td1^{A1-5} neurons in the VNC. GFP expression shows the normal expression pattern of *35B01-Gal4* line. The cell bodies and their arborizations are normal. **B** Dissecting the VNCs immediately after twelve hours of heat shock at 30 °C labels fewer cell bodies and damaged neuronal processes represented by faint GFP staining and distorted processes. **C** However, 48 hours after heat shock barely any arborization or cell bodies are visible. **D** On average the loss of GFP in cell bodies after the shock is not immediately noticeable, but after two days the number of visible cell bodies drops significantly. **E** The average surface area of the cell bodies increases immediately after cell killing but significantly drops after two days. **F** The mean fluorescence value of GFP expression in cell bodies does not immediately drop after heat shock but two days later significantly drops. * = $p \leq 0.05$, ** = $p < 0.001$, and *** = $p < 0.0001$. ns = not significantly different. *Scale bars*: 50 µm.

3. Kir2.1 can effectively silence clock neurons

Expression of potassium inward rectifying channel 2.1 (*UAS-Kir2.1*) was used to electrically silence the neurons. To assess the effectiveness of Kir2.1, locomotor activity assays of flies with silenced clock neurons (*Clk856> Kir2.1*) were monitored using the TriKinetics *Drosophila* Activity Monitor 2 system (TriKinetics Inc, Waltham, MA USA). The activity of

two control groups (w^{1118}> *Kir2.1* and *Clk856*> w^{1118}) was monitored as well. All flies were entrained in 12:12 LD conditions and monitoring was done in constant DD (see Materials and Methods 6). The rhythmicity of the locomotor activity was measured using LS analysis. The experimental group immediately showed an arrhythmic averaged activity pattern (Figure 6.3 A and D) while the control groups remained rhythmic after 25 days (Figure 6.3 B-C and E-F). The LS analysis also showed the experimental group is arrhythmic with a period of 17.93 hours (Figure 6.3 D). The Gal4 control had a period of 23.82 which is close to 24 hours (Figure 6.3 E). However, despite being rhythmic the UAS control had a shorter free-running period of 22.75 hours (Figure 6.3 F). This experiment showed that Kir2.1 is capable of successfully silencing the clock neurons. Hence, it was used to silence other neurons in this thesis (see Results I.1.a, I.3, IV.1.d, and IV.3.b).

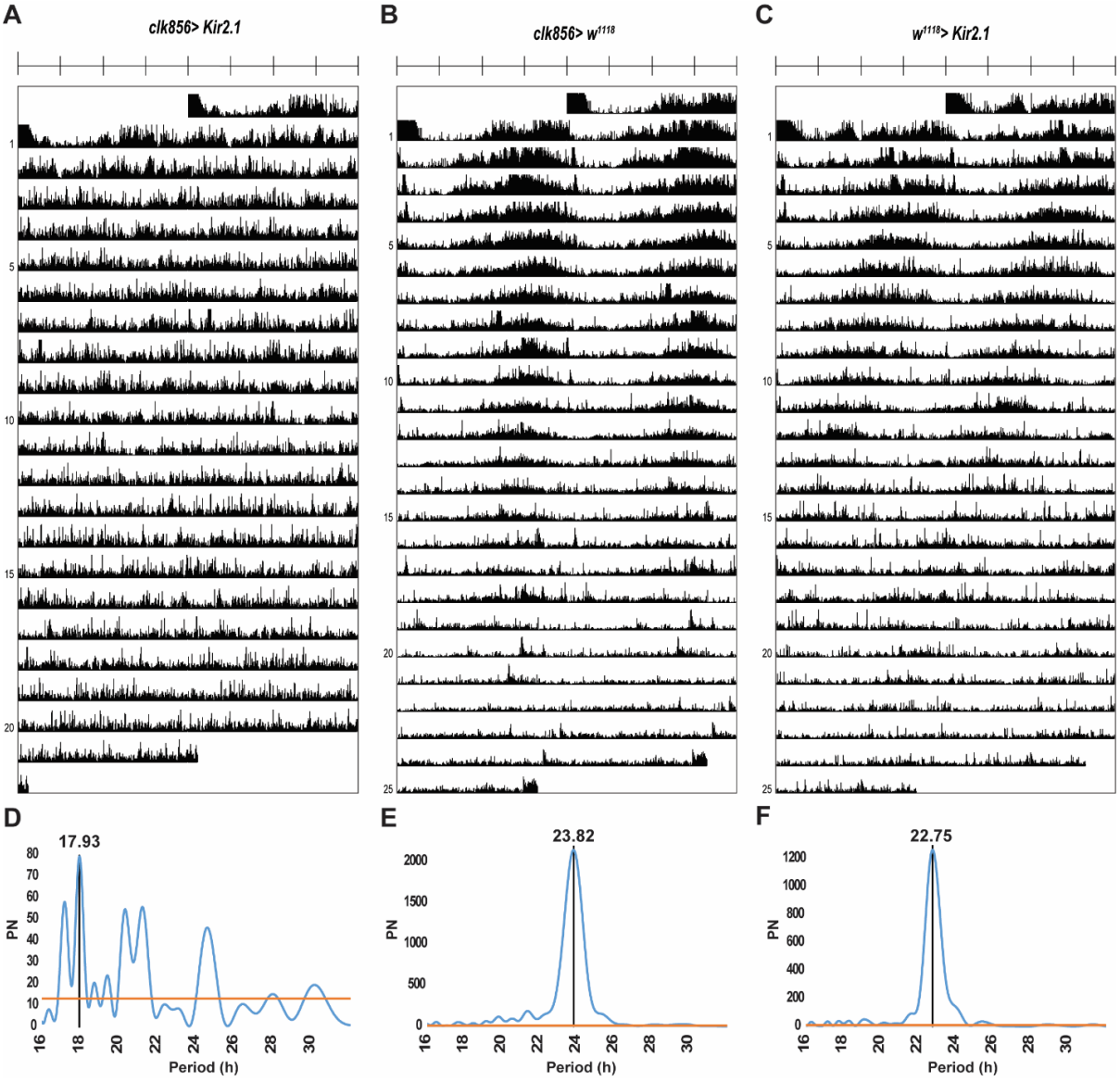

Figure 6.3. Kir2.1 efficiently silences the clock neurons. A The expression of Kir2.1 in all clock neurons (*Clk856*> *Kir2.1*) shows arrhythmic locomotor activity in DD. The average activity of 32 flies shows no distinctive bimodal pattern. **B** The Gal4 control (*Clk856*> w^{1118}) shows a very distinctive averaged bimodal activity pattern with a free-running period close to 24 hours (n=32). **C** The UAS control (w^{1118}> *Kir2.1*) also shows averaged bimodal activity with a free-running period shorter than 24 hours (n=32). **D** LS analysis of the experimental groups confirms the arrhythmicity of averaged

locomotor activity with a period of 17.93 hours. **E** The averaged locomotor activity of the Gal4 control group has a period of 23.82 hours, **F** while the UAS control group shows a period of 22.75 hours.

4. *R43D05-LexA* drives expression in most clock neurons

To identify the clock neurons providing input to PTTH or EH neurons BAcTrace was used (see Results I.2 and II.1). BAcTrace requires a LexA line able to label expression in the hypothesized presynaptic neurons (Cachero et al., 2020). For this reason, the GMR line *R43D05-LexA* was used. To check if this line efficiently labels clock neurons and to compare its expression pattern with *Clk856-Gal4*, double staining was performed. The nuclear mCherry was expressed in most of the clock neurons using *Clk856-Gal4> UAS-mCherry.nls* (Figure 6.4 A"). The membrane-bound GFP was expressed using the *R43D05-LexA> LexAop-myr::GFP* to label the morphology of the neurons expressed by the GMR driver (Figure 6.4 A). The GFP and mCherry signals were successfully colocalized in all four sLN_vs (Figure 6.4 B'), 3-5 of the LN_ds (Figure 6.4 C'), both $DN1_as$ (Figure 6.4 D') and both DN2s (Figure 6.4 E'). This line was unable to show any of the $DN1_ps$ or DN3s. Based on this expression pattern *R43D05-LexA* was used to identify the presynaptic clock neurons to PTTHn and EH neurons using BAcTrace.

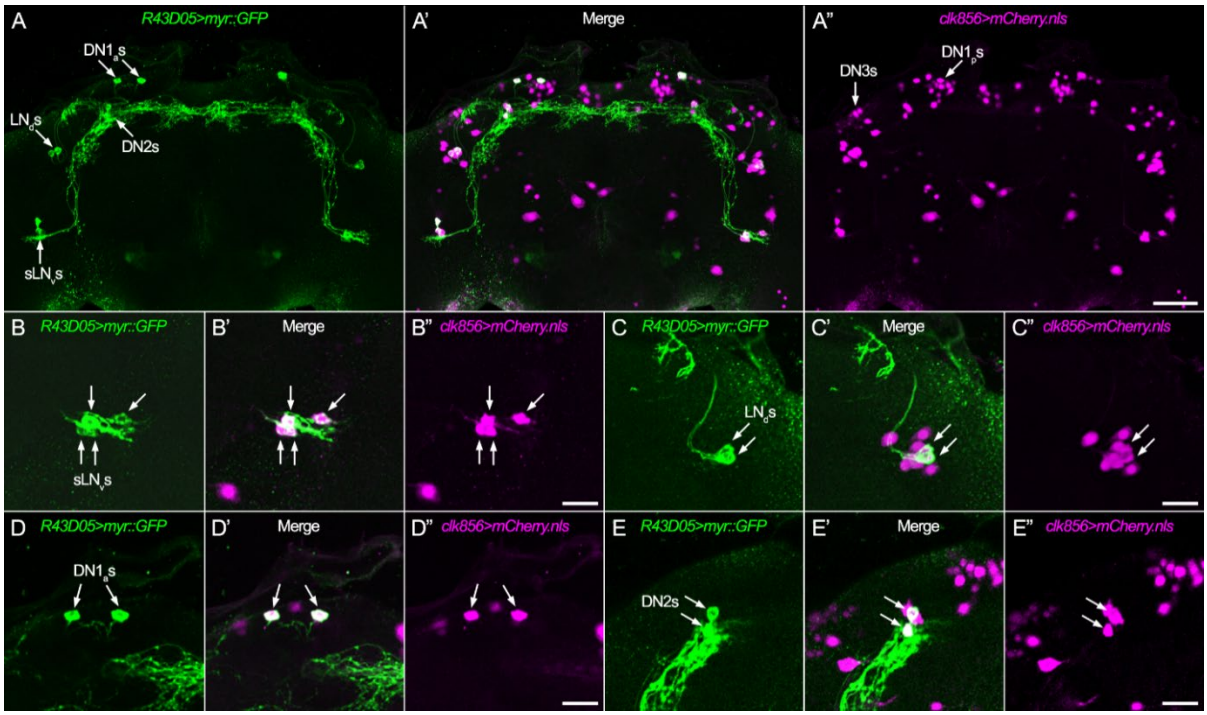

Figure 6.4. The colocalization of *Clk865-Gal4* driven mCherry and *R43D05-LexA* driven GFP shows which clock neurons labeled with this *R43D05-LexA* line. A myr::GFP is expressed in clock neurons using *R43D05> myr::GFP*. **A'** Colocalization of GFP and mCherry identifies the clock neurons labeled by both driver lines. **A"** *Clk856> mCherry.nls* expresses nuclear mCherry in all clock neurons except lLN_vs and ectopically is some non-clock neurons as well. The clock neurons labeled by both drivers are **B-B"** all sLN_vs (arrows), **C-C"** some of LN_ds (arrows), **D-D"** both $DN1_as$ (arrows) and **E-E"** both DN2s (arrows). *Scale bars:* A 50 µm and B-E 20 µm.

5. The specificity of the clock driver lines used in silencing the clock neuronal clusters

To specifically silence the clock neurons (see Results I.3), two split lines, one Flylight GMR, and a combined Gal4-Gal80 line were used. To check their expression patterns, *UAS-myr::GFP* was used. The split-Gal4 lines were previously described (Sekiguchi et al., 2020). *R43D05-p65.AD; R93B11.DBD* line could effectively and efficiently label $DN1_a$ neurons. It did not drive expression in any other neuron (Figure 6.5 A) and, therefore had a very specific expression pattern. The other split-Gal4 line, *R11B03-p65.AD; R65D05.DBD*, successfully labeled LPNs. Despite being very specific, it was not strong. The GFP expression driven by *R11B03-p65.AD; R65D05.DBD* in LPNs was very weak (Figure 6.5 D). The GMR line R51H05-Gal4 could successfully and strongly drive myr::GFP expression in 10-12 of the $DN1_p$s. It showed unspecific expression in the optic lobe projecting neurons and GFP expression was visible in the medulla, lobula, and posterior optic commissure. Weak GFP expression was also present in some neurons in the posterior medial protocerebrum (Figure 6.5 B). The *Clk-9M-Gal4; LN-Gal80* line when crossed to *UAS-myr::GFP* specifically only labeled the DN2 neurons (Figure 6.5 C). However, GFP expression with *Clk-9M-Gal4; LN-Gal80* was not strong. In summary, all lines that were used in silencing the clock neurons could specifically target the clock clusters of interest. However, considering the strength of GFP expression by LPN and DN2 drivers, it is possible that they weakly expressed Kir2.1 in the temperature-entrained eclosion rhythmicity experiments (see Results I.3 and Figure 1.4) as well.

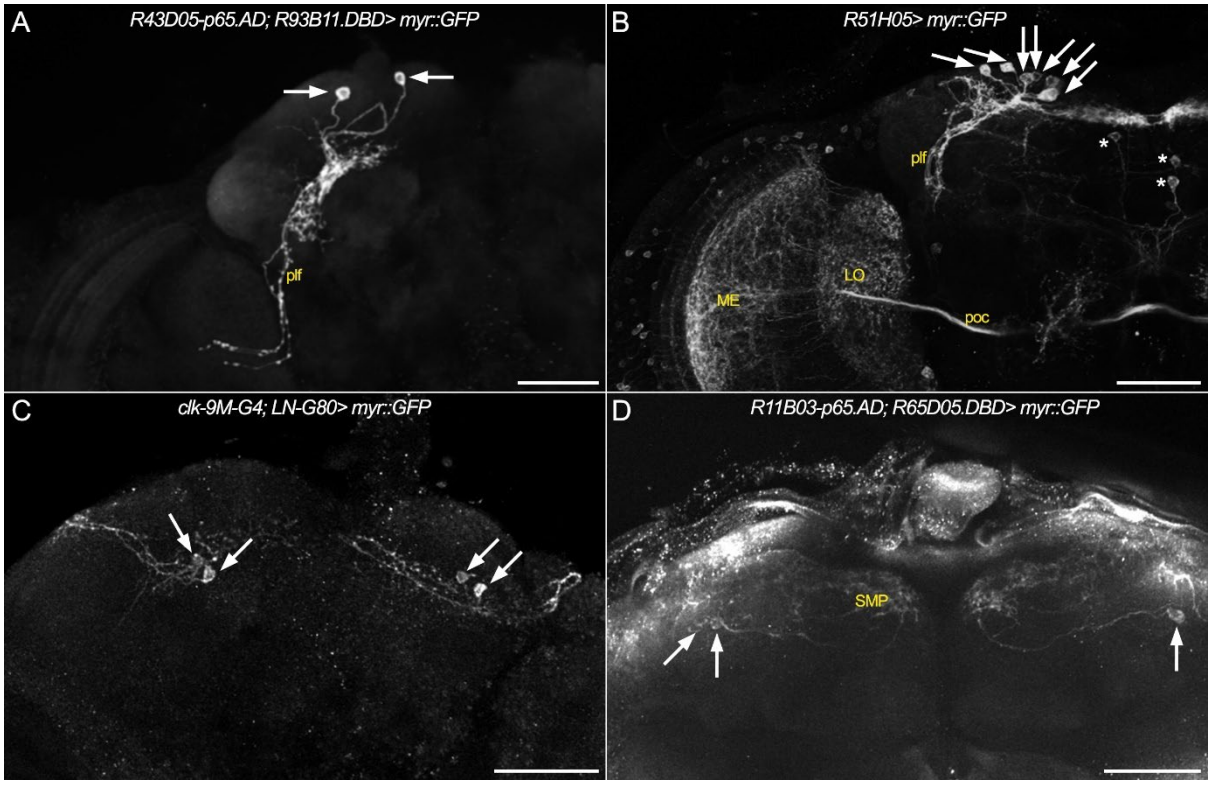

Figure 6.5. The specificity of individual clock neuron driver lines was tested with myr::GFP expression. A *R43D05-p65.AD; R93B11.DBD> myr::GFP* only expresses GFP in the $DN1_a$ neurons (arrows) and labels their processes that project through the posterior lateral fascicle (plf) to AME. The GFP expression in $DN1_a$ neurons is strong. **B** *R51H05> myr::GFP* expresses GFP strongly in twelve

$DN1_p$ neurons (arrows) but also other neurons. Most of the cell bodies of these non-clock neurons are located at the optic lobe cell body rim and project to the medulla (ME), and lobula (LO), and pass through the posterior optic commissure (poc) to the other hemisphere. Other non-clock neuron cell bodies are located at the posterior medial protocerebrum (asterisks). **C** The DN2s can be labeled with *Clk-9M-gal4; LN-Gal80> myr::GFP* (arrows). *Clk-9M-gal4; LN-Gal80* GFP expression pattern is very specific but not strong. **D** The weakest GFP expression belongs to the split-Gal4 line that labels LPNs. The *R11B03-p65.AD; R65D05.DBD> myr::GFP* specifically labels all LPNs but its GFP signal is very weak. The names of the neuropils are shown in capital yellow and the names of the fibers with lowercase yellow letters. *Scale bars*: 50 µm.

6. The expression pattern of the myosuppressin-T2A driver line

The *Ms::2A-Gal4* driver line labels about 180 neurons (Figure 6.6). Unfortunately, due to dense arborizations in most cases, it was not possible to correctly specify the arborization patterns of the neuronal clusters. In the anterior ventral side of the brain ten large neurons projected to the periesophageal neuropils. Specifically, 20-22 small neurons in each hemisphere project to the PRW region of periesophageal neuropils. Only five neurons with large cell bodies projected to the optic lobes, two send their axons to the lobula, and three to the medulla. Ten to13 neurons with large cell bodies sitting at PI sent their axons through the MBDL to the SMP and PRW. About 30 neurons located at the posterior dorsal side of the brain projected to the central complex neuropils, like fan-shaped body, and the BU neuropils. In each hemisphere, four to seven neurons penetrated the AL. The rest of the neurons could not be identified based on their projections. They were categorized based on the location and size of their cell bodies into three groups. The dorsal cluster contained 15 neurons in each hemisphere that projected to superior neuropils, LH, and CL. The small and large posterior clusters each respectively contained five and twelve neurons in each hemisphere.

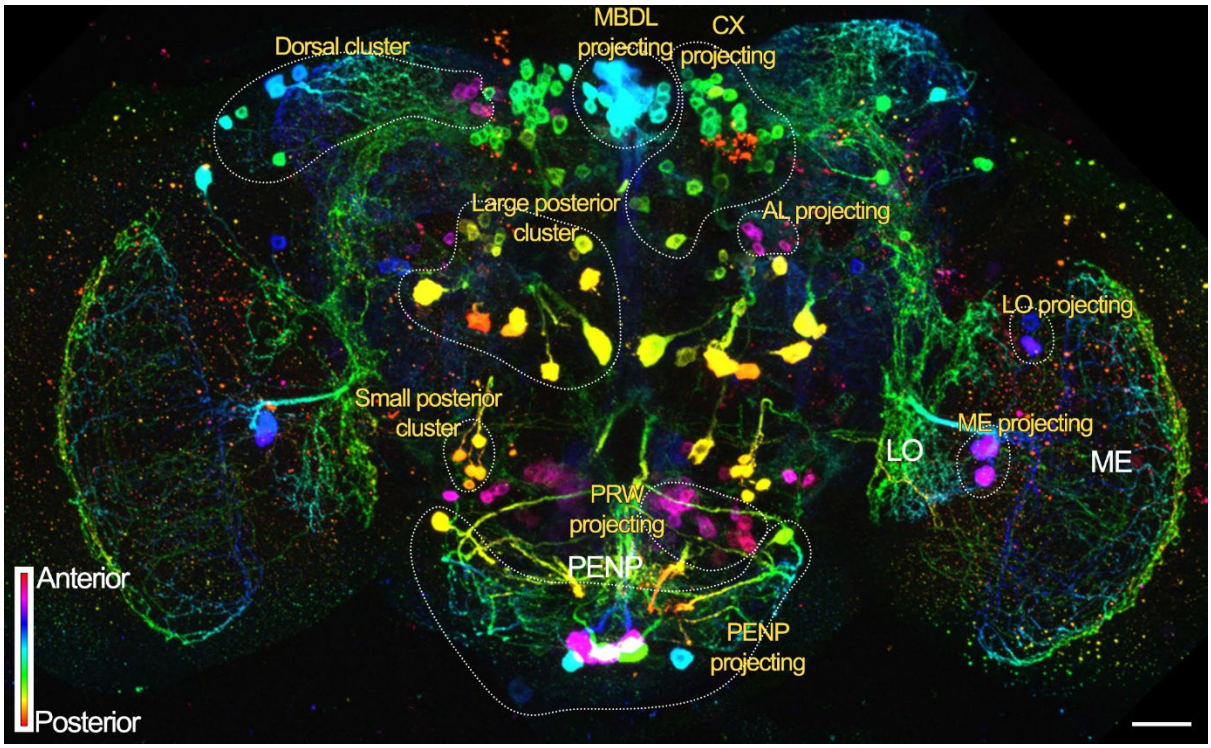

Figure 6.6. Most of the 180 Ms neurons have large cell bodies and they spread in various parts of the brain. Based on their arborization patterns and sizes of cell bodies the Ms neurons are divided into

different clusters. False color coding indicates the location of the cell bodies from anterior to posterior.13 large neurons residing at PI project down to the prow (PRW) neuropils. Five neurons project to the medulla (ME) and lobula (LO) of the optic lobes. Ten large neurons project to the periesophageal neuropils (PENP) and specifically 20-22 small neurons project to PRW. Four to seven neurons project to the antennal lobes (AL) and 30 to the central complex (CX). The unidentified neurons are divided into three clusters. The small- (5 neurons) and large posterior (12 neurons) cluster and dorsal cluster (15) in each hemisphere house these neurons that project to various neuropils. *Scale bar*: 50 µm. The names of the neuropils are shown in capital white and the names of the groups with yellow letters.

7. The expression pattern of the allatostatin A-T2A driver line

AstA::2A-Gal4 line drove myr::GFP expression in around 400 neurons (Figure 6.7). These neurons based on their cell body location and the neuropil system that they project into were divided into ten groups. Three different groups project into the optic lobes. A group of 40 neurons projected to the medulla, 20-22 neurons projected to the lobula, and eight to the lobula plate. The central complex and mainly the fan-shaped body were the target of axonal projections of 74 posterior neurons. The fifth group projected into the periesophageal neuropils such as gnathal ganglia, SAD, FLA, and PRW. Unfortunately, it was not possible to distinguish between the projections of these 42 neurons and which periesophageal neuropils they exactly penetrated. At the dorsolateral part of the brain, four to five neurons entered LH, ten projected to the CL, and 14-16 neurons projected to the superior protocerebrum neuropils such as SLP and SMP. At the anterior side, seven neurons sent their axons to the AL, and 20-23 projected to ventrolateral neuropils and mostly anterior ventrolateral protocerebrum neuropil. The rest of the neurons (11-12) were located on the posterior side of the brain. Where exactly they projected to cannot be known but LPN clock neurons were among them. The posterior slope was one of the neuropils that these posterior neurons projected into.

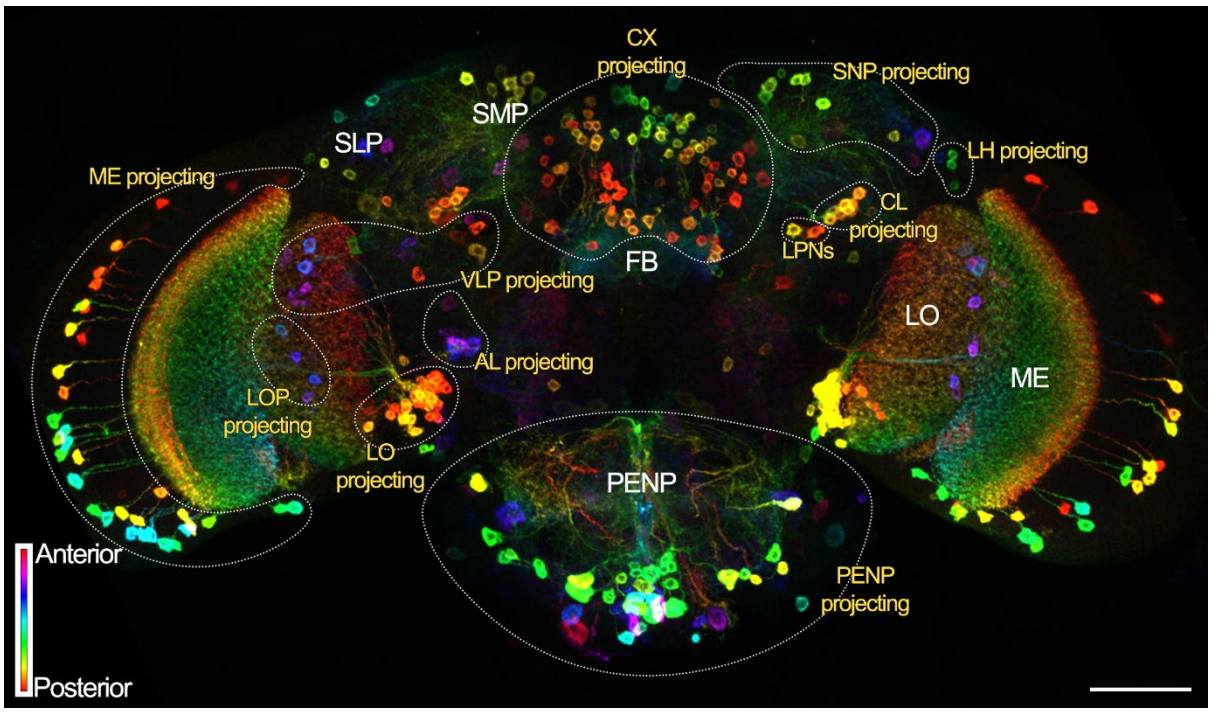

Figure 6.7. Around 400 neurons can be targeted with the AstA::T2A line. Based on the location of the cell bodies and their projections these neurons can be defined into ten groups. False color coding indicates the location of the cell bodies from anterior to posterior. The optic lobe projecting groups are

medulla (ME), lobula (LO), and lobula plate (LOP) projecting neurons. The central complex and especially the Fan-shaped body (FB) is the second distinctive neuropil system that houses AstA neurons. The rest of the neuropil systems that have AstA neurons are periesophageal neuropils (PENP), antennal lobe (AL), ventrolateral neuropils (VLP), superior neuropils (SNP), lateral horn (LH), and clamp (CL). The rest of the neurons are located posteriorly but where they project into is not identified. *Scale bar*: 50 µm. The names of the neuropils are shown in capital white and the names of the groups with yellow letters.

8. The expression pattern of the allatostatin C-T2A driver line

The *AstC::2A-Gal4* driver line drives myr::GFP expression in more than 440 neurons (Figure 6.8) most of which were associated with the central complex neuropils, optic lobes, and periesophageal neuropils. The central complex neurons projected into the fan-shaped body (12 neurons), ellipsoid body (six neurons), and protocerebral bridge (23-24 neurons in each hemisphere). 13-15 neurons in each hemisphere were the tubercle-bulb neurons. The periesophageal neuropils projecting neurons were divided into two groups. One posterior group containing 10-15 neurons projected to cantle and FLA. The other contained 31-35 (in each hemisphere) mostly large cell-bodied neurons in the ventral part of the brain and projected to SEZ neuropils such as SAD, PRW, and gnathal ganglia. The optic lobes were housing several groups of neurons. A cluster of small neurons (25-30) sat on the dorsal part of the medulla and projected to it. A group of 18-20 neurons projected to both medulla and lobula. 30 posteriorly located neurons projected to the posterior optic commissure. At the anterior side of the brain 18 neurons projected to CL. Finally, one more group was defined based on their cell body locations and not their projections. These 30-32 neurons resided in the dorsal brain and projected to various neuropils. Some of the DN1$_{p}$s and DN3 clock neurons are among these neurons.

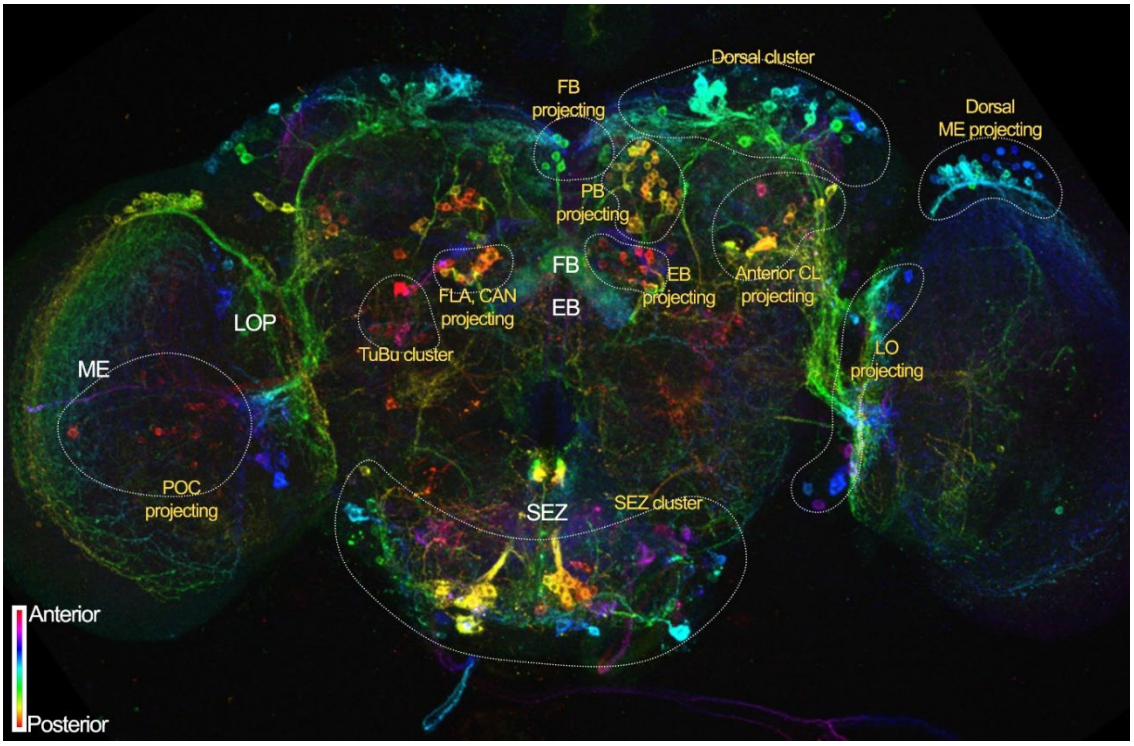

Figure 6.8. More than 440 neurons in the brain express AstC. The AstC neurons reside in different neuronal clusters. False color coding indicates the location of the cell bodies from anterior to posterior.

Some of these neurons project to central complex neuropils such as fan-shaped body (FB), ellipsoid body (EB), and protocerebral bridge (PB). There is a tubercle-bulb (TuBu) neuronal group. Two periesophageal neuropils (PENP) clusters project to the suboesophageal zone (SEZ) and the cantle (CAN) and flange (FLA). The optic lobe-associated neurons reside in the dorsal medulla- (ME), lobula- (LO), and posterior optic commissure (POC) projecting neurons. 18 neurons project to clamp (CL). The dorsal cluster contains neurons that project to various neuropils, among which the $DN1_p$s and DN3 clock neurons reside.

9. List of receptors investigated in this study and the prediction of their Gα subunit using PRED-COUPLE 2.00:

The following is the list of the receptors of the peptides released by the clock neurons. The Isoform, CG number, FB number, protein sequence, and type of each receptor were obtained from the Flybase. The protein sequence was used with PRED-COUPLE 2.00 bioinformatic database to predict the Gα subunit of the GPCR, hence predicting its mechanism of function.

- ***PDFR*** **(CG13758)**

PRED-COUPLE 2.00 prediction: **$G\alpha_{i/o}$: 0.96**, **$G\alpha_s$: 0.65**, $G\alpha_{q/11}$: 0.08, and $G\alpha_{12/13}$: 0.00.

- ***sNPF-R*** **(CG7395)**

PRED-COUPLE 2.00 prediction: **$G\alpha_{i/o}$: 0.99**, **$G\alpha_{q/11}$: 0.56**, **$G\alpha_{12/13}$: 0.38**, and $G\alpha_s$: 0.00.

- ***AstA-R1*** **(CG2872)**

PRED-COUPLE 2.00 prediction: **$G\alpha_{i/o}$: 0.92,** $G\alpha_s$: 0.01, $G\alpha_{q/11}$: 0.00, and $G\alpha_{12/13}$: 0.09.

- ***AstA-R2^C*** **(CG10001)**

PRED-COUPLE 2.00 prediction: **$G\alpha_{i/o}$: 0.83**, $G\alpha_{q/11}$: 0.21, $G\alpha_s$: 0.07, and $G\alpha_{12/13}$: 0.00.

- ***AstC-R1*** **(CG7285)**

PRED-COUPLE 2.00 prediction: **$G\alpha_{q/11}$: 0.95**, $G\alpha_{i/o}$: 0.19, $G\alpha_s$: 0.02, and $G\alpha_{12/13}$: 0.00.

- ***AstC-R2*** **(CG13702)**

PRED-COUPLE 2.00 prediction: **$G\alpha_{q/11}$: 0.92**, $G\alpha_{i/o}$: 0.11, $G\alpha_s$: 0.01, and $G\alpha_{12/13}$: 0.00.

- ***Dh31-R^C*** **(CG32843)**

PRED-COUPLE 2.00 prediction: **$G\alpha_{i/o}$: 0.94**, **$G\alpha_s$: 0.91**, $G\alpha_{q/11}$: 0.04, and $G\alpha_{12/13}$: 0.00.

- ***MsR1^B*** **(CG8985)**

PRED-COUPLE 2.00 prediction: **$G\alpha_{i/o}$: 0.96**, $G\alpha_s$: 0.08, $G\alpha_{q/11}$: 0.02, and $G\alpha_{12/13}$: 0.00.

- ***MsR2^C*** **(CG43745)**

PRED-COUPLE 2.00 prediction: **$G\alpha_{i/o}$: 0.99**, $G\alpha_s$: 0.12, $G\alpha_{q/11}$: 0.05, and $G\alpha_{12/13}$: 0.05.

10. Calculation of the time of eclosion in *ppk> ARG-Luc* data independent of photographs

To investigate the activity of C4da neurons and to see how this activity correlates with the activity of PTTHn and V_m neurons, *ppk> ARG-Luc* flies were used. However, due to the crashing of the TopCount Multiplate Reader, the data was mainly lost. The machine could record only about three days (less than 72 hours). Therefore, the eclosion data was available only for six flies and five of them had low photon counts. After sorting the data based on

photographs that captured the moment of eclosion, the overall activity of C4da neurons was obtained (Figure 6.9). The average data showed activity at -7h. The eclosion peak artifact was mainly lost due to low counts except for one fly. On the day of eclosion, each fly data showed a different activity pattern. However, on the next day, a large and broad activity peak was present in average data.

This pattern was used to analyze the data obtained previously (on 04.08.2022) but without photographs. 23 flies showed C4da activity. In each fly a peak at around -10h to -6h before eclosion was present and they all showed the eclosion artifact peak. Each fly showed random C4da activity on the day of eclosion and the day after showed increased activity followed by a drop to zero (Figure 4.11). Therefore, the data was aligned based on the eclosion artifact peak and presented in Chapter IV (see Results IV.3.d).

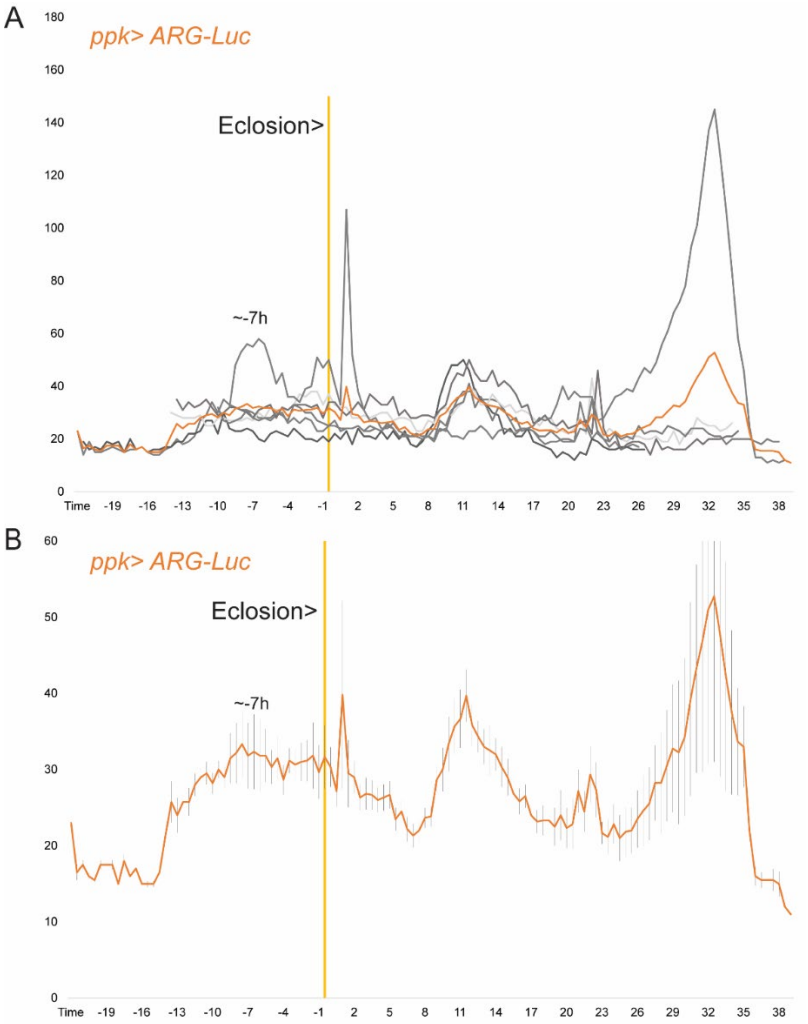

Figure 6.9. Activity of C4da neurons before and after eclosion. A Data from six *ppk> ARG-Luc* flies are shown in different shades of gray and the average is shown in orange. The C4da neurons start their activity between ten to seven hours before eclosion. On the first day after eclosion, different flies show different activities. **B** The average activity of six *ppk> ARG-Luc* flies is shown in orange. A broad activity peak is present around seven hours before eclosion. On day two after eclosion a large peak is present.

Affidavit

I, Emad Amini, hereby confirm that this thesis entitled **"How central and peripheral clocks and the neuroendocrine system interact to time eclosion behavior in *Drosophila melanogaster*"** is the result of my own work. I did not receive any help or support from any commercial consultants. All the sources and/or materials applied are listed and specified in the thesis.

Furthermore, I confirm that this thesis has not yet been submitted as part of another examination process neither in identical nor in similar form.

Würzburg, 15.01.2024

Place, Date Signature

Eidesstattliche Erklärung

Hiermit bestätige ich, Emad Amini, dass diese Arbeit mit dem Titel **„Wie zentrale und periphere Uhren und das neuroendokrine System zusammenwirken, um das Schlupfverhalten von *Drosophila melanogaster* zeitlich festzulegen"** das Ergebnis meiner eigenen Arbeit ist. Ich habe keine Hilfe oder Unterstützung von kommerziellen Beratern erhalten. Alle verwendeten Quellen und/oder Materialien sind in der Arbeit aufgeführt und spezifiziert.

Weiterhin versichere ich, dass diese Arbeit bisher weder in gleicher noch in ähnlicher Form im Rahmen eines anderen Prüfungsverfahrens eingereicht worden ist.

Würzburg, 15.01.2024

Ort, Datum Unterschrift